QCD quantum correlation and multi-parton dynamics

by

Zhongbo Kang

A dissertation submitted to the graduate faculty

in partial fulfillment of the requirements for the degree of

DOCTOR OF PHILOSOPHY

Major: Nuclear Physics

Program of Study Committee:
Jian-Wei Qiu, Major Professor
Mark Gordon
John Hill
John Lajoie
Marshall Luban

Iowa State University

Ames, Iowa

2009

DEDICATION

I would like to dedicate this work to my family, who always love me, support me and appreciate me ...

TABLE OF CONTENTS

LIST OF FIGURES

ACKNOWLEDGEMENTS

I would like to take this opportunity to express my thanks to those who helped me with various aspects of conducting research and the writing of this thesis.

First and foremost, I would like to thank my Ph.D advisor Dr. Jian-Wei Qiu for his guidance, patience and support throughout the research and the writing of this thesis. I thank him for spending a significant effort and time to teach me new valuable knowledge and skills. I am also very grateful for his willingness to answer countless questions and patiently discuss with me even the smallest technical detail.

I would like to thank my collaborators Drs. Werner Vogelsang and Feng Yuan for working with me, for their encouragement and suggestions. Furthermore, I thank Drs. Marshal Luban and Xiaofeng Guo for their encouragements, Dr. German Valencia for teaching me high energy physics and for his valuable suggestions and encouragement. Thanks must go as well to Drs. John Lajoie, Kirill Tuchin, Ming Liu and Andreas Metz for many interesting discussions.

I would like to thank Feng Wei and Jian Zhou for lots of valuable discussions on various physics problems. Thanks also go to my friends Andrew Ansorge, Alina Negoita, Jun Li, Oleg Antipin, Alberto Accardi, Ricardo Rodriguez, Jie Ma, Qian Wang, Asif Imran, and Ben-Wei Zhang for their friendship and for discussion on everything, including the future of the career.

I wish to thank my parents, Linzhi Yang and Jianting Kang for their unconditional love. They support every step of my life. Their love is beyond words. I thank my parents-in-law, Shuxian Yang and Rongshan Ni, and my sister Zhonglei Kang for their love, understanding and encouragements. Finally, I would like to thank my wife, Ni Ni, for her love and her support all these years. Perhaps none of this work would be completed without her love, encouragements and appreciation. I feel deeply blessed for having this lovely wife.

ABSTRACT

Protons and neutrons are known to be the building blocks of matter, and also known to be the bound states of quarks and gluons - the partons, whose dynamics is best described by Quantum Chromodynamics (QCD). Perturbative QCD has been very successful in interpreting and predicting high-energy hadronic scattering processes by factorizing the leading contribution to the physical cross sections into a convolution of the perturbatively calculable short-distance part and the universal long-distance parton distribution functions (PDFs) of colliding hadrons. Besides testing QCD dynamics at the short-distance, these cross sections also probe partonic structure inside a colliding hadron via PDFs, which are often interpreted as the probability densities of finding a parton inside a hadron with a given longitudinal momentum fraction.

In this thesis I discuss the possibilities to explore the rich partonic dynamics inside a hadron or a large nucleus beyond the probability distributions. I will first explain why a difference of two transverse-spin dependent cross sections (or the measurement of the single transverse-spin asymmetry) can directly probe a set of new three-parton correlation functions. These correlation functions provide the first direct information on quantum correlation between quarks and gluons inside a polarized hadron. I will describe the basic formalism and the experimental measurements of these correlation functions. I will present the first derivation of evolution equations (or renormalization group equations) for these correlation functions. I will then discuss how to use the nuclear dependence of high energy nuclear collisions to extract the information on four-parton correlations inside a large nucleus or a nuclear medium. The measurements of the spin asymmetry and the anomalous nuclear dependence provide us new opportunities to explore the QCD dynamics and hadron structure beyond the parton probability distributions.

CHAPTER 1. Introduction

1.1 Structure of matter: History towards QCD

What is the world made of? What are the most fundamental constituents of matter? Present-day particle physics research represents man's most ambitious and most organized effort to answer these questions. The earliest attempt dates to at least 6th century BC, when ancient Greek philosophers were studying the philosophical doctrine of atomism and the nature of their basic building blocks. These ideas were founded in abstract, philosophical reasoning, thus remained only a speculation for the next 2400 years. In the early nineteenth century investigators applied the method of experimental science to study this problem and raise these ideas to the level of a full-fledged scientific theory.

In 1803, English natural philosopher John Dalton proposed the atomic theory in chemistry, in which the concept of atoms was introduced and used to explain various new discoveries in chemistry. In 1911, Ernest Rutherford from New Zealand discovered that atoms have a small charged nucleus. The atomic nucleus was originally thought to be made of protons only, until English physicist James Chadwick discovered neutrons in 1932. Until then, the general understanding was that matter in the universe is composed of atoms which consist of a nucleus and electrons. The nucleus is further made of protons and neutrons, collectively called nucleons.

Since particle accelerators were introduced in late 1920s, many new particles have been discovered in scattering experiments. It has become clear that the neutron and proton were not alone. They turned out to be just the lightest particles in a spectrum of strongly interacting fermion states, called baryons. There is also another sequence of strongly interacting bosons, called mesons, in which pion is the lightest. Baryons and mesons are collectively called hadrons, which add up to more than several hundred.

With a bewildering variety of particles, it becomes difficult to believe that all of them are fundamental. In 1964 Gell-Mann [1] and Zweig [2] proposed the quark model to classify all hadrons in terms of their more fundamental building blocks, named quarks: three quarks for baryons and a quark-antiquark pair for mesons. These so called "constituent quarks" are spin-1/2 fermions with fractional electric charges and new quantum numbers of flavor, ie, up, down, strange, charm, bottom and top.

However, there is a difficulty in constructing low-lying baryon states in this naive quark model. For example, Δ^{++} with spin 3/2, is made of three u-quark. To satisfy the Pauli exclusion principle, a hidden degrees of freedom "color" was introduced for the quarks. We suppose that quarks come in three primary colors, usually called red, green and blue, and the baryon wave functions are totally antisymmetric in this new quantum number. Since we do not observe the color degrees of freedom directly, we may assume that the hadronic phenomena be unaltered under the exchange of colors. In other words, all hadron states and physical observables are color-singlets.

The quark model with flavor and color quantum numbers can successfully describe most of the basic properties and the qualitative features of the observed low-energy hadronic states. It was thus natural to try to detect the quarks in high energy scattering experiments, and to explore the dynamics between them. The first experimental attempt to directly "see" the substructure of the hadron (proton) was initiated at SLAC in the late 1960s [3, 4], so called electron proton deep inelastic scattering (DIS). The famous Bjorken scaling [5] of the structure functions and the so-called Callan-Gross relation [6] between them inspired Feynman to propose his parton model [7]: the hadrons are composed of pointlike spin-1/2 partons, interacting weakly at high energy. It then became natural to identify Feynman's partons with the quarks proposed by Gell-Mann and Zweig. However, the total momentum carried by these partons is only around 50% of the proton's momentum. It suggests that there are other particles inside the proton, which should be electric neutral and thus do not interact with electrons. It was then assumed that these are gluons, which carry color charge and mediate strong interactions between the quarks.

However, one has never observed an isolated quark indicating that they are strongly confined inside the hadron. On the other hand, they appear almost free at high energy DIS experiments. To solve this dynamical difficulty, we need to build a theory of strong interactions. Following the pioneering work on non-Abelian gauge symmetries by C. N. Yang and R. L. Mills [8], Fritzsch et al. [9] introduced the gauge theory of strong interaction in 1973: Quantum Chromodynamics (QCD), which preserves the local color SU(3) gauge symmetry. It was soon realized that QCD has the feature of asymptotic freedom [10, 11]: the interaction between the quarks and gluons becomes weaker at shorter distances. Because of this property, physical observable (for example, cross section) related to parton interactions at high energy can be calculated as a series in the small QCD running coupling α_s in so called "perturbative QCD".

On the other hand, because of parton confinement, any physical observable involving hadrons contains both short- and long-distance physics, which requires a systematic separation of the dynamics between them. The possibilities for such separation are proven by QCD factorization theorems [12], which factorize the physical observable into perturbatively calculable short-distant hard parts convoluted with universal long-distant distribution functions. Predictions follow when processes with different hard scatterings but the same distribution functions are compared. This approach has been very successful in interpreting and predicting almost all existing data from high energy collisions with momentum transfer larger than a few GeV [13, 14]. It it fair to say that the faith in QCD as a true physics theory ultimately founded, at least up to now, on the successes of perturbative QCD.

In this chapter, we would like to give an elementary introduction to the fundamental formulation of perturbative QCD: QCD Lagrangian, asymptotic freedom, and factorization. Finally I propose how to go beyond the so-called leading twist formalism, to study the strong interaction beyond simple probabilities.

1.2 QCD: Lagrangian, asymptotic freedom

1.2.1 QCD Lagrange density

QCD is a quantum field theory of quarks and gluons endowed with a non-abelian gauge symmetry group - SU(3) of color. The classical Lagrangian which explicitly exhibits this symmetry is given by the Yang-Mills formula:

$$\mathcal{L}_{\text{invariant}} = \sum_f \bar{\psi}_{f,i}(i\gamma^\mu D_{\mu,ij} - m_f\delta_{ij})\psi_{f,j} - \frac{1}{4}(F^a_{\mu\nu})^2. \tag{1.1}$$

Here $D_\mu = \partial_\mu + igA^a_\mu t^a$, g is the gauge coupling constant, the quark fields are ψ_f of mass m_f ($f = 1, ..., n_f$ labels flavor) with color index $i = 1, 2, 3$ ($N_c = 3$). The gluon fields are A^a_μ, $a = 1, 2, .., 8$ ($N_c^2 - 1 = 8$), and the corresponding non-Abelian gauge field strength is given by

$$F^a_{\mu\nu} = \partial_\mu A^a_\nu - \partial_\nu A^a_\mu - gf^{abc}A^b_\mu A^c_\nu \tag{1.2}$$

with f^{abc} the structure constants of SU(3), which define its Lie algebra.

The gauge invariance of $\mathcal{L}_{\text{invariant}}$ actually makes it difficult to quantize. This problem is solved by adding to $\mathcal{L}_{\text{invariant}}$ a gauge-fixing density, $\mathcal{L}_{\text{gauge}}$, given by

$$\mathcal{L}_{\text{gauge}} = -\frac{\lambda}{2}(\eta^\mu A^a_\mu)^2, \tag{1.3}$$

which fixes the gauge $\eta \cdot A = 0$. η is typically chosen as the gradient ∂ (covariant gauge) or as a fixed vector n (axial gauge). In covariant gauges, a ghost term $\mathcal{L}_{\text{ghost}}$ is also needed

$$\mathcal{L}_{\text{ghost}} = \eta^\mu \bar{c}^a(\partial_\mu\delta^{ad} - gf^{abd}A^b_\mu)c^d, \tag{1.4}$$

with ghost fields c^a. So in general a quantized QCD Lagrangian can be written as

$$\mathcal{L}_{\text{QCD}}(\psi_f, A_\mu) = \mathcal{L}_{\text{invariant}} + \mathcal{L}_{\text{gauge}} + \mathcal{L}_{\text{ghost}}. \tag{1.5}$$

1.2.2 Asymptotic freedom

Given the QCD Lagrangian in Eq. (1.5), it is straightforward to derive the Feynman rules for QCD perturbation theory. However, similar to other field theories, Green functions, and consequently cross sections, calculated according to these unmodified Feynman rules suffer a severe problem when we include diagrams with loops. These are the ultraviolet (UV) divergences, associated with infinite loop momenta. Therefore, perturbative calculations need to be regularized, and renormalized. The term "renormalization" means, together with the redefinition of the mass and coupling constant, the readjustment of the normalization of cross sections by suitable multiplicative factors which may eliminate possible infinities in the cross section. Physical predictions of the theory come only after the divergences are systematically removed.

Renormalization in QCD can be summarized as follows. Start with the QCD Lagrangian in Eq. (1.5), we define

$$\begin{aligned} \mathcal{L}_{\rm Renormalized}(\psi_R, A_R, Z's) &\equiv \mathcal{L}_{\rm Classical}(\psi_R, A_R) + \mathcal{L}_{\rm counterterm}(\psi_R, A_R, Z's) \\ &= \mathcal{L}_{\rm Bare}(\psi_0, A_0), \end{aligned} \tag{1.6}$$

where $\mathcal{L}_{\rm Classical}(\psi_R, A_R)$ and $\mathcal{L}_{\rm Bare}(\psi_0, A_0)$ have the same functional form as $\mathcal{L}_{\rm QCD}(\psi, A)$ in Eq. (1.5). $\mathcal{L}_{\rm Bare}(\psi_0, A_0)$ is presented in terms of "bare" (unrenormalized) quantities (fields, coupling constants, and mass parameters) while $\mathcal{L}_{\rm Classical}(\psi_R, A_R)$ is given in terms of renormalized ones. $Z's$ are renormalization constants, which define the relation between the renormalized and bare quantities,

$$\begin{aligned} \psi_{f,0} &= Z_\psi^{1/2}(\mu)\psi_{f,R}(\mu), \\ A^a_{\mu,0} &= Z_A^{1/2}(\mu)A^a_{\mu,R}(\mu), \\ c^a_0 &= Z_c^{1/2}(\mu)c^a_R(\mu), \\ g_0 &= Z_g(\mu)\, g(\mu), \\ m_{f,0} &= Z_m(\mu)m_{f,R}(\mu), \end{aligned} \tag{1.7}$$

where μ is the renormalization scale.

When QCD is renormalized, an arbitrary scale μ arises. However, a physically observed quantity (e.g., the cross section σ) should be independent of this scale, ie,

$$\mu^2 \frac{d}{d\mu^2} \sigma \left(\frac{Q_{ij}^2}{\mu^2}, \alpha_s(\mu), \mu \right) = 0, \tag{1.8}$$

where Q_{ij}^2 are Lorentz invariants constructed from external momenta and $\alpha_s = g^2/4\pi$. We can then derive a renormalization group equation as

$$\left(\mu^2 \frac{\partial}{\partial \mu^2} + \beta(\alpha_s) \frac{\partial}{\partial \alpha_s} + \omega \right) \sigma \left(\frac{Q_{ij}^2}{\mu^2}, \alpha_s(\mu), \mu \right) = 0. \tag{1.9}$$

Here $\beta(\alpha_s)$ is defined as

$$\beta(\alpha_s) = \mu^2 \frac{\partial \alpha_s}{\partial \mu^2}, \tag{1.10}$$

which measures the change of the coupling constant α_s as one changes the renormalization scale μ. This leads to an important concept: running coupling constant, whose strength depends on the renormalization scale, and it represents an effective "local" interaction including a lot of high mass states. The running coupling constant $\alpha_s(\mu^2)$ is controlled by the QCD β-function, which has the perturbative expansion

$$\beta(\alpha_s) = -\frac{\beta_0}{2\pi} \alpha_s^2 - \frac{\beta_1}{4\pi^2} \alpha_s^3 - \frac{\beta_2}{64\pi^3} \alpha_s^4 - \ldots, \tag{1.11}$$

where

$$\begin{aligned} \beta_0 &= 11 - \frac{2}{3} n_f \\ \beta_1 &= 51 - \frac{19}{3} n_f \\ \beta_2 &= 2857 - \frac{5033}{9} n_f + \frac{325}{27} n_f^2 \end{aligned} \tag{1.12}$$

The solution to the lowest order approximation to Eq. (1.10) can be written as

$$\alpha_s(\mu^2) = \frac{\alpha_s(\mu_0^2)}{1 + (\beta_0/4\pi)\alpha_s(\mu_0^2)\ln(\mu^2/\mu_0^2)}, \tag{1.13}$$

where the value of $\alpha_s(\mu_0^2)$ gives the boundary condition for the solution of the differential equation. Since $\alpha_s(\mu_0^2)$ and μ_0^2 are not independent, it is more convenient to introduce a common constant, $\Lambda_{\rm QCD}$,

$$\Lambda_{\rm QCD}^2 = \mu_0^2\, e^{4\pi/\beta_0\alpha_s(\mu_0^2)}, \tag{1.14}$$

such that

$$\alpha_s(\mu^2) = \frac{4\pi}{\beta_0 \ln(\mu^2/\Lambda_{\rm QCD}^2)}, \tag{1.15}$$

where the famous $\Lambda_{\rm QCD}$ is of the order 200 MeV determined from the experiments, and it has the qualitative definition of being the momentum scale at which the QCD coupling constant is large thus perturbative QCD is not applicable. From Eq. (1.15), the running coupling $\alpha_s(\mu^2)$ decreases to zero as μ^2 becomes very large, see Fig. 1.1. This is known as asymptotic freedom [10, 11] for QCD perturbation theory.

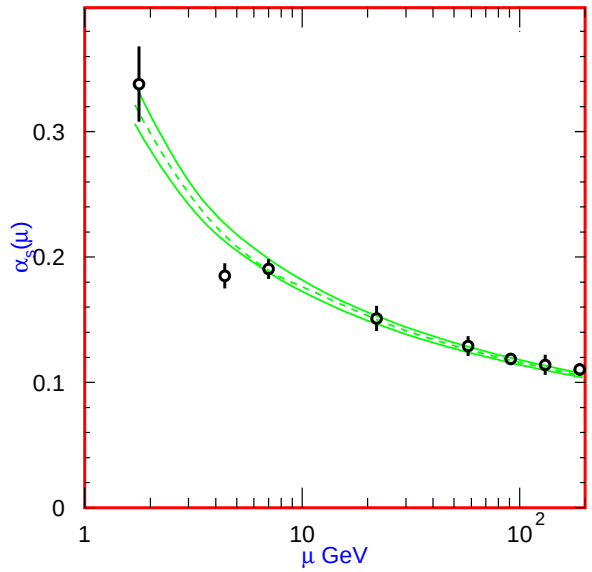

Figure 1.1 The QCD coupling constant $\alpha_s(\mu^2)$ as a function of μ from measurements. (Compiled from Ref. [15])

1.3 Factorization and probability distributions

With asymptotic freedom, one could in principle apply QCD perturbation theory to physical observables at high energy where coupling constant α_s is small. However, most of the physical processes involve hadrons. Typically there are two scales in the physical observable (e.g., cross section):

- the energy exchange Q in the hard scattering: usually larger than a few GeV,

- the scale of hadron wavefunction: $1/R$, with R the hadron mean radius, around the order of $\Lambda_{\rm QCD} \sim 200$ MeV.

This kind of processes contain both short- and long-distance physics. Certainly the perturbative techniques only apply for short-distance part where $\alpha_s(Q)$ is small, but not for long-distance part where $\alpha_s(1/R)$ is relevant and large. A way out is through the factorization theorems [12]. According to these theorems, for many scattering processes, a physical measured quantity can be factorized into some perturbatively calculable short-distant hard parts convoluted with non-perturbative but universal long-distant distribution functions (or matrix elements). The interference between these two scales are power suppressed.

Take the single inclusive hard-scattering process,

$$h_1(p_1) + h_2(p_2) \to H(Q) + X, \tag{1.16}$$

as an example. Here the colliding hadrons h_1 and h_2 have momenta p_1 and p_2, H denotes the observed particle or jets and X stands for any unobserved particles produced by the collisions. The typical scale Q of the scattering process is set by the invariant mass or the transverse momentum of the observed particle or jets. For example, the hard process may be the production of a $W^{\pm}$ boson, or the production of a pion with large transverse momentum.

According to the factorization theorem [12], the cross section for this process can be written

as

$$\begin{aligned}\sigma(p_1,p_2,Q) &= \sum_{a,b}\int dx_1 dx_2 f_{a/h_1}(x_1,Q^2) f_{b/h_2}(x_2,Q^2)\hat{\sigma}_{ab}(x_1p_1,x_2p_2,Q,\alpha_s(Q)) \\ &+ \mathcal{O}\left((\Lambda_{\rm QCD}/Q)^p\right) \end{aligned} \tag{1.17}$$

Here the indices $a,b = q,\bar{q},g$ denote parton flavors; $\hat{\sigma}_{ab}$ is the short-distance coefficient function (partonic cross section); $f_{a/h}(x,Q^2)$ is a non-perturbative, long-distance matrix element on the hadron state, which is interpreted as the probability density to find a parton of flavor a inside a hadron h with momentum fraction x (or parton distributions of flavor a). See Fig. 1.2 for a diagram illustration of this factorization. The partonic cross section $\hat{\sigma}_{ab}$ is computable as a power series expansion in the QCD coupling $\alpha_s(Q)$. On the other hand, parton distribution functions $f_{a/h}(x,Q^2)$ are independent of the details of collision, and they are universal. Thus one could measure them in one experiment (or one process), or obtain them through a global fitting procedure, then use the same set of distribution functions to make predictions. This formalism, so called leading twist (power) collinear pQCD factorization formalism, has been very successful in interpreting and predicting almost all existing data from high energy collisions with momentum transfer larger than a few GeV.

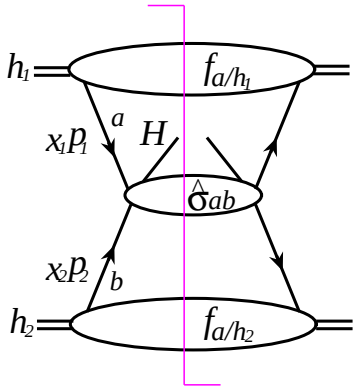

Figure 1.2 Perturbative QCD factorization corresponds to Eq. (1.17)

What happen to the power suppressed terms $\mathcal{O}\left((\Lambda_{\rm QCD}/Q)^p\right)$? Do they have any effect, or any significance at all? These are the key questions this thesis is trying to investigate and answer. We will find that in some cases, these power suppressed terms have important effects

and lead to non-trivial and very interesting phenomena. They give us new opportunities to study the structure of the hadron and the quantum correlation between quarks and gluons beyond what have been learned so far. It also provides us new insights into nonperturbative regime of QCD through multiparton correlation matrix elements.

In the 1990s Qiu and Sterman has developed and proved a factrorization formalism beyond leading power (higher twist) in hadronic collisions [16, 17, 18, 19]. This formalism can be schematically written as

$$\sigma(Q) = H_0 \otimes f_2 \otimes f_2 + \left(\frac{1}{Q}\right)^N H_1 \otimes f_2 \otimes f_{2+N} + \mathcal{O}\left(\frac{1}{Q}\right)^{N+1}, \tag{1.18}$$

where $N = 1$ for transversely polarized scatterings, while $N = 2$ for unpolarized scattering. The H_0 and H_1 are perturbatively calculable coefficient functions in power series of α_s, and f_n are non-perturbative matrix elements of the products of fields on the light cone and are often loosely referred as "twist-n" parton distribution or correlation functions. In Eq. (1.18), the "$\otimes$" represents the convolution over partons' momentum fractions.

Using this formalism, we will first explain why and how a difference of two transverse-spin dependent cross sections (or the measurement of the single transverse-spin asymmetry) can directly probe new sets of twist-3 three-parton correlation functions in Chapter 2. We will construct two sets of correlation functions that are responsible for generating the novel single transverse spin asymmetries (SSAs). These correlation functions provide the first direct information on quantum correlation between quarks and gluons inside a polarized hadron. In Chapter 3, we calculate the SSAs for the open charm production and propose to use it to access one set of correlation functions, so called tri-gluon correlation functions, which represent the role gluon has played in generating the SSAs. In chapter 4, we study how to go beyond the leading order formalism and present the necessary step: the first derivation of evolution equations (or renormalization group equations) for these correlation functions. In chapter 5, we study the SSAs in a complementary approach - TMD approach, ie, calculate the SSAs in terms of transverse-momentum-dependent (TMD) distribution. In chapter 6 and 7, we discuss the close connection between QCD partonic multiple scattering and nuclear dependence in high

energy nuclear collisions, and demonstrate how to use the nuclear dependence of high energy nuclear collisions to extract the information on four-parton correlations inside a large nucleus or a nuclear medium. As an example, we investigate the transverse momentum broadening of vector boson production in hadron-nucleus and nucleus-nuclues collisions. We summarize our results in chapter 8. Taking advantages of the spin and/or nuclear dependence will enable us to explore the hadron structure beyond the probability distributions.

CHAPTER 2. Single transverse-spin asymmetry: Overview

Single transverse-spin asymmetries (SSAs) in high energy collisions are important phenomena and have been observed for more than three decades in various processes [20, 21, 22, 23]. In these processes, a transversely polarized nucleon scatters off an unpolarized nucleon (or virtual photon) target, the observed final-state hadrons show an asymmetric distribution in a plane perpendicular to the beam direction depending on the polarization vector of the scattering nucleon. The spin-averaged cross section and the corresponding spin-dependent cross section may be represented as

$$\begin{aligned} \sigma &\equiv \frac{1}{2}\left[\sigma(s_T) + \sigma(-s_T)\right], \\ \Delta\sigma(s_T) &\equiv \frac{1}{2}\left[\sigma(s_T) - \sigma(-s_T)\right], \end{aligned} \tag{2.1}$$

respectively, where s_T is the transverse spin vector of the initial hadron. The SSA is often defined as a dimensionless ratio of spin-dependent and spin-averaged cross sections as $A_N = \Delta\sigma(s_T)/\sigma$. Starting from the 1970s and 1980s, surprisingly large SSAs, as large as 30 percent, have been consistently observed in various experiments at different collision energies [24], such as in $p^{\uparrow}p \to \pi + X$ at $\sqrt{s} = 200$ GeV at Relativistic Heavy Ion Collider (RHIC).

Despite the conceptual simplicity of A_N, the theoretical description of SSAs has proven to be a challenge [24], since the leading power collinear QCD factorization contribution to the asymmetries vanishes as discovered long ago in [25]. Efremov and Teryaev [26] later point out that a nonvanishing SSA can be obtained in perturbative QCD if one goes beyond the leading power. Such asymmetries were later consistently evaluated and the details were worked out by Qiu and Sterman [16] in terms of generalized factorization theorems [18, 19] in perturbative

QCD. The asymmetries are presented as a convolution of a twist-2 parton distribution from the unpolarized hadron, a twist-3 quark-gluon correlation function from the polarized hadron, and a short-distant partonic hard part calculable in perturbative QCD. This is so-called Efremov-Teryaev-Qiu-Sterman (ETQS) mechanism, or twist-3 approach to the SSAs.

In this chapter, we will first review the basic idea of this mechanism. We then identify other twist-3 contributions and construct the corresponding correlation functions beyond the twist-3 quark-gluon correlation function that has been studied originally by Qiu and Sterman.

2.1 Twist-3 approach: quark-gluon correlation function

In this section, we review the basic Qiu-Sterman formalism to set up the notation and terminology. We will use the following example

$$A(P, s_T) + B(P') \to h(\ell) + X, \tag{2.2}$$

where A is a transversely polarized spin-1/2 hadron with momentum P and spin vector s_T, B is an unpolarized hadron with momentum P', and h is the hadron produced with momentum ℓ.

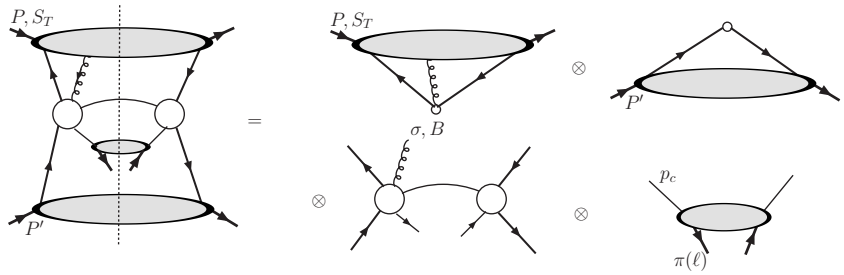

Figure 2.1 Generic Feynman diagram contributing to the single transverse-spin asymmetry for inclusive hadron production in proton-proton scattering at leading twist (twist-three). The polarized cross section can be factorized into convolutions of the following terms: twist-three quark-gluon correlation functions for the transversely polarized proton, parton distributions for the unpolarized proton, hadron fragmentation functions, and hard-scattering functions calculable in QCD perturbation theory.

Following the generalized factorization theorem [16, 17, 18], the transverse spin-dependent cross section for large ℓ_T hadron can be written as

$$d\Delta\sigma_{AB\to hX}(\ell_T, s_T) = \sum_{abc} f^{(3)}_{a/A}(x_1, x_2, s_T) \otimes f_{b/B}(x') \otimes H_{ab\to c} \otimes D_{c\to h}(z) + \ldots, \qquad (2.3)$$

where the symbol $\otimes$ denotes an appropriate convolution in partonic light-cone momentum fractions, $f_{b/B}(x')$ and $D_{c\to h}(z)$ are the standard twist-2 unpolarized parton distributions, and the fragmentation functions, respectively. $f^{(3)}_{a/A}(x_1, x_2, s_T)$ is the twist-3 correlation functions, and $H_{ab\to c}$ is the partonic hard scattering. This contribution can be represented by a generic Feynman diagram shown in Fig. 2.1.

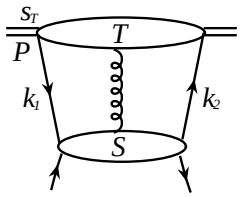

Figure 2.2 Generic Feynman diagram

In order to find the field-theoretic expression for the twist-3 function, and to get the master formula in this approach, we start with a generic diagram in Fig. 2.2 and it can be written as

$$d\Delta\sigma(s_T) \equiv \frac{1}{2S} \sum_a \int \frac{d^4k_1}{(2\pi)^4} \frac{d^4k_2}{(2\pi)^4} \left[T_a(k_1, k_2, s_T)\, S_a(k_1, k_2)\right], \qquad (2.4)$$

where $1/2S$ is the flux factor, $\sum_a$ runs over the quark (antiquark) flavor, T_a is proportional to the nonperturbative matrix element of quark-gluon operator between polarized initial hadron states (a twist-3 matrix element) and S_a refers to the rest of the process. Expanding S_a in the collinear approximation enables us to reduce the four-dimensional integrals to convolutions in the momentum fractions of partons with $k_i^\mu = x_i P^\mu + k_{i,\perp}^\mu$, we have

$$S_a(k_1, k_2) = S_a(x_1, x_2) + \frac{\partial S_a}{\partial k_1^\rho}(x_1, x_2)(k_1 - x_1 P)^\rho + \frac{\partial S_a}{\partial k_2^\rho}(x_1, x_2)(k_2 - x_2 P)^\rho + \ldots \qquad (2.5)$$

One then derives

$$d\Delta\sigma(s_T) = \frac{1}{2S}\sum_a \int dx_1 dx_2 \left[i\epsilon^{\rho s_T n\bar{n}} \frac{\partial S_a}{\partial k_2^\rho}(x_1, x_2) \right] T_{a,F}(x_1, x_2), \tag{2.6}$$

where $\epsilon^{\rho s_T n\bar{n}} = \epsilon^{\rho\sigma\mu\nu} s_{T\sigma} n_\mu \bar{n}_\nu$, n and $\bar{n}$ are light-like unit vectors whose spatial components are parallel to those of P' and P, respectively. Usually one chooses the polarized beam P along $+z$ direction, and P' along $-z$ direction, thus

$$n^\mu = \left[n^+, n^-, n_\perp\right] = \left[0, 1, 0_\perp\right], \qquad \bar{n}^\mu = \left[1, 0, 0_\perp\right], \tag{2.7}$$

where the light-cone momentum components are defined as $V^\pm = (V^0 \pm V^3)/\sqrt{2}$ for a general four-vector V^μ. n^μ and $\bar{n}^\mu$ has the following properties:

$$V \cdot n = V^+, \qquad V \cdot \bar{n} = V^-, \qquad n \cdot \bar{n} = 1. \tag{2.8}$$

$T_{a,F}(x_1, x_2)$ in Eq. (2.6) is called quark-gluon correlation function and has the following operator definition,

$$\begin{aligned} T_{a,F}(x_1, x_2) \;=\; & \int \frac{dy_1^- dy_2^-}{2\pi}\, e^{ix_1 P^+ y_1^-}\, e^{i(x_2 - x_1)P^+ y_2^-} \\ & \times \langle P, s_T | \overline{\psi}_a(0)\, \frac{\gamma^+}{2}\, \left[\epsilon^{s_T \sigma n\bar{n}} {F_\sigma}^+(y_2^-)\right] \psi_a(y_1^-) | P, s_T \rangle\,, \end{aligned} \tag{2.9}$$

with ${F_\sigma}^+$ the gluon field strength. Since $T_{a,F}$ is real, one needs a phase to generate a nonvanishing SSA. This phase will come from the pole structure of S_a. The details how this pole appears will be presented in chapter 3 when we discuss the single transverse spin asymmetry of open charm.

The last step is to factorize the remaining function S_a into a perturbatively calculable partonic term, $H_{ab\to c}$, a corresponding target parton distribution, $f_{b/B}$, and a fragmentation

function, $D_{c\to h}$:

$$d\Delta\sigma(s_T) = \frac{1}{2S}\sum_{abc}\int dz D_{c\to h}(z)\int\frac{dx'}{x'}f_{b/B}(x')\int dx_1 dx_2\, T_{a,F}(x_1,x_2) \times\left[i\,\epsilon^{\rho s_T n\bar{n}}\frac{\partial}{\partial k_2^\rho}H_{ab\to c}(x_1,x_2,x',z)\right]_{k_2^\rho=0}. \quad (2.10)$$

Working out the partonic hard parts, one ends up with the following final result:

$$E_\ell\frac{d^3\Delta\sigma(s_T)}{d^3\ell} = \frac{\alpha_s^2}{S}\sum_{a,b,c}\int_{z_{\min}}^1\frac{dz}{z^2}\,D_{c\to h}(z)\int_{x'_{\min}}^1\frac{dx'}{x'}\,\frac{1}{x'S+T/z}\,f_{b/B}(x')\sqrt{4\pi\alpha_s} \times\left(\frac{\epsilon^{\ell s_T n\bar{n}}}{z\hat{u}}\right)\frac{1}{x}\left[T_{a,F}(x,x)-x\left(\frac{d}{dx}T_{a,F}(x,x)\right)\right]H_{ab\to c}(\hat{s},\hat{t},\hat{u})\ , \quad (2.11)$$

where $\hat{s},\hat{t},\hat{u}$ are the standard partonic Mandelstam variables, $H_{ab\to c}(\hat{s},\hat{t},\hat{u})$ are given in Ref. [27]. It is interesting to note that the asymmetry calculated here depends only on the diagonal part of the quark-gluon correlation functions $T_{a,F}(x_1,x_2)$ with $x_1=x_2=x$. This is generally true for the process with single hard scale in the scattering, in which only "soft-pole" contributes. In our case, $T_{a,F}(x,x)$ corresponds to the situation in which the momentum of the extra gluon from the initial state goes to zero. This contribution is so-called "soft-gluonic pole" contributions. In general, the so-called "soft-fermionic pole" contributions, for which the pole in the hard-scattering is taken in such a way that the initial quark becomes soft, could also exist. This corresponds to the contribution proportional to $T_{a,F}(0,x)$. Soft-gluonic pole and soft-fermionic pole contributions are both the special case of the more general contribution from $T_{a,F}(x_1,x_2)$, which will be discussed a bit more in the next section.

In order to perform a phenomenological study, one needs the information for the unknown but universal twist-3 quark-gluon correlation functions. The ordinary quark parton distribution functions are defined as

$$f_a(x)=\int\frac{dy_1^-}{2\pi}e^{ixP^+y_1^-}\langle P|\bar{\psi}_a(0)\frac{\gamma^+}{2}\psi_a(y_1^-)|P\rangle. \quad (2.12)$$

Realizing the $T_{a,F}(x,x)$ function is based on the above parton distribution function with the

following operator insertion,

$$\left[\int dy_2^- \, \epsilon^{s_T \sigma n \bar{n}} F_\sigma{}^+(y_2^-)\right], \tag{2.13}$$

the most natural ansatz for $T_{a,F}(x,x)$ is:

$$T_{a,F}(x,x) = N_a(x) f_a(x) \tag{2.14}$$

Initially a simple functional form with $N_a(x) = \kappa_a \lambda_F$ was adopted [16], where $\lambda_F \approx 0.07$ GeV and $\kappa_{u,d} = \pm 1$ (for a proton). The comparison with the Fermilab data is impressive, see Fig. 2.3.

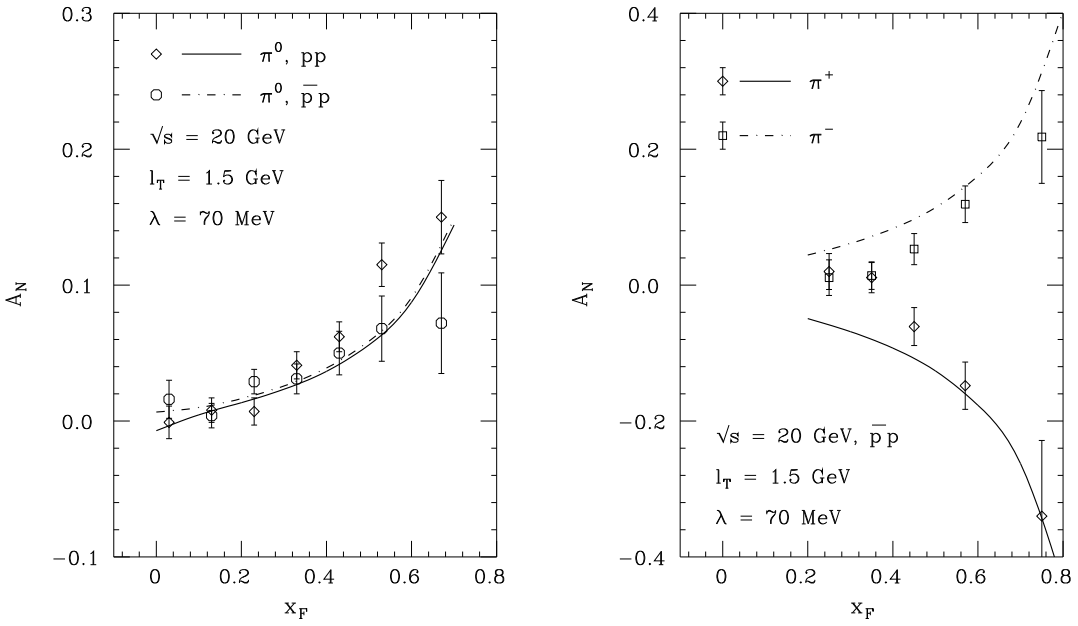

Figure 2.3 Single transverse spin asymmetry of π^0 (left) and π^+, π^- (right) compared with Fermilab data. (Compiled from Ref. [16])

More recently, with more data having become available, a more general form has been adopted [27] , $N_a(x) = N_a x^{\alpha_a}(1-x)^{\beta_a}$. The formalism can describe both the Fermilab and RHIC data simultaneously, see Fig. 2.4 for the comparison with the RHIC data.

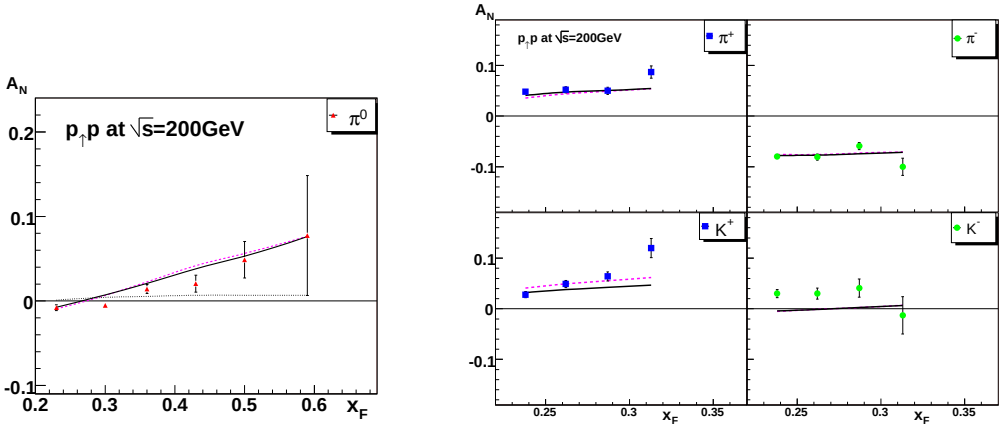

Figure 2.4 Single transverse spin asymmetry compared with recent STAR (left) and BRAMHS (right) data. (Compiled from Ref. [27])

2.2 Twist-3 correlation functions relevant to SSAs

There are other twist-3 correlation functions besides the quark-gluon correlation function $T_{q,F}(x_1, x_2)$ discussed in previous section. In this section, we will identify other twist-3 contributions. We will find that there will be another set of quark-gluon correlation functions, and the tri-gluon correlation function, which represents the role of gluon played in single transverse spin asymmetry.

We construct two sets of twist-3 correlation functions that are responsible for generating the nonvanishing SSAs in the QCD collinear factorization approach. We start with two general twist-3 correlation functions: quark-gluon correlation function $\widetilde{\mathcal{T}}_{q,F,\sigma}(x_1, x_2, s_T)$ and tri-gluon correlation function $\widetilde{\mathcal{T}}^{(f,d)}_{G,F,\sigma}(x_1, x_2, s_T)$ defined as

$$\widetilde{\mathcal{T}}_{q,F,\sigma}(x_1, x_2, s_T) \equiv \int \frac{dy_1^- dy_2^-}{(2\pi)^2} e^{ix_1 P^+ y_1^-} e^{i(x_2-x_1)P^+ y_2^-} \times \langle P, s_T | \overline{\psi}_q(0) \frac{\gamma^+}{2} \left[F_\sigma{}^+(y_2^-)\right] \psi_q(y_1^-) | P, s_T \rangle \,, \tag{2.15}$$

$$\widetilde{\mathcal{T}}^{(f,d)}_{G,F,\sigma}(x_1, x_2, s_T) \equiv \int \frac{dy_1^- dy_2^-}{(2\pi)^2} e^{ix_1 P^+ y_1^-} e^{i(x_2-x_1)P^+ y_2^-} \frac{1}{P^+} \times \langle P, s_T | F^{+\rho}(0) \left[F_\sigma{}^+(y_2^-)\right] F^{+\lambda}(y_1^-) | P, s_T \rangle \, (-g_{\rho\lambda}) \,, \tag{2.16}$$

where the subscript "F" indicates that a field strength operator (not a covariant derivative

operator [16]) is inserted in the middle of the bi-local operator that defines the twist-2 spin-averaged quark (q) or gluon (G) distribution function. There is one quark-gluon correlation function, $\widetilde{\mathcal{T}}_{q,F,\sigma}$, for each quark (antiquark) flavor $q\,(\bar{q})$. However, there are two independent tri-gluon correlation functions, $\widetilde{\mathcal{T}}^{(f)}_{G,F,\sigma}$ and $\widetilde{\mathcal{T}}^{(d)}_{G,F,\sigma}$, because of the fact that the color of the three gluon field strengths in Eq. (2.16) can be neutralized by contracting with either the antisymmetric if_{abc} or the symmetric d_{abc} tensors with color indices, a, b, and c.

The reality property of these two functions can be expressed as [16],

$$\begin{aligned}
\widetilde{\mathcal{T}}_{q,F,\sigma}(x_1,x_2,s_T)^* &= \widetilde{\mathcal{T}}_{q,F,\sigma}(x_2,x_1,s_T)\,, \\
\widetilde{\mathcal{T}}^{(f,d)}_{G,F,\sigma}(x_1,x_2,s_T)^* &= \widetilde{\mathcal{T}}^{(f,d)}_{G,F,\sigma}(x_2,x_1,s_T)\,.
\end{aligned} \tag{2.17}$$

That is, the real part of these two functions are symmetric in the exchange of x_1 and x_2, while the imaginary part is antisymmetric. Similarly, from the parity and time-reversal invariance, we find [16]

$$\begin{aligned}
\widetilde{\mathcal{T}}_{q,F,\sigma}(x_1,x_2,s_T) &= -\widetilde{\mathcal{T}}_{q,F,\sigma}(x_2,x_1,-s_T)\,, \\
\widetilde{\mathcal{T}}^{(f,d)}_{G,F,\sigma}(x_1,x_2,s_T) &= -\widetilde{\mathcal{T}}^{(f,d)}_{G,F,\sigma}(x_2,x_1,-s_T)\,.
\end{aligned} \tag{2.18}$$

That is, these two functions are antisymmetric when the transverse spin vector s_T reverses its direction.

From the definition in Eq. (2.15) and the symmetry properties in Eqs. (2.17) and (2.18), we construct a twist-3 quark-gluon correlation function that is relevant to the SSA as follows,

$$\begin{aligned}
\mathcal{T}_{q,F}(x_1,x_2) &\equiv \epsilon^{s_T\sigma n\bar{n}}\,\frac{1}{2}\left[\widetilde{\mathcal{T}}_{q,F,\sigma}(x_1,x_2,s_T) - \widetilde{\mathcal{T}}_{q,F,\sigma}(x_1,x_2,-s_T)\right] \\
&= \epsilon^{s_T\sigma n\bar{n}}\,\frac{1}{2}\left[\widetilde{\mathcal{T}}_{q,F,\sigma}(x_1,x_2,s_T) + \widetilde{\mathcal{T}}_{q,F,\sigma}(x_2,x_1,s_T)\right] \\
&\equiv \frac{1}{2}\left[\widetilde{\mathcal{T}}_{q,F}(x_1,x_2,s_T) + \widetilde{\mathcal{T}}_{q,F}(x_2,x_1,s_T)\right] \\
&= \mathrm{Re}\left[\widetilde{\mathcal{T}}_{q,F}(x_1,x_2,s_T)\right]\,,
\end{aligned} \tag{2.19}$$

where the spin-dependent twist-3 quark-gluon correlation function is defined as

$$\begin{aligned}
\widetilde{\mathcal{T}}_{q,F}(x_1,x_2,s_T) &\equiv \int \frac{dy_1^- dy_2^-}{(2\pi)^2}\, e^{ix_1P^+y_1^-}\, e^{i(x_2-x_1)P^+y_2^-} \\
&\quad \times\langle P,s_T|\overline{\psi}_q(0)\,\frac{\gamma^+}{2}\left[\epsilon^{s_T\sigma n\bar{n}}F_\sigma{}^+(y_2^-)\right]\psi_q(y_1^-)|P,s_T\rangle \\
&= \widetilde{\mathcal{T}}_{q,F}(x_2,x_1,-s_T)\,. \qquad (2.20)
\end{aligned}$$

As shown in Eq. (2.19), the twist-3 quark-gluon correlation function $\mathcal{T}_{q,F}(x_1,x_2)$ is *real* and *symmetric* when the active momentum fraction x_1 exchanges with x_2.

Similarly, we can construct the tri-gluon correlation function relevant to the SSA as,

$$\begin{aligned}
\mathcal{T}_{G,F}^{(f,d)}(x_1,x_2) &\equiv \epsilon^{s_T\sigma n\bar{n}}\,\frac{1}{2}\left[\widetilde{\mathcal{T}}_{G,F,\sigma}^{(f,d)}(x_1,x_2,s_T)-\widetilde{\mathcal{T}}_{G,F,\sigma}^{(f,d)}(x_1,x_2,-s_T)\right] \\
&= \epsilon^{s_T\sigma n\bar{n}}\,\frac{1}{2}\left[\widetilde{\mathcal{T}}_{G,F,\sigma}^{(f,d)}(x_1,x_2,s_T)+\widetilde{\mathcal{T}}_{G,F,\sigma}^{(f,d)}(x_2,x_1,s_T)\right] \\
&\equiv \frac{1}{2}\left[\widetilde{\mathcal{T}}_{G,F}^{(f,d)}(x_1,x_2,s_T)+\widetilde{\mathcal{T}}_{G,F}^{(f,d)}(x_2,x_1,s_T)\right] \\
&= \mathrm{Re}\left[\widetilde{\mathcal{T}}_{G,F}^{(f,d)}(x_1,x_2,s_T)\right]\,, \qquad (2.21)
\end{aligned}$$

where the spin-dependent twist-3 tri-gluon correlation function is defined as

$$\begin{aligned}
\widetilde{\mathcal{T}}_{G,F}^{(f,d)}(x_1,x_2,s_T) &\equiv \int \frac{dy_1^- dy_2^-}{(2\pi)^2}\, e^{ix_1P^+y_1^-}\, e^{i(x_2-x_1)P^+y_2^-}\,\frac{1}{P^+} \\
&\quad \times\langle P,s_T|F^{+\rho}(0)\left[\epsilon^{s_T\sigma n\bar{n}}F_\sigma{}^+(y_2^-)\right]F^{+\lambda}(y_1^-)|P,s_T\rangle(-g_{\rho\lambda}) \\
&= \widetilde{\mathcal{T}}_{G,F}^{(f,d)}(x_2,x_1,-s_T)\,. \qquad (2.22)
\end{aligned}$$

The tri-gluon correlation function $\mathcal{T}_{G,F}^{(f,d)}(x_1,x_2)$ is also *real* and *symmetric* in the exchange of x_1 and x_2.

For later convenience, we also define the diagonal correlation functions $T_{q,F}(x,x)$ and $T_{G,F}^{(f,d)}(x,x)$ as

$$\begin{aligned}
T_{q,F}(x,x) &= \int dx'\,\left[2\pi\,\delta(x'-x)\right]\,\mathcal{T}_{q,F}(x,x') = 2\pi\,\mathcal{T}_{q,F}(x,x)\,, \\
T_{G,F}^{(f,d)}(x,x) &= \int dx'\,\left[2\pi\,\delta(x'-x)\right]\,\left(\frac{1}{x}\right)\mathcal{T}_{G,F}^{(f,d)}(x,x') = 2\pi\,\frac{\mathcal{T}_{G,F}^{(f,d)}(x,x)}{x}\,. \qquad (2.23)
\end{aligned}$$

Notice that the new tri-gluon correlation function, $\mathcal{T}_{G,F}(x,x')$, is symmetric in the exchange of x and x', while a direct generalization of the diagonal tri-gluon correlation function in Eq. (2.23), $T_{G,F}(x,x') \equiv 2\pi\,\mathcal{T}_{G,F}(x,x')/x$ is not symmetric in exchanging x and x'.

In addition to the gluonic pole contribution, the SSA could also be generated by the fermionic pole of partonic hard scattering [17, 26]. The fermionic pole contribution at twist-3 is proportional to the off-diagonal part of the correlation functions $\mathcal{T}_{q,F}$ and $\mathcal{T}_{G,F}$, as well as a new set of twist-3 correlation functions which vanishes when $x_2 = x_1$ [17, 28]. To construct this new set of twist-3 correlation functions, we introduce two new twist-3 correlation functions,

$$\begin{aligned}
\widetilde{\mathcal{T}}_{\Delta q,F,\sigma}(x_1,x_2,s_T) &\equiv \int \frac{dy_1^- dy_2^-}{(2\pi)^2}\, e^{ix_1P^+y_1^-}\, e^{i(x_2-x_1)P^+y_2^-} \\
&\quad \times \langle P,s_T|\overline{\psi}_q(0)\,\frac{\gamma^+\gamma^5}{2}\left[i\,F_\sigma{}^+(y_2^-)\right]\psi_q(y_1^-)|P,s_T\rangle\,, \qquad (2.24)\\
\widetilde{\mathcal{T}}^{(f,d)}_{\Delta G,F,\sigma}(x_1,x_2,s_T) &\equiv \int \frac{dy_1^- dy_2^-}{(2\pi)^2}\, e^{ix_1P^+y_1^-}\, e^{i(x_2-x_1)P^+y_2^-}\,\frac{1}{P^+} \\
&\quad \times \langle P,s_T|F^{+\rho}(0)\left[i\,F_\sigma{}^+(y_2^-)\right]F^{+\lambda}(y_1^-)|P,s_T\rangle\,(i\epsilon_{\perp\rho\lambda})\,, \qquad (2.25)
\end{aligned}$$

where the antisymmetric tensor $\epsilon_{\perp\rho\lambda} = \epsilon_\perp^{\rho\lambda} = -\epsilon^{\rho\lambda n\bar{n}}$ and subscript "Δq" and "ΔG" indicate that the field strength operator is inserted in the middle of the bi-local field operators that define the twist-2 quark helicity distribution Δq and the gluon helicity distribution ΔG, respectively. Similar to Eq. (2.17), the reality property of these two new twist-3 correlation functions can be expressed as,

$$\begin{aligned}
\widetilde{\mathcal{T}}_{\Delta q,F,\sigma}(x_1,x_2,s_T)^* &= -\widetilde{\mathcal{T}}_{\Delta q,F,\sigma}(x_2,x_1,s_T)\,, \\
\widetilde{\mathcal{T}}^{(f,d)}_{\Delta G,F,\sigma}(x_1,x_2,s_T)^* &= -\widetilde{\mathcal{T}}^{(f,d)}_{\Delta G,F,\sigma}(x_2,x_1,s_T)\,. \qquad (2.26)
\end{aligned}$$

That is, the real part of these two new functions are *antisymmetric* in the exchange of x_1 and x_2, while the imaginary part is symmetric. This reality property is different from that of the

functions $\mathcal{T}_{q,F,\sigma}$ and $\mathcal{T}_{G,F,\sigma}$. Similarly, from the parity and time-reversal invariance, we find,

$$\begin{aligned}
\widetilde{\mathcal{T}}_{\Delta q,F,\sigma}(x_1,x_2,s_T) &= \widetilde{\mathcal{T}}_{\Delta q,F,\sigma}(x_2,x_1,-s_T)\,, \\
\widetilde{\mathcal{T}}^{(f,d)}_{\Delta G,F,\sigma}(x_1,x_2,s_T) &= \widetilde{\mathcal{T}}^{(f,d)}_{\Delta G,F,\sigma}(x_2,x_1,-s_T)\,.
\end{aligned} \tag{2.27}$$

That is, these two functions are *symmetric* when the transverse spin vector s_T reverses its direction.

From the definition of these new correlation functions in Eqs. (2.24) and (2.25) and their properties in Eqs. (2.26) and (2.27), we construct the second set of twist-3 quark-gluon and tri-gluon correlation functions that could also contribute to the SSAs. The new quark-gluon correlation function is defined as,

$$\begin{aligned}
\mathcal{T}_{\Delta q,F}(x_1,x_2) &\equiv s_T^\sigma \frac{1}{2}\left[\widetilde{\mathcal{T}}_{\Delta q,F,\sigma}(x_1,x_2,s_T) - \widetilde{\mathcal{T}}_{\Delta q,F,\sigma}(x_1,x_2,-s_T)\right] \\
&= s_T^\sigma \frac{1}{2}\left[\widetilde{\mathcal{T}}_{\Delta q,F,\sigma}(x_1,x_2,s_T) - \widetilde{\mathcal{T}}_{\Delta q,F,\sigma}(x_2,x_1,s_T)\right] \\
&\equiv \frac{1}{2}\left[\widetilde{\mathcal{T}}_{\Delta q,F}(x_1,x_2,s_T) - \widetilde{\mathcal{T}}_{\Delta q,F}(x_2,x_1,s_T)\right] \\
&= \mathrm{Re}\left[\widetilde{\mathcal{T}}_{\Delta q,F}(x_1,x_2,s_T)\right]\,,
\end{aligned} \tag{2.28}$$

where the spin-dependent new twist-3 quark-gluon correlation function is defined as

$$\begin{aligned}
\widetilde{\mathcal{T}}_{\Delta q,F}(x_1,x_2,s_T) &\equiv \int \frac{dy_1^- dy_2^-}{(2\pi)^2}\, e^{ix_1P^+y_1^-}\, e^{i(x_2-x_1)P^+y_2^-} \\
&\quad \times \langle P,s_T|\overline{\psi}_q(0)\,\frac{\gamma^+\gamma^5}{2}\left[i\,s_T^\sigma\, F_\sigma{}^+(y_2^-)\right]\psi_q(y_1^-)|P,s_T\rangle\,, \\
&= -\widetilde{\mathcal{T}}_{\Delta q,F}(x_2,x_1,-s_T)
\end{aligned} \tag{2.29}$$

which was also discussed in Ref. [28]. As shown in Eq. (2.28), this new twist-3 quark-gluon correlation function $\mathcal{T}_{\Delta q,F}(x_1,x_2)$ that is relevant to the SSA is also *real*, but, is *antisymmetric*

in the exchange of x_1 and x_2. Similarly, the new tri-gluon correlation function is defined as,

$$\begin{aligned}
\mathcal{T}^{(f,d)}_{\Delta G,F}(x_1,x_2) &\equiv s_T^\sigma \frac{1}{2}\left[\widetilde{\mathcal{T}}^{(f,d)}_{\Delta G,F,\sigma}(x_1,x_2,s_T) - \widetilde{\mathcal{T}}^{(f,d)}_{\Delta G,F,\sigma}(x_1,x_2,-s_T)\right] \\
&= s_T^\sigma \frac{1}{2}\left[\widetilde{\mathcal{T}}^{(f,d)}_{\Delta G,F,\sigma}(x_1,x_2,s_T) - \widetilde{\mathcal{T}}^{(f,d)}_{\Delta G,F,\sigma}(x_2,x_1,s_T)\right] \\
&\equiv \frac{1}{2}\left[\widetilde{\mathcal{T}}^{(f,d)}_{\Delta G,F}(x_1,x_2,s_T) - \widetilde{\mathcal{T}}^{(f,d)}_{\Delta G,F}(x_2,x_1,s_T)\right] \\
&= \mathrm{Re}\left[\widetilde{\mathcal{T}}^{(f,d)}_{\Delta G,F}(x_1,x_2,s_T)\right], \qquad (2.30)
\end{aligned}$$

where the spin-dependent new twist-3 tri-gluon correlation function is defined as

$$\begin{aligned}
\widetilde{\mathcal{T}}^{(f,d)}_{\Delta G,F}(x_1,x_2,s_T) &\equiv \int \frac{dy_1^- dy_2^-}{(2\pi)^2}\, e^{ix_1P^+y_1^-}\, e^{i(x_2-x_1)P^+y_2^-}\, \frac{1}{P^+} \\
&\quad \times \langle P,s_T|F^{+\rho}(0)\left[i\, s_T^\sigma\, F_\sigma{}^+(y_2^-)\right] F^{+\lambda}(y_1^-)|P,s_T\rangle\, (i\epsilon_{\perp\rho\lambda}) \\
&= -\widetilde{\mathcal{T}}^{(f,d)}_{\Delta G,F}(x_2,x_1,-s_T). \qquad (2.31)
\end{aligned}$$

From Eq. (2.30), it is clear that the new twist-3 tri-gluon correlation function $\mathcal{T}^{(f,d)}_{\Delta G,F}(x_1,x_2)$ is also *real*, but, *antisymmetric* in the exchange of x_1 and x_2. Consequently, the diagonal part of these two new correlation functions vanishes,

$$\begin{aligned}
T_{\Delta q,F}(x,x) &\equiv \int dx' \left[2\pi\,\delta(x'-x)\right] \mathcal{T}_{\Delta q,F}(x,x') = 0\,, \\
T^{(f,d)}_{\Delta G,F}(x,x) &\equiv \int dx' \left[2\pi\,\delta(x'-x)\right] \left(\frac{1}{x}\right) \mathcal{T}^{(f,d)}_{\Delta G,F}(x,x') = 0\,. \qquad (2.32)
\end{aligned}$$

That is, this set of twist-3 correlation functions does not directly generate soft gluonic pole contribution to the SSAs [17, 28].

For phenomenological studies, conventionally we use the following definition for the corre-

lation functions

$$\begin{aligned} T_{q,F}(x,x') &= 2\pi\, \mathcal{T}_{q,F}(x,x') \\ T_{G,F}(x,x') &= 2\pi\, \frac{\mathcal{T}_{G,F}(x,x')}{x} \\ T_{\Delta q,F}(x,x') &= 2\pi\, \mathcal{T}_{\Delta q,F}(x,x') \\ T^{(f,d)}_{\Delta G,F}(x,x') &= 2\pi\, \frac{\mathcal{T}_{\Delta G,F}(x,x')}{x} \end{aligned} \tag{2.33}$$

To complete this section, we summarize the key properties of these twist-3 correlation functions that are responsible for generating the SSAs from the unpinched gluonic and fermionic poles of partonic scattering in the QCD collinear factorization approach. From their operator structure, these correlation functions can be grouped into two sets. One set is for the $\mathcal{T}_{q,F}$ and $\mathcal{T}^{(f,d)}_{G,F}$, and the other includes $\mathcal{T}_{\Delta q,F}$ and $\mathcal{T}^{(f,d)}_{\Delta G,F}$. The operators for the first set of correlation functions, $\mathcal{T}_{q,F}$ and $\mathcal{T}^{(f,d)}_{G,F}$, are constructed from the bi-local operators that define the twist-2 *spin-averaged* PDFs with an insertion of the following operator,

$$\int \frac{dy_2^-}{2\pi}\, e^{ix_2P^+y_2^-}\, \left[\epsilon^{s_T\sigma n\bar{n}}\, F_\sigma{}^+(y_2^-)\right] = i\int \frac{dy_2^-}{2\pi}\, e^{ix_2P^+y_2^-}\, \left[i\,\epsilon_\perp^{\rho\sigma}\, s_{T\rho}\, F_\sigma{}^+(y_2^-)\right]\,; \tag{2.34}$$

and the operators for the second set of correlation functions, $\mathcal{T}_{\Delta q,F}$ and $\mathcal{T}^{(f,d)}_{\Delta G,F}$, are constructed from the bi-local operators that define the twist-2 *spin-dependent* parton helicity distributions with an insertion of a slightly different operator,

$$i\int \frac{dy_2^-}{2\pi}\, e^{ix_2P^+y_2^-}\, \left[s_T^\sigma\, F_\sigma{}^+(y_2^-)\right]\,. \tag{2.35}$$

The $i\epsilon_\perp^{\rho\sigma}$ in Eq. (2.34) takes care of the parity invariance of the spin asymmetry for the first set of correlation functions, while the same property was taken care of naturally by the γ^5 or $i\epsilon_{\perp\rho\lambda}$ in the operator definition of the spin-dependent helicity distributions. The extra "i" in both Eq. (2.34) and Eq. (2.35) provides the necessary phase for the SSAs and is a result of taking the contribution from the gluonic or fermionic pole of partonic scattering [17].

CHAPTER 3. Tri-gluon correlations and single transverse spin asymmetry in open charm production

We have identified four twist-3 correlation functions which are responsible for the single transverse spin asymmetry: $T_{q,F}$, $T_{G,F}^{(f,d)}$, $T_{\Delta q,F}$, and $T_{\Delta G,F}^{(f,d)}$. The diagonal part of $T_{\Delta q,F}$ and $T_{\Delta G,F}^{(f,d)}$ vanish, thus their contribution to the SSAs might be small. The contribution of $T_{q,F}$ to the SSAs has been studied extensively, which represents the role quarks play in generating the SSAs. The tri-gluon correlation functions $T_{G,F}^{(f,d)}$ represents the role gluon plays in generating the SSAs. Since the gluon is an essential component of QCD dynamics and has played a dominant role in many high energy hadronic scattering processes. To fully understand the physics of the SSAs requires us to investigate the role of gluons in generating the SSAs. In this chapter, we study the contribution of $T_{G,F}^{(f,d)}$ to the SSAs, ie, the role of gluons in the QCD collinear factorization approach. We calculate the SSAs for open charm production in both Semi-Inclusive lepton-hadron Deep Inelastic Scattering (SIDIS) and hadronic collisions. We find that the asymmetry is sensitive to the tri-gluon correlation functions and could be used to extract the tri-gluon correlations.

3.1 SSAs for open charm production in SIDIS

In this section, we present our calculation of the SSAs for open charm production in SIDIS. We first introduce the relevant kinematics of open charm production in SIDIS and present the formula for the unpolarized cross section. We then derive the twist-three formula for the SSA in QCD collinear factorization approach and express the asymmetry in terms of the tri-gluon correlation functions, $T_{G,F}^{(f,d)}(x,x)$.

3.1.1 Kinematics

We start this subsection by specifying our notation and kinematics of SIDIS. We consider the scattering processes of an unpolarized lepton, e, on a polarized hadron, p,

$$e(\ell) + p(P, s_T) \to e(\ell') + h(P_h) + X, \tag{3.1}$$

where s_T is the transverse spin vector defined below, h represents the observed D meson with momentum P_h and mass m_h. We work in the approximation of one-photon exchange, and define the virtual photon momentum $q = \ell - \ell'$ and its invariant mass $Q^2 = -q^2$. The usual SIDIS variables are defined as:

$$S_{ep} = (P + \ell)^2, \qquad x_B = \frac{Q^2}{2P \cdot q}, \qquad y = \frac{P \cdot q}{P \cdot \ell} = \frac{Q^2}{x_B S_{ep}}, \qquad z_h = \frac{P \cdot P_h}{P \cdot q}. \tag{3.2}$$

It is also convenient to introduce the "transverse" component of the virtual photon momentum, q, as

$$q_t^\mu = q^\mu - \frac{q \cdot P_h}{P \cdot P_h} P^\mu - \frac{q \cdot P}{P \cdot P_h} P_h^\mu, \tag{3.3}$$

which is orthogonal to both P and P_h. q_t^μ is a space-like vector, we thus define

$$\vec{q}_\perp^{\,2} \equiv -q_t^\mu q_{t\mu} = Q^2 \left[1 + \frac{1}{x_B} \frac{q \cdot P}{P \cdot P_h} \right] - \frac{m_h^2}{z_h^2}. \tag{3.4}$$

To completely specify the kinematics, we will work in the so-called *hadron frame* [30], where the virtual photon and the polarized proton are taken to have only one spatial component that is in the z-direction:

$$P^\mu = P^+ \bar{n}^\mu, \qquad q^\mu = -x_B P^+ \bar{n}^\mu + \frac{Q^2}{2 x_B P^+} n^\mu, \tag{3.5}$$

where $\bar{n}^\mu$ and n^μ are given in Eq. (2.7). The momentum of final-state D-meson can be written as

$$P_h^\mu = \frac{x_B P^+}{z_h Q^2} m_{h\perp}^2 \bar{n}^\mu + \frac{z_h Q^2}{2 x_B P^+} n^\mu + P_{h\perp}^\mu, \tag{3.6}$$

where $m_{h\perp}^2 = m_h^2 + P_{h\perp}^2$ with $P_{h\perp} = \sqrt{\vec{P}_{h\perp}^2}$. From Eq. (3.4) one can show that $q_\perp \equiv \sqrt{\vec{q}_\perp^2} = P_{h\perp}/z_h$ in this hadron frame, independent of mass m_h.

In this hadron frame, usually, one chooses the coordinate system such that the virtual photon has a vanishing energy component, corresponding to $P^+ = Q/\sqrt{2}x_B$, and P_h lies in the xz-plane (known as the *hadron plane*), as shown in Fig. 3.1. The lepton momenta, ℓ and ℓ' define the *lepton plane* and can be expressed in terms of variables ψ and ϕ as follows [30],

$$\begin{aligned} \ell^\mu &= \frac{Q}{2}\left(\cosh\psi, \sinh\psi\cos\phi, \sinh\psi\sin\phi, -1\right), \\ \ell'^\mu &= \frac{Q}{2}\left(\cosh\psi, \sinh\psi\cos\phi, \sinh\psi\sin\phi, +1\right), \end{aligned} \tag{3.7}$$

where ϕ is the azimuthal angle between the hadron and lepton plane, as indicated in Fig. 3.1, and

$$\cosh\psi = \frac{2x_B S_{ep}}{Q^2} - 1 = \frac{2}{y} - 1. \tag{3.8}$$

We parametrize the transverse spin vector of the initial proton s_T as

$$s_T = (0, \cos\phi_s, \sin\phi_s, 0), \tag{3.9}$$

where ϕ_s is the azimuthal angle of s_T measured from the hadron plane, as shown in Fig. 3.1. If one uses the lepton plane as the reference to define the azimuthal angle of s_T as Φ_S, and that of hadron plane as Φ_h, one has the relation $\phi_s = \Phi_S - \Phi_h$ and $\phi = -\Phi_h$.

To be more precise, the single transverse-spin asymmetry is defined by the ratio of the

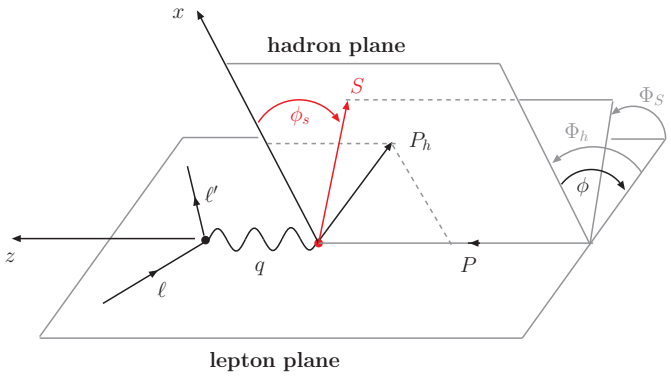

Figure 3.1 Kinematics of the SIDIS process in hadron frame.

following deferential cross sections as

$$A_N = \frac{d\Delta\sigma(s_T)}{dx_B dy dz_h dP_{h\perp}^2 d\phi} \Big/ \frac{d\sigma}{dx_B dy dz_h dP_{h\perp}^2 d\phi} \,. \tag{3.10}$$

In the following subsections, we will first review the unpolarized cross section at leading order, and then derive the single-transverse polarized cross sections, $\Delta\sigma(s_T)$.

3.1.2 Unpolarized cross section

The unpolarized differential SIDIS cross section may be calculated from the formula

$$\frac{d\sigma}{dx_B dy dz_h dP_{h\perp}^2 d\phi} = \frac{\pi\alpha_{em}^2 y}{Q^4} L_{\mu\nu}(\ell,\, q) W^{\mu\nu}(P,\, q,\, P_h), \tag{3.11}$$

where $L_{\mu\nu}$ and $W^{\mu\nu}$ are the leptonic and hadronic tensors, respectively. The leptonic tensor is given by

$$L_{\mu\nu}(\ell,\, q) = 2\left(\ell_\mu \ell'_\nu + \ell'_\nu \ell_\mu - g_{\mu\nu} Q^2/2\right). \tag{3.12}$$

The hadronic tensor has the following expression in QCD:

$$W^{\mu\nu}(P,\, q,\, P_h) = \frac{1}{4z_h} \sum_X \int \frac{d^4\xi}{(2\pi)^4} e^{iq\cdot\xi} \langle P|J_\mu(\xi)|X\, P_h\rangle\langle X\, P_h|J_\nu(0)|P\rangle, \tag{3.13}$$

where J^μ is the quark electromagnetic current and X represents all other final-state hadrons other than the observed open charm meson h.

The hadronic tensor can be decomposed in terms of five parity and current conserving tensors $\mathcal{V}_i^{\mu\nu}$ [30]:

$$W^{\mu\nu} = \sum_{i=1}^{5} \mathcal{V}_i^{\mu\nu} W_i, \tag{3.14}$$

where the W_i are structure functions which may be projected out from $W^{\mu\nu}$ by $W_i = W_{\rho\sigma}\tilde{\mathcal{V}}_i^{\rho\sigma}$, with the corresponding inverse tensors $\tilde{\mathcal{V}}_i$. Both $\mathcal{V}_i$ and $\tilde{\mathcal{V}}_i$ can be constructed from four orthonormal basis vectors:

$$\begin{aligned}
T^\mu &= \frac{1}{Q}\left(q^\mu + 2x_B P^\mu\right), \\
X^\mu &= \frac{1}{q_\perp}\left[\frac{P_h^\mu}{z_h} - q^\mu - \left(1 + \frac{q_\perp^2 + m_h^2/z_h^2}{Q^2}\right) x_B P^\mu\right], \\
Y^\mu &= \epsilon^{\mu\nu\rho\sigma} Z_\nu X_\rho T_\sigma, \\
Z^\mu &= -\frac{q^\mu}{Q},
\end{aligned} \tag{3.15}$$

with normalization $T^2 = 1$ and $X^2 = Y^2 = Z^2 = -1$, which are reduced to those in [30] when $m_h = 0$. The tensor $\mathcal{V}_5$ does not contribute to the cross section when it is contracted with a symmetric $L_{\mu\nu}$, the other four tensors and their inverse are given as [30]:

$$\begin{aligned}
&\mathcal{V}_1^{\mu\nu} = X^\mu X^\nu + Y^\mu Y^\nu, \qquad \mathcal{V}_2^{\mu\nu} = g^{\mu\nu} + Z^\mu Z^\nu, \\
&\mathcal{V}_3^{\mu\nu} = T^\mu X^\nu + T^\nu X^\mu, \qquad \mathcal{V}_4^{\mu\nu} = X^\mu X^\nu - Y^\mu Y^\nu,
\end{aligned} \tag{3.16}$$

$$\begin{aligned}
&\tilde{\mathcal{V}}_1^{\mu\nu} = \frac{1}{2}\left(2T^\mu T^\nu + X^\mu X^\nu + Y^\mu Y^\nu\right), \qquad \tilde{\mathcal{V}}_2^{\mu\nu} = T^\mu T^\nu, \\
&\tilde{\mathcal{V}}_3^{\mu\nu} = -\frac{1}{2}\left(T^\mu X^\nu + T^\nu X^\mu\right), \qquad \tilde{\mathcal{V}}_4^{\mu\nu} = \frac{1}{2}\left(X^\mu X^\nu - Y^\mu Y^\nu\right).
\end{aligned} \tag{3.17}$$

The contraction of $L_{\mu\nu}$ and $\mathcal{V}_i^{\mu\nu}$ leads to various angular distributions. Let $\mathcal{A}_i = L_{\mu\nu}\mathcal{V}_i^{\mu\nu}/Q^2$,

we have

$$\mathcal{A}_1 = 1 + \cosh^2\psi, \qquad \mathcal{A}_2 = -2, \qquad \mathcal{A}_3 = -\cos\phi \sinh 2\psi, \qquad \mathcal{A}_4 = \cos 2\phi \sinh^2\psi. \quad (3.18)$$

We can then write the cross section in Eq. (3.11) as

$$\frac{d\sigma}{dx_B dy dz_h dP_{h\perp}^2 d\phi} = \frac{\pi \alpha_{em}^2 y}{Q^2} \sum_{i=1}^{4} \mathcal{A}_i W_i. \quad (3.19)$$

At large $P_{h\perp} \sim Q$, the collinear factorization is expected to be valid, and W_i can be factorized into a convolution of the parton distribution function, the fragmentation function for the produced D meson, and a short-distance partonic hard part. The lowest-order (LO) contribution to the partonic hard part comes from the photon-gluon fusion subprocess $\gamma^* + g \to Q(p_c) + \bar{Q}(p_{\bar{c}})$, see Fig. 3.2, which gives the leading order cross section as

$$\begin{aligned} \frac{d\sigma}{dx_B dy dz_h dP_{h\perp}^2 d\phi} &= \sigma_0 \int_{x_{\min}}^{1} \frac{dx}{x} \int \frac{dz}{z} G(x) D(z)\, \delta\left(\frac{P_{h\perp}^2}{z_h^2} - \frac{(1-\hat{x})(1-\hat{z})}{\hat{x}\hat{z}} Q^2 + \hat{z}^2 m_c^2\right) \\ &\quad \times \left(\frac{1}{2}\right) \sum_{i=1}^{4} \mathcal{A}_i \hat{W}_i, \end{aligned} \quad (3.20)$$

where $\sigma_0 = e_c^2 \alpha_{em}^2 \alpha_s y/(8\pi z_h^2 Q^2)$, $\hat{x} = x_B/x$, $\hat{z} = z_h/z$, and e_c and m_c are the fractional charge and mass of the charm quark, respectively. The $P_{h\perp}^2/z_h^2$ in the δ-function could be replaced by $q_\perp^2$, and the 1/2 is the color factor. In Eq. (3.20), $G(x)$ is the unpolarized gluon distribution

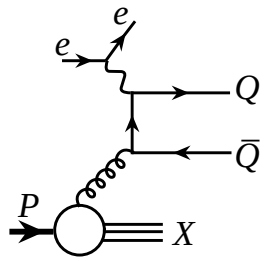

Figure 3.2 Leading order contribution to the partonic hard part comes from the photon-gluon fusion channel.

function with gluon momentum fraction x, and $D(z)$ is the fragmentation function for the

charm quark to become a D meson with $z = P\cdot P_h/P\cdot p_c$. We have suppressed the dependence on the factorization and renormalization scales for simplicity. We used $P_{h\perp} \approx z p_{c\perp}$ inside the δ-function, which fixes the z integration. The lower limit of x integration $x_{\min}$ is given by:

$$x_{\min} = \begin{cases} x_B\left[1+\frac{P_{h\perp}^2+m_c^2}{z_h(1-z_h)Q^2}\right], & \text{if } z_h+\sqrt{z_h^2+\frac{P_{h\perp}^2}{m_c^2}} \geq 1; \\ \\ x_B\left[1+\frac{2m_c^2}{Q^2}\left(1+\sqrt{1+\frac{P_{h\perp}^2}{z_h^2 m_c^2}}\right)\right], & \text{if } z_h+\sqrt{z_h^2+\frac{P_{h\perp}^2}{m_c^2}} \leq 1. \end{cases} \tag{3.21}$$

The short-distance parts $\hat{W}_i$ are calculated from the photon-gluon scattering and are given by

$$\begin{aligned} \hat{W}_1 &= 2\left[\frac{\hat{u}}{\hat{t}}+\frac{\hat{t}}{\hat{u}}-\frac{2\hat{s}Q^2}{\hat{t}\hat{u}}+\frac{4\hat{x}^2\hat{s}}{Q^2}\right] \\ &\quad +4m_c^2\left[\frac{Q^2-2\hat{t}}{\hat{t}^2}+\frac{Q^2-2\hat{u}}{\hat{u}^2}-\frac{2\hat{x}^2}{Q^2}\left(\frac{\hat{u}}{\hat{t}}+\frac{\hat{t}}{\hat{u}}+2\right)\right]-8m_c^4\left[\frac{1}{\hat{t}}+\frac{1}{\hat{u}}\right]^2, \\ \hat{W}_2 &= \frac{16\hat{x}^2}{Q^2}\left[\hat{s}-m_c^2\left(\frac{\hat{u}}{\hat{t}}+\frac{\hat{t}}{\hat{u}}+2\right)\right], \\ \hat{W}_3 &= 4\hat{x}\hat{z}\frac{q_\perp}{Q}(\hat{u}-\hat{t})\left[\frac{\hat{s}-Q^2}{\hat{t}\hat{u}}-2m_c^2\left(\frac{1}{\hat{t}}+\frac{1}{\hat{u}}\right)^2\right], \\ \hat{W}_4 &= 8\hat{z}^2q_\perp^2\left[\frac{Q^2}{\hat{t}\hat{u}}+m_c^2\left(\frac{1}{\hat{t}}+\frac{1}{\hat{u}}\right)^2\right], \end{aligned} \tag{3.22}$$

where $\hat{s},\hat{t},\hat{u}$ are defined at the partonic level as

$$\begin{aligned} \hat{s} &\equiv (xP+q)^2 = \frac{1-\hat{x}}{\hat{x}}Q^2, \\ \hat{t} &\equiv (p_c-q)^2-m_c^2 = -\frac{1-\hat{z}}{\hat{x}}Q^2, \\ \hat{u} &\equiv (xP-p_c)^2-m_c^2 = -\frac{\hat{z}}{\hat{x}}Q^2\,, \end{aligned} \tag{3.23}$$

which are different from some definitions used in the literature. We found that this definition makes the expression of $\hat{W}_i$ for massive quark production simpler. Taking $m_c = 0$ in Eqs. (3.22) and (3.23), one recovers the results for the production of massless quark derived in [28, 31].

3.1.3 Twist-three polarized cross section

We now proceed to derive the single transverse-spin dependent cross section by applying the method [16, 17, 27] reviewed in chapter 2. When both physically observed scales $Q, P_{h\perp} \gg \Lambda_{\rm QCD}$, the spin-dependent cross section for D-meson production is expected to be factorized in terms of twist-three transverse-spin dependent tri-gluon correlation function [18],

$$d\Delta\sigma(s_T) \propto \frac{1}{2S_{ep}} \int dz D(z) \int dx_1 dx_2 \widetilde{T}_{G,F}^{(f,d)}(x_1,x_2)\; i\epsilon^{\rho s_T n\bar{n}} \lim_{k_\perp \to 0} \frac{\partial}{\partial k_\perp^\rho} H(x_1,x_2,k_\perp), \quad (3.24)$$

where $1/2S_{ep}$ is the flux factor and

$$\begin{aligned} \widetilde{T}_{G,F}^{(f,d)}(x_1,x_2) &= \int \frac{P^+ dy_1^- dy_2^-}{2\pi} e^{ix_1P^+y_1^- + i(x_2-x_1)P^+y_2^-} \\ &\quad \times d_{\alpha\beta} \langle P, s_T | A^\alpha(0) \left[\epsilon^{s_T\sigma n\bar{n}} F_\sigma{}^+(y_2^-)\right] A^\beta(y_1^-) | P, s_T\rangle, \end{aligned} \quad (3.25)$$

where $d_{\alpha\beta} = -g_{\alpha\beta} + \bar{n}_\alpha n_\beta + \bar{n}_\beta n_\alpha$. $\widetilde{T}_{G,F}^{(f,d)}(x_1,x_2)$ is related to the tri-gluon correlation function through $T_{G,F}^{(f,d)}(x,x) = x\widetilde{T}_{G,F}^{(f,d)}(x,x)$. Since $\widetilde{T}_{G,F}^{(f,d)}(x_1,x_2)$ is real, we need an imaginary part of the hard-scattering function $H(x_1,x_2,k_\perp)$ to contract with $i\epsilon^{\rho s_T n\bar{n}}$ in order to obtain a real $\Delta\sigma(s_T)$. This imaginary part comes from the interference between a real part of scattering amplitude with a single gluon initial state and an imaginary part of the partonic scattering amplitude with an extra gluon, see Fig. 3.3. Technically, the imaginary part, or the phase, "i", arises when the virtual momentum integral of the extra gluon is evaluated by the residue of an unpinched pole from a propagator in the amplitude with an extra gluon. Such propagator is indicated by the one marked with a short bar in the diagrams in Fig. 3.4.

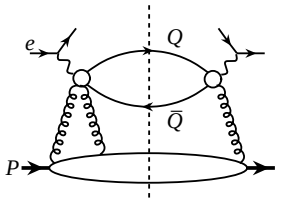

Figure 3.3 A typical diagram that gives a non-vanishing contribution to the SSA.

There are a total of eight partonic diagrams contributing to the twist-three polarized cross sections, $\Delta\sigma(s_T)$. Four of them are shown in Fig. 3.4, and the other four are obtained by attaching the extra gluon in the same way on the right side of the final-state cut. When the extra gluon is attached to the left side of the final-state cut, as shown in Fig. 3.4, the phase from the propagator marked by the bar arises effectively as

$$\begin{aligned}\frac{1}{(p_c-(x_2-x_1)P-k_\perp)^2-m_c^2+i\epsilon} &= \frac{1}{2P\cdot p_c}\frac{1}{x_1-x_2+v_1\cdot k_\perp+i\epsilon}+\mathcal{O}(k_\perp^2)\\ &\to \frac{-i\pi}{2P\cdot p_c}\delta(x_1-x_2+v_1\cdot k_\perp),\end{aligned} \tag{3.26}$$

to fix the virtual loop momentum fraction $x_1 = x_2 - v_1\cdot k_\perp$ with $v_1^\mu = -2p_c^\mu/2P\cdot p_c$. On the

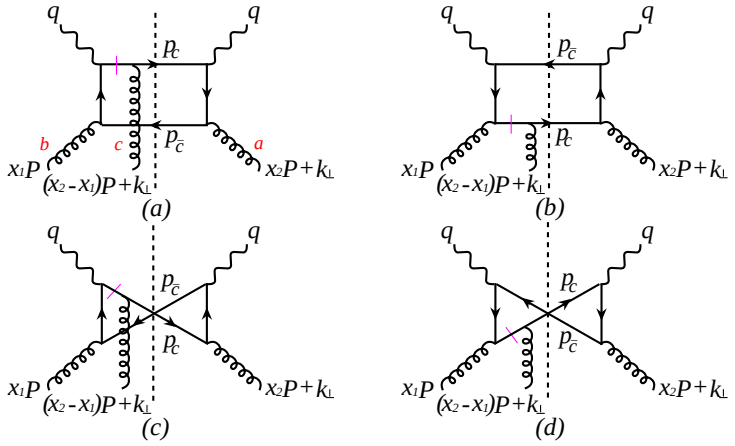

Figure 3.4 Feynman diagrams that give the twist-three contribution to the spin-dependent cross section. The short bar indicates the propagator that produces the pole. The letters, a, b and c in Fig. (a), represent the color of the initial-state gluons.

other hand, the on-shell condition associated with the unobserved anti-charm quark fixes the momentum fraction of the active initial-state gluon as

$$\begin{aligned}\delta(p_{\bar{c}}^2-m_c^2) &= \delta\left((x_2P+k_\perp+q-p_c)^2-m_c^2\right)\\ &= \frac{1}{2P\cdot(q-p_c)}\delta(x_2-x-v_2\cdot k_\perp),\end{aligned} \tag{3.27}$$

where terms at $\mathcal{O}(k_\perp^2)$ and higher are neglected and

$$x = -\frac{(q-p_c)^2 - m_c^2}{2P\cdot(q-p_c)}, \qquad v_2^\mu = \frac{2p_c^\mu}{2P\cdot(q-p_c)}. \tag{3.28}$$

When the extra gluon is attached to the right hand side of the cut, the phase arises as

$$\begin{aligned}\frac{1}{(p_c+(x_2-x_1)P+k_\perp)^2 - m_c^2 - i\epsilon} &= \frac{1}{2P\cdot p_c}\frac{1}{x_2-x_1-v_1\cdot k_\perp - i\epsilon} + \mathcal{O}(k_\perp^2)\\ &\to \frac{i\pi}{2P\cdot p_c}\delta(x_2-x_1-v_1\cdot k_\perp),\end{aligned} \tag{3.29}$$

and the on-shell condition of the unobserved anti-charm quark gives

$$\delta(p_{\bar{c}}^2 - m_c^2) = \frac{1}{2P\cdot(q-p_c)}\delta(x_1-x), \tag{3.30}$$

which has no $k_\perp$-dependence.

Applying these delta functions in Eq. (3.24), we have the following general expression:

$$\begin{aligned}&\lim_{k_\perp\to 0}\frac{\partial}{\partial k_\perp^\rho}\int dx_1\int dx_2\,\widetilde{T}_{G,F}^{(f,d)}(x_1,x_2)\,[H_L(x_1,x_2,k_\perp)\delta(x_1-x_2+v_1\cdot k_\perp)\delta(x_2-x-v_2\cdot k_\perp)\\ &-H_R(x_1,x_2,k_\perp)\delta(x_2-x_1-v_1\cdot k_\perp)\delta(x_1-x)]\\ &= (v_2-v_1)^\rho H_L(x,x,0)\frac{d}{dx}\left(\frac{T_{G,F}^{(f,d)}(x,x)}{x}\right) + \frac{T_{G,F}^{(f,d)}(x,x)}{x}\\ &\times\lim_{k_\perp\to 0}\frac{\partial}{\partial k_\perp^\rho}\left[H_L(x+(v_2-v_1)\cdot k_\perp, x+v_2\cdot k_\perp, k_\perp) - H_R(x,x+v_1\cdot k_\perp,k_\perp)\right],\end{aligned} \tag{3.31}$$

where we have already used the facts that $H_L(x,x,0) = H_R(x,x,0)$ and $T_{G,F}^{(f,d)}(x,x) = x\widetilde{T}_{G,F}^{(f,d)}(x,x)$. The fact that Eq. (3.31) depends only on the diagonal part of the tri-gluon correlation function, $T_{G,F}^{(f,d)}(x_1,x_2)$, with $x_1 = x_2 = x$ is a consequence of that the photon-gluon fusion subprocess at this order has only the so-called "soft-pole" contribution to the SSA [17, 32]. Therefore, the measurement of the SSA in D-meson production in SIDIS is a direct measurement of the tri-gluon correlation function, $T_{G,F}^{(f,d)}(x,x)$.

In terms of $\hat{s}, \hat{t}, \hat{u}$ defined in the previous subsection, we have

$$v_1^\mu = \frac{2x}{\hat{u}} p_c^\mu, \qquad v_2^\mu = -\frac{2x}{\hat{t}} p_c^\mu, \qquad (v_2 - v_1)^\mu = -\frac{2x}{\hat{t}} \left(1 + \frac{\hat{t}}{\hat{u}}\right) p_c^\mu. \tag{3.32}$$

Using Eqs. (3.24), (3.31), and adding the contributions from the eight diagrams together, we derive the fully differential single-transverse-spin-dependent cross section for D meson production:

$$\begin{aligned} \frac{d\Delta\sigma(s_T)}{dx_B dy dz_h dP_{h\perp}^2 d\phi} &= \sigma_0 \int_{x_{\min}}^1 \frac{dx}{x} \int \frac{dz}{z} D(z) \delta\left(\frac{P_{h\perp}^2}{z_h^2} - \frac{(1-\hat{x})(1-\hat{z})}{\hat{x}\hat{z}} Q^2 + \hat{z}^2 m_c^2\right) \\ &\times \left(\frac{1}{4}\right) \left[\epsilon^{P_h s_T n \bar{n}} \left(\frac{\sqrt{4\pi\alpha_s}}{z\hat{t}}\right) \left(1 + \frac{\hat{t}}{\hat{u}}\right)\right] \\ &\times \sum_{j=f,d} \sum_{i=1}^4 \mathcal{A}_i \left[-x^2 \frac{d}{dx}\left(\frac{T_{G,F}^{(j)}(x,x)}{x}\right) \hat{W}_i + T_{G,F}^{(j)}(x,x) \hat{N}_i\right] \end{aligned} \tag{3.33}$$

Here 1/4 is the color factor, $\hat{W}_i$ are given in Eq. (3.22), and the hard parts for the "non-derivative" term, $\hat{N}_i$, are given by

$$\begin{aligned} \hat{N}_1 &= 4\left[\frac{2m_c^2 - Q^2}{\hat{t}\hat{u}} + \frac{6\hat{x}^2}{Q^2}\right] \left[(\hat{s} - Q^2) - 2m_c^2 \left(\frac{\hat{u}}{\hat{t}} + \frac{\hat{t}}{\hat{u}} + 2\right)\right], \\ \hat{N}_2 &= \frac{16\hat{x}^2}{Q^2} \left[(\hat{s} - Q^2) - 2m_c^2 \left(\frac{\hat{u}}{\hat{t}} + \frac{\hat{t}}{\hat{u}} + 2\right)\right], \\ \hat{N}_3 &= \frac{2Q}{\hat{z} q_\perp} (\hat{u} - \hat{t}) \left[\left(\frac{4\hat{z}^2 q_\perp^2}{\hat{t}\hat{u}} - \frac{1}{Q^2 + \hat{s}}\right) \left(2m_c^2 \left(\frac{1}{\hat{t}} + \frac{1}{\hat{u}}\right) - \frac{Q^2 - \hat{s}}{Q^2 + \hat{s}}\right) - 2\hat{z} q_\perp^2\right], \\ \hat{N}_4 &= 8\left[2\hat{z} q_\perp^2 - \frac{\hat{t}\hat{u}}{Q^2 + \hat{s}}\right] \left[\frac{Q^2}{\hat{t}\hat{u}} + m_c^2 \left(\frac{1}{\hat{t}} + \frac{1}{\hat{u}}\right)^2\right]. \end{aligned} \tag{3.34}$$

Eq. (3.33) is our main result for the leading order twist-three $T_{G,F}^{(f,d)}(x,x)$ contribution to the fully differential polarized cross section, $\Delta\sigma(s_T)$, of D-meson production in SIDIS. The single transverse-spin asymmetry for the D-meson production in SIDIS is obtained by substituting Eqs. (3.20) and (3.33) into Eq. (3.10).

Similarly, by attaching the extra gluon to the final anti-charm quark instead of charm quark, we could calculate the SSAs for producing a $\bar{D}$ meson, which is fragmented from an anti-charm quark. We find that attaching the gluon to the anti-charm quark leads to an opposite phase

compared to the attachment to the charm quark, thus the partonic hard parts change sign. On the other hand, the color factor associated with $T^{(f)}_{G,F}(x,x)$ will also change sign due to the antisymmetric nature of the color structure constant f^{abc}. But for the symmetric one d^{abc}, the color factor remains the same. The combined effect is that the SSA for $\bar{D}$ meson has the same functional form as that for the D meson production except that the sum of the trigluon correlation functions, $T^{(f)}_{G,F}(x,x)+T^{(d)}_{G,F}(x,x)$ in Eq. (3.33) is replaced by the difference, $T^{(f)}_{G,F}(x,x) - T^{(d)}_{G,F}(x,x)$. That is, the D and $\bar{D}$ meson production should have the same SSAs if $T^{(d)}_{G,F}(x,x) = 0$, but, with an opposite sign if $T^{(f)}_{G,F}(x,x) = 0$. We could gain valuable information on both tri-gluon correlation functions by comparing the SSAs for producing D and $\bar{D}$-mesons in SIDIS.

Similar to the twist-three contributions to the SSAs generated by the fermionic quark-gluon correlation function, $T_{q,F}(x,x)$, the gluonic twist-three contribution to the SSA of D-meson production in Eq. (3.33) has both the "derivative" and "non-derivative" terms, a unique feature of twist-three contribution. It was found that the fermionic "non-derivative" and "derivative" terms can be combined into a simple form $T_{q,F}(x,x) - xT'_{q,F}(x,x)$ [27, 29]. Realizing that

$$-x^2\frac{d}{dx}\left[\frac{T^{(f,d)}_{G,F}(x,x)}{x}\right] = T^{(f,d)}_{G,F}(x,x) - x\frac{d}{dx}T^{(f,d)}_{G,F}(x,x), \tag{3.35}$$

we found that the first term in Eq. (3.33) follows the same simple combination for tri-gluon correlation function. However, the terms $\propto \hat{N}_i$ introduce the violation of this simple form.

3.2 SSAs for open charm production in hadronic collisions

Studying SSAs for open charm in SIDIS helps us to extract tri-gluon correlation functions. However, it does not provide a test of the QCD collinear factorization approach to the SSAs. In order to better test this approach, we need to test the universality of these tri-gluon correlation functions. For this purpose, we also study the SSAs for open charm production in hadronic collisions. We calculate the SSAs in the same approach, and demonstrate that the SSAs depend on the same tri-gluon correlations. Comparing SSAs for physical cross sections

involving the same non-perturbative twist-three correlation functions but different partonic hard subprocesses will provide stringent tests of QCD dynamics and the twist-3 factorization we use.

We consider inclusive single charm meson production in a scattering process between a polarized proton A of momentum P and transverse spin vector s_T and an unpolarized proton B of momentum P',

$$A(P, s_T) + B(P') \to h(P_h) + X, \tag{3.36}$$

where h represents the observed open charm (D or $\bar{D}$) meson with momentum P_h and mass m_h. The single transverse-spin asymmetry A_N can be written as

$$A_N = E_{P_h} \frac{d\Delta\sigma(P_h, s_T)}{d^3P_h} \Big/ E_{P_h} \frac{d\sigma(P_h)}{d^3P_h} \ , \tag{3.37}$$

for the single hadron differential cross sections.

The spin-averaged differential cross section for D meson production at large transverse momentum, $P_{h\perp} > m_h$, can be expressed in the following factorized form [12]:

$$\begin{aligned} E_{P_h} \frac{d\sigma}{d^3P_h} &= \frac{\alpha_s^2}{S} \sum_{a,b} \int \frac{dz}{z^2} D_{c\to h}(z) \int \frac{dx'}{x'} f_{b/B}(x') \int \frac{dx}{x} f_{a/A}(x) \\ &\quad \times \delta\left(\tilde{s} + \tilde{t} + \tilde{u}\right) H^U_{ab\to c}(\tilde{s}, \tilde{t}, \tilde{u}), \end{aligned} \tag{3.38}$$

where $\sum_{a,b}$ represents the sum over all light parton flavors and $S = (P + P')^2$ is the total collision energy squared. $f_{a/A}(x)$ and $f_{b/B}(x')$ are the standard parton distribution functions, and $D_{c\to h}(z)$ is the fragmentation function for a charm quark c fragmenting into a D meson. We have neglected all dependence on the factorization and renormalization scales in (3.38).

In Eq. (3.38), $H^U_{ab\to c}$ is a short-distance hard part for two partons of flavor a and b to produce a charm quark c. At the lowest order, it gets contributions from the light quark-antiquark annihilation and gluon-gluon fusion subprocesses, as sketched in Fig. 3.5, and is

given by

$$\begin{aligned} H^U_{q\bar{q}\to c} &= \frac{C_F}{N_C}\left[\frac{\tilde{t}^2+\tilde{u}^2+2m_c^2\tilde{s}}{\tilde{s}^2}\right], \\ H^U_{gg\to c} &= \frac{1}{2N_C}\left[\frac{1}{\tilde{t}\tilde{u}}-\frac{N_C}{C_F}\frac{1}{\tilde{s}^2}\right]\left[\tilde{t}^2+\tilde{u}^2+4m_c^2\tilde{s}-\frac{4m_c^4\tilde{s}^2}{\tilde{t}\tilde{u}}\right], \end{aligned} \tag{3.39}$$

where $\tilde{s},\tilde{t},\tilde{u}$ are defined at the partonic level as

$$\tilde{s}=(xP+x'P')^2, \qquad \tilde{t}=(xP-p_c)^2-m_c^2, \qquad \tilde{u}=(x'P'-p_c)^2-m_c^2, \tag{3.40}$$

with p_c and m_c the momentum and mass of the charm quark that fragments into the D meson, respectively.

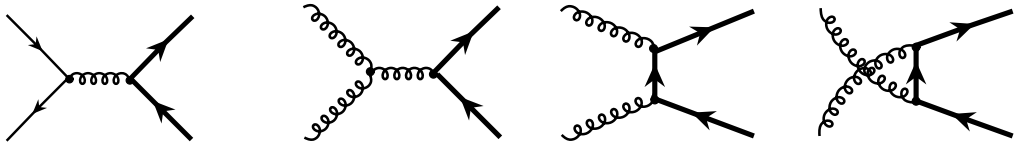

Figure 3.5 Lowest order Feynman diagram for light quark-antiquark annihilation (a) and for gluon-gluon fusion to a pair of heavy quarks.

The transverse spin-dependent cross section now gets contributions from both the $q\bar{q}$ annihilation and gg fusion channels. Following the same method [16, 17, 27], the cross section in the $q\bar{q}$ annihilation channel can be expressed in terms of the twist-3 quark-gluon correlation function $T_{q,F}(x_1,x_2)$,

$$\begin{aligned} d\Delta\sigma(s_T) \;\propto\; & \frac{1}{2S}\sum_q \int dz D_{c\to h}(z)\int\frac{dx'}{x'}f_{\bar{q}/B}(x')\int dx_1dx_2T_{q,F}(x_1,x_2) \\ & \times\, i\epsilon^{\rho s_T n\bar{n}}\lim_{k_\perp\to 0}\frac{\partial}{\partial k_\perp^\rho}H_{q\bar{q}\to c}(x_1,x_2,k_\perp), \end{aligned} \tag{3.41}$$

with $T_{q,F}(x_1,x_2)$ given in chapter 2.

Again, the strong interaction phase needed to generate a non-vanishing SSA comes from the interference between a real part of the scattering amplitude and an imaginary part of the

partonic scattering amplitude with an extra gluon, as shown in Fig. 3.6. The propagator which provides the unpinched poles is indicated by the short bars in the diagrams in Fig. 3.6, just as in the last section. The phase can arise from the attachment of the extra gluon to either the initial-state parton, or the final-state charm quark, which we will refer to as initial-state and final-state interactions, respectively.

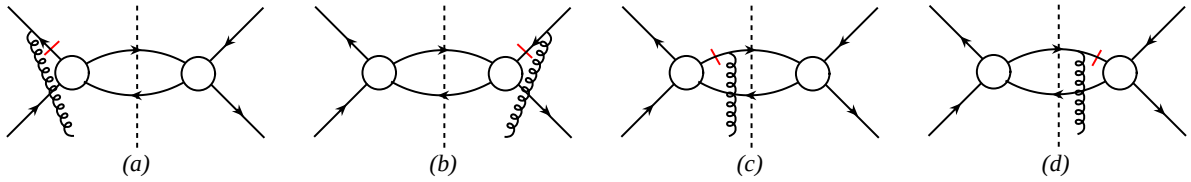

Figure 3.6 Feynman diagrams that give the twist-3 contribution to the spin-dependent cross section in the quark-antiquark annihilation channel: initial-state interaction (a), (b), and final-state interaction (c), (d). The short bar indicates the propagator that produces the unpinched pole.

At lowest order, there are four diagrams contributing to the twist-3 polarized cross section in the quark-antiquark annihilation channel, as sketched in Fig. 3.6, where the blob is given by the diagram in Fig. 3.5(a). Using the same techniques as in last section, we have

$$\begin{aligned} E_{P_h}\frac{d\Delta\sigma}{d^3P_h}\bigg|_{q\bar{q}\to c\bar{c}} &= \frac{\alpha_s^2}{S}\sum_q \int\frac{dz}{z^2}D_{c\to h}(z)\int\frac{dx'}{x'}f_{\bar{q}/B}(x')\int\frac{dx}{x} \\ &\quad\times\sqrt{4\pi\alpha_s}\left(\frac{\epsilon^{P_h s_T n\bar{n}}}{z\tilde{u}}\right)\delta\left(\tilde{s}+\tilde{t}+\tilde{u}\right) \\ &\quad\times\left[\left(T_{q,F}(x,x)-x\frac{d}{dx}T_{q,F}(x,x)\right)H_{q\bar{q}\to c}(\tilde{s},\tilde{t},\tilde{u})\right. \\ &\quad\left.+T_{q,F}(x,x)\mathcal{H}_{q\bar{q}\to c}(\tilde{s},\tilde{t},\tilde{u})\right], \end{aligned} \tag{3.42}$$

where $H_{q\bar{q}\to c}$ can be written as

$$H_{q\bar{q}\to c} = H^I_{q\bar{q}\to c} + H^F_{q\bar{q}\to c}\left(1+\frac{\tilde{u}}{\tilde{t}}\right), \tag{3.43}$$

and likewise for $\mathcal{H}_{q\bar{q}\to c}$, and where the corresponding hard parts are given by

$$\begin{aligned} H^I_{q\bar{q}\to c} &= \frac{1}{2N_C^2}\left[\frac{\tilde{t}^2+\tilde{u}^2+2m_c^2\tilde{s}}{\tilde{s}^2}\right], \\ H^F_{q\bar{q}\to c} &= \frac{N_C^2-2}{2N_C^2}\left[\frac{\tilde{t}^2+\tilde{u}^2+2m_c^2\tilde{s}}{\tilde{s}^2}\right], \qquad (3.44) \\ \mathcal{H}^I_{q\bar{q}\to c} &= \frac{1}{2N_C^2}\left[\frac{2m_c^2}{\tilde{s}}\right], \\ \mathcal{H}^F_{q\bar{q}\to c} &= \frac{N_C^2-2}{2N_C^2}\left[\frac{2m_c^2}{\tilde{s}}\right]. \qquad (3.45) \end{aligned}$$

Note that $\mathcal{H}^I_{q\bar{q}\to c}$ and $\mathcal{H}^F_{q\bar{q}\to c}$ are proportional to the charm quark mass. As a check of our results, when $m_c^2 \to 0$ the spin-dependent cross section in Eq. (3.42) becomes identical to the one for pion production through the $q\bar{q} \to q'\bar{q}'$ channel [27] (if one replaces the D meson fragmentation function by the pion fragmentation function).

The spin-dependent cross section for $\bar{D}$ meson production can be calculated in the same way. The Feynman diagrams are the same as those for D meson production in Fig. 3.6, except that the extra gluon should be attached to the anti-charm $\bar{c}$ quark for the final-state interaction. The cross section for $\bar{D}$ meson production has the same factorized form as that in Eq. (3.42), with the fragmentation function $D_{c\to D}(z)$ replaced by $D_{\bar{c}\to\bar{D}}(z)$, and the hard parts given by

$$\begin{aligned} H^I_{q\bar{q}\to\bar{c}} &= \frac{1}{2N_C^2}\left[\frac{\tilde{t}^2+\tilde{u}^2+2m_c^2\tilde{s}}{\tilde{s}^2}\right], \\ H^F_{q\bar{q}\to\bar{c}} &= \frac{1}{N_C^2}\left[\frac{\tilde{t}^2+\tilde{u}^2+2m_c^2\tilde{s}}{\tilde{s}^2}\right], \qquad (3.46) \\ \mathcal{H}^I_{q\bar{q}\to\bar{c}} &= \frac{1}{2N_C^2}\left[\frac{2m_c^2}{\tilde{s}}\right], \\ \mathcal{H}^F_{q\bar{q}\to\bar{c}} &= \frac{1}{N_C^2}\left[\frac{2m_c^2}{\tilde{s}}\right]. \qquad (3.47) \end{aligned}$$

These short-distance hard parts are consistent with those presented in the calculation of the SSAs for heavy quark and anti-quark production in hadronic collisions [33]. We note that the hard parts for $\bar{q}q$ scattering are obtained from those for $q\bar{q}$ by $H^{I,F}_{\bar{q}q\to c} = -H^{I,F}_{q\bar{q}\to\bar{c}}$ and $H^{I,F}_{\bar{q}q\to\bar{c}} = -H^{I,F}_{q\bar{q}\to c}$, and likewise for the $\mathcal{H}^{I,F}$.

Similar to Eq. (3.41), the spin-dependent cross section for the gg fusion channel has the

following factorized form:

$$d\Delta\sigma(s_T) \propto \frac{1}{2S}\int dz D_{c\to h}(z)\int\frac{dx'}{x'}f_{g/B}(x')\int dx_1 dx_2 \widetilde{T}^{(f,d)}_{G,F}(x_1,x_2) \times i\epsilon^{\rho s_T n\bar{n}}\lim_{k_\perp\to 0}\frac{\partial}{\partial k_\perp^\rho}H_{gg\to c}(x_1,x_2,k_\perp), \tag{3.48}$$

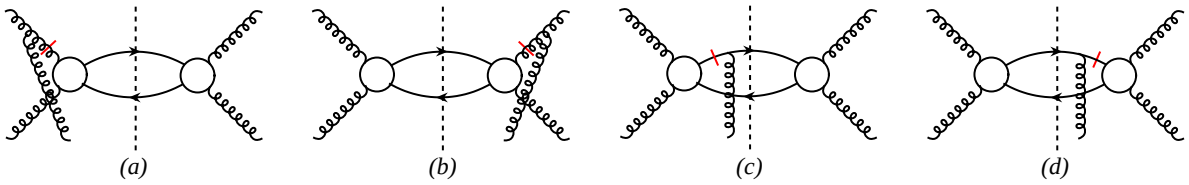

Figure 3.7 Feynman diagrams that give the twist-3 contribution to the spin-dependent cross section in the gluon-gluon fusion channel: initial-state interaction (a), (b), and final-state interaction (c), (d). The short bar indicates the propagator that produces the pole.

To calculate the partonic hard part, $H_{gg\to c}$, in Eq. (3.48), we need to consider Feynman diagrams with either initial-state or final-state interactions, as sketched in Fig. 3.7, where the blob is given by the sum of the three diagrams in Fig. 3.5(b). Hence, each diagram in Fig. 3.7 corresponds to nine diagrams. Instead of four diagrams in Fig. 3.6 for the quark-antiquark annihilation subprocess, we have a total of 36 diagrams for gluon-gluon fusion. By evaluating these diagrams, we obtain the contribution to the spin-dependent cross section,

$$\begin{aligned} E_{P_h}\frac{d\Delta\sigma}{d^3P_h}\bigg|_{gg\to c\bar{c}} &= \frac{\alpha_s^2}{S}\sum_{i=f,d}\int\frac{dz}{z^2}D_{c\to h}(z)\int\frac{dx'}{x'}f_{g/B}(x')\int\frac{dx}{x} \\ &\times\sqrt{4\pi\alpha_s}\left(\frac{\epsilon^{P_h s_T n\bar{n}}}{z\tilde{u}}\right)\delta\left(\tilde{s}+\tilde{t}+\tilde{u}\right) \\ &\times\left[\left(T_G^{(i)}(x,x)-x\frac{d}{dx}T_G^{(i)}(x,x)\right)H^{(i)}_{gg\to c}(\tilde{s},\tilde{t},\tilde{u})\right. \\ &\left.+T_G^{(i)}(x,x)\mathcal{H}^{(i)}_{gg\to c}(\tilde{s},\tilde{t},\tilde{u})\right], \end{aligned} \tag{3.49}$$

where the sum, $\sum_{i=f,d}$, is over the two correlation functions $T^{(f)}_{G,F}(x,x)$ and $T^{(d)}_{G,F}(x,x)$. The

partonic hard part $H_{gg\to c}^{(i)}$ can be written as

$$H_{gg\to c}^{(i)} = H_{gg\to c}^{I(i)} + H_{gg\to c}^{F(i)}\left(1+\frac{\tilde{u}}{\tilde{t}}\right), \tag{3.50}$$

and likewise for $\mathcal{H}_{gg\to c}^{(i)}$, and we find

$$\begin{aligned}
H_{gg\to c}^{I(f)} &= -\frac{1}{8C_F}\frac{\tilde{t}^2+\tilde{u}^2}{\tilde{t}\tilde{u}\tilde{s}^2}\left[\tilde{t}^2+\tilde{u}^2+4m_c^2\tilde{s}-\frac{4m_c^4\tilde{s}^2}{\tilde{t}\tilde{u}}\right], \\
H_{gg\to c}^{I(d)} &= -\frac{1}{8C_F}\frac{\tilde{u}-\tilde{t}}{\tilde{t}\tilde{u}\tilde{s}}\left[\tilde{t}^2+\tilde{u}^2+4m_c^2\tilde{s}-\frac{4m_c^4\tilde{s}^2}{\tilde{t}\tilde{u}}\right], \qquad (3.51) \\
H_{gg\to c}^{F(f)} &= H_{gg\to c}^{F(d)} \\
&= \left[\frac{N_C}{4\left(N_C^2-1\right)}\frac{\tilde{u}}{\tilde{t}\tilde{s}^2}-\frac{1}{4N_C\left(N_C^2-1\right)}\frac{1}{\tilde{t}\tilde{u}}\right]\left[\tilde{t}^2+\tilde{u}^2+4m_c^2\tilde{s}-\frac{4m_c^4\tilde{s}^2}{\tilde{t}\tilde{u}}\right], \qquad (3.52) \\
\mathcal{H}_{gg\to c}^{I(f)} &= -\frac{1}{2C_F}\frac{m_c^2\left(\tilde{t}^2+\tilde{u}^2\right)\left(\tilde{t}\tilde{u}-2m_c^2\tilde{s}\right)}{\tilde{s}\tilde{t}^2\tilde{u}^2}, \\
\mathcal{H}_{gg\to c}^{I(d)} &= -\frac{1}{2C_F}\frac{m_c^2\left(\tilde{u}-\tilde{t}\right)\left(\tilde{t}\tilde{u}-2m_c^2\tilde{s}\right)}{\tilde{t}^2\tilde{u}^2}, \\
\mathcal{H}_{gg\to c}^{F(f)} &= \mathcal{H}_{gg\to c}^{F(d)} = -\left[\frac{1}{N_C(N_C^2-1)}\frac{1}{\tilde{u}^2}-\frac{N_C}{N_C^2-1}\frac{1}{\tilde{s}^2}\right]\frac{m_c^2\tilde{s}(\tilde{t}\tilde{u}-2m_c^2\tilde{s})}{\tilde{t}^2}. \qquad (3.53)
\end{aligned}$$

The gluon-gluon subprocess of course also contributes to the cross section for $\bar{D}$ meson production. The corresponding partonic hard parts for producing an anti-charm quark are given by

$$\begin{aligned}
H_{gg\to\bar{c}}^{(f)} &= H_{gg\to c}^{(f)}, \qquad H_{gg\to\bar{c}}^{(d)} = -H_{gg\to c}^{(d)}, \\
\mathcal{H}_{gg\to\bar{c}}^{(f)} &= \mathcal{H}_{gg\to c}^{(f)}, \qquad \mathcal{H}_{gg\to\bar{c}}^{(d)} = -\mathcal{H}_{gg\to c}^{(d)}, \qquad (3.54)
\end{aligned}$$

where the sign difference of the partonic hard parts for the $T_{G,F}^{(d)}$ contribution will be responsible for the difference of the SSAs for D and $\bar{D}$ meson production that will be discussed in the next section. We note that this sign difference can also be observed in the expressions for the "gluonic pole matrix elements" given in [34].

We point out that the compact dependence of the spin-dependent cross section on the combinations $T_{q,F}(x,x) - xT'_{q,F}(x,x)$ of the twist-3 correlation functions found in Ref. [27] for

the "massless" case of pion production in hadronic collisions, is violated for the production of D (or $\bar{D}$) mesons by the additional non-derivative terms in Eqs. (3.42) and (3.49). The violation is caused by the heavy quark mass since the additional terms vanish when $m_c \to 0$. In fact, we observe that the hard parts we have derived satisfy the following relation:

$$\mathcal{H}^{I,F}_{ab\to c} = m_c^2 \frac{dH^{I,F}_{ab\to c}}{dm_c^2} \,, \tag{3.55}$$

separately for any of the various contributions considered above (and likewise for $\bar{c}$ production). This connection is likely a consequence of the "master formula" for twist-3 soft-gluon-pole contributions derived in [29].

We also note that "soft-fermion pole" contributions [17], for which the pole in the hard-scattering function is taken in such a way that the initial quark, rather than the initial gluon, becomes soft, are absent for the $q\bar{q}$ process at the leading order. This is because $q\bar{q}$ annihilation proceeds through an s-channel diagram, whereas soft-fermion poles would only appear in t-channel diagrams. If they were present, such contributions would involve the function $T_{q,F}(0,x)$. For the tri-gluon correlation contribution, terms proportional to $T^{(f)}_{G,F}(0,x)$ and $T^{(d)}_{G,F}(0,x)$ are automatically included in our calculations. This is due to the symmetry of the partonic hard part under interchange of two gluon lines, and to the fact that field operators commute on the light-cone [19]. This leads to the symmetry properties $T_{G,F}(x,x) = T_{G,F}(0,x) = T_{G,F}(x,0)$ [35].

Combining the factorized cross sections in Eqs. (3.42) and (3.49) with the corresponding partonic hard parts, we have

$$E_{P_h}\frac{d\Delta\sigma}{d^3P_h} = E_{P_h}\frac{d\Delta\sigma}{d^3P_h}\bigg|_{q\bar{q}\to c\bar{c}} + E_{P_h}\frac{d\Delta\sigma}{d^3P_h}\bigg|_{gg\to c\bar{c}} \tag{3.56}$$

for the leading-order contribution to the transverse-spin-dependent cross section for D (or $\bar{D}$) meson production in hadronic collisions. The corresponding single transverse-spin asymmetry is obtained by substituting Eqs. (3.38) and (3.56) into Eq. (3.37).

3.3 Phenomenology

In order to estimate the SSAs for the production of D or $\bar{D}$ mesons, we need the unknown, but universal, tri-gluon correlation functions $T_{G,F}^{(f,d)}(x,x)$. Similar to the ansatz for quark-gluon correlation function $T_{q,F}(x,x)$, which was originally introduced in [16] and found to be consistent with the latest experimental data [27], we model the tri-gluon correlation function $T_{G,F}^{(f,d)}(x,x)$ as

$$T_{G,F}^{(f)}(x,x) = \lambda_f\, G(x), \qquad T_{G,F}^{(d)}(x,x) = \lambda_d\, G(x) \tag{3.57}$$

with $G(x)$ the normal unpolarized gluon distribution function. Because of its non-perturbative nature, $T_{G,F}^{(f,d)}(x,x)$ should be extracted from the experiments and the values and the signs of $\lambda_{f,d}$ should be fixed by future data. For the following numerical estimate, we assume that $\lambda_{f,d}$ has the same size as that for quark-gluon correlation function $T_{q,F}(x,x)$ [16], choose $|\lambda_f| = |\lambda_d| = \lambda_F = 0.07$ GeV.

For open charm production in hadronic collisions, we will also need the quark-gluon correlation functions $T_{q,F}(x,x)$. Recently an updated form for $T_{q,F}(x,x)$ has been extracted from experimental data on the SSAs in $pp \to \pi X$ including both fix-target [21] and RHIC [23] data. In the following, we will adopt the set referred to as "Fit II" in [27] for $T_{q,F}(x,x)$.

We will use CTEQ6L parton distribution functions [13], and charm-to-D fragmentation functions from Ref. [36]. We further assume that $D_{\bar{c}\to\bar{D}}(z) = D_{c\to D}(z)$ for the $\bar{D}$ meson fragmentation functions. We choose the factorization scale to be equal to the renormalization scale throughout, and set $\mu = \sqrt{Q^2 + m_c^2 + P_{h\perp}^2}$ for SIDIS and $\mu = \sqrt{m_c^2 + P_{h\perp}^2}$ for hadronic case with $m_c = 1.3$ GeV.

3.3.1 Numerical estimate of the SSAs in SIDIS

In this section we first evaluate the inclusive D-meson production rate at large $P_{h\perp}$ in SIDIS. We then estimate the size of SSA for the D-meson production in SIDIS.

The charm meson's transverse momentum, $P_{h\perp}$, is chosen to be along the x-direction in

the *hadron frame*, and therefore, $\epsilon^{P_h s_T n\bar{n}} = -P_{h\perp} \sin\phi_s$. The fully differential cross sections in Eqs. (3.20) and (3.33) can be decomposed in terms of the independent angular distributions as follows,

$$\begin{aligned} \frac{d\sigma}{dx_B dy dz_h dP_{h\perp}^2 d\phi} &= \sigma_0^U + \sigma_1^U \cos\phi + \sigma_2^U \cos 2\phi, \\ \frac{d\Delta\sigma}{dx_B dy dz_h dP_{h\perp}^2 d\phi} &= \sin\phi_s \left(\Delta\sigma_0 + \Delta\sigma_1 \cos\phi + \Delta\sigma_2 \cos 2\phi\right). \end{aligned} \tag{3.58}$$

Before evaluating the SSA, we first estimate the D-meson production rate in the unpolarized SIDIS by using our LO formula in Eq. (3.20).

In the following plots, we choose two sets of kinematic variables. The first one is $S_{ep} = 300$ GeV^2, $x_B = 0.01$ and $Q = 1$ GeV, which is close to the COMPASS kinematics. The other is $S_{ep} = 2500$ GeV^2, $x_B = 0.01$ and $Q = 4$ GeV, which is more relevant to the planned eRHIC experiment [37].

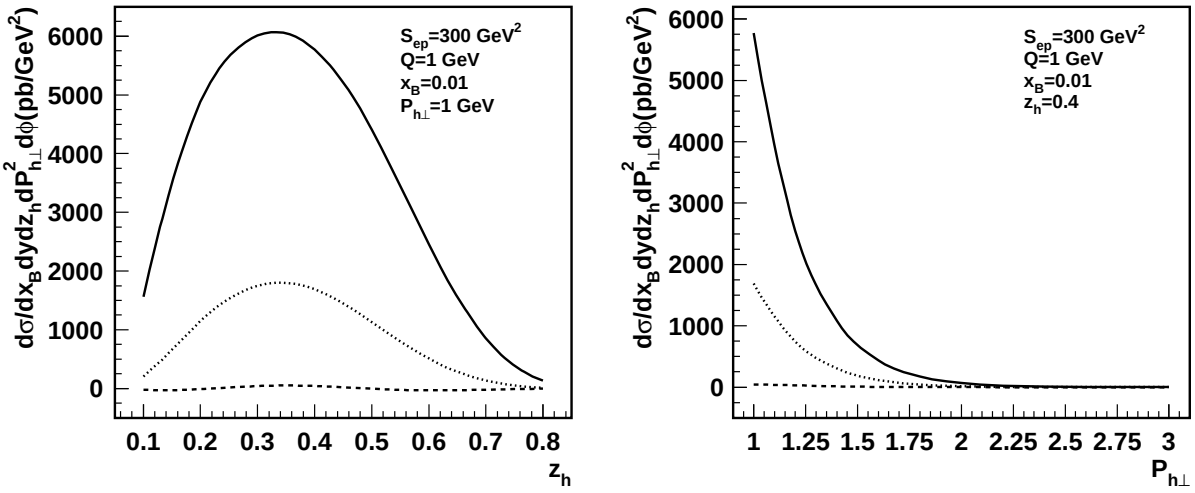

Figure 3.8 The fully differential unpolarized cross section for D^0 production in SIDIS for COMPASS kinematics. The curves represent: σ_0^U(solid), σ_1^U(dashed), and σ_2^U(dotted) in Eq. (3.58).

In Fig. 3.8, we show individual coefficients of the angular distribution, σ_0^U, σ_1^U, and σ_2^U, of the *fully differential* unpolarized cross section for D^0 production in Eq. (3.58) as a function of both z_h and $P_{h\perp}$ for the kinematics relevant to COMPASS experiment. It is clear that the angular dependent pieces $\sigma_1^U, \sigma_2^U \ll \sigma_0^U$, and might be too small to be significant. Without

worrying about the detection efficiency, the D-meson production at $P_{h\perp} \sim 1$ GeV could be measurable. Likewise, Fig. 3.9 shows the *fully differential* unpolarized cross section for D^0 production for eRHIC kinematics. With larger Q and $P_{h\perp}$, the production rate is smaller but may still have enough events with a high luminosity.

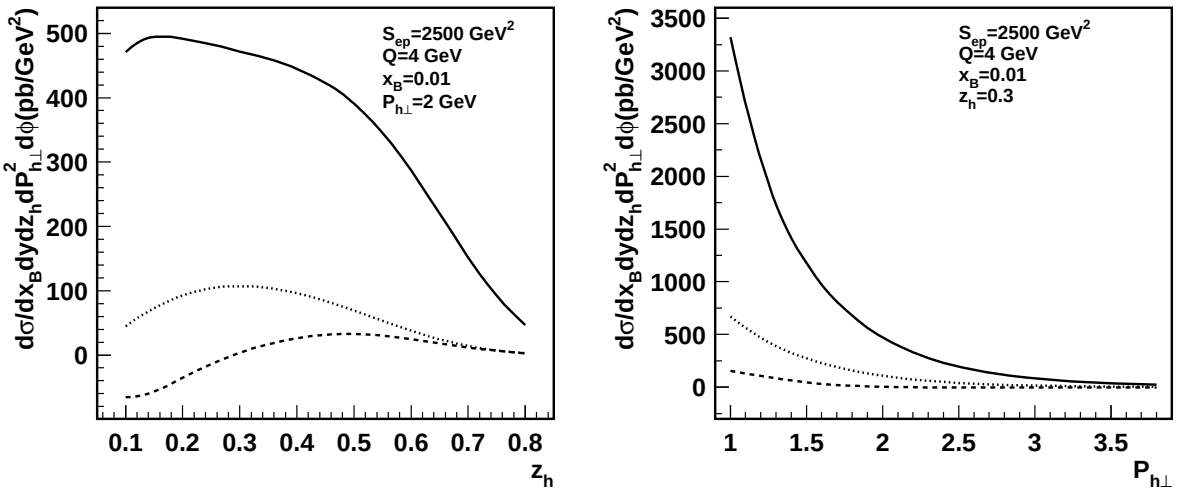

Figure 3.9 The fully differential unpolarized cross section for D^0 production in SIDIS at the future eRHIC. The curves represent: σ_0^U(solid), σ_1^U(dashed), and σ_2^U(dotted) in Eq. (3.58).

In order to obtain the numerical estimate for the SSAs of D-meson production, we use the model for tri-gluon correlation function $T_{G,F}^{(f,d)}(x,x)$ proposed in Eq. (3.57). Since the SSAs in SIDIS has relatively simple dependence on the tri-gluon correlation functions, we choose $\lambda_f = +0.07$ GeV and present in the following the SSAs of D meson production coming from the contribution of $T_{G,F}^{(f)}(x,x)$ only. The full dependence is easily recovered: if the contribution from $T_{G,F}^{(d)}(x,x)$ is also included, the SSAs for D meson will be doubled if $T_{G,F}^{(d)} = T_{G,F}^{(f)}$ and vanish if $T_{G,F}^{(d)} = -T_{G,F}^{(f)}$. However, the situation will be opposite for $\bar{D}$ meson.

In order to present the SSA and its angular dependence on the ϕ, the angle between the hadron plane and the lepton plane, we define the ϕ-integrated single spin azimuthal asymmetries as

$$\langle \cos(n\phi) \rangle = \frac{1}{\sin\phi_s} \frac{\int_0^{2\pi} d\phi \cos(n\phi) \frac{d\Delta\sigma(s_T)}{dx_B dy dz_h dP_{h\perp}^2 d\phi}}{\int_0^{2\pi} d\phi \frac{d\sigma}{dx_B dy dz_h dP_{h\perp}^2 d\phi}}, \tag{3.59}$$

which gives

$$\langle 1\rangle = \frac{\Delta\sigma_0}{\sigma_0^U}, \qquad \langle \cos\phi\rangle = \frac{\Delta\sigma_1}{2\sigma_0^U}, \qquad \langle \cos 2\phi\rangle = \frac{\Delta\sigma_2}{2\sigma_0^U}. \tag{3.60}$$

In Fig. 3.10 we plot the SSAs as a function of z_h (left) and $P_{h\perp}$ (right) for the COMPASS kinematics. The asymmetries, $\langle 1\rangle$, $\langle\cos\phi\rangle$, and $\langle\cos 2\phi\rangle$, defined in Eq. (3.60), are shown by the solid, dot-dashed, and dotted curves, respectively. For a comparison between the size of the "derivative" and the "non-derivative" terms, we also show, by the dashed curves, the contribution to the SSA, $\langle 1\rangle$, from the derivative term only. It is clear that the derivative term dominates over the whole kinematic region. The asymmetries, $\langle\cos\phi\rangle$ and $\langle\cos 2\phi\rangle$, are too small to be observed experimentally. The SSA, $\langle 1\rangle$, is of the order of 10%, and could be measurable at COMPASS experiment.

Fig. 3.10 indicates that the SSA hits a minimum at $z_h \sim 0.5$ and increases very fast when z_h becomes very large or very small. This is because the SSA, $\langle 1\rangle \sim 1/(1-x_{\rm min})$, due to the derivative of $T_{G,F}^{(f,d)}(x,x)$ [16]. From the definition of $x_{\rm min}$ in Eq. (3.21), the $z_h(1-z_h)$ has a maximum at $z_h = 0.5$. Therefore, $x_{\rm min}$ increases, equivalently, the SSA increases when z_h becomes either smaller or larger than 0.5. When z_h is much further away from the central value 0.5, the $x_{\rm min}$ becomes so large that the perturbatively calculated asymmetry could increase sharply, which could signal a breakdown of the twist-three approximation and a need of higher power corrections. Nevertheless, the increase of the SSA when z_h is moving away from the central value 0.5 has the same physics origin as the observed increase of the SSA as a function of increasing x_F (or rapidity y) in the hadronic pion production [21, 23], and it could be tested in the COMPASS experiment.

Fig. 3.10 also indicates a monotonic increase of the SSA as a function of $P_{h\perp}$. Although we expect the SSA to fall when $P_{h\perp}$ increases, a natural behavior of the twist-three effect in QCD collinear factorization, the enhancement from the derivative of the $T_{G,F}^{(f,d)}(x,x)$ at large x wins over the suppression from large $P_{h\perp}$ due to the limited phase space at COMPASS kinematics. As we will see below, the decrease of the SSA as the increase of $P_{h\perp}$ is clearly seen at the eRHIC kinematics.

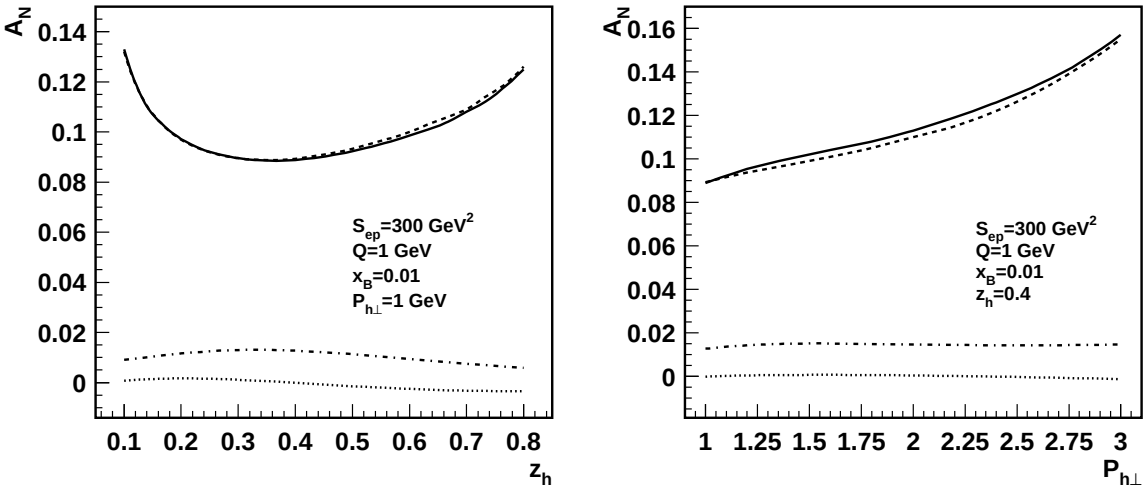

Figure 3.10 Single-transverse-spin-asymmetries defined in Eq. (3.60) for D^0 production in SIDIS for COMPASS kinematics. The curves are: solid-$\langle 1\rangle$, dashed-$\langle 1\rangle$ with derivative-term only, dot-dashed-$\langle\cos\phi\rangle$, and dotted-$\langle\cos 2\phi\rangle$.

Similarly, we plot the SSAs for D^0 production for the eRHIC kinematics in Fig. 3.11. Due to the higher collision energy, the effective gluon momentum fraction x that dominates the SSAs is smaller, which leads to a smaller derivative of $T_{G,F}^{(f,d)}(x,x)$ and a smaller SSAs. Similar feature has been seen in the SSA for hadronic pion production when we compare the data from the fixed-target experiments with that from RHIC experiments. The 5% SSA for D-meson production at eRHIC could be significant.

The slightly different shape of the SSA as a function of z_h is purely a consequence of the difference in effective range of parton momentum fraction x. That is, the z_h-dependence of the SSA provides a good measurement of the x-dependence of the correlation function, $T_{G,F}^{(f,d)}(x,x)$. On the other hand, the slow falloff of the SSA as a function $P_{h\perp}$ is natural due to the asymptotic $\lambda_f/P_{h\perp}$ behavior of the twist-3 contribution when $P_{h\perp}$ increases. Of course, as discussed above, the $1/(1-x_{\min})$ dependence of the twist-three formalism compensates some of the $1/P_{h\perp}$ falloff due to the phase space limit on parton momentum fraction x.

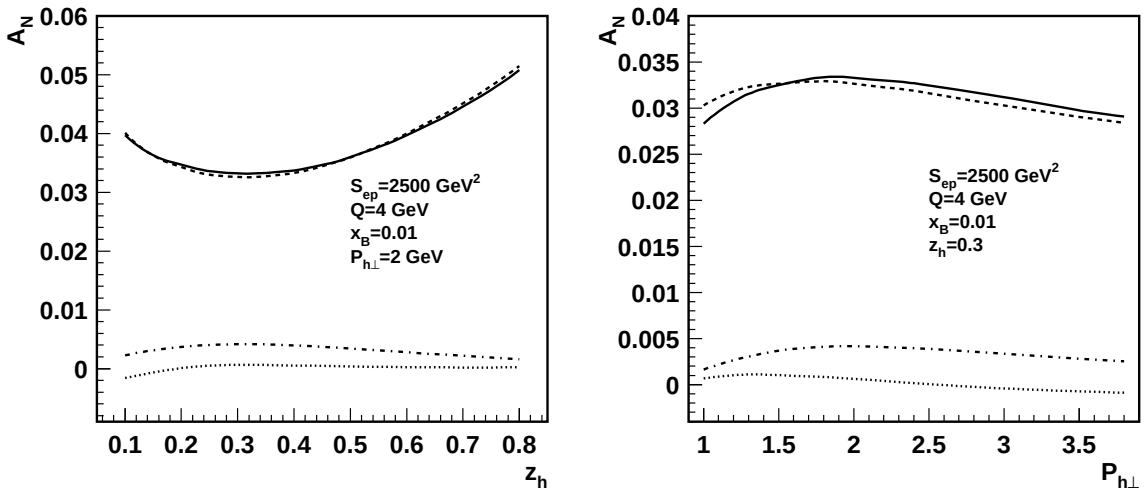

Figure 3.11 Single-transverse-spin-asymmetries defined in Eq. (3.60) for D^0 production in SIDIS for eRHIC kinematics. The curves are: solid-$\langle 1\rangle$, dashed-$\langle 1\rangle$ with derivative-term only, dot-dashed-$\langle\cos\phi\rangle$, and dotted-$\langle\cos 2\phi\rangle$.

3.3.2 Numerical estimate of the SSAs in hadronic collisions

In this section, we estimate the size of the SSAs for D and $\bar{D}$ meson production in $p^{\uparrow}p$ collisions at RHIC at $\sqrt{s} = 200$ GeV.

In order to treat the kinematic charm mass effects in the fragmentation process, we adopt one of the choices introduced in Ref. [38], which corresponds to setting $P_{h\perp} = zp_{c\perp}$ and $y_D = y_c \equiv y$, where $P_{h\perp}$ ($p_{c\perp}$) and y_D (y_c) are the transverse momentum and rapidity of the D meson (charm quark), respectively. With this choice, we then have for $\tilde{s}, \tilde{t}, \tilde{u}$ and the Feynman variable x_F:

$$\tilde{s} = x'xS, \qquad \tilde{t} = -xm_{c\perp}\sqrt{S}e^{-y}, \qquad \tilde{u} = -x'm_{c\perp}\sqrt{S}e^{y}, \qquad x_F = \frac{m_{h\perp}}{\sqrt{S}}\left(e^{y} - e^{-y}\right), \tag{3.61}$$

where $m_{c\perp} = \sqrt{m_c^2 + p_{c\perp}^2}$ and $m_{h\perp} = \sqrt{m_h^2 + P_{h\perp}^2}$.

Since the SSAs of open charm production in hadronic collisions depend on both quark-gluon and tri-gluon correlation functions, the situation is slightly more complicated than that in SIDIS. In order to cover a range of possibilities for the nonperturbative correlation functions, we introduce three sets of values for the parameters λ_f and λ_d: (1) $\lambda_f = \lambda_d = 0.07$ GeV, (2)

$\lambda_f = \lambda_d = 0$, and (3) $\lambda_f = -\lambda_d = 0.07$ GeV, corresponding to the assumptions: $T^{(f)}_{G,F} = T^{(d)}_{G,F}$, $T^{(f)}_{G,F} = T^{(d)}_{G,F} = 0$, and $T^{(f)}_{G,F} = -T^{(d)}_{G,F}$, respectively. In principle, the signs and the values of λ_f and λ_d, as well as the functional form of the correlation functions should be fixed by future data.

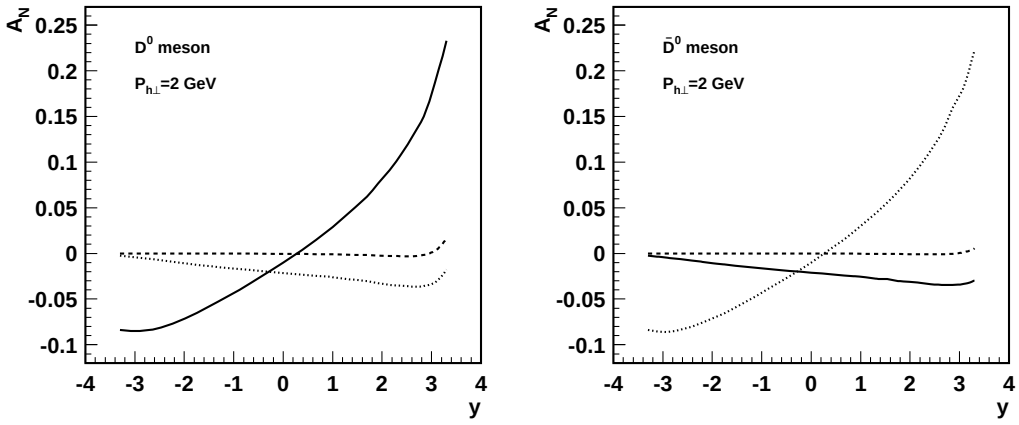

Figure 3.12 The SSA as a function of rapidity y for D^0 meson (left) and $\bar{D}^0$ meson production (right) at $\sqrt{s} = 200$ GeV and $P_{h\perp} = 2$ GeV. The curves are: solid ($\lambda_f = \lambda_d = 0.07$ GeV), dashed ($\lambda_f = \lambda_d = 0$), dotted ($\lambda_f = -\lambda_d = 0.07$ GeV).

In Figs. 3.12 and 3.13 we plot the SSAs, A_N, for the production of D and $\bar{D}$ mesons as functions of rapidity y and Feynman-x_F, respectively. We count positive rapidity in the forward direction of the polarized proton. The solid, dashed, and dotted curves correspond to the three sets of parameters: $\lambda_f = \lambda_d = 0.07$ GeV, $\lambda_f = \lambda_d = 0$, and $\lambda_f = -\lambda_d = 0.07$ GeV, respectively. From the dashed curves in Figs. 3.12 and 3.13, it is clear that the quark-gluon correlation function $T_{q,F}$ alone generates a very small single transverse-spin asymmetry at RHIC energy. This is because of the dominance of the gg fusion contribution over the $q\bar{q}$ one in the spin-averaged cross section in the denominator of A_N. In other words, any significant size of the SSA in open charm production signals the discovery of tri-gluon correlations inside a polarized proton.

The difference between the solid and dotted curves in Figs. 3.12 and 3.13 indicates that the two tri-gluon correlation functions, $T^{(f)}_{G,F}$ and $T^{(d)}_{G,F}$, may both play very important, but different, roles for the SSA in D and $\bar{D}$ meson production. In the case of D mesons, a large

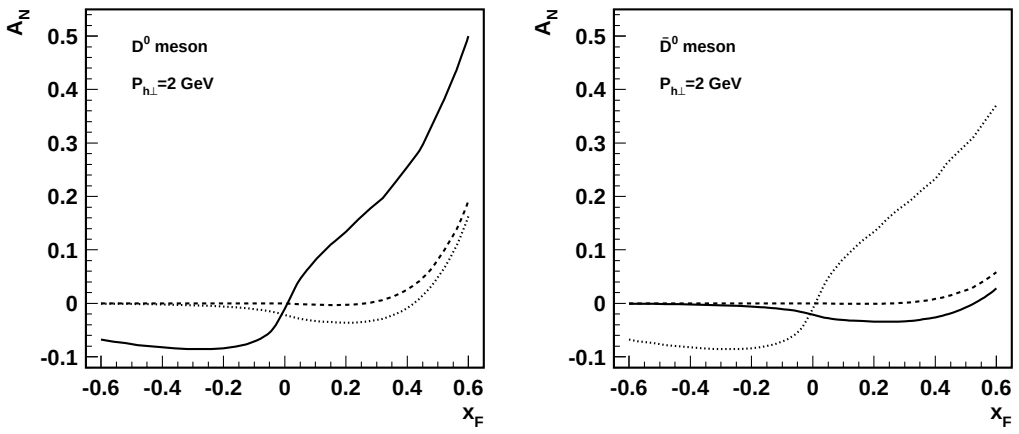

Figure 3.13 Same as Fig. 3.12, but as a function of Feynman-x_F.

A_N (see the solid curve) is obtained when $\lambda_f = \lambda_d = 0.07$ GeV, i.e., when $T_{G,F}^{(f)}$ and $T_{G,F}^{(d)}$ have the same sign. However, when their signs are opposite, their contributions to the SSA tend to cancel, leading to a much smaller SSA (dotted curve). On the contrary, for $\bar{D}$ meson production, the largest A_N is found when $T_{G,F}^{(f)}$ and $T_{G,F}^{(d)}$ have opposite signs. This is due to the fact that, as shown in Eq. (3.54), the partonic hard parts associated with $T_{G,F}^{(d)}$ change sign when going from charm to anti-charm production, while the hard parts for $T_{G,F}^{(f)}$ remain the same. As a result, the SSA for $\bar{D}$ mesons is much smaller if $T_{G,F}^{(f)}$ and $T_{G,F}^{(d)}$ have the same sign. In addition, as seen from Figs. 3.12 and 3.13, scans of the SSA from the forward to the backward region may provide good sources of information on the x-dependence or the functional form of the tri-gluon correlation functions, in particular if a sign change occurs. It is also striking to see that the asymmetry for either D or $\bar{D}$ mesons may become very large at forward rapidities at RHIC (but not for both simultaneously).

In Figs. 3.14 and 3.15, we show A_N for D^0 and $\bar{D}^0$ meson production as a function of $P_{h\perp}$, at mid-rapidity ($y = 0$) and forward-rapidity ($y = 1.8$), respectively. The absolute values of the SSAs decrease as a function of $P_{h\perp}$, which is a natural behavior of the twist-3 effect in QCD collinear factorization. As before, while the contribution by the quark-gluon correlation functions is very small, the two tri-gluon correlation functions can make sizable, and very different, contributions to the SSA, thanks to the difference in the partonic hard parts in Eq. (3.54).

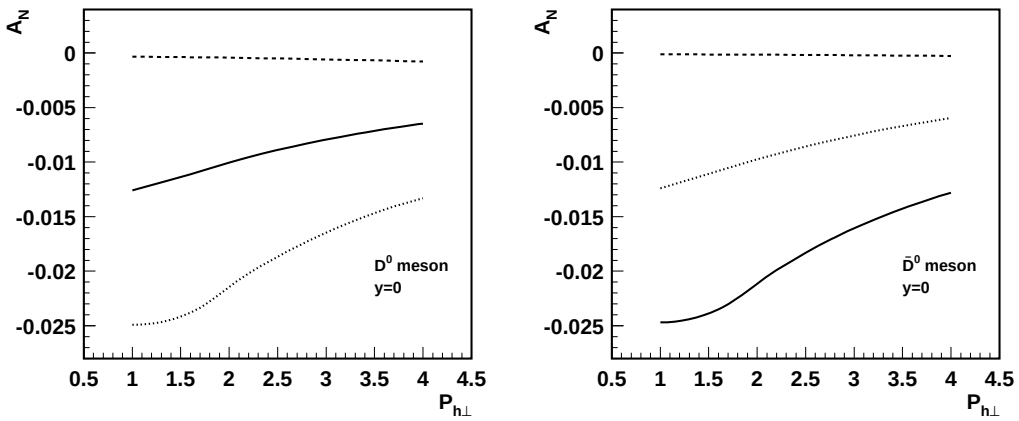

Figure 3.14 The SSA as a function of $P_{h\perp}$ for D^0 (left) and $\bar{D}^0$ mesons (right) at mid-rapidity, $y = 0$, and $\sqrt{s} = 200$ GeV. The curves are: solid ($\lambda_f = \lambda_d = 0.07$ GeV), dashed ($\lambda_f = \lambda_d = 0$), dotted ($\lambda_f = -\lambda_d = 0.07$ GeV).

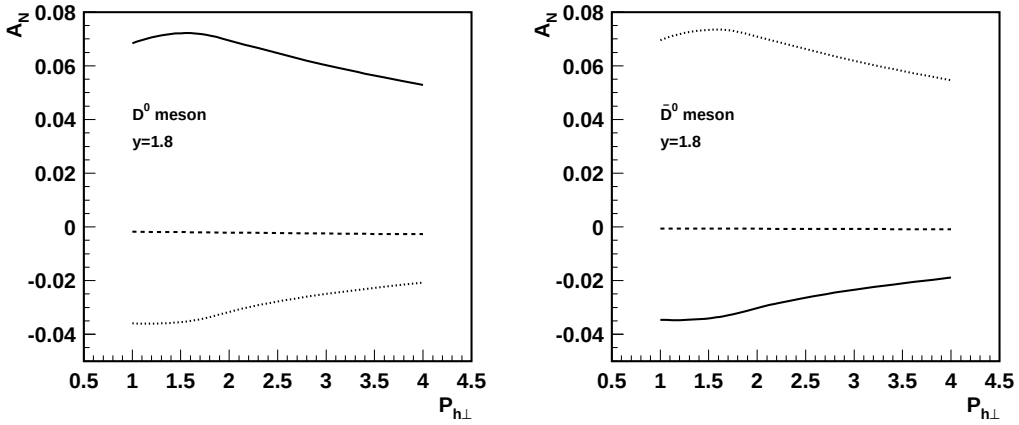

Figure 3.15 Same as Fig. 3.14, but at forward rapidity, $y = 1.8$.

3.3.3 Current experimental status

The first experimental data on the SSAs for open charm production are now emerging from PHENIX group at RHIC [39]. The first measurement of A_N of single muons from open heavy flavor decay has been made as a function of p_T in the forward and backward rapidities, see Fig. 3.16.

Obviously, the uncertainties are currently too large to allow distinction of the various models we have proposed, but the measurements are certainly very encouraging. With the Forward Vertex Detector available in the future [40], we expect great improvement and much better

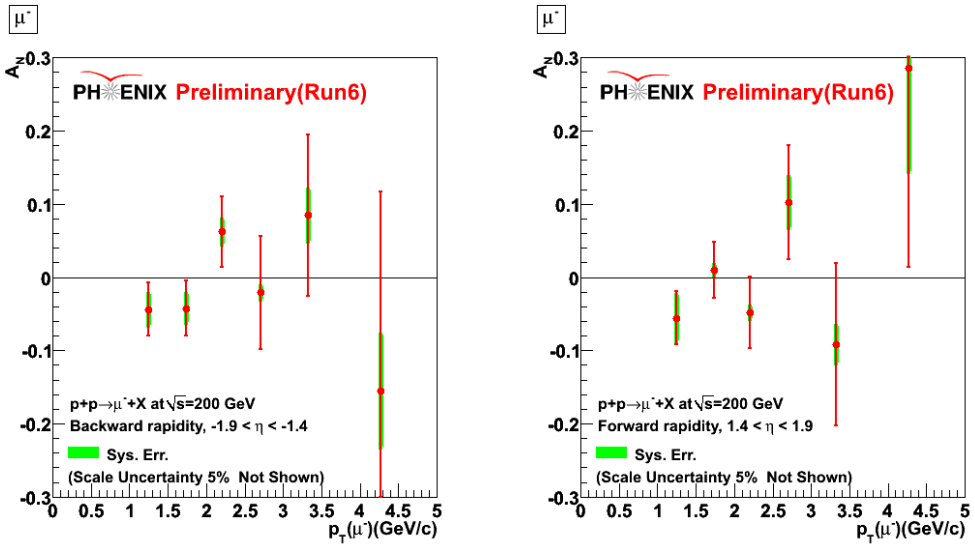

Figure 3.16 Transverse single spin asymmetry of prompt single muons (most from open flavor (charm and bottom) decay) at backward (left) and forward (right) rapidities in RHIC. (Compiled from Ref. [39])

measurements for the single transverse spin asymmetry in open charm production. With better data from RHIC and perhaps in the future in SIDIS, we will be able to extract the tri-gluon correlation functions and to learn for the first time about the dynamics of quantum correlations of gluons inside a polarized proton.

CHAPTER 4. Evolution of twist-3 correlation functions

Almost all the existing perturbative calculations of single transverse spin asymmetry, including those presented in the previous two chapters are at the leading order (LO) in strong coupling constant, $\alpha_s(\mu)$. Only very recently, a calculation of next leading order (NLO) result becomes available for Drell-Yan production [41]. A LO formalism has a strong dependence on the choice of the renormalization scale μ as well as the factorization scale μ_F, while the physically observed SSAs should not depend on the choice of the renormalization and/or the factorization scale. The strong dependence on the choice of renormalization and factorization scale is an artifact of the lowest order perturbative calculation, and a significant cancellation of the scale dependence between the leading and the next-to-leading order (NLO) contribution is expected from the QCD factorization theorem [12, 13, 14, 19]. In order to test QCD dynamics for SSAs, it is necessary to calculate the evolution (or the scale dependence) of the universal long-distance distributions and to evaluate the perturbative short-distance contribution beyond the lowest order.

In this chapter, we derive the evolution equations of the correlation functions constructed in Chapter 2. We first introduce the Feynman diagram representation for these twist-3 correlation functions that are relevant to the SSAs. From the operator definition of the twist-3 correlation functions, we then derive the cut vertices in momentum space to explicitly connect these correlation functions to Feynman diagrams [42]. Following the technique introduced in Ref. [43], we derive the evolution equations in two steps. First, we factorize, in terms of QCD collinear factorization approach [12, 44, 45], the perturbative modification to the twist-3 correlation functions into a convolution of the short-distance evolution kernels with the twist-3 correlation functions. Then, we calculate corresponding evolution kernels in the light-cone

gauge. We also provide the prescription to calculate the evolution kernels in a covariant gauge which should give the same results. Finally we discuss the scale dependence of these correlation functions by solving the evolution equations.

4.1 Feynman diagram representation and cut vertex

In this section we introduce the Feynman diagram representation of the twist-3 quark-gluon and tri-gluon correlation functions constructed in chapter 2. We derive cut vertices in momentum space to connect the Feynman diagrams to specific twist-3 correlation functions [42].

In QCD collinear factorization approach to SSAs, the twist-3 three-parton correlation functions measure the net effect of the quantum interference between two scattering amplitudes of the transversely polarized hadron: one with single active parton and the other with two active partons, participating in the short-distance hard scattering [16]. Like the normal PDFs, the quark-gluon and tri-gluon correlation functions could be represented by the cut forward scattering diagrams as sketched in Figs. 4.1(a) and 4.1(b), respectively. The cut represents a particular final-state. The Feynman diagrams in Fig. 4.1 should include all possible cuts to sum over all possible final states. We suppress the explicit cuts for the diagrams in Fig. 4.1 since the matrix element of the three-parton correlation functions with the middle gluon field strength in the left side of the cut is equal to the matrix element with the gluon field strength in the right side of the final-state cut. This is because the field operators of hadronic matrix elements commute on the light-cone [19, 46]. Because of the odd number of active fields defining the twist-3 correlation functions, unlike the normal PDFs, these correlation functions do not have a probability interpretation.

As discussed in chapter 2, one set of twist-3 correlation functions is expressed in terms of a *sum* of two spin-dependent twist-3 correlation functions, as in Eqs. (2.19) and (2.21), and the other by a *difference* of two spin-dependent twist-3 correlation functions, as in Eqs. (2.28) and (2.30). These spin-dependent twist-3 correlation functions are given in terms of explicit matrix elements of the transverse-spin dependent hadronic state and could be represented by Feynman

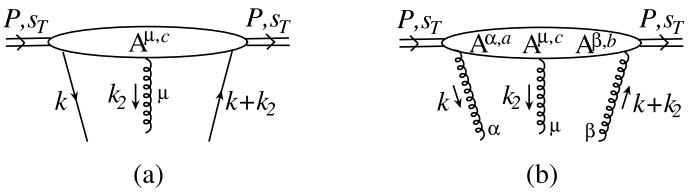

Figure 4.1 Feynman diagrams that contribute to the twist-3 quark-gluon (a) and tri-gluon (b) correlation functions. α, β, μ and a, b, c are Lorentz and color indices of gluon field operators, respectively.

diagrams. However, since all gluon lines in Feynman diagrams are connected to gluon fields, calculating the Feynman diagrams in Fig. 4.1 does not immediately give the twist-3 correlation functions whose gluonic degree of freedom is represented by the field strength, $F^{+\mu}$, not the gluon field, A^μ. Therefore, in order to fully define the Feynman diagram representation of the spin-dependent twist-3 correlation functions, we need to derive the cut vertex [42] to connect the operator definition of the spin-dependent twist-3 correlation functions to the cut forward scattering Feynman diagrams in Fig. 4.1. With different cut vertices, the same diagrams in Fig. 4.1 can represent both sets of the spin-dependent twist-3 correlation functions.

To derive the cut vertex to connect the spin-dependent quark-gluon correlation function in Eq. (2.20) to the Feynman diagram in Fig. 4.1(a), we reexpress the operator definition of the correlation function in Eq. (2.20) in terms of hadronic matrix elements of quark and gluon operators in momentum space and find,

$$\begin{aligned}
\widetilde{\mathcal{T}}_{q,F}(x, x+x_2, \mu_F, s_T) &= \int \frac{d^4k}{(2\pi)^4}\,\frac{d^4k_2}{(2\pi)^4}\,\langle P, s_T|\,\widetilde{\overline{\psi}}_{q,i}(-k-k_2) \\
&\quad \times \left[\frac{\gamma^+}{2P^+}\,\delta\left(x-\frac{k^+}{P^+}\right) x_2\,\delta\left(x_2-\frac{k_2^+}{P^+}\right)\left(i\,\epsilon^{s_T\sigma n\bar{n}}\right)\right. \\
&\quad \left.\times\left(-g_{\sigma\mu}+\frac{k_{2\sigma}n_\mu}{k_2^+}\right)\right](\mathcal{C}_q)^c_{ij}\,\widetilde{A}^{\mu,c}(k_2)\,\widetilde{\psi}_{q,j}(k)\,|P,s_T\rangle\,, \qquad (4.1)
\end{aligned}$$

where the fermionic color contraction factor $\mathcal{C}_q$ is given by

$$(\mathcal{C}_q)^c_{ij} = (t^c)_{ij}\ , \qquad (4.2)$$

with quark and gluon color indices, $i, j = 1, 2, 3 = N_c$ and $c = 1, 2, ..., 8 = N_c^2 - 1$, respectively,

and t^c are the generators of the fundamental representation of SU(3) color. The field operators listed with "$\sim$" in Eq. (4.1) represent the momentum space field operators of those in Eq. (2.20). The matrix element, $\langle P, s_T | \, \widetilde{\overline{\psi}}_{q,i}(-k-k_2) \widetilde{A}^{\mu,c}(k_2) \, \widetilde{\psi}_{q,j}(k) \, | P, s_T \rangle$, in Eq. (4.1) can be represented by the Feynman diagram in Fig. 4.1(a). By comparing the definition of quark-gluon correlation function in Eq. (4.1) and the Feynman diagram in Fig. 4.1(a), it is clear that we can derive the quark-gluon correlation function, $\widetilde{\mathcal{T}}_{q,F}$, from the Feynman diagram in Fig. 4.1(a) by contracting the quark and gluon lines with the expression in the square brackets and the color contraction factor $(t^c)_{ij}$, plus the integration over the loop momenta in Eq. (4.1). The expression in the square brackets plus the color contraction factor $\mathcal{C}_q$ defines the cut vertex that connects the Feynman diagram in Fig. 4.1(a) to the quark-gluon correlation function $\widetilde{\mathcal{T}}_{q,F}$ in Eq. (2.20),

$$\mathcal{V}_{q,F} \equiv \frac{\gamma^+}{2P^+} \, \delta\left(x - \frac{k^+}{P^+}\right) \left(i \, \epsilon^{s_T \sigma n \bar{n}}\right) \, x_2 \, \delta\left(x_2 - \frac{k_2^+}{P^+}\right) \left[-g_{\sigma\mu} \, + \frac{k_{2\sigma} n_\mu}{k_2^+} \right] \mathcal{C}_q \, . \tag{4.3}$$

Similarly, we can rewrite the tri-gluon correlation function in Eq. (2.22) as

$$\begin{aligned} \widetilde{\mathcal{T}}_{G,F}^{(f,d)}(x, x+x_2, \mu_F, s_T) \;\; = \;\; & \int \frac{d^4k}{(2\pi)^4} \, \frac{d^4k_2}{(2\pi)^4} \, \langle P, s_T | \, \widetilde{A}^{\beta,b}(-k-k_2) \, \widetilde{A}^{\mu,c}(k_2) \, \widetilde{A}^{\alpha,a}(k) \, | P, s_T \rangle \\ & \times \left[\left(-g_{\alpha\beta} + \frac{(k+k_2)_\alpha n_\beta}{(k+k_2)^+} + \frac{k_\beta \, n_\alpha}{k^+} - \frac{k \cdot (k+k_2) \, n_\alpha n_\beta}{k^+ \, (k+k_2)^+} \right) \right. \\ & \times x(x+x_2) \delta\left(x - \frac{k^+}{P^+}\right) x_2 \, \delta\left(x_2 - \frac{k_2^+}{P^+}\right) \\ & \left. \times \left(i \, \epsilon^{s_T \sigma n \bar{n}}\right) \left(-g_{\sigma\mu} + \frac{k_{2\sigma} \, n_\mu}{k_2^+} \right) \right] (\mathcal{C}_g)_{bca}^{(f,d)} \, , \end{aligned} \tag{4.4}$$

where the gluonic color contraction factor $\mathcal{C}_g$ is given by

$$(\mathcal{C}_g)_{bca}^{(f)} = i f_{bca} = (\mathcal{F}^c)_{ba} \, , \quad \text{and} \quad (\mathcal{C}_g)_{bca}^{(d)} = d_{bca} \, , \tag{4.5}$$

where $\mathcal{F}^c$ are the generators of adjoint representation of SU(3) color. In Eq. (4.4), the matrix element $\langle P, s_T | \, \widetilde{A}^{\beta,b}(-k-k_2) \, \widetilde{A}^{\mu,c}(k_2) \, \widetilde{A}^{\alpha,a}(k) \, | P, s_T \rangle$ can be represented by the Feynman diagram in Fig. 4.1(b). Similar to the situation of quark-gluon correlation, the expression in the square brackets plus the color contraction factor $\mathcal{C}_{bca}^{(f,d)}$ defines the cut vertex for calculating

the tri-gluon correlation function $\widetilde{\mathcal{T}}_{G,F}^{(f,d)}$ from the diagram in Fig. 4.1(b),

$$\begin{aligned}\mathcal{V}_{G,F} &\equiv x(x+x_2)\left(-g_{\alpha\beta}+\frac{(k+k_2)_\alpha n_\beta}{(k+k_2)^+}+\frac{k_\beta\, n_\alpha}{k^+}-\frac{k\cdot(k+k_2)\, n_\alpha n_\beta}{k^+\,(k+k_2)^+}\right)\\ &\quad\times\delta\left(x-\frac{k^+}{P^+}\right)x_2\,\delta\left(x_2-\frac{k_2^+}{P^+}\right)\left(i\,\epsilon^{s_T\sigma n\bar{n}}\right)\left[-g_{\sigma\mu}+\frac{k_{2\sigma}\,n_\mu}{k_2^+}\right](\mathcal{C}_g)_{bca}^{(f,d)}\ . \quad (4.6)\end{aligned}$$

Similarly, by rewriting the operator definitions of the second set of spin-dependent twist-3 correlation functions in terms of quark and gluon field operators in momentum space, we derive the following cut vertices,

$$\mathcal{V}_{\Delta q,F}\equiv\frac{\gamma^+\gamma^5}{2P^+}\,\delta\left(x-\frac{k^+}{P^+}\right)(-s_T^\sigma)\;x_2\,\delta\left(x_2-\frac{k_2^+}{P^+}\right)\left[-g_{\sigma\mu}\;+\frac{k_{2\sigma}n_\mu}{k_2^+}\right]\mathcal{C}_q \quad (4.7)$$

for connecting the same Feynman diagram in Fig. 4.1(a) to the second set quark-gluon correlation function $\widetilde{\mathcal{T}}_{\Delta q,F}(x,x+x_2,\mu_F,s_T)$ in Eq. (2.29), and

$$\begin{aligned}\mathcal{V}_{\Delta G,F} &\equiv x(x+x_2)\,(i\epsilon_{\perp\rho\lambda})\left[-g^{\rho\beta}+\frac{(k+k_2)^\rho n^\beta}{(k+k_2)^+}\right]\left[-g^{\lambda\alpha}+\frac{k_\lambda\, n_\alpha}{k^+}\right]\delta\left(x-\frac{k^+}{P^+}\right)\\ &\quad\times x_2\,\delta\left(x_2-\frac{k_2^+}{P^+}\right)(-s_T^\sigma)\;\left[-g_{\sigma\mu}+\frac{k_{2\sigma}\,n_\mu}{k_2^+}\right]\mathcal{C}_g^{(f,d)} \quad (4.8)\end{aligned}$$

for connecting the same Feynman diagram in Fig. 4.1(b) to the second set tri-gluon correlation function $\widetilde{\mathcal{T}}_{\Delta G,F}(x,x+x_2,\mu_F,s_T)$ in Eq. (2.31). The color factors in Eqs. (4.7) and Eqs. (4.8) are the same as those in Eqs. (4.3) and Eqs. (4.6), respectively.

For our calculation of the evolution kernels in the next section in the light-cone gauge, $n\cdot A=0$, the cut vertices are simplified as,

$$\mathcal{V}_{q,F}^{\rm LC} = \frac{\gamma^+}{2P^+}\,\delta\left(x-\frac{k^+}{P^+}\right)x_2\,\delta\left(x_2-\frac{k_2^+}{P^+}\right)\left(i\,\epsilon^{s_T\sigma n\bar{n}}\right)[-g_{\sigma\mu}]\;\mathcal{C}_q \quad (4.9)$$

$$\mathcal{V}_{G,F}^{\rm LC} = x(x+x_2)\,(-g_{\alpha\beta})\,\delta\left(x-\frac{k^+}{P^+}\right)x_2\,\delta\left(x_2-\frac{k_2^+}{P^+}\right)\left(i\,\epsilon^{s_T\sigma n\bar{n}}\right)[-g_{\sigma\mu}]\;\mathcal{C}_g^{(f,d)} \quad (4.10)$$

$$\mathcal{V}_{\Delta q,F}^{\rm LC} = \frac{\gamma^+\gamma^5}{2P^+}\,\delta\left(x-\frac{k^+}{P^+}\right)x_2\,\delta\left(x_2-\frac{k_2^+}{P^+}\right)(-s_T^\sigma)\;[-g_{\sigma\mu}]\;\mathcal{C}_q \quad (4.11)$$

$$\mathcal{V}_{\Delta G,F}^{\rm LC} = x(x+x_2)\left(i\epsilon_\perp^{\beta\alpha}\right)\delta\left(x-\frac{k^+}{P^+}\right)x_2\,\delta\left(x_2-\frac{k_2^+}{P^+}\right)(-s_T^\sigma)\;[-g_{\sigma\mu}]\;\mathcal{C}_g^{(f,d)} \quad (4.12)$$

for correlation functions, $\widetilde{\mathcal{T}}_{q,F}$, $\widetilde{\mathcal{T}}_{G,F}^{(f,d)}$, $\widetilde{\mathcal{T}}_{\Delta q,F}$, $\widetilde{\mathcal{T}}_{\Delta G,F}^{(f,d)}$, respectively.

4.2 Factorization and evolution equations

In order to derive the evolution equations and evolution kernels from the definition of the twist-3 correlation functions, we need to compute the perturbative modification to these correlation functions caused by the quark-gluon interaction in QCD [43]. For example, we need to calculate the diagram in Fig. 4.2 for extracting the flavor non-singlet evolution kernel of the quark-gluon correlation function.

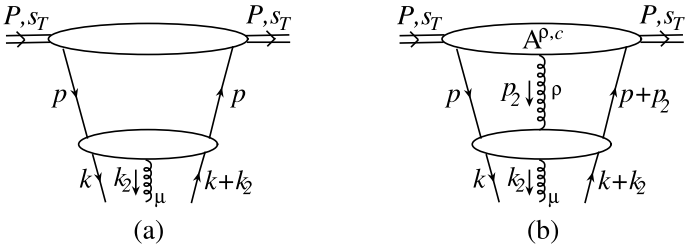

Figure 4.2 Feynman diagrams that contribute to the flavor non-singlet change of the twist-3 quark-gluon correlation function where μ, ρ and c are Lorentz and color indices of gluon field operators, respectively. The lower part of quark and gluon lines are contracted to the cut vertex that defines the quark-gluon correlation function.

We first evaluate the perturbative change to all spin-dependent correlation functions, $\widetilde{\mathcal{T}}_{q,F}$, $\widetilde{\mathcal{T}}_{G,F}^{(f,d)}$, $\widetilde{\mathcal{T}}_{\Delta q,F}$, and $\widetilde{\mathcal{T}}_{\Delta G,F}^{(f,d)}$, because they are defined in terms of hadronic matrix elements and represented by the Feynman diagrams with proper cut vertices. We follow the standard QCD collinear factorization approach to factorize the perturbative change to these spin-dependent correlation functions into short-distance evolution kernels convoluted with corresponding gauge invariant long-distance matrix elements or the correlation functions [43, 44, 45]. From Eqs. (2.19), (2.21), (2.28), and (2.30), we then derive the evolution equations for the two sets of twist-3 correlation functions that are responsible for generating the SSAs in QCD collinear factorization approach.

4.2.1 Non-singlet case: quark-gluon correlations

We start with the flavor non-singlet change to the quark-gluon correlation function, $\widetilde{\mathcal{T}}_{q,F}$, as represented by the diagrams in Fig. 4.2 with the cut vertex in Eq. (4.3). For the twist-3 correlation functions relevant to the SSAs, we are interested in the difference of the diagrams in Fig. 4.2 with hadron spin s_T and that with $-s_T$. The only surviving leading twist matrix element from the top of the diagram in Fig. 4.2(a) after taking the difference is the transversity distribution that does not contribute to the change of the quark-gluon correlation function of massless quark due to the symmetry of time-reversal or simply due to an odd number of gamma matrices in the spinor trace. However, the twist-3 or sub-leading contribution from the diagram in Fig. 4.2(a) can be combined with the leading contribution of the diagram in Fig. 4.2(b) due to color gauge invariance [19, 28, 44, 45]. Long-distance physics of the combined contribution from two diagrams in Fig. 4.2 could be expressed in terms of four twist-3 long-distance matrix elements or correlation functions, $T^{(V,A)}_{(D,F)}$, as defined in Ref. [17], where superscripts V and A represent the vector and axial vector current, respectively, and subscripts, D and F, refer to the standard QCD covariant derivative and field strength, respectively. The correlation functions, T^V_F and T^A_F, correspond to our spin-dependent quark-gluon correlation functions, $\widetilde{\mathcal{T}}_{q,F}$ and $\widetilde{\mathcal{T}}_{\Delta q,F}$, respectively, while the other two functions could be obtained by replacing the field strength operator ${F_\sigma}^+$ by the covariant derivative operator D_σ. As explained in Ref. [17], the two correlation functions with the covariant derivative operator do not contribute to the SSAs.

We now provide a detailed derivation of the projection operator for extracting the flavor non-singlet evolution kernels or the short-distance contribution from both diagrams in Fig. 4.2. There are two sources of twist-3 or subleading power contribution from the diagram in Fig. 4.2(a) [19, 44, 45]. One is from the transverse momentum expansion of the parton momenta entering the bottom part of the diagram, which leads to the contribution associated with matrix elements, $T^{V,A}_D$, thus does not contribute to the SSAs. The other is from the spinor trace decomposition when the bottom part of the diagram is contracted by $\gamma \cdot n$ instead of the leading $\gamma \cdot P$ [44, 45], so-called contact contribution [19, 45]. Although the matrix element of

this term has only two quark field operators, it can be expressed in terms of the same matrix element of two quark fields and a gluon field, $T_F^{V,A}$, after applying the equation of motion [44]. That is, this part of subleading contribution from the diagram in Fig. 4.2(a) can be represented by the same diagram in Fig. 4.2(b) except that the partonic Feynman diagrams in the bottom part of the diagram are given by the diagrams with the contact interaction [19, 45]. Therefore, we can derive the full flavor non-singlet evolution kernels from the diagram in Fig. 4.2(b) with the understanding that the bottom part of the diagram also includes those with the contact interaction or the special propagator [19, 45].

We represent the perturbative change to $\widetilde{\mathcal{T}}_{q,F}$ from the diagram in Fig. 4.2(b) as

$$d\widetilde{\mathcal{T}}_{q,F}(x, x+x_2, \mu_F, s_T) \equiv \int \frac{d^4p\, d^4p_2}{(2\pi)^8}\ \mathrm{Tr}\left[\hat{T}^\rho(p, p_2, P, s_T)\hat{H}_\rho(p, p_2, x, x_2, \mu_F)\right], \tag{4.13}$$

where the "Tr" represents the trace over the fermion fields' spinor indices, and $\hat{T}$ and $\hat{H}$ represent the top part and the bottom part of the Feynman diagram, respectively. In the momentum space, the $\hat{T}$ is given by the matrix element,

$$\hat{T}^\rho(p, p_2, P, s_T) = \langle P, s_T|\, \widetilde{\overline{\psi}}_{q,i}(-p-p_2)\widetilde{A}^{\rho,c}(p_2)\, \widetilde{\psi}_{q,j}(p)\, |P, s_T\rangle\,, \tag{4.14}$$

where i, j are color indices of the quark fields and ρ, c are Lorentz and color indices of the gluon field, respectively. The $\hat{H}$ represents the bottom blob that includes all cut Feynman diagrams for the given external quark and gluon lines. The list of all cut diagrams at order of α_s will be given in the next section when we present the calculation of evolution kernels. The bottom quark and gluon lines of these diagrams are contracted by the cut vertex that defines the correlation function. The dependence of x and x_2 in the argument of $\hat{H}$ in Eq. (4.13) is from the cut vertex, and the scale μ_F represents the hardness or the off-shellness of the parton momenta, k and k_2. To pick up the leading power contribution from the perturbative modification to the quark-gluon correlation function, we first separate the spinor trace for the

case of massless partons by [45]

$$\hat{H}_\rho(p,p_2,x,x_2,\mu_F) \approx H_{\rho,\alpha}(p,p_2,x,x_2,\mu_F)\left(\frac{1}{2}\gamma^\alpha\right) + \widetilde{H}_{\rho,\alpha}(p,p_2,x,x_2,\mu_F)\left(\frac{1}{2}\gamma^\alpha\left(i\gamma^5\right)\right)+\dots, \tag{4.15}$$

where "..." represents terms with even number of γ-matrices and subleading, and

$$H_{\rho,\alpha}(p,p_2,x,x_2,\mu_F) = \frac{1}{2}\mathrm{Tr}\left[\hat{H}_\rho(p,p_2,x,x_2,\mu_F)\gamma_\alpha\right], \tag{4.16}$$

$$\widetilde{H}_{\rho,\alpha}(p,p_2,x,x_2,\mu_F) = \frac{1}{2}\mathrm{Tr}\left[\hat{H}_\rho(p,p_2,x,x_2,\mu_F)\gamma_\alpha\left(i\gamma^5\right)\right]. \tag{4.17}$$

In order to derive the contribution from the first term in Eq. (4.15) in details, we introduce

$$I_q \equiv \int \frac{d^4p\,d^4p_2}{(2\pi)^8}\; T^{\rho,\alpha}(p,p_2,P,s_T)H_{\rho,\alpha}(p,p_2,x,x_2,\mu_F), \tag{4.18}$$

with

$$T^{\rho,\alpha}(p,p_2,P,s_T) = \frac{1}{2}\mathrm{Tr}\left[\hat{T}^\rho(p,p_2,P,s_T)\gamma^\alpha\right]. \tag{4.19}$$

We then apply the strong ordering in the off-shellness of active partons, $|p^2| \ll \mu_F^2$ and $|p_2^2| \ll \mu_F^2$, and make the collinear approximation to expand the parton momenta entering into the $\hat{H}$ in Fig. 4.2(b) around $p = \xi P$ and $p_2 = \xi_2 P$ as

$$H_{\rho,\alpha}(p,p_2,x,x_2,\mu_F) \approx H_{\rho,\alpha}(\xi P,\xi_2 P,x,x_2,\mu_F) + \frac{\partial H_{\rho,\alpha}(\xi P,\xi_2 P,x,x_2,\mu_F)}{\partial p^\beta}(p-\xi P)^\beta + \frac{\partial H_{\rho,\alpha}(\xi P,\xi_2 P,x,x_2,\mu_F)}{\partial p_2^\beta}(p_2-\xi_2 P)^\beta+\dots. \tag{4.20}$$

By substituting Eq. (4.20) into Eq. (4.18), we can rewrite the I_q as

$$\begin{aligned} I_q \;\approx\; & \int d\xi\, d\xi_2\, T^{\rho,\alpha}(\xi,\xi+\xi_2)\, H_{\rho,\alpha}(\xi,\xi_2,x,x_2,\mu_F) \\ & + \int d\xi\, d\xi_2\, T_1^{\rho,\alpha,\beta}(\xi,\xi+\xi_2)\, \frac{\partial H_{\rho,\alpha}(\xi,\xi_2,x,x_2,\mu_F)}{\partial p^\beta} \\ & + \int d\xi\, d\xi_2\, T_2^{\rho,\alpha,\beta}(\xi,\xi+\xi_2)\, \frac{\partial H_{\rho,\alpha}(\xi,\xi_2,x,x_2,\mu_F)}{\partial p_2^\beta} + \dots\,, \end{aligned} \tag{4.21}$$

where the explicit P dependence in $H_{\rho,\alpha}$ is suppressed. The correlation functions in Eq. (4.21) are given by

$$\begin{aligned} T^{\rho,\alpha}(\xi,\xi+\xi_2) &= \int \frac{d^4p\, d^4p_2}{(2\pi)^8}\, \delta\left(\xi-\frac{p^+}{P^+}\right)\delta\left(\xi_2-\frac{p_2^+}{P^+}\right) \\ &\quad \times\langle P,s_T|\,\widetilde{\overline{\psi}}_{q,i}(-p-p_2)\frac{\gamma^\alpha}{2}\widetilde{A}^{\rho,c}(p_2)\,\widetilde{\psi}_{q,j}(p)\,|P,s_T\rangle\,; \\ T_1^{\rho,\alpha,\beta}(\xi,\xi+\xi_2) &= \int \frac{d^4p\, d^4p_2}{(2\pi)^8}\, \delta\left(\xi-\frac{p^+}{P^+}\right)\delta\left(\xi_2-\frac{p_2^+}{P^+}\right)(p-\xi P)^\beta \\ &\quad \times\langle P,s_T|\,\widetilde{\overline{\psi}}_{q,i}(-p-p_2)\frac{\gamma^\alpha}{2}\widetilde{A}^{\rho,c}(p_2)\,\widetilde{\psi}_{q,j}(p)\,|P,s_T\rangle\,; \\ T_2^{\rho,\alpha,\beta}(\xi,\xi+\xi_2) &= \int \frac{d^4p\, d^4p_2}{(2\pi)^8}\, \delta\left(\xi-\frac{p^+}{P^+}\right)\delta\left(\xi_2-\frac{p_2^+}{P^+}\right)(p_2-\xi_2 P)^\beta \\ &\quad \times\langle P,s_T|\,\widetilde{\overline{\psi}}_{q,i}(-p-p_2)\frac{\gamma^\alpha}{2}\widetilde{A}^{\rho,c}(p_2)\,\widetilde{\psi}_{q,j}(p)\,|P,s_T\rangle\,. \end{aligned} \tag{4.22}$$

Finally, we decouple the contraction of Lorentz indices in the RHS of Eq. (4.21) to express the quark-gluon correlation functions in terms of the $\widetilde{\mathcal{T}}_{q,F}$, defined in Eq. (4.1), so that we can factorize the leading term of the RHS of Eq. (4.21) into a convolution of the $\widetilde{\mathcal{T}}_{q,F}$ and corresponding evolution kernel. We find

$$T^{\rho,\alpha}(\xi,\xi+\xi_2) \approx \left[\widetilde{\mathcal{C}}_q\left(\frac{-1}{\xi_2}\right)\left(i\,\epsilon^{s_T\rho n\bar{n}}\right)P^\alpha\right]\widetilde{\mathcal{T}}_{q,F}^{(\mathrm{LC})}(\xi,\xi+\xi_2,s_T)+\dots \tag{4.23}$$

where the factorization scale dependence is suppressed and the fermionic color projection operator $\widetilde{\mathcal{C}}_q$ is given by

$$(\widetilde{\mathcal{C}}_q)^c_{ji} = 2/(N_c^2-1)(t^c)_{ji}\,, \tag{4.24}$$

with the quark and gluon color indices ij and c as labeled in Fig. 4.2(a), so that $\widetilde{\mathcal{C}}_q\,\mathcal{C}_q = 1$. In Eq. (4.23), the quark-gluon correlation function $\widetilde{\mathcal{T}}_{q,F}^{(\mathrm{LC})}$ has the same definition as that of $\widetilde{\mathcal{T}}_{q,F}$ in Eq. (2.20), except the cut vertex in the square brackets is replaced by the cut vertex in the light-cone gauge in Eq. (4.9). The superscript "LC" indicates that this quark-gluon correlation function is calculated by using the light-cone gauge cut vertex instead of the full cut vertex. We find that the term proportional to $T_1^{\rho,\alpha,\beta}(\xi,\xi+\xi_2)$ in Eq. (4.21) does not give the leading power contribution. For the third term in Eq. (4.21), we have

$$T_2^{\rho,\alpha,\beta}(\xi,\xi+\xi_2) \approx \left[\widetilde{\mathcal{C}}_q\left(i\,\epsilon^{s_T\beta n\bar{n}}\right)P^\rho\,P^\alpha\right]\widetilde{\mathcal{T}}_{q,F}^{(\mathrm{CO})}(\xi,\xi+\xi_2,s_T)+\ldots \tag{4.25}$$

where the long-distance quark-gluon correlation function, $\widetilde{\mathcal{T}}_{q,F}^{(\mathrm{CO})}$, has the same definition as that of $\widetilde{\mathcal{T}}_{q,F}$ in Eq. (2.20), except the cut vertex in the square brackets is replaced by

$$\frac{\gamma^+}{2P^+}\,\delta\left(\xi-\frac{p^+}{P^+}\right)\left(i\,\epsilon^{s_T\sigma n\bar{n}}\right)\xi_2\,\delta\left(\xi_2-\frac{p_2^+}{P^+}\right)\frac{p_{2\sigma}\,n_\rho}{p_2^+}\;(\mathcal{C}_q)_{ij}^c\;, \tag{4.26}$$

which corresponds to the second term in the square brackets in Eq. (4.3). The superscript "CO" indicates that this term provides the leading contribution in a covariant gauge calculation of the correlation functions [19, 47]. From the factorized expression for the first and the third term, we find the leading contribution from the RHS of Eq. (4.21) can be factorized as

$$\begin{aligned} I_q \;\approx\; & \int d\xi\,d\xi_2\left\{\widetilde{\mathcal{T}}_{q,F}^{(\mathrm{LC})}(\xi,\xi+\xi_2,s_T)\left[\widetilde{\mathcal{C}}_q\left(\frac{-1}{\xi_2}\right)\left(i\,\epsilon^{s_T\rho\,n\bar{n}}\right)P^\alpha\,H_{\rho,\alpha}(\xi,\xi_2,x,x_2,\mu_F)\right]\right. \\ & \left.+\widetilde{\mathcal{T}}_{q,F}^{(\mathrm{CO})}(\xi,\xi+\xi_2,s_T)\left[\widetilde{\mathcal{C}}_q\left(i\,\epsilon^{s_T\beta\,n\bar{n}}\right)P^\rho\,P^\alpha\;\frac{\partial H_{\rho,\alpha}(\xi,\xi_2,x,x_2,\mu_F)}{\partial p_2^\beta}\bigg|_{p_2=\xi_2 P}\right]\right\} \\ & +\ldots\,, \end{aligned} \tag{4.27}$$

where the "..." again represents the subleading term which includes the contribution from the $T_1^{\rho,\alpha,\beta}$ in Eq. (4.21). From the definitions of $\widetilde{\mathcal{T}}_{q,F}^{(\mathrm{LC})}(\xi,\xi+\xi_2,s_T)$ and $\widetilde{\mathcal{T}}_{q,F}^{(\mathrm{CO})}(\xi,\xi+\xi_2,s_T)$, we have

$$\widetilde{\mathcal{T}}_{q,F}(\xi,\xi+\xi_2,s_T) = \widetilde{\mathcal{T}}_{q,F}^{(\mathrm{LC})}(\xi,\xi+\xi_2,s_T)+\widetilde{\mathcal{T}}_{q,F}^{(\mathrm{CO})}(\xi,\xi+\xi_2,s_T)\,. \tag{4.28}$$

Therefore, QCD color gauge invariance requires

$$\widetilde{\mathcal{C}}_q\left(\frac{-1}{\xi_2}\right)\left(i\,\epsilon^{s_T\rho\,n\bar{n}}\right)P^\alpha\,H^{(\mathrm{LC})}_{\rho,\alpha}(\xi,\xi_2,x,x_2,\mu_F)$$
$$=\widetilde{\mathcal{C}}_q\left(i\,\epsilon^{s_T\beta\,n\bar{n}}\right)P^\rho\,P^\alpha\,\left.\frac{\partial H^{(\mathrm{CO})}_{\rho,\alpha}(\xi,\xi_2,x,x_2,\mu_F)}{\partial p_2^\beta}\right|_{p_2=\xi_2 P}, \tag{4.29}$$

when the LHS is evaluated in the light-cone gauge and the RHS is evaluated in a covariant gauge. Then, the two terms in Eq. (4.27) can be combined into one term proportional to the quark-gluon correlation function, $\widetilde{\mathcal{T}}_{q,F}(\xi,\xi+\xi_2,s_T)$. Since $\widetilde{\mathcal{T}}^{(\mathrm{CO})}_{q,F}(\xi,\xi+\xi_2,s_T)$ vanishes in the light-cone gauge, the left-hand-side (LHS) of the equality in Eq. (4.29) represents the short-distance partonic part calculated in the light-cone gauge. On the other hand, the RHS of the equality in Eq. (4.29) represents the short-distance partonic part calculated in a covariant gauge [19]. This is because the matrix element $\widetilde{\mathcal{T}}^{(\mathrm{CO})}_{q,F}(\xi,\xi+\xi_2,s_T)$ dominates over $\widetilde{\mathcal{T}}^{(\mathrm{LC})}_{q,F}(\xi,\xi+\xi_2,s_T)$ in a covariant gauge calculation [19, 47]. That is, the equality in Eq. (4.29) provides an excellent consistency test for the perturbative modification of the quark-gluon correlation functions evaluated in different gauges.

By using Eqs. (4.28) and (4.29), we can combine the two factorized terms in Eq. (4.27) into one factorized term as

$$I_q \approx \int d\xi\,d\xi_2\,\widetilde{\mathcal{T}}_{q,F}(\xi,\xi+\xi_2,s_T)\,dK_{qq}(\xi,\xi+\xi_2,x,x+x_2,\mu_F)+\dots\,, \tag{4.30}$$

where the perturbative modification to the correlation function, $dK_{qq}(\xi,\xi+\xi_2,x,x+x_2,\mu_F)$, can be calculated by using either side of the equality in Eq. (4.29) depending on the gauge used for the calculation. For the light-cone gauge calculation,

$$dK_{qq}(\xi,\xi+\xi_2,x,x+x_2,\mu_F)=\widetilde{\mathcal{C}}_q\left(\frac{-1}{\xi_2}\right)\left(i\,\epsilon^{s_T\rho\,n\bar{n}}\right)P^\alpha\,H^{(\mathrm{LC})}_{\rho,\alpha}(\xi,\xi_2,x,x_2,\mu_F)\,. \tag{4.31}$$

From Eqs. (4.16) and Eq. (4.31), we derive the projection operator in the light-cone gauge,

$$\mathcal{P}^{(\mathrm{LC})}_{q,F}=\frac{1}{2}\,\gamma\cdot P\left(\frac{-1}{\xi_2}\right)\left(i\,\epsilon^{s_T\rho\,n\bar{n}}\right)\widetilde{\mathcal{C}}_q\,, \tag{4.32}$$

for extracting the perturbative modification dK_{qq} from the partonic diagram in Fig. 4.3(a), which is equal to the lower blob of the diagram in Fig. 4.2(b) plus all diagrams with the contact interaction. From the RHS of Eq. (4.29), we have the projection operator for the covariant gauge calculation

$$\mathcal{P}_{q,F}^{(\mathrm{CO})} = \frac{1}{2}\,\gamma\cdot P\; P^{\rho}\,\left(i\,\epsilon^{s_T\beta\,n\bar{n}}\right)\,\widetilde{\mathcal{C}}_q\;\frac{\partial}{\partial p_2^{\beta}}\,, \tag{4.33}$$

where the p_2 is set to $\xi_2 P$ following the derivative [19].

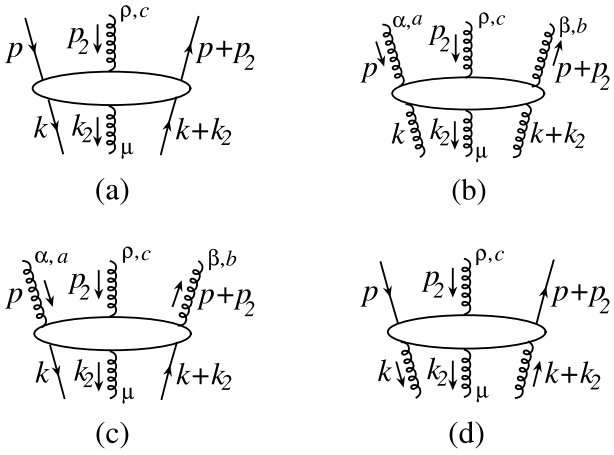

Figure 4.3 Partonic Feynman diagrams that contribute to the evolution kernels of the twist-3 correlation functions.

In order to derive the leading contribution from the second term in Eq. (4.15), we introduce

$$I_{\Delta q} \equiv \int \frac{d^4p\,d^4p_2}{(2\pi)^8}\;\widetilde{T}^{\rho,\alpha}(p,p_2,P,s_T)\widetilde{H}_{\rho,\alpha}(p,p_2,x,x_2,\mu_F)\,, \tag{4.34}$$

with

$$\widetilde{T}^{\rho,\alpha}(p,p_2,P,s_T) = \frac{1}{2}\mathrm{Tr}\left[\hat{T}^{\rho}(p,p_2,P,s_T)\gamma^{\alpha}\left(i\gamma^5\right)\right]\,. \tag{4.35}$$

Following the same derivation as that for I_q, we find

$$
\begin{aligned}
I_{\Delta q} &\approx \int d\xi\, d\xi_2 \left\{ \widetilde{\mathcal{T}}^{(\mathrm{LC})}_{\Delta q,F}(\xi,\xi+\xi_2,s_T) \left[\widetilde{\mathcal{C}}_q \left(\frac{-1}{\xi_2} \right) \left(i\, s_T^\rho \right) P^\alpha\, \widetilde{H}_{\rho,\alpha}(\xi,\xi_2,x,x_2,\mu_F) \right] \right. \\
&\quad \left. + \widetilde{\mathcal{T}}^{(\mathrm{CO})}_{\Delta q,F}(\xi,\xi+\xi_2,s_T) \left[\widetilde{\mathcal{C}}_q \left(i\, s_T^\beta \right) P^\rho\, P^\alpha\, \left. \frac{\partial \widetilde{H}_{\rho,\alpha}(\xi,\xi_2,x,x_2,\mu_F)}{\partial p_2^\beta} \right|_{p_2=\xi_2 P} \right] \right\} \\
&\quad + \ldots \qquad (4.36) \\
&\equiv \int d\xi\, d\xi_2\, \widetilde{\mathcal{T}}_{\Delta q,F}(\xi,\xi+\xi_2,s_T)\, dK_{q\Delta q}(\xi,\xi+\xi_2,x,x+x_2,\mu_F) + \ldots\,, \qquad (4.37)
\end{aligned}
$$

where the perturbative modification to $\widetilde{\mathcal{T}}_{q,F}$ from $\widetilde{\mathcal{T}}_{\Delta q,F}$ is given by

$$
\begin{aligned}
dK_{q\Delta q}(\xi,\xi+\xi_2,x,x+x_2,\mu_F) &= \widetilde{\mathcal{C}}_q \left(\frac{-1}{\xi_2} \right) \left(i\, s_T^\rho \right) P^\alpha\, \widetilde{H}^{(\mathrm{LC})}_{\rho,\alpha}(\xi,\xi_2,x,x_2,\mu_F) \\
&= \widetilde{\mathcal{C}}_q \left(i\, s_T^\beta \right) P^\rho\, P^\alpha\, \left. \frac{\partial \widetilde{H}^{(\mathrm{CO})}_{\rho,\alpha}(\xi,\xi_2,x,x_2,\mu_F)}{\partial p_2^\beta} \right|_{p_2=\xi_2 P} \qquad (4.38)
\end{aligned}
$$

where the subscript "LC" ("CO") again indicates the light-cone (covariant) gauge calculation. From Eq. (4.38), we obtain the projection operator,

$$
\mathcal{P}^{(\mathrm{LC})}_{\Delta q,F} = \frac{1}{2}\, \gamma\cdot P\, \gamma^5 \left(\frac{-1}{\xi_2} \right) \left(-s_T^\rho \right) \widetilde{\mathcal{C}}_q\,, \qquad (4.39)
$$

for extracting $dK_{q\Delta q}$ from the same diagram in Fig. 4.3(a) in the light-cone gauge. Similarly, one can easily derive the projection operator for the covariant gauge calculation from Eq. (4.38).

By adding contributions from Eqs. (4.30) and (4.37), we obtain the factorized perturbative modification to $\widetilde{\mathcal{T}}_{q,F}$,

$$
\begin{aligned}
d\widetilde{\mathcal{T}}_{q,F}(x,x+x_2,\mu_F,s_T) &\approx \int d\xi\, d\xi_2 \left[\widetilde{\mathcal{T}}_{q,F}(\xi,\xi+\xi_2,s_T)\, dK_{qq}(\xi,\xi+\xi_2,x,x+x_2,\mu_F) \right. \\
&\quad \left. + \widetilde{\mathcal{T}}_{\Delta q,F}(\xi,\xi+\xi_2,s_T)\, dK_{q\Delta q}(\xi,\xi+\xi_2,x,x+x_2,\mu_F) \right]\,. \qquad (4.40)
\end{aligned}
$$

As shown in the next section, the leading power perturbative modification, dK_{ij} with $i,j =$

$q, \Delta q, g, \Delta g$, can be expressed as

$$dK_{ij}(\xi, \xi+\xi_2, x, x+x_2, \mu_F) = \int^{\mu_F^2} \frac{dk_T^2}{k_T^2}\, K_{ij}(\xi, \xi+\xi_2, x, x+x_2, \alpha_s) + \dots \,, \tag{4.41}$$

where $K_{ij}(\xi, \xi+\xi_2, x, x+x_2, \alpha_s)$ is referred as the short-distance perturbative evolution kernel. Substituting Eq. (4.41) into Eq. (4.40) and taking the derivative with respect to the factorization scale μ_F in both sides in Eq. (4.40), we derive the leading order flavor non-singlet evolution equation for the quark-gluon correlation function,

$$\begin{aligned}
&\mu_F^2 \frac{\partial}{\partial \mu_F^2} \widetilde{\mathcal{T}}_{q,F}(x, x+x_2, \mu_F, s_T) \\
&= \int d\xi\, d\xi_2 \, \Big[\widetilde{\mathcal{T}}_{q,F}(\xi, \xi+\xi_2, \mu_F, s_T)\, K_{qq}(\xi, \xi+\xi_2, x, x+x_2, \alpha_s) \\
&\qquad + \widetilde{\mathcal{T}}_{\Delta q,F}(\xi, \xi+\xi_2, \mu_F, s_T)\, K_{q\Delta q}(\xi, \xi+\xi_2, x, x+x_2, \alpha_s) \Big] \,,
\end{aligned} \tag{4.42}$$

which has the generic homogeneous differential-integral form of the typical evolution equation, such as the DGLAP evolution equation of PDFs [43, 48].

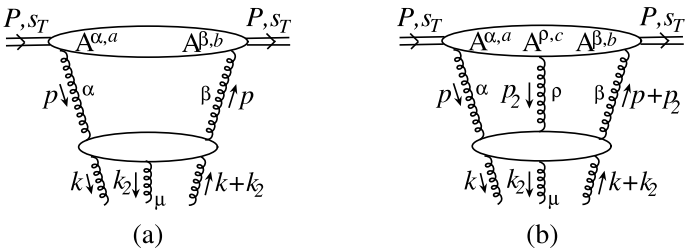

Figure 4.4 Feynman diagrams that contribute to the change of the twist-3 tri-gluon correlation functions where α, β, μ, ρ and a, b, c are Lorentz and color indices of gluon field operators, respectively. The lower part of gluon lines are contracted to the cut vertices that define the tri-gluon correlation functions.

4.2.2 Non-singlet case: tri-gluon correlations

Next, we derive the perturbative change of tri-gluon correlation function $\widetilde{\mathcal{T}}_{G,F}^{(f,d)}$ from the diagrams in Fig. 4.4. Since gluon transversity distribution vanishes [49], there is no leading twist or leading power contribution to the evolution of the tri-gluon correlation functions from

Fig. 4.4(a). Similar to the case of the flavor non-singlet change of quark-gluon correlation function discussed above, the subleading power contribution from the diagram in Fig. 4.4(a) can be combined with the leading contribution of the diagram in Fig. 4.4(b) [45]. We can then derive the projection operator for calculating the gluonic evolution kernel by factorizing the diagram in Fig. 4.4(b).

We express the diagram in Fig. 4.4(b) as

$$\begin{aligned} d\widetilde{\mathcal{I}}^{(i)}_{G,F}(x, x+x_2, \mu_F, s_T) &\equiv \int \frac{d^4p\, d^4p_2}{(2\pi)^8} \sum_{\rho,\alpha,\beta} \Big[T^{\rho,\alpha,\beta}(p, p_2, P, s_T)\, H^{(i)}_{\rho,\alpha,\beta}(p, p_2, x, x_2, \mu_F) \Big] \\ &\equiv I^{(i)}_G + I^{(i)}_{\Delta G}\,, \end{aligned} \tag{4.43}$$

where the superscript $i = f, d$ from the cut vertex and I_G ($I_{\Delta G}$) represents the part of the perturbative change that is symmetric (antisymmetric) in the exchange of the Lorentz indices α and β. In Eq. (4.43), the partonic part $H_{\rho,\alpha,\beta}$ is given by the bottom part of the diagram in Fig. 4.4(b) plus diagrams with the contact interaction from the subleading contribution of the diagram in Fig. 4.4(a). All partonic diagrams are contracted by the cut vertex in Eq. (4.6). The tri-gluon matrix element $T^{\rho,\alpha,\beta}$ in Eq. (4.43) is defined as

$$T^{\rho,\alpha,\beta}(p, p_2, P, s_T) = \langle P, s_T |\, \widetilde{A}^{\beta,b}(-p-p_2)\, \widetilde{A}^{\rho,c}(p_2)\, \widetilde{A}^{\alpha,a}(p)\, | P, s_T \rangle \tag{4.44}$$

with the gluon color indices, b, c, a and is represented by the top part of the Feynman diagram in Fig. 4.4(b). Following the same steps used to factorize the diagram in Fig. 4.2(b), we can

factorize the leading power contribution to the part that is symmetric in α and β as

$$
\begin{aligned}
I_G^{(i)} \;\approx\; & \int d\xi\, d\xi_2 \Bigg\{ \left[\frac{\widetilde{\mathcal{T}}_{G,F}^{(j)(\mathrm{LC})}(\xi, \xi+\xi_2, s_T)}{\xi(\xi+\xi_2)} \right] \\
& \times \left[\widetilde{\mathcal{C}}_g^{(j)} \; \frac{1}{2}\, d^{\alpha\beta} \left(\frac{-1}{\xi_2} \right) \left(i\, \epsilon^{s_T \rho\, n\bar{n}} \right) H_{\rho,\alpha,\beta}^{(i)}(\xi, \xi_2, x, x_2, \mu_F) \right] \\
& + \left[\frac{\widetilde{\mathcal{T}}_{G,F}^{(j)(\mathrm{CO})}(\xi, \xi+\xi_2, s_T)}{\xi(\xi+\xi_2)} \right] \\
& \times \left[\widetilde{\mathcal{C}}_g^{(j)} \; \frac{1}{2} d^{\alpha\beta}\, P^\rho \, \left(i\, \epsilon^{s_T \sigma\, n\bar{n}} \right) \left. \frac{\partial H_{\rho,\alpha,\beta}^{(i)}(\xi, \xi_2, x, x_2, \mu_F)}{\partial p_2^\sigma} \right|_{p_2 = \xi_2 P} \right] \Bigg\} + \dots \,,
\end{aligned}
\tag{4.45}
$$

where the transverse polarization tensor $d^{\alpha\beta} \equiv -g^{\alpha\beta} + n^\alpha \bar{n}^\beta + \bar{n}^\alpha n^\beta$ and the gluonic color projection operators $\widetilde{\mathcal{C}}_g^{(i)}$ with $j = f, d$ are given by

$$
(\widetilde{\mathcal{C}}_g^{(f)})_{acb} = \frac{1}{N_c(N_c^2-1)}\, i f_{acb}\,, \quad \text{and} \quad (\widetilde{\mathcal{C}}_g^{(d)})_{acb} = \frac{N_c}{(N_c^2-4)(N_c^2-1)}\, d_{acb}\,,
\tag{4.46}
$$

for color indices labeled in Fig. 4.4(b), so that $\widetilde{\mathcal{C}}_g^{(j)}\, \mathcal{C}_g^{(j)} = 1$ for $j = f, d$. In Eq. (4.45), $\widetilde{\mathcal{T}}_{G,F}^{(j)(\mathrm{LC})}$ and $\widetilde{\mathcal{T}}_{G,F}^{(j)(\mathrm{CO})}$ with $j = f, d$ are tri-gluon correlation functions that have the same definition as that of $\widetilde{\mathcal{T}}_{G,F}^{(f,d)}$ in Eq. (4.4), except that the cut vertex is now replaced by the corresponding one in the light-cone gauge and the one in a covariant gauge, respectively, and they satisfy

$$
\widetilde{\mathcal{T}}_{G,F}^{(f,d)}(\xi, \xi+\xi_2, s_T) = \widetilde{\mathcal{T}}_{G,F}^{(f,d)(\mathrm{LC})}(\xi, \xi+\xi_2, s_T) + \widetilde{\mathcal{T}}_{G,F}^{(f,d)(\mathrm{CO})}(\xi, \xi+\xi_2, s_T)\,.
\tag{4.47}
$$

Again, the color gauge invariance requires

$$
\begin{aligned}
& \frac{1}{2}\, d^{\alpha\beta} \left(\frac{-1}{\xi_2} \right) \left(i\, \epsilon^{s_T \rho\, n\bar{n}} \right) H_{\rho,\alpha,\beta}^{(i)(\mathrm{LC})}(\xi, \xi_2, x, x_2, \mu_F) \\
& = \frac{1}{2} d^{\alpha\beta}\, P^\rho \, \left(i\, \epsilon^{s_T \sigma\, n\bar{n}} \right) \left. \frac{\partial H_{\rho,\alpha,\beta}^{(i)(\mathrm{CO})}(\xi, \xi_2, x, x_2, \mu_F)}{\partial p_2^\sigma} \right|_{p_2 = \xi_2 P} \,,
\end{aligned}
\tag{4.48}
$$

when the LHS is evaluated in the light-cone gauge and the RHS in a covariant gauge. Therefore,

the two leading terms in Eq. (4.45) can be combined together as

$$I_G^{(i)} \approx \int d\xi\, d\xi_2\, \widetilde{\mathcal{T}}_{G,F}^{(j)}(\xi, \xi+\xi_2, s_T)\, dK_{gg}^{(ij)}(\xi, \xi+\xi_2, x, x+x_2, \mu_F) \tag{4.49}$$

with

$$\begin{aligned} &dK_{gg}^{(ij)}(\xi, \xi+\xi_2, x, x+x_2, \mu_F) \\ &= \widetilde{\mathcal{C}}_g^{(j)}\, \frac{1}{2}\, d^{\alpha\beta} \frac{1}{\xi(\xi+\xi_2)} \left(\frac{-1}{\xi_2}\right) \left(i\,\epsilon^{s_T \rho\, n\bar{n}}\right) H_{\rho,\alpha,\beta}^{(i)(\mathrm{LC})}(\xi, \xi_2, x, x_2, \mu_F) \end{aligned} \tag{4.50}$$

in the light-cone gauge. The $dK_{gg}^{(ij)}$ can also be derived in a covariant gauge from the RHS of Eq. (4.48). The equality in Eq. (4.48) provides an independent check of perturbative calculation done in different gauges. From Eq. (4.50), we obtain the light-cone gauge projection operator,

$$\mathcal{P}_{G,F}^{(f,d)(\mathrm{LC})} = \frac{1}{2}\, d^{\alpha\beta}\, \frac{1}{\xi(\xi+\xi_2)} \left(\frac{-1}{\xi_2}\right) \left(i\,\epsilon^{s_T \rho\, n\bar{n}}\right)\, \widetilde{\mathcal{C}}_g^{(f,d)}\,; \tag{4.51}$$

for calculating the perturbative modification to the tri-gluon correlation function $\widetilde{\mathcal{T}}_{G,F}^{(f,d)}$ from the diagrams in Fig. 4.3(b), which includes all the partonic Feynman diagrams from the lower blob of the diagram in Fig. 4.4(b) plus corresponding twist-3 contribution from the diagram in Fig. 4.4(a) expressed in terms of diagrams with the contact interaction [45]. Similar projection operator can be derived from the RHS of Eq. (4.48) for the covariant gauge calculation.

Similarly, we derive the perturbative modification to $\widetilde{\mathcal{T}}_{G,F}^{(f,d)}$ from the tri-gluon correlation function $\widetilde{\mathcal{T}}_{\Delta G,F}^{(f,d)}$,

$$I_{\Delta G}^{(i)} \approx \int d\xi\, d\xi_2\, \widetilde{\mathcal{T}}_{\Delta G,F}^{(j)}(\xi, \xi+\xi_2, s_T)\, dK_{g\Delta g}^{(ij)}(\xi, \xi+\xi_2, x, x+x_2, \mu_F) \tag{4.52}$$

with

$$\begin{aligned} &dK_{g\Delta g}^{(ij)}(\xi, \xi+\xi_2, x, x+x_2, \mu_F) \\ &= \widetilde{\mathcal{C}}_g^{(j)}\, \frac{1}{2}\, \left(i\epsilon_\perp^{\alpha\beta}\right)\, \frac{1}{\xi(\xi+\xi_2)} \left(\frac{-1}{\xi_2}\right) \left(-s_T^\rho\right) H_{\rho,\alpha,\beta}^{(i)(\mathrm{LC})}(\xi, \xi_2, x, x_2, \mu_F) \end{aligned} \tag{4.53}$$

in the light-cone gauge. One can easily derive the expression for $dK_{g\Delta g}^{(ij)}$ in a covariant gauge as well. From Eq. (4.53), we obtain the light-cone gauge projection operator,

$$\mathcal{P}_{\Delta G,F}^{(f,d)(\mathrm{LC})} = \frac{1}{2}\left(i\epsilon_{\perp}^{\alpha\beta}\right)\frac{1}{\xi(\xi+\xi_2)}\left(\frac{-1}{\xi_2}\right)\left(-s_T^{\rho}\right)\widetilde{\mathcal{C}}_g^{(f,d)}\,; \tag{4.54}$$

for calculating the perturbative modification from the tri-gluon correlation function $\widetilde{\mathcal{T}}_{\Delta G,F}^{(f,d)}$ from the same diagrams in Fig. 4.3(b).

Using the generic expression of the leading power contribution to the perturbative modification factor dK_{ij} in Eq. (4.41), we derive the evolution equation for the factorization scale dependence of the tri-gluon correlation function $\widetilde{\mathcal{T}}_{G,F}^{(f,d)}$ by factorizing the perturbative correction from the diagrams in Fig. 4.4,

$$\begin{aligned}
&\mu_F^2\frac{\partial}{\partial\mu_F^2}\widetilde{\mathcal{T}}_{G,F}^{(i)}(x,x+x_2,\mu_F,s_T)\\
&=\sum_{j=f,d}\int d\xi\,d\xi_2\,\Big[\widetilde{\mathcal{T}}_{G,F}^{(j)}(\xi,\xi+\xi_2,\mu_F,s_T)\,K_{gg}^{(ji)}(\xi,\xi+\xi_2,x,x+x_2,\alpha_s)\\
&\qquad\qquad+\widetilde{\mathcal{T}}_{\Delta G,F}^{(j)}(\xi,\xi+\xi_2,\mu_F,s_T)\,K_{g\Delta g}^{(ji)}(\xi,\xi+\xi_2,x,x+x_2,\alpha_s)\Big]\,,
\end{aligned} \tag{4.55}$$

where the superscript $i,j=f,d$, $K_{gg}^{(ji)}$ and $K_{g\Delta g}^{(ji)}$ are evolution kernels that can be perturbatively calculated from the diagram in Fig. 4.3(b) with proper projection operators as discussed above.

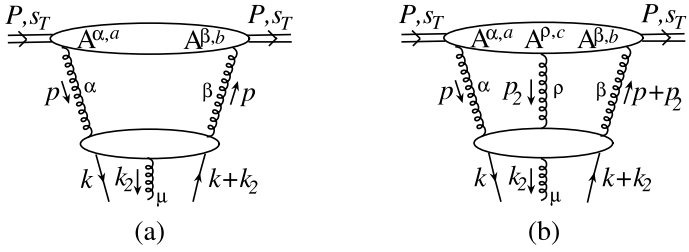

Figure 4.5 Feynman diagrams that contribute to the change of the twist-3 quark-gluon correlation function where α,β,μ,ρ and a,b,c are Lorentz and color indices of gluon field operators, respectively. The lower part of quark and gluon lines are contracted to the cut vertex that defines the quark-gluon correlation function.

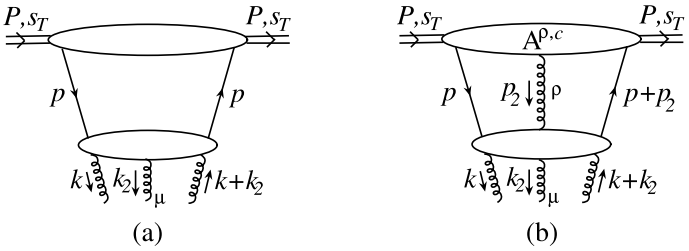

Figure 4.6 Feynman diagrams that contribute to the change of the twist-3 tri-gluon correlation functions from the interaction initiated from the quark-gluon correlation functions. The lower part of gluon lines are contracted to the cut vertices that define the tri-gluon correlation functions.

4.2.3 Complete evolution equations

The evolution equation for the scale dependence of the quark-gluon correlation function in Eq. (4.42) can also get contributions from the tri-gluon correlation functions via the diagrams in Fig. 4.5. Similarly, the evolution equation for the tri-gluon correlation functions in Eq. (4.55) can get additional contribution from the quark-gluon correlation function via the diagrams in Fig. 4.6.

Following the same procedure to factorize the diagrams in Fig. 4.4, we derive the additional contribution to the evolution of the quark-gluon correlation function from the tri-gluon correlation functions and have,

$$
\begin{aligned}
&\mu_F^2 \frac{\partial}{\partial \mu_F^2} \widetilde{\mathcal{T}}_{q,F}(x, x+x_2, \mu_F, s_T) \\
&= \int d\xi\, d\xi_2 \, \Big[\widetilde{\mathcal{T}}_{q,F}(\xi, \xi+\xi_2, \mu_F, s_T)\, K_{qq}(\xi, \xi+\xi_2, x, x+x_2, \alpha_s) \\
&\qquad\qquad + \widetilde{\mathcal{T}}_{\Delta q,F}(\xi, \xi+\xi_2, \mu_F, s_T)\, K_{q\Delta q}(\xi, \xi+\xi_2, x, x+x_2, \alpha_s) \Big] \\
&\quad + \sum_{i=f,d} \int d\xi\, d\xi_2 \, \Big[\widetilde{\mathcal{T}}^{(i)}_{G,F}(\xi, \xi+\xi_2, \mu_F, s_T)\, K^{(i)}_{qg}(\xi, \xi+\xi_2, x, x+x_2, \alpha_s) \\
&\qquad\qquad + \widetilde{\mathcal{T}}^{(i)}_{\Delta G,F}(\xi, \xi+\xi_2, \mu_F, s_T)\, K^{(i)}_{q\Delta g}(\xi, \xi+\xi_2, x, x+x_2, \alpha_s) \Big] \, . \qquad (4.56)
\end{aligned}
$$

The evolution kernels from the tri-gluon correlation functions to the quark-gluon correlation function, $K_{qg}^{(f,d)}$ and $K_{q\Delta g}^{(f,d)}$, can be obtained by calculating the diagram in Fig. 4.3(c) with

proper projection operators. If the kernels are evaluated in the light-cone gauge, the three gluon lines on the top of the diagram are contracted by the projection operator in Eqs. (4.51) and (4.54), respectively. The diagram in Fig. 4.3(c) includes all Feynman diagrams from the bottom part of the diagram in Fig. 4.5(b) plus diagrams from the subleading contribution of the diagram in Fig. 4.5(a), which can be effectively expressed in terms of the diagrams with the contact interaction and the same external lines as those in Fig. 4.5(b). The combination of these diagrams forms a gauge invariant set [45].

Similarly, following the same procedure to factorize the diagrams in Fig. 4.2, we derive the additional contribution to the evolution equation of the tri-gluon correlation functions from the quark-gluon correlation functions and have,

$$
\begin{aligned}
&\mu_F^2 \frac{\partial}{\partial \mu_F^2} \widetilde{\mathcal{T}}^{(i)}_{G,F}(x, x+x_2, \mu_F, s_T) \\
&= \sum_{j=f,d} \int d\xi\, d\xi_2 \, \Big[\widetilde{\mathcal{T}}^{(j)}_{G,F}(\xi, \xi+\xi_2, \mu_F, s_T)\, K^{(ji)}_{gg}(\xi, \xi+\xi_2, x, x+x_2, \alpha_s) \\
&\qquad\qquad + \widetilde{\mathcal{T}}^{(j)}_{\Delta G,F}(\xi, \xi+\xi_2, \mu_F, s_T)\, K^{(ji)}_{g\Delta g}(\xi, \xi+\xi_2, x, x+x_2, \alpha_s) \Big] \\
&\quad + \sum_q \int d\xi\, d\xi_2 \, \Big[\widetilde{\mathcal{T}}_{q,F}(\xi, \xi+\xi_2, \mu_F, s_T)\, K^{(i)}_{gq}(\xi, \xi+\xi_2, x, x+x_2, \alpha_s) \\
&\qquad\qquad + \widetilde{\mathcal{T}}_{\Delta q,F}(\xi, \xi+\xi_2, \mu_F, s_T)\, K^{(i)}_{g\Delta q}(\xi, \xi+\xi_2, x, x+x_2, \alpha_s) \Big] \, . \qquad (4.57)
\end{aligned}
$$

where $\sum_q$ runs over all quark and antiquark flavors, the superscript, $i, j = f, d$. The evolution kernels from the quark-gluon correlation functions to the tri-gluon correlation functions, $K^{(f,d)}_{gq}$ and $K^{(f,d)}_{g\Delta q}$, can be obtained by calculating the diagram in Fig. 4.3(d) with proper projection operators. If the evolution kernels are evaluated in the light-cone gauge, the quark and gluon lines on the top of the diagram are contracted by the projection operator in Eqs. (4.32) and (4.39), respectively. The diagram in Fig. 4.3(d) includes all partonic Feynman diagrams from the bottom part of the diagram in Fig. 4.6(b) plus the diagrams with the contact interaction representing the subleading contribution of the diagram in Fig. 4.6(a).

Following the same derivation for the perturbative corrections to the first set twist-3 correlation functions, we derive the evolution equations for the second set of twist-3 correlation

functions,

$$\begin{aligned}
&\mu_F^2\frac{\partial}{\partial\mu_F^2}\widetilde{\mathcal{T}}_{\Delta q,F}(x,x+x_2,\mu_F,s_T)\\
&=\int d\xi\,d\xi_2\,\Big[\widetilde{\mathcal{T}}_{\Delta q,F}(\xi,\xi+\xi_2,\mu_F,s_T)\,K_{\Delta q\Delta q}(\xi,\xi+\xi_2,x,x+x_2,\alpha_s)\\
&\qquad\qquad+\widetilde{\mathcal{T}}_{q,F}(\xi,\xi+\xi_2,\mu_F,s_T)\,K_{\Delta q\,q}(\xi,\xi+\xi_2,x,x+x_2,\alpha_s)\Big]\\
&\quad+\sum_{i=f,d}\int d\xi\,d\xi_2\,\Big[\widetilde{\mathcal{T}}^{(i)}_{G,F}(\xi,\xi+\xi_2,\mu_F,s_T)\,K^{(i)}_{\Delta q\,g}(\xi,\xi+\xi_2,x,x+x_2,\alpha_s)\\
&\qquad\qquad+\widetilde{\mathcal{T}}^{(i)}_{\Delta G,F}(\xi,\xi+\xi_2,\mu_F,s_T)\,K^{(i)}_{\Delta q\Delta g}(\xi,\xi+\xi_2,x,x+x_2,\alpha_s)\Big]\ , \quad (4.58)
\end{aligned}$$

and

$$\begin{aligned}
&\mu_F^2\frac{\partial}{\partial\mu_F^2}\widetilde{\mathcal{T}}^{(i)}_{\Delta G,F}(x,x+x_2,\mu_F,s_T)\\
&=\sum_{j=f,d}\int d\xi\,d\xi_2\,\Big[\widetilde{\mathcal{T}}^{(j)}_{\Delta G,F}(\xi,\xi+\xi_2,\mu_F,s_T)\,K^{(ji)}_{\Delta g\Delta g}(\xi,\xi+\xi_2,x,x+x_2,\alpha_s)\\
&\qquad\qquad+\widetilde{\mathcal{T}}^{(j)}_{G,F}(\xi,\xi+\xi_2,\mu_F,s_T)\,K^{(ji)}_{\Delta g\,g}(\xi,\xi+\xi_2,x,x+x_2,\alpha_s)\Big]\\
&\quad+\sum_{q}\int d\xi\,d\xi_2\,\Big[\widetilde{\mathcal{T}}_{q,F}(\xi,\xi+\xi_2,\mu_F,s_T)\,K^{(i)}_{\Delta g\,q}(\xi,\xi+\xi_2,x,x+x_2,\alpha_s)\\
&\qquad\qquad+\widetilde{\mathcal{T}}_{\Delta q,F}(\xi,\xi+\xi_2,\mu_F,s_T)\,K^{(i)}_{\Delta g\Delta q}(\xi,\xi+\xi_2,x,x+x_2,\alpha_s)\Big]\ . \quad (4.59)
\end{aligned}$$

All evolution kernels in Eqs. (4.58) and (4.59) can be derived by calculating diagrams in Fig. 4.3 with proper projection operators discussed in this section.

Equations (4.56), (4.57), (4.58), and (4.59) form a closed set of evolution equations for the scale dependence of the two sets of twist-3 quark-gluon and tri-gluon correlation functions defined in the last section. From these evolution equations, we can construct the evolution

equations of twist-3 correlation functions that are responsible for the SSAs as,

$$\mu_F^2\frac{\partial}{\partial\mu_F^2}\mathcal{T}_{q,F}(x,x+x_2,\mu_F) = \frac{1}{2}\left[\mu_F^2\frac{\partial}{\partial\mu_F^2}\widetilde{\mathcal{T}}_{q,F}(x,x+x_2,\mu_F,s_T) + \mu_F^2\frac{\partial}{\partial\mu_F^2}\widetilde{\mathcal{T}}_{q,F}(x+x_2,x,\mu_F,s_T)\right], \tag{4.60}$$

$$\mu_F^2\frac{\partial}{\partial\mu_F^2}\mathcal{T}^{(i)}_{G,F}(x,x+x_2,\mu_F) = \frac{1}{2}\left[\mu_F^2\frac{\partial}{\partial\mu_F^2}\widetilde{\mathcal{T}}^{(i)}_{G,F}(x,x+x_2,\mu_F,s_T) + \mu_F^2\frac{\partial}{\partial\mu_F^2}\widetilde{\mathcal{T}}^{(i)}_{G,F}(x+x_2,x,\mu_F,s_T)\right], \tag{4.61}$$

$$\mu_F^2\frac{\partial}{\partial\mu_F^2}\mathcal{T}_{\Delta q,F}(x,x+x_2,\mu_F) = \frac{1}{2}\left[\mu_F^2\frac{\partial}{\partial\mu_F^2}\widetilde{\mathcal{T}}_{\Delta q,F}(x,x+x_2,\mu_F,s_T) - \mu_F^2\frac{\partial}{\partial\mu_F^2}\widetilde{\mathcal{T}}_{\Delta q,F}(x+x_2,x,\mu_F,s_T)\right], \tag{4.62}$$

$$\mu_F^2\frac{\partial}{\partial\mu_F^2}\mathcal{T}^{(i)}_{\Delta G,F}(x,x+x_2,\mu_F) = \frac{1}{2}\left[\mu_F^2\frac{\partial}{\partial\mu_F^2}\widetilde{\mathcal{T}}^{(i)}_{\Delta G,F}(x,x+x_2,\mu_F,s_T) - \mu_F^2\frac{\partial}{\partial\mu_F^2}\widetilde{\mathcal{T}}^{(i)}_{\Delta G,F}(x+x_2,x,\mu_F,s_T)\right]. \tag{4.63}$$

As we show in the next section, the sum or the difference in the RHS of above equations determines the symmetry property of these correlation functions when the active momentum fractions x and $x+x_2$ are switched.

4.3 Evolution kernels

In the previous two chapters, the calculated SSAs for single inclusive particle production depend on the first set of twist-3 correlation function, more precisely, they are so-called gluonic pole contribution or the diagonal part of the correlation functions. The evolution of these diagonal correlation functions can be derived by calculating the evolution kernels for the evolution equations that are derived in the last section at $x_2 = 0$.

The evolution kernels can be derived from the order of α_s diagrams in Fig. 4.3 after setting $x_2 = 0$ or integrating over x_2 weighted by $\delta(x_2)$. We use the light-cone gauge *cut vertices* and *projection operators* derived in the last section to contract the quark and gluon lines at the *bottom* and the *top* of these diagrams, respectively. Since the cut vertices with the middle gluon in the LHS of the cut are the same as that with the gluon in the RHS of the cut, we

only need to calculate the cut Feynman diagrams in Fig. 4.3 that have the middle gluon at the *bottom* part of the diagrams in *one* side of the cut. On the other hand, the sum of the all final-state cuts requires us to calculate all diagrams with the middle gluon on the *top* part of the diagrams in *both* sides of the cut. In addition, we need to calculate the same diagrams in Fig. 4.3 with the active momentum fractions x and $x + x_2$ switched, as indicated by the equations in Eq. (4.60) to Eq. (4.63).

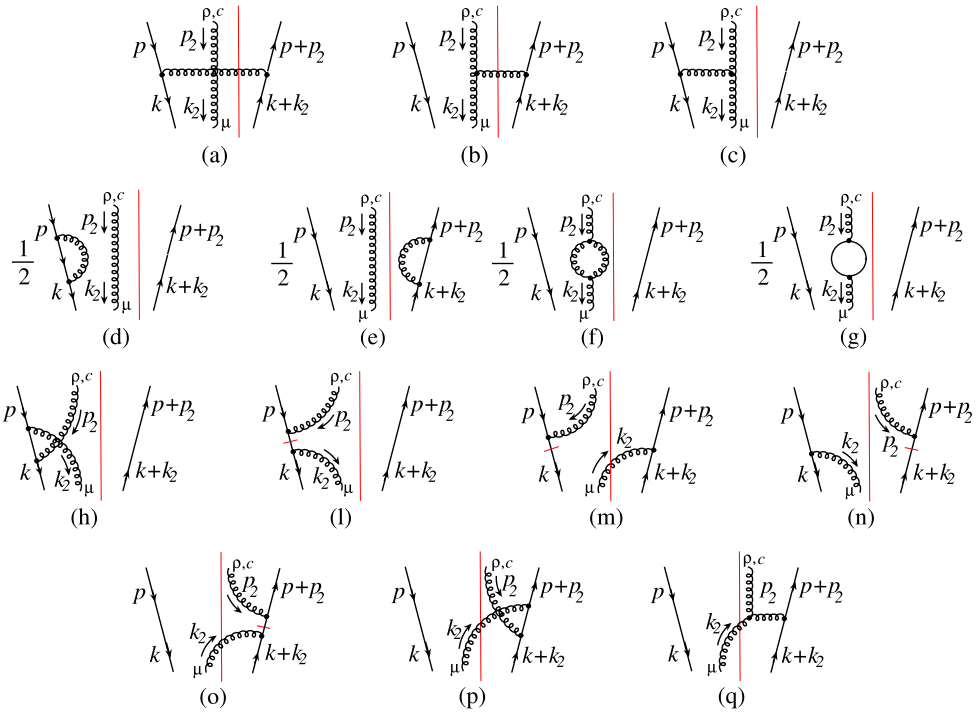

Figure 4.7 Feynman diagrams that contribute to the leading order flavor non-singlet evolution kernel of the twist-3 quark-gluon correlation function.

We start with a detailed calculation of the order of α_s evolution kernels for the evolution equations of $\widetilde{\mathcal{T}}_{q,F}(x, x+x_2, \mu_F, s_T)$ and $\widetilde{\mathcal{T}}_{q,F}(x+x_2, x, \mu_F, s_T)$, and then, we construct the evolution equation for $\mathcal{T}_{q,F}(x, x, \mu_F)$ from Eq. (4.60). Finally, from Eq. (2.23), we have the diagonal correlation function, $T_{q,F}(x, x, \mu_F) = 2\pi\mathcal{T}_{q,F}(x, x, \mu_F)$. We define

$$d\mathcal{I}_{qq} \equiv \int dx_2\, \delta(x_2)\, dK_{qq}(\xi, \xi+\xi_2, x, x+x_2, \alpha_s)\,, \tag{4.64}$$

where dK_{qq} is given by the diagrams in Fig. 4.3(a) with the cut vertex in Eq. (4.9) and the projection operator in Eq. (4.32). We list in Fig. 4.7 all cut Feynman diagrams at order of α_s with the gluon at the cut vertex in the LHS of the cut. Diagrams labeled from (a) to (m) have the top middle gluon in the LHS of the cut while the diagrams from (n) to (q) have the top middle gluon in the RHS of the cut. The quark propagator with a short bar for the diagrams labeled by (l), (m), (n), and (o) is the special propagator introduced in Ref. [45] to represent the contact interaction. These diagrams represent the contribution from the diagram in Fig. 4.2(a) that is necessary to make the full twist-3 contribution gauge invariant. In the $n \cdot A = 0$ light-cone gauge, the Feynman rule for the special quark propagator of momentum k is [45]

$$\frac{i\gamma \cdot n}{2k \cdot n} \frac{k^2}{k^2 + i\epsilon} \,. \tag{4.65}$$

Having the cut vertex and the projection operator for the bottom and top quark and gluon lines, respectively, calculation of these Feynman diagrams in Fig. 4.7 is straightforward. In particular, after setting $x_2 = 0$ or integrating over x_2 weighted by the $\delta(x_2)$, all diagrams labeled from (f) to (q) give the vanishing contribution to the diagonal evolution kernel, $K_{qq}(\xi, \xi + \xi_2, x, x, \alpha_s)$. Using the technique introduced in Ref. [43], we find the following results for the rest of diagrams,

$$d\mathcal{I}_{qq}^{(a)} = \delta(\xi_2) \frac{1}{\xi} \int^{\mu_F^2} \frac{dk_T^2}{k_T^2} \left[C_F - \frac{C_A}{2} \right] \frac{\alpha_s}{2\pi} \left(\frac{1+z^2}{1-z} \right) , \tag{4.66}$$

$$d\mathcal{I}_{qq}^{(b)} = \delta(\xi - x) \frac{1}{\xi_2} \int^{\mu_F^2} \frac{dk_T^2}{k_T^2} \left[\frac{C_A}{2} \right] \frac{\alpha_s}{2\pi} \left(\frac{1}{2} \frac{2x + \xi_2}{x + \xi_2} \right) , \tag{4.67}$$

$$d\mathcal{I}_{qq}^{(c)} = \delta(\xi + \xi_2 - x) \frac{1}{\xi} \int^{\mu_F^2} \frac{dk_T^2}{k_T^2} \left[\frac{C_A}{2} \right] \frac{\alpha_s}{2\pi} \left(\frac{1}{2} \frac{1+z}{1-z} \right) , \tag{4.68}$$

$$d\mathcal{I}_{qq}^{(d+e)} = -\delta(\xi_2)\, \delta(\xi - x) \int^{\mu_F^2} \frac{dk_T^2}{k_T^2} \int_0^1 dz \, [C_F] \frac{\alpha_s}{2\pi} \left(\frac{1+z^2}{1-z} \right) . \tag{4.69}$$

In above equations, $z = x/\xi$ and the color factor for each diagram is explicitly shown in the square brackets with $C_F = (N_c^2 - 1)/2N_c$, $C_A = N_c$ and $N_c = 3$, the number of color. We notice that the RHS of the last equation from the diagrams (d) and (e) is infrared divergent, and the divergence is needed to cancel the infrared divergence from the term proportional to

C_F in Eq. (4.66) when $z \to 1$. This cancellation of infrared divergence between the real and virtual diagrams is the same as that takes place in the evolution kernel of normal PDFs [43]. The remaining infrared divergence as $z \to 1$ in Eq. (4.66) is proportional to a different color factor, $C_A/2$, and is cancelled by the contribution from diagrams (b) and (c).

From the same Feynman diagrams in Fig. 4.7, we can also calculate the contribution from $\widetilde{\mathcal{T}}_{\Delta q,F}$,

$$d\mathcal{I}_{q\Delta q} \equiv \int dx_2\, \delta(x_2)\, dK_{q\Delta q}(\xi, \xi+\xi_2, x, x+x_2, \alpha_s) \tag{4.70}$$

by using the projection operator in Eq. (4.39). In this case, only diagrams (b) and (c) give nonvanishing results,

$$d\mathcal{I}^{(b)}_{q\Delta q} = \delta(\xi - x) \int^{\mu_F^2} \frac{dk_T^2}{k_T^2} \left[\frac{C_A}{2}\right] \frac{\alpha_s}{2\pi} \left(\frac{1}{2}\, \frac{1}{x+\xi_2}\right), \tag{4.71}$$

$$d\mathcal{I}^{(c)}_{q\Delta q} = -\delta(\xi + \xi_2 - x)\, \frac{1}{\xi} \int^{\mu_F^2} \frac{dk_T^2}{k_T^2} \left[\frac{C_A}{2}\right] \frac{\alpha_s}{2\pi} \left(\frac{1}{2}\right). \tag{4.72}$$

By comparing above calculated results with Eq. (4.41), we extract evolution kernels, $K_{qq}(\xi, \xi+\xi_2, x, x)$ and $K_{q\Delta q}(\xi, \xi+\xi_2, x, x)$. By calculating the same diagrams in Fig. 4.3 with momentum fractions ξ and x switched with $\xi+\xi_2$ and $x+x_2$, respectively, we derive evolution kernels, $K_{qq}(\xi+\xi_2, \xi, x, x)$ and $K_{q\Delta q}(\xi+\xi_2, \xi, x, x)$. By integrating Eq. (4.60) over x_2 weighted by $\delta(x_2)$ or simply setting $x_2 = 0$, we obtain the order of α_s evolution equation for $\mathcal{T}_{q,F}(x, x, \mu_F)$ from flavor non-singlet interactions,

$$\begin{aligned}
\frac{\partial \mathcal{T}_{q,F}(x,x,\mu_F)}{\partial \ln \mu_F^2} = \frac{\alpha_s}{2\pi} \int_x^1 \frac{d\xi}{\xi} \Bigg\{ & P_{qq}(z)\, \mathcal{T}_{q,F}(\xi, \xi, \mu_F) \\
& + \frac{C_A}{2} \left[\frac{1+z^2}{1-z} \left[\mathcal{T}_{q,F}(\xi, x, \mu_F) - \mathcal{T}_{q,F}(\xi, \xi, \mu_F) \right] + z\, \mathcal{T}_{q,F}(\xi, x, \mu_F) \right] \\
& + \frac{C_A}{2} \left[\mathcal{T}_{\Delta q,F}(x, \xi, \mu_F) \right] \Bigg\},
\end{aligned} \tag{4.73}$$

where

$$P_{qq}(z) = C_F \left[\frac{1+z^2}{(1-z)_+} + \frac{3}{2}\,\delta(1-z) \right] \tag{4.74}$$

is the LO quark-to-quark splitting function for the normal PDFs. The standard definition of "+" distribution is

$$\int_x^1 dz\, \frac{f(z)}{(1-z)_+} = \int_x^1 dz\, \frac{f(z)-f(1)}{1-z} + f(1)\, \ln(1-x) \tag{4.75}$$

for a smooth function $f(z)$. In deriving Eq. (4.73), Eqs. (2.19) and (2.28) were used. It is clear from Eq. (4.73) that the flavor non-singlet evolution kernels for the diagonal twist-3 quark-gluon correlation function $T_{q,F}(x,x,\mu_F) = 2\pi \mathcal{T}_{q,F}(x,x,\mu_F)$ are all infrared safe. The evolution equation for the diagonal correlation function $\mathcal{T}_{q,F}(x,x,\mu_F)$ is not a closed one since it gets contribution not only from the same diagonal function $\mathcal{T}_{q,F}(\xi,\xi,\mu_F)$ but also from the off-diagonal part of the same function as well as gets the contribution from a different function $\mathcal{T}_{\Delta q,F}(x,\xi,\mu_F)$.

In the rest of this section, we derive the order of α_s evolution kernels involving gluons as well as those with the flavor change. In Fig. 4.8, we list all cut Feynman diagrams at the order of α_s that could contribute to the evolution kernels, $K_{gg}^{(ij)}$ and $K_{\Delta g \Delta g}^{(ij)}$ with $i,j = f,d$, when proper cut vertices and projection operators are used. The gluon propagator with a short bar in the diagrams (l), (m), (n), and (o) is the gluonic special propagator defined in Ref. [45], given by

$$\frac{in^\alpha n^\beta}{(k\cdot n)^2} \frac{k^2}{k^2+i\epsilon}\,, \tag{4.76}$$

which represents the contact interaction. The diagrams with the contact interaction are responsible for the twist-3 contribution from the diagram in Fig. 4.4(a). We calculate all diagrams with the cut vertices and projection operators derived in last section and setting $x_2 = 0$. We find that after taking $x_2 = 0$ or integrating over x_2 weighted with $\delta(x_2)$, only diagrams (a),

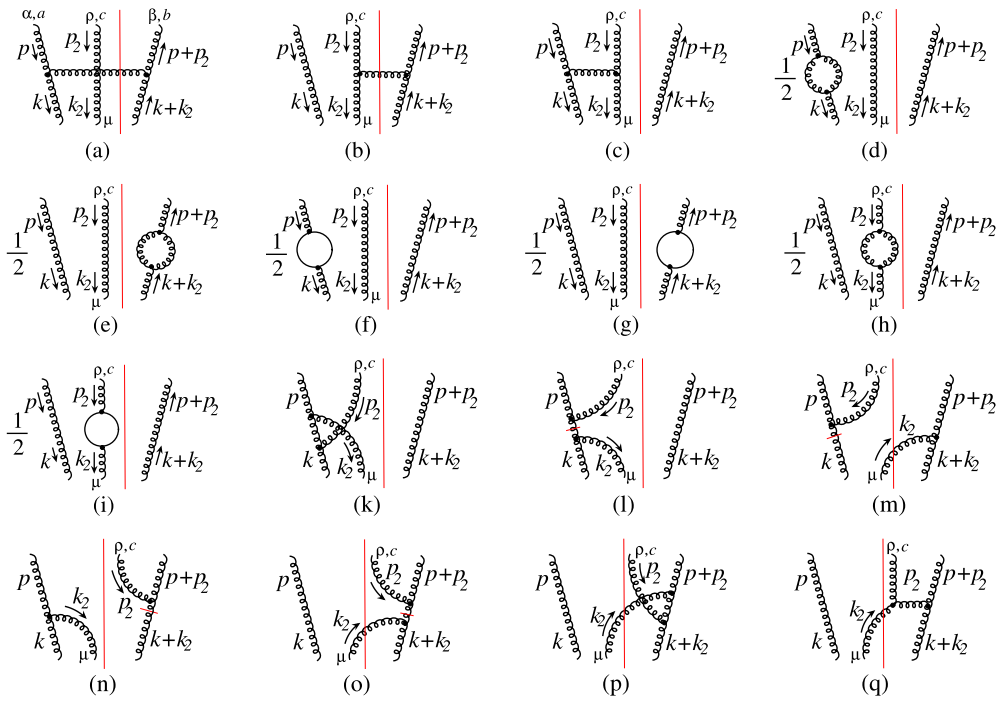

Figure 4.8 Feynman diagrams that contribute to the leading order evolution kernel from the tri-gluon correlation functions to the tri-gluon correlation function.

(b), (c), (d), (e), (f), and (g) give the nonvanishing contribution to the evolution kernel, $K_{gg}^{(i,j)}$,

$$d\mathcal{I}_{gg}^{(a)} = 2\pi\,\delta(\xi_2)\,\frac{1}{\xi}\int^{\mu_F^2}\frac{dk_T^2}{k_T^2}\left[C_A-\frac{C_A}{2}\right]\frac{\alpha_s}{2\pi}\,2z\left(\frac{z}{1-z}+\frac{1-z}{z}+z(1-z)\right); \quad (4.77)$$

$$d\mathcal{I}_{gg}^{(b)} = 2\pi\,\delta(\xi-x)\,\frac{1}{\xi_2}\int^{\mu_F^2}\frac{dk_T^2}{k_T^2}\left[\frac{C_A}{2}\right]\frac{\alpha_s}{2\pi}\left(\frac{1}{2}\,\frac{x^2+(x+\xi_2)^2}{(x+\xi_2)^2}\right); \quad (4.78)$$

$$d\mathcal{I}_{gg}^{(c)} = 2\pi\,\delta(\xi+\xi_2-x)\,\frac{1}{\xi}\int^{\mu_F^2}\frac{dk_T^2}{k_T^2}\left[\frac{C_A}{2}\right]\frac{\alpha_s}{2\pi}\left(\frac{1}{2}\,\frac{1+z^2}{1-z}\right); \quad (4.79)$$

$$d\mathcal{I}_{gg}^{(d+e)} = -2\pi\,\delta(\xi_2)\,\delta(\xi-x)\int^{\mu_F^2}\frac{dk_T^2}{k_T^2}\int_0^1 dz\,\frac{1}{2}\,[C_A] \times\frac{\alpha_s}{2\pi}\,2\left(\frac{z}{1-z}+\frac{1-z}{z}+z(1-z)\right); \quad (4.80)$$

$$d\mathcal{I}_{gg}^{(f+g)} = -2\pi\,\delta(\xi_2)\,\delta(\xi-x)\int^{\mu_F^2}\frac{dk_T^2}{k_T^2}\int_0^1 dz\,\frac{1}{2}\,(2\,n_f)\left[\frac{1}{2}\right]\frac{\alpha_s}{2\pi}\left((1-z)^2+z^2\right), \quad (4.81)$$

where $n_f = 1, 2, ...$ the number of active quark flavors and the color factors are shown in the square brackets. We find that the results from Eq. (4.77) to (4.81) are the same for the evolution

kernel $K_{gg}^{(ff)}$ and $K_{gg}^{(dd)}$. All evolution kernels of the crossing contribution $K_{gg}^{(fd)} = K_{gg}^{(df)} = 0$.

By adding the flavor changing contribution to the evolution kernels from Figs. 4.9 and 4.10, and adding the contributions from the same diagrams but with their parton momentum fractions ξ and $\xi + \xi_2$ switched, we derive the order of α_s evolution equations for the diagonal

twist-3 quark-gluon and tri-gluon correlation functions defined in Eq. (2.23),

$$\begin{aligned}
\frac{\partial T_{q,F}(x,x,\mu_F)}{\partial \ln \mu_F^2} &= \frac{\alpha_s}{2\pi}\int_x^1 \frac{d\xi}{\xi}\Bigg\{P_{qq}(z)\,T_{q,F}(\xi,\xi,\mu_F) \\
&+\frac{C_A}{2}\left[\frac{1+z^2}{1-z}\left[T_{q,F}(\xi,x,\mu_F)-T_{q,F}(\xi,\xi,\mu_F)\right]+z\,T_{q,F}(\xi,x,\mu_F)\right] \\
&+\frac{C_A}{2}\left[T_{\Delta q,F}(x,\xi,\mu_F)\right] \\
&+P_{qg}(z)\left(\frac{1}{2}\right)\left[T_{G,F}^{(d)}(\xi,\xi,\mu_F)+T_{G,F}^{(f)}(\xi,\xi,\mu_F)\right]\Bigg\}; \qquad (4.82)\\
\frac{\partial T_{\bar q,F}(x,x,\mu_F)}{\partial \ln \mu_F^2} &= \frac{\alpha_s}{2\pi}\int_x^1 \frac{d\xi}{\xi}\Bigg\{P_{qq}(z)\,T_{\bar q,F}(\xi,\xi,\mu_F) \\
&+\frac{C_A}{2}\left[\frac{1+z^2}{1-z}\left[T_{\bar q,F}(\xi,x,\mu_F)-T_{\bar q,F}(\xi,\xi,\mu_F)\right]+z\,T_{\bar q,F}(\xi,x,\mu_F)\right] \\
&+\frac{C_A}{2}\left[T_{\Delta \bar q,F}(x,\xi,\mu_F)\right] \\
&+P_{qg}(z)\left(\frac{1}{2}\right)\left[T_{G,F}^{(d)}(\xi,\xi,\mu_F)-T_{G,F}^{(f)}(\xi,\xi,\mu_F)\right]\Bigg\}; \qquad (4.83)\\
\frac{\partial T_{G,F}^{(f)}(x,x,\mu_F)}{\partial \ln \mu_F^2} &= \frac{\alpha_s}{2\pi}\int_x^1 \frac{d\xi}{\xi}\Bigg\{P_{gg}(z)\,T_G^{(f)}(\xi,\xi,\mu_F) \\
&+\frac{C_A}{2}\left[2\left(\frac{z}{1-z}+\frac{1-z}{z}+z(1-z)\right)\left[T_{G,F}^{(f)}(\xi,x,\mu_F)-T_{G,F}^{(f)}(\xi,\xi,\mu_F)\right]\right. \\
&\qquad \left.+2\left(1-\frac{1-z}{2z}-z(1-z)\right)T_{G,F}^{(f)}(\xi,x,\mu_F)\right] \\
&+\frac{C_A}{2}\left[(1+z)\,T_{\Delta G,F}^{(f)}(x,\xi,\mu_F)\right] \\
&+P_{gq}(z)\left(\frac{N_c^2}{N_c^2-1}\right)\sum_q\left[T_{q,F}(\xi,\xi,\mu_F)-T_{\bar q,F}(\xi,\xi,\mu_F)\right]\Bigg\}; \qquad (4.84)\\
\frac{\partial T_{G,F}^{(d)}(x,x,\mu_F)}{\partial \ln \mu_F^2} &= \frac{\alpha_s}{2\pi}\int_x^1 \frac{d\xi}{\xi}\Bigg\{P_{gg}(z)\,T_{G,F}^{(d)}(\xi,\xi,\mu_F) \\
&+\frac{C_A}{2}\left[2\left(\frac{z}{1-z}+\frac{1-z}{z}+z(1-z)\right)\left[T_{G,F}^{(d)}(\xi,x,\mu_F)-T_{G,F}^{(d)}(\xi,\xi,\mu_F)\right]\right. \\
&\qquad \left.+2\left(1-\frac{1-z}{2z}-z(1-z)\right)T_{G,F}^{(d)}(\xi,x,\mu_F)\right] \\
&+\frac{C_A}{2}\left[(1+z)\,T_{\Delta G,F}^{(d)}(x,\xi,\mu_F)\right] \\
&+P_{gq}(z)\left(\frac{N_c^2-4}{N_c^2-1}\right)\sum_q\left[T_{q,F}(\xi,\xi,\mu_F)+T_{\bar q,F}(\xi,\xi,\mu_F)\right]\Bigg\}. \qquad (4.85)
\end{aligned}$$

In above evolution equations, the LO quark-to-quark splitting function is given in Eq. (4.74),

and the rest LO parton-to-parton splitting functions for the normal PDFs are given by

$$
\begin{aligned}
P_{qg}(z) &= \frac{1}{2}\left[(1-z)^2+z^2\right], \\
P_{gg}(z) &= 2\,C_A\left[\frac{z}{(1-z)_+}+\frac{1-z}{z}+z(1-z)\right]+\left(C_A\frac{11}{6}-\frac{n_f}{3}\right)\delta(1-z), \\
P_{gq}(z) &= C_F\left[\frac{(1-z)^2+1}{z}\right].
\end{aligned}
\tag{4.86}
$$

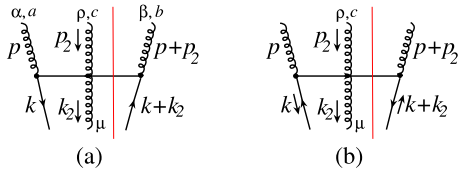

Figure 4.9 Feynman diagrams that contribute to the leading order evolution kernel from the tri-gluon correlation functions to the quark-gluon correlation function.

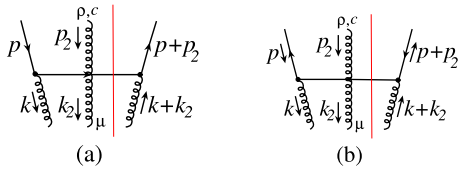

Figure 4.10 Feynman diagrams that contribute to the leading order evolution kernel from the quark-gluon correlation functions to the tri-gluon correlation functions.

Our explicit calculation also verifies that evolution equations for the *diagonal* parts of the second set of twist-3 correlation functions vanish,

$$
\frac{\partial T_{\Delta q(\bar{q}),F}(x,x,\mu_F)}{\partial \ln \mu_F^2}=0\,, \quad \frac{\partial T^{(f,d)}_{\Delta G,F}(x,x,\mu_F)}{\partial \ln \mu_F^2}=0\,,
\tag{4.87}
$$

which are consistent with the antisymmetric nature of the second set of twist-3 correlation functions. The *off-diagonal* correlation functions in Eqs. (4.82) to (4.85) are defined as in Eq. (2.33).

Equations from (4.82) to (4.85) plus Eq. (4.87) form a complete set of evolution equations of the *diagonal* twist-3 correlation functions relevant to the leading gluonic pole contribution to the SSAs. All evolution kernels at the order of α_s are infrared safe and perturbatively calculated. However, unlike the evolution equations for the full twist-3 correlation functions from Eq. (4.60) to Eq. (4.63), these evolution equations do not form a closed equation set.

The evolution equations of the diagonal twist-3 correlation functions have a lot in common with the DGLAP evolution equations of normal PDFs. Every channel of parton-to-parton evolution kernel is led by a term that is proportional to the DGLAP splitting function and the diagonal twist-3 correlation functions. All other terms are either proportional to the difference between the diagonal and the off-diagonal correlation functions or proportional to the off-diagonal correlation functions. Therefore, we expect that the scale dependence of the diagonal part of the twist-3 correlation functions is more close to the scale dependence of spin-averaged PDFs, not the spin-dependent helicity distributions.

Unlike the normal PDFs, the quark-gluon and antiquark-gluon correlation functions could have a different evolution equation unless the tri-gluon correlation function $T_{G,F}^{(f)} = 0$. The difference was caused by the difference in color contraction for $T_{G,F}^{(f)}$ and $T_{G,F}^{(d)}$. As we show in Chapter 3, the production of open charm mesons in SIDIS or hadron-hadron collisions can provide the excellent information on the tri-gluon correlation functions. If $T_{G,F}^{(f)} \neq 0$, the difference between the quark-gluon and antiquark-gluon correlation functions could be enhanced as the scale evolves. The difference should lead to interesting measurable consequences when we compare the SSAs generated by the quark-gluon correlation with that by the antiquark-gluon correlation.

It was argued in Ref. [50] that one of the two tri-gluon correlation functions $T_{G,F}^{(f)}$ can be related to the moment of a TMD gluon distribution, known as the gluonic Sivers function, in terms of their operator definitions. However, the other tri-gluon correlation function $T_{G,F}^{(d)}$ does not have a direct operator connection to the TMD gluon distribution. Equation (4.85) indicates that within QCD collinear factorization formalism, the $T_{G,F}^{(d)}$ can be generated perturbatively from the quark-gluon and antiquark-gluon correlation functions as long as $T_{q,F}(x,x,\mu_F) +$

$T_{\bar{q},F}(x,x,\mu_F) \neq 0$ or $T^{(d)}_{\Delta G,F}(x,\xi,\mu_F) \neq 0$, even if $T^{(d)}_{G,F}$ vanishes at one scale.

To complete this section, we state that we also examined the infrared sensitivity of the order of α_s evolution kernels for correlation functions that give the leading fermionic pole contribution to the SSAs. The fermionic pole contribution is generated by the off-diagonal correlation functions, $\mathcal{T}_{q,F}(0,x,\mu_F)$, $\mathcal{T}_{G,F}(0,x,\mu_F)$, $\mathcal{T}_{\Delta q,F}(0,x,\mu_F)$, and $\mathcal{T}_{\Delta G,F}(0,x,\mu_F)$ (or equivalently from $\mathcal{T}_{q,F}(x,0,\mu_F)$, $\mathcal{T}_{G,F}(x,0,\mu_F)$, $\mathcal{T}_{\Delta q,F}(x,0,\mu_F)$, and $\mathcal{T}_{\Delta G,F}(x,0,\mu_F)$ for the diagrams in which the gluon at the cut vertex is in the RHS of the cut). At the order of α_s, all evolution kernels are also infrared safe. For example, the flavor non-singlet evolution kernel for the quark-gluon correlation function $\widetilde{\mathcal{T}}_{q,F}$ can be calculated from the diagrams in Fig. 4.7 by setting $x = 0$. We find that after setting $x = 0$, only diagrams (a), (b), (c), (e), (f), and (g) in Fig. 4.7 give nonvanishing contribution to the evolution kernel. Again, the evolution kernel is infrared safe and all infrared divergences cancel between diagrams. It will be interesting to derive the full evolution equations for the off-diagonal twist-3 correlation functions in the future.

4.4 Scale dependence

In this section, we study the scale dependence of the diagonal twist-3 quark-gluon and tri-gluon correlation functions relevant to SSAs by solving the evolution equations derived in the last section.

Since the evolution equations for the diagonal twist-3 correlation functions from Eq. (4.82) to (4.85) do not form a closed set of differential equations, we need to make a model for off-diagonal correlation functions before we can study the scale dependence of the diagonal correlation functions. For the following numerical study, we introduce the following model to express the *symmetric* off-diagonal correlation functions in terms of diagonal correlation functions and a universal width,

$$\begin{aligned} T_{q,F}(x_1,x_2,\mu_F) &= \frac{1}{2}\left[T_{q,F}(x_1,x_1,\mu_F) + T_{q,F}(x_2,x_2,\mu_F)\right] e^{-\frac{(x_1-x_2)^2}{2\sigma^2}}, \\ \mathcal{T}^{(f,d)}_{G,F}(x_1,x_2,\mu_F) &= \frac{1}{2}\left[\mathcal{T}^{(f,d)}_{G,F}(x_1,x_1,\mu_F) + \mathcal{T}^{(f,d)}_{G,F}(x_2,x_2,\mu_F)\right] e^{-\frac{(x_1-x_2)^2}{2\sigma^2}}, \end{aligned} \tag{4.88}$$

where both $T_{q,F}$ and $\mathcal{T}_{G,F}^{(f,d)}$ are symmetric in exchange of x_1 and x_2 and the σ is a width for the strength of the off-diagonal correlation. However, the off-diagonal correlation function $T_{G,F}^{(f,d)}(x_1, x_2, \mu_F)$ defined in Eq. (2.33) is not symmetric. From Eq. (4.88), we have

$$T_{G,F}^{(f,d)}(x_1, x_2, \mu_F) = \frac{1}{2}\left[T_{G,F}^{(f,d)}(x_1, x_1, \mu_F) + \frac{x_2}{x_1}\, T_{G,F}^{(f,d)}(x_2, x_2, \mu_F)\right] e^{-\frac{(x_1-x_2)^2}{2\sigma^2}} . \tag{4.89}$$

We choose the width σ such that

$$e^{-\frac{(x_1-x_2)^2}{2\sigma^2}} \sim 0 \tag{4.90}$$

when $|x_1 - x_2| \to 1$. In Fig. 4.11, we plot the factor $e^{-\frac{x^2}{2\sigma^2}}$ as a function of x for $\sigma = 1/4$ (solid line) and $1/8$ (dashed line).

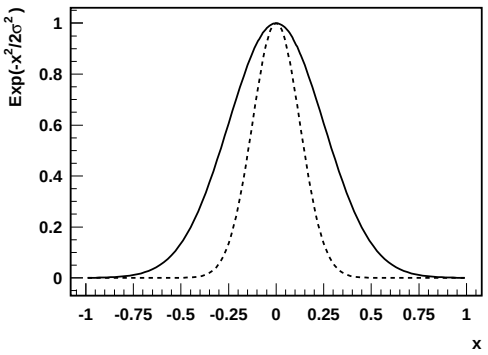

Figure 4.11 The factor $e^{-\frac{x^2}{2\sigma^2}}$ as a function of x for $\sigma = 1/4$ (solid) and $\sigma = 1/8$ (dashed).

To numerically solve the evolution equations in Eqs. (4.82) to (4.85), we choose the following input correlation functions at $\mu_{F0} = 2$ GeV. For the quark-gluon correlation function $T_{q,F}(x, x, \mu_{F0})$, we choose the Fit. II of the quark-gluon correlation function $T_{q,F}(x, x, \mu_F)$ from Ref. [27]. For the tri-gluon correlation functions, we follow Eq. (3.57) in chapter 3,

$$T_{G,F}^{(f)}(x, x, \mu_{F0}) = \lambda_f\, G(x, \mu_{F0}) \qquad T_{G,F}^{(d)}(x, x, \mu_{F0}) = \lambda_d\, G(x, \mu_{F0}) \tag{4.91}$$

with $\lambda_f = \lambda_d = +0.07$ GeV at $\mu_{F0} = 2$ GeV and CTEQ6L unpolarized gluon distribution

[13]. As an approximation, we also set $T_{\Delta q,F}(x,\xi,\mu_F) = 0$ and $T_{\Delta G,F}(x,\xi,\mu_F) = 0$ for less parameters since they have vanishing diagonal contribution and the size of the off-diagonal part could be smaller than that of set one correlation functions. For a better convergence of the numerical solution, we use the linear combination of the two tri-gluon correlation functions, $T^{(\pm)}_{G,F} = T^{(d)}_{G,F} \pm T^{(f)}_{G,F}$, when we solve for the evolution equations.

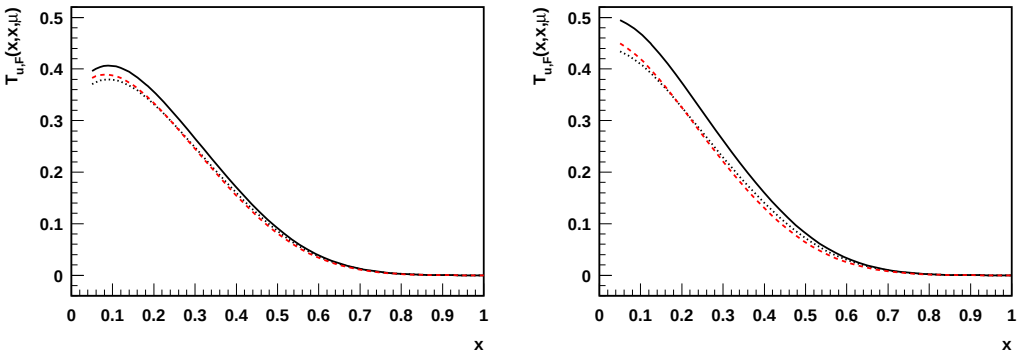

Figure 4.12 Twist-3 up-quark-gluon correlation $T_{u,F}(x,x,\mu_F)$ as a function of x at $\mu_F = 4$ GeV (left) and $\mu_F = 10$ GeV (right). The factorization scale dependence is a solution of the flavor non-singlet evolution equation in Eq. (4.73). Solid and dotted curves correspond to $\sigma = 1/4$ and $1/8$, while the dashed curve is obtained by keeping only the DGLAP evolution kernel $P_{qq}(z)$ in Eq. (4.73).

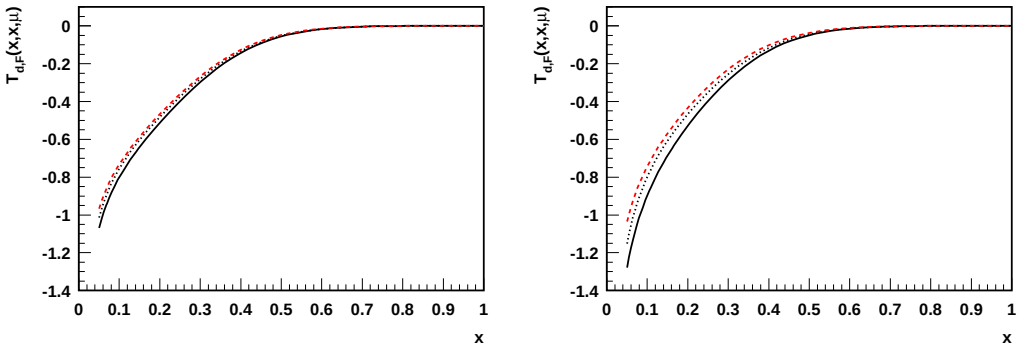

Figure 4.13 Twist-3 down-quark-gluon correlation $T_{d,F}(x,x,\mu_F)$ as a function of x at $\mu_F = 4$ GeV (left) and $\mu_F = 10$ GeV (right). Solid and dotted curves correspond to $\sigma = 1/4$ and $1/8$, while the dashed curve is obtained by keeping only the DGLAP evolution kernel $P_{qq}(z)$ in Eq. (4.73).

We first solve the flavor non-singlet evolution equation for the quark-gluon correlation function in Eq. (4.73) to test the relative role of the normal DGLAP evolution term that is proportional to $P_{qq}(z)$ and the new piece that depends on the off-diagonal correlation function. In Fig. 4.12, we plot the twist-3 up-quark-gluon correlation $T_{u,F}(x,x,\mu_F)$ as a function of x at the factorization scale $\mu_F = 4$ GeV (left) and $\mu_F = 10$ GeV (right). The difference between the left figure and the one on the right indicates the evolution of the twist-3 correlation functions. The factorization scale dependence is a solution of the flavor non-singlet evolution equation in Eq. (4.73). Solid and dotted curves correspond to two different choices of the width for the off-diagonal input correlation function at $\sigma = 1/4$ and $1/8$, respectively. The dashed curve is obtained by keeping only the DGLAP evolution kernel $P_{qq}(z)$ when we solve the flavor non-singlet evolution equation in Eq. (4.73). Similarly, we plot the twist-3 down-quark-gluon correlation $T_{d,F}(x,x,\mu_F)$ as a function of x at the factorization scale $\mu_F = 4$ GeV (left) and $\mu_F = 10$ GeV (right) in Fig. 4.13. Unlike the up-quark-gluon correlation function $T_{u,F}$, the down-quark-gluon correlation function $T_{d,F}$ is negative [16]. Figures 4.12 and 4.13 clearly show that the scale dependence of the diagonal twist-3 quark-gluon correlation function does follow the evolution of the unpolarized quark distribution. The difference between the solid and the dashed curves indicates that the effect of non-DGLAP type contribution from the off-diagonal correlation function could be very important at small x if the width of the off-diagonal correlation function is large.

In Figs. 4.14 and 4.15, we plot the twist-3 up-quark-gluon and down-quark-gluon correlation functions, $T_{u,F}(x,x,\mu_F)$ and $T_{d,F}(x,x,\mu_F)$, as a function of x at $\mu_F = 4$ GeV (left) and $\mu_F = 10$ GeV (right). The only difference between the solid and dotted curves in these figures and those in Figs. 4.12 and 4.13 is that we use the full set of evolution equations in Eq. (4.82) through (4.85) to solve for the factorization scale dependence of these correlation functions. The dashed curves represent the quark-gluon correlation functions obtained from the parametrization of Fit II in Ref. [27] by assuming all quark-gluon and tri-gluon correlation functions obey the DGLAP evolution. We find that non-DGLAP terms in the full evolution equations for the diagonal twist-3 correlation functions play a significant role in modifying the

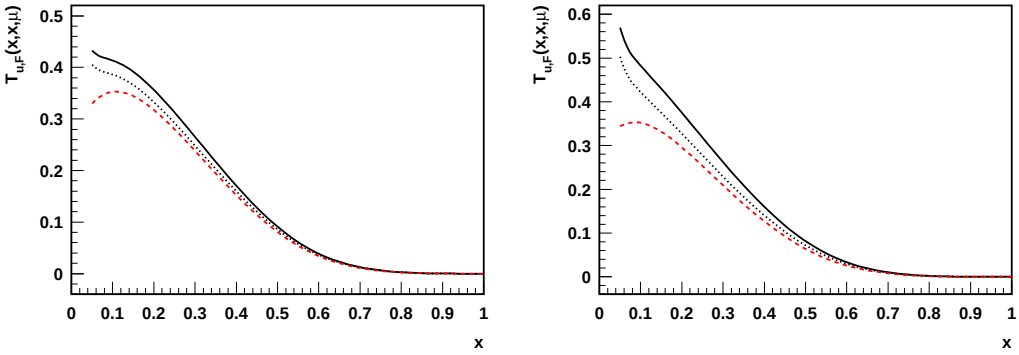

Figure 4.14 Twist-3 up-quark-gluon correlation $T_{u,F}(x,x,\mu_F)$ as a function of x at $\mu_F = 4$ GeV (left) and $\mu_F = 10$ GeV (right). The factorization scale dependence is obtained by solving the full set of evolution equations in Eq. (4.82) through (4.85). Solid and dotted curves correspond to $\sigma = 1/4$ and $1/8$ for the width of input off-diagonal correlation functions. The dashed curves represent the quark-gluon correlation functions obtained from the parametrization of Fit II in Ref. [27] by assuming all quark-gluon and tri-gluon correlation functions obey the DGLAP.

evolution of these correlation functions at small x, where the role of the off-diagonal correlation functions is enhanced due to a larger available phase space for the evolution kernels. The extra enhancement of the solid and dotted curves over the dashed curves in Figs. 4.14 and 4.15 is mainly from the term proportional to the sum of both tri-gluon correlation functions $T_{G,F}^{(f)}$ and $T_{G,F}^{(d)}$ that we assumed to have the same sign.

In Figs. 4.16 and 4.17, we plot the twist-3 tri-gluon correlation functions, $T_{G,F}^{(f)}(x,x,\mu_F)$ and $T_{G,F}^{(d)}(x,x,\mu_F)$, as a function of x at $\mu_F = 4$ GeV (left) and $\mu_F = 10$ GeV (right), respectively. Solid and dotted curves are from solving the full evolution equations with the input correlation functions evaluated at $\sigma = 1/4$ and $1/8$, respectively. Dashed curves are given by the normal CTEQ6L gluon distribution multiplied by the normalization constant λ_f (or λ_d), which corresponds to making an assumption that all twist-3 correlation functions obey the DGLAP evolution, like the normal unpolarized PDFs. We notice that for the evolution of tri-gluon correlation functions, the difference in color factor for the DGLAP-type terms in the full evolution equations tends to compensate the contribution from the terms proportional to the

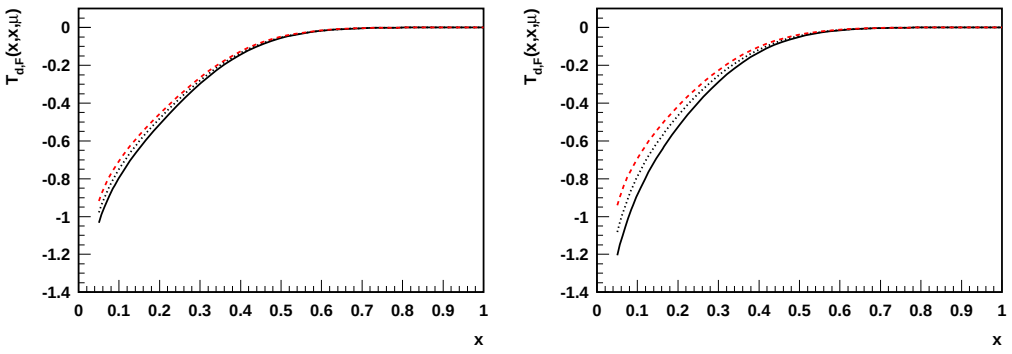

Figure 4.15 Twist-3 down-quark-gluon correlation $T_{d,F}(x, x, \mu_F)$ as a function of x at $\mu_F = 4$ GeV (left) and $\mu_F = 10$ GeV (right). all curves are defined in the same way as those in Fig. 4.14.

off-diagonal correlation functions, so that the evolution of the tri-gluon correlation functions follow more closely to the DGLAP evolution as shown in Figs. 4.16 and 4.17.

We complete this section by stressing that the scale dependence presented in this section is sensitive to our assumption to neglect the role of the second set of twist-3 correlation functions and our model for the input tri-gluon correlation functions (equal and positive at the input scale). Although the overall features found here should be valid, the precise numerical values of these correlation functions should be extracted from a consistent global QCD analysis by comparing experimental data on SSAs and corresponding theoretical calculations, like what have been done to test the leading power QCD factorization formalism [13, 14]. The new evolution equation derived here is the necessary step to make such a consistent global QCD analysis possible for twist-3 correlation functions relevant to SSAs.

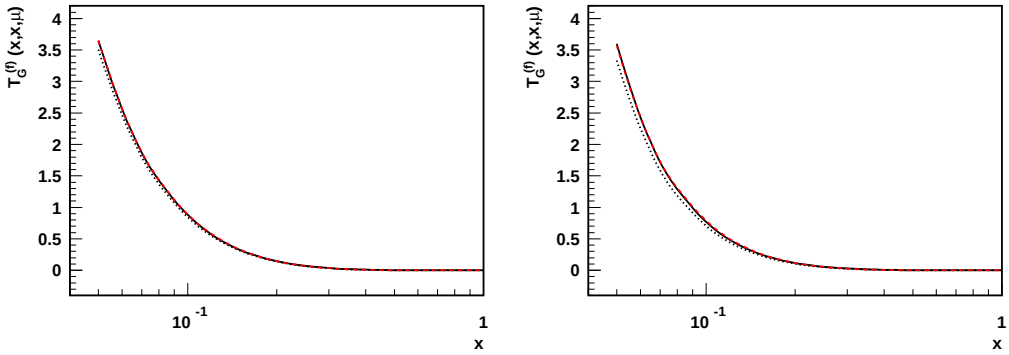

Figure 4.16 Twist-3 tri-gluon correlation function $T_{G,F}^{(f)}(x,x,\mu_F)$ as a function of x at $\mu_F = 4$ GeV (left) and $\mu_F = 10$ GeV (right). Dashed curves are from $T_{G,F}^{(f)}(x,x,\mu_F) = \lambda_f\, G(x,\mu_F)$, and solid and dotted curves are from solving the full evolution equations with $\sigma = 1/4$ and $1/8$ for the input correlation functions, respectively.

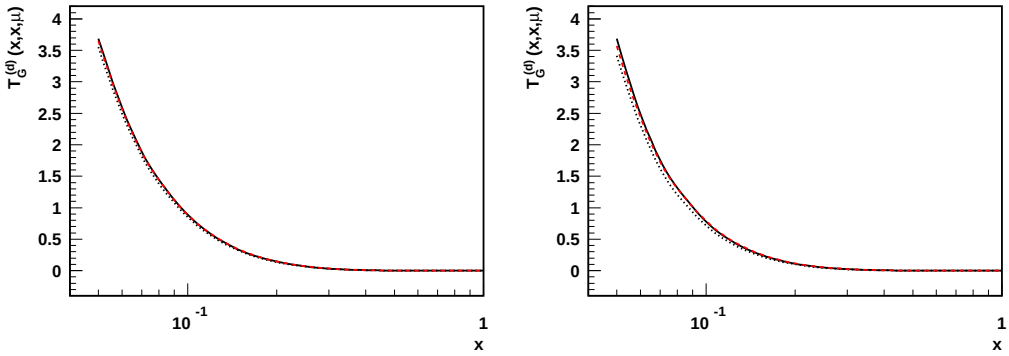

Figure 4.17 Twist-3 tri-gluon correlation function $T_{G,F}^{(d)}(x,x,\mu_F)$ as a function of x at $\mu_F = 4$ GeV (left) and $\mu_F = 10$ GeV (right). Dashed curves are from $T_{G,F}^{(d)}(x,x,\mu_F) = \lambda_d\, G(x,\mu_F)$, and solid and dotted curves are from solving the full evolution equations with $\sigma = 1/4$ and $1/8$ for the input correlation functions, respectively.

CHAPTER 5. Transverse momentum dependent parton distributions

We have demonstrated that SSAs of cross sections, whose observed momentum scales are much larger than $\Lambda_{\rm QCD}$, can be described in terms of the collinear factorization approach. When the momentum transfer of the partonic collisions Q is much larger than the typical transverse momentum of active partons $k_\perp$, the collinear factorization approach expands the active parton momentum entering the hard collision around its large collinear component $k \approx k_\parallel \sim Q$. The leading contribution of the collinear expansion does not generate the SSAs because of the parity and time-reversal invariance of QCD. That is, the nonvanishing SSA has to be a consequence of parton's transverse motion or quantum interference between scattering amplitudes with different number of active partons. As demonstrated in last three chapters, SSAs in the collinear factorization approach are determined by the twist-3 three-parton correlation functions. These correlation functions can be related to the moments of transverse momentum dependent (TMD) parton distributions [51]

$$T_{q,F}(x,x) = \int d^2k_\perp k_\perp \frac{1}{2}\Delta^N f_{q/h^\uparrow}(x,k_\perp)\,. \tag{5.1}$$

That is, the SSA in the collinear factorization approach measures the integrated effect of the parton's transverse motion inside a transversely polarized hadron. This is because the cross sections with one large momentum transfer Q is not very sensitive to the parton's transverse motion when $k_\perp \ll Q$.

The TMD function $\Delta^N f_{q/h^\uparrow}(x,k_\perp)$ is the spin-dependent part of the TMD parton distribution $f_{q/h^\uparrow}(x,\mathbf{k}_\perp,\vec{S}_\perp)$, which is interpreted to be a probability density to find a parton of flavor q with longitudinal momentum fraction x and transverse momentum $k_\perp$ inside a hadron h of transverse spin $\vec{S}_\perp$ [54, 55, 56, 57, 58]. Unlike the three-parton correlation function in the

collinear factorization approach, which provides the net or integrated spin dependence of the parton's transverse motion inside a polarized hadron, TMD parton distribution provides the direct information on the spin dependence of parton's transverse motion at a given transverse momentum $k_\perp$. Extracting the TMD parton distribution provides very valuable information on partonic dynamics inside a polarized hadron.

However, high energy collision experiments measure the cross section and the spin dependence of the cross sections. It is the QCD factorization that connects the measured cross sections to the gauge invariant nonperturbative distributions or correlation functions. That is, we need to factorize the cross sections in terms of TMD parton distributions.

It has been shown that cross sections with two very different momentum scales $Q \gg q_T \gtrsim \Lambda_{\rm QCD}$, such as Drell-Yan dilepton production with lepton pair's invariant mass Q much larger than the pair's transverse momentum q_T, could be factorized in terms of the TMD parton distributions [56]. In this TMD factorization approach, the SSAs are attributed to the Sivers function [59], which is the spin dependent part of the TMD parton distributions. If a final-state hadron was observed, the SSAs could be generated by the Collins function [60], which describes the asymmetric hadron formation around the direction of a transversely polarized parton. This TMD factorization approach to the SSAs has also been applied extensively in phenomenological studies of SSAs [24].

The twist-3 collinear factorization approach is more relevant to the cross section with all observed momentum scales are much larger than $\Lambda_{\rm QCD}$. On the other hand, the TMD factorization approach is more relevant to the observables with at least one large momentum scale to ensure the perturbative calculation and at least one small scale that is sensitive to the parton's transverse momentum. Although the twist-3 collinear approach and the TMD approach each have their kinematic domain of validity, they were shown to be consistent with each other in the kinematic regime where they both apply [32]. Each approach has its advantage and disadvantage. The twist-3 collinear factorization approach seems to work for more high energy observables or cross sections, but, it only probes the integrated effect of parton's transverse motion. On the other hand, the TMD factorization approach relates the

cross section to TMD parton distributions, and directly probe the spin dependence of parton's transverse motion at a given $k_\perp$. But, the TMD factorization can only apply to a very limited number of cross sections [58]. These two approaches complement to each other.

However, there is one crucial difference between these two factorization approaches besides the difference in kinematic regimes where they apply. The Sivers function in the TMD factorization approach could be process dependent, while all distribution functions in the collinear factorization approach are universal. It was predicted by Collins [54] on the basis of time-reversal arguments that the quark Sivers function in semi-inclusive deep inelastic scattering (SIDIS) and in Drell-Yan process (DY) have the same functional form but an *opposite sign*, a time-reversal modified universality. In this chapter, we derive the same time-reversal modified universality for both quark and gluon Sivers function from the parity and time-reversal invariance of QCD.

The experimental check of this time-reversal modified universality of the Sivers function would provide a critical test for the TMD factorization approach [54, 55, 56, 57, 58]. Recently, the quark Sivers function has been extracted from data of SIDIS experiments [61]. Future measurements of the SSAs in DY production have been planned [62]. Since the W production shares the same Sivers function as DY, and will be available very soon at RHIC [63], we calculate the SSAs of W production, and the induced SSAs of the inclusive single lepton production from the decay of W bosons at RHIC experiment. We find that although the asymmetry is diluted from the decay of W bosons, the lepton asymmetry is significant and measurable for a good range of lepton rapidity at RHIC. We show that the lepton SSAs provide the better flavor separation of the quark Sivers function than what the standard DY can do. We also show that the lepton SSAs are sharply peaked at transverse momentum $p_T \sim M_W/2$ with W mass M_W. Since leptons from heavy quarkonium decay and other potential backgrounds are unlikely to be peaked at the $p_T \sim M_W/2$, we argue that the SSA of inclusive high p_T leptons at RHIC is an excellent observable for testing the time-reversal modified universality of the Sivers function.

5.1 The QCD prediction

The predictive power of the TMD factorization approach to the SSAs relies on the universality of the TMD parton distributions. For the lepton-hadron SIDIS, $\ell(l) + h(p, \vec{S}) \to \ell'(l') + h'(p') + X$, the factorized TMD quark distribution has the following gauge invariant operator definition [64],

$$\begin{aligned} f_{q/h^\uparrow}^{\rm SIDIS}(x, \mathbf{k}_\perp, \vec{S}) &= \int \frac{dy^- d^2\mathbf{y}_\perp}{(2\pi)^3} e^{ixp^+y^- - i\,\mathbf{k}_\perp\cdot\mathbf{y}_\perp} \langle p, \vec{S}|\bar{\psi}(0^-, \mathbf{0}_\perp)\Phi_n^\dagger(\{\infty, 0\}, \mathbf{0}_\perp) \\ &\quad \times \Phi_{\mathbf{n}_\perp}^\dagger(\infty, \{\mathbf{y}_\perp, \mathbf{0}_\perp\})\frac{\gamma^+}{2}\Phi_n(\{\infty, y^-\}, \mathbf{y}_\perp)\psi(y^-, \mathbf{y}_\perp)|p, \vec{S}\rangle, \end{aligned} \tag{5.2}$$

where $y^+ = 0^+$ dependence is suppressed and the gauge links from the final-state interaction of SIDIS are

$$\begin{aligned} \Phi_n(\{\infty, y^-\}, \mathbf{y}_\perp) &\equiv \mathcal{P}e^{-ig\int_{y^-}^{\infty} dy_1^- n^\mu A_\mu(y_1^-, \mathbf{y}_\perp)}, \\ \Phi_{\mathbf{n}_\perp}(\infty, \{\mathbf{y}_\perp, \mathbf{0}_\perp\}) &\equiv \mathcal{P}e^{-ig\int_{\mathbf{0}_\perp}^{\mathbf{y}_\perp} d\mathbf{y}'_\perp \mathbf{n}_\perp^\mu A_\mu(\infty, \mathbf{y}'_\perp)}, \end{aligned} \tag{5.3}$$

where $\mathcal{P}$ indicates the path ordering and the direction $\mathbf{n}_\perp$ is pointed from $\mathbf{0}_\perp$ to $\mathbf{y}_\perp$, n^μ and $\bar{n}^\mu$ are given in Eq. (2.7).

For the DY, $h(p, \vec{S}) + h'(p') \to \gamma^*(Q)[\to \ell^+\ell^-] + X$, the factorized TMD quark distribution is given by

$$\begin{aligned} f_{q/h^\uparrow}^{\rm DY}(x, \mathbf{k}_\perp, \vec{S}) &= \int \frac{dy^- d^2\mathbf{y}_\perp}{(2\pi)^3} e^{ixp^+y^- - i\,\mathbf{k}_\perp\cdot\mathbf{y}_\perp} \langle p, \vec{S}|\bar{\psi}(0^-, \mathbf{0}_\perp)\Phi_n^\dagger(\{-\infty, 0\}, \mathbf{0}_\perp) \\ &\quad \times \Phi_{\mathbf{n}_\perp}^\dagger(-\infty, \{\mathbf{y}_\perp, \mathbf{0}_\perp\})\frac{\gamma^+}{2}\Phi_n(\{-\infty, y^-\}, \mathbf{y}_\perp)\psi(y^-, \mathbf{y}_\perp)|p, \vec{S}\rangle, \end{aligned} \tag{5.4}$$

where the past pointing gauge links were caused by the initial-state interactions of DY production [54]. From Eqs. (5.2) and (5.4), it is easy to show that the collinear quark distributions are process independent,

$$\int d^2\mathbf{k}_\perp f_{q/h^\uparrow}^{\rm SIDIS}(x, \mathbf{k}_\perp, \vec{S}) = \int d^2\mathbf{k}_\perp f_{q/h^\uparrow}^{\rm DY}(x, \mathbf{k}_\perp, \vec{S}), \tag{5.5}$$

if the same renormalization scheme was used for the ultraviolet divergence of the $\mathbf{k}_\perp$ integration.

Let $|\alpha\rangle = |p, \vec{S}\rangle$ and $\langle\beta|$ be equal to the rest of the matrix element in Eq. (5.2) [65]. From the parity and time-reversal invariance of QCD, $\langle\alpha_P|\beta_P\rangle = \langle\alpha|\beta\rangle$ and $\langle\beta_T|\alpha_T\rangle = \langle\alpha|\beta\rangle$, where $|\alpha_P\rangle$ and $|\beta_P\rangle$, and $|\alpha_T\rangle$ and $|\beta_T\rangle$ are the parity and time-reversal transformed states from the states $|\alpha\rangle$ and $|\beta\rangle$, respectively, we derive

$$f^{\rm SIDIS}_{q/h^\uparrow}(x, \mathbf{k}_\perp, \vec{S}) = f^{\rm DY}_{q/h^\uparrow}(x, \mathbf{k}_\perp, -\vec{S})\,, \tag{5.6}$$

thus the spin-averaged TMD quark distributions are process independent. Following the notation of Ref. [61], we expand the TMD quark distribution as

$$f_{q/h^\uparrow}(x, \mathbf{k}_\perp, \vec{S}) \equiv f_{q/h}(x, k_\perp) + \frac{1}{2}\Delta^N f_{q/h^\uparrow}(x, k_\perp)\, \vec{S} \cdot \left(\hat{p} \times \hat{\mathbf{k}}_\perp\right) \tag{5.7}$$

where $k_\perp = |\mathbf{k}_\perp|$, $\hat{p}$ and $\hat{\mathbf{k}}_\perp$ are the unit vectors of $\vec{p}$ and $\mathbf{k}_\perp$, respectively, $f_{q/h}(x, k_\perp)$ is the spin-averaged TMD distribution, and $\Delta^N f_{q/h^\uparrow}(x, k_\perp)$ is the Sivers function [59]. Substituting Eq. (5.7) into Eq. (5.6), we obtain,

$$\Delta^N f^{\rm SIDIS}_{q/h^\uparrow}(x, k_\perp) = -\Delta^N f^{\rm DY}_{q/h^\uparrow}(x, k_\perp)\,, \tag{5.8}$$

which confirms the Collins' prediction [54] that the Sivers function in SIDIS and in DY differ by a sign.

We define the gauge invariant TMD gluon distribution in SIDIS and in DY by replacing the quark operator $\bar{\psi}(\gamma^+/2)\psi$ in Eqs. (5.2) and (5.4) by the gluon operator $F^{+\mu}F^{+\nu}(-g_{\mu\nu})$, and the gauge links by those in the adjoint representation of SU(3) color. From the parity and time-reversal invariance of the matrix elements of the TMD gluon distribution, we find, like Eq. (5.6),

$$f^{\rm SIDIS}_{g/h^\uparrow}(x, \mathbf{k}_\perp, \vec{S}) = f^{\rm DY}_{g/h^\uparrow}(x, \mathbf{k}_\perp, -\vec{S})\,. \tag{5.9}$$

Applying Eq. (5.7) to the gluon TMD distribution, we derive the same time-reversal modified

universality for the gluon Sivers function,

$$\Delta^N f_{g/h^\uparrow}^{\rm SIDIS}(x,k_\perp) = -\Delta^N f_{g/h^\uparrow}^{\rm DY}(x,k_\perp)\,. \tag{5.10}$$

The sign change of the Sivers function is a property of the gauge invariant TMD parton distributions.

5.2 SSAs from W production

In this section, we first calculate the SSAs of W production at RHIC and then the SSAs of single lepton production from the decay of W bosons.

5.2.1 SSAs for W boson

We consider the following process,

$$A(p_A,\vec{S}_\perp) + B(p_B) \to W^\pm(q) + X\,, \tag{5.11}$$

where A is a proton with momentum p_A and transverse spin vector $\vec{S}_\perp$, B is another colliding proton with momentum p_B. We will use the TMD factorization formalism because W bosons at RHIC are likely produced with transverse momentum $|\mathbf{q}_\perp| \ll M_W$ [63]. We work in a frame in which the polarized hadron A moves in the $+z$-direction. For the production of reconstructed W bosons, we label the momenta of colliding partons and the W in light-cone component as

$$\begin{aligned}
p_a^\mu &= \left[x_a\sqrt{\frac{s}{2}},\, \frac{\mathbf{k}_{a\perp}^2}{x_a\sqrt{2\,s}},\, \mathbf{k}_{a\perp}\right]\,,\\
p_b^\mu &= \left[\frac{\mathbf{k}_{b\perp}^2}{x_b\sqrt{2\,s}},\, x_b\sqrt{\frac{s}{2}},\, \mathbf{k}_{b\perp}\right]\,,\\
q^\mu &= \left[\frac{M_T}{\sqrt{2}}e^{y_W},\, \frac{M_T}{\sqrt{2}}e^{-y_W},\, \mathbf{q}_\perp\right]\,,
\end{aligned} \tag{5.12}$$

where y_W is W rapidity and $M_T \equiv \sqrt{M_W^2 + |\mathbf{q}_\perp|^2}$. At leading order, we have the spin-averaged W cross section,

$$\begin{aligned}\frac{d\sigma_{AB\to W}}{dy_W\, d^2\mathbf{q}_\perp} &= \sigma_0 \sum_{a,b} |V_{ab}|^2 \int d^2\mathbf{k}_{a\perp} d^2\mathbf{k}_{b\perp} f_{a/A}(x_a, k_{a\perp}) \\ &\quad \times f_{b/B}(x_b, k_{b\perp})\, \delta^2(\mathbf{q}_\perp - \mathbf{k}_{a\perp} - \mathbf{k}_{b\perp}), \end{aligned} \tag{5.13}$$

where $\sigma_0 = (\pi/3)\sqrt{2}\,\mathrm{G_F} M_W^2/s$ is the lowest order partonic cross section with the Fermi weak coupling constant G_F and $s = (p_A + p_B)^2$, $\sum_{ab}$ runs over all light (anti)quark flavors, V_{ab} are the CKM matrix elements for the weak interaction, and $f_{i/h}(x_i, k_{i\perp})$ with $i = a, b$ and $h = A, B$ are spin-averaged TMD (anti)quark distribution of flavor i in hadron h, which are process independent. The parton momentum fractions in Eq. (5.13) are given by

$$x_a = \frac{M_W}{\sqrt{s}}\, e^{y_W}, \quad x_b = \frac{M_W}{\sqrt{s}}\, e^{-y_W} \tag{5.14}$$

to the leading power in $q_\perp^2/M_W^2$. Similarly, we have the leading order factorized spin-dependent W cross section $\Delta\sigma(\vec{S}_\perp)$ as

$$\begin{aligned}\frac{d\Delta\sigma_{A^\uparrow B\to W}(\vec{S}_\perp)}{dy_W\, d^2\mathbf{q}_\perp} &= \frac{\sigma_0}{2} \sum_{a,b} |V_{ab}|^2 \int d^2\mathbf{k}_{a\perp} d^2\mathbf{k}_{b\perp}\, \vec{S}_\perp \cdot (\hat{p}_A \times \hat{\mathbf{k}}_{a\perp}) \\ &\quad \times \Delta^N f_{a/A^\uparrow}^{\mathrm{DY}}(x_a, k_{a\perp}) f_{b/B}(x_b, k_{b\perp})\, \delta^2(\mathbf{q}_\perp - \mathbf{k}_{a\perp} - \mathbf{k}_{b\perp})\,. \end{aligned} \tag{5.15}$$

The SSA of W production is then defined as,

$$A_N^{(W)} \equiv \frac{d\Delta\sigma(\vec{S}_\perp)_{A^\uparrow B\to W}}{dy_W\, d^2\mathbf{q}_\perp} \Bigg/ \frac{d\sigma_{AB\to W}}{dy_W\, d^2\mathbf{q}_\perp}\,, \tag{5.16}$$

whose sign depends on the sign of the Sivers function and the direction of the spin vector $\vec{S}_\perp$.

To evaluate the SSA in Eq. (5.16), we use the parameterization of TMD parton distributions

in Ref. [61],

$$f_{q/h}(x,k_\perp) = f_q(x)\,\frac{1}{\pi\langle k_\perp^2\rangle}\,e^{-k_\perp^2/\langle k_\perp^2\rangle}, \tag{5.17}$$

$$\Delta^N f_{q/h^\uparrow}^{\rm SIDIS}(x,k_\perp) = 2\mathcal{N}_q(x)\,h(k_\perp)\,f_{q/h}(x,k_\perp), \tag{5.18}$$

$$h(k_\perp) = \sqrt{2e}\,\frac{k_\perp}{M_1}\,e^{-k_\perp^2/M_1} \tag{5.19}$$

where $f_q(x)$ is the standard unpolarized parton distribution of flavor q, $\langle k_\perp^2\rangle$ and M_1 are fitting parameters, and $\mathcal{N}_q(x)$ is a fitted distribution given in Ref. [61]. By carrying out the integration $d^2\mathbf{k}_{a\perp}d^2\mathbf{k}_{b\perp}$ in Eqs. (5.13) and (5.15) analytically, we obtain,

$$\begin{aligned} A_N^{(W)} &= \vec{S}_\perp\cdot(\hat{p}_A\times\mathbf{q}_\perp)\,\frac{2\langle k_s^2\rangle^2}{[\langle k_\perp^2\rangle+\langle k_s^2\rangle]^2}\,e^{-\left[\frac{\langle k_\perp^2\rangle-\langle k_s^2\rangle}{\langle k_\perp^2\rangle+\langle k_s^2\rangle}\right]\frac{\mathbf{q}_\perp^2}{2\langle k_\perp^2\rangle}} \\ &\quad\times\frac{\sqrt{2e}}{M_1}\,\frac{\sum_{ab}|V_{ab}|^2\,[-\mathcal{N}_a(x_a)]\,f_a(x_a)\,f_b(x_b)}{\sum_{ab}|V_{ab}|^2\,f_a(x_a)\,f_b(x_b)}, \end{aligned} \tag{5.20}$$

where $\langle k_s^2\rangle = M_1^2\,\langle k_\perp^2\rangle/[M_1^2+\langle k_\perp^2\rangle]$ and the "$-$" sign in front of $\mathcal{N}_a(x_a)$ is from Eq. (5.8), ie, due to the fact that the Sivers function in W production is opposite to those in SIDIS process. If we choose the $\vec{S}_\perp$ along the y-axis as in Ref. [61], $\vec{S}_\perp\cdot(\hat{p}_A\times\mathbf{q}_\perp) = q_T\cos(\phi_W)$ with $q_T\equiv|\mathbf{q}_\perp|$ and azimuthal angle ϕ_W. For our numerical predictions below, we choose $\phi_W = 0$ and the GRV98LO parton distribution [67] for $f_q(x)$ to be consistent with the usage of the TMD distributions of Ref. [61].

In Figs. 5.1 and 5.2, we plot the A_N from Eq. (5.20) at $\sqrt{s} = 500$ GeV. The W asymmetry is peaked at $q_T \ll M_W$ and is much larger than that of DY production [62]. This is because the u and d Sivers functions have an opposite sign, and they partially cancel each other in their contribution to the DY asymmetry, while they contribute to the W^+ and W^- separately. The large W^- asymmetry is caused by a large d Sivers function [61]. The negative d Sivers function in SIDIS gives the positive W^- asymmetry. The rapidity dependence in Fig. 5.1 provides excellent informations for the flavor separation as well as the functional form of the Sivers function if we could reconstruct the W bosons.

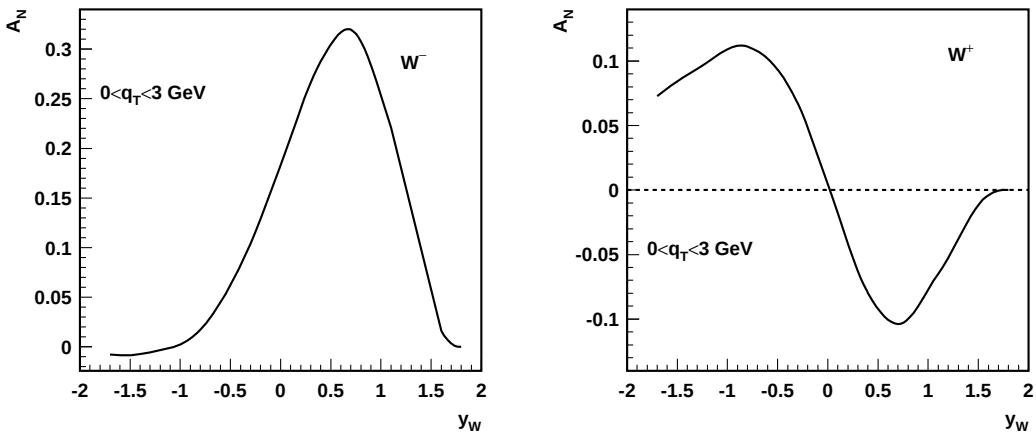

Figure 5.1 A_N as a function of W-boson rapidity for W^- (left) and W^+ (right). We have integrated over the q_T range from 0 to 3 GeV.

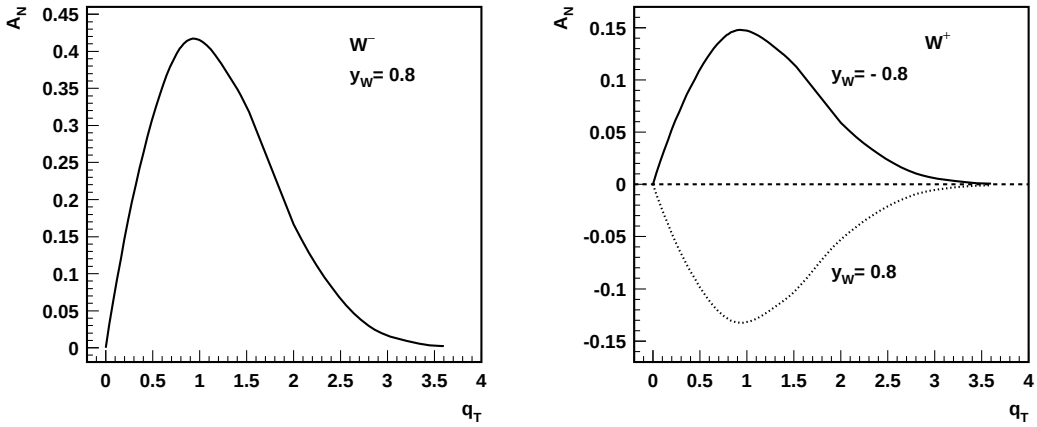

Figure 5.2 A_N as a function of W-boson transverse momentum for W^- (left) and W^+ (right).

5.2.2 SSAs for single lepton production from the decay of W boson

The SSAs of W production at RHIC were originally proposed in Refs. [66] to measure the Sivers function. As we have shown in last subsection, the SSAs of W boson is very large and should be a perfect channel to measure the Sivers functions and verify the time-reversal modified universality of the Sivers functions. However, it is difficult to reconstruct W bosons by the current detectors at RHIC [63]. It is the lepton from the decay of W bosons that is readily measured at RHIC. In this subsection, we will present our calculation for the SSAs of

the inclusive lepton production from W decay, ie, we now consider

$$A(p_A, \vec{S}_\perp) + B(p_B) \to \left[W^\pm(q) \to \ell^\pm(p)\right] + X\,. \tag{5.21}$$

Since we do not measure the (anti)neutrino, we integrate over the momentum of (anti)neutrino from the W decay. We then obtain the leading order factorized cross section for the production of leptons of rapidity y and transverse momentum $\mathbf{p}_\perp$,

$$\begin{aligned}\frac{d\sigma_{A^\uparrow B\to\ell(p)}(\vec{S}_\perp)}{dy\,d^2\mathbf{p}_\perp} &= \sum_{a,b}|V_{ab}|^2\int dx_a\,d^2\mathbf{k}_{a\perp}\int dx_b\,d^2\mathbf{k}_{b\perp}f^{\rm DY}_{a/A^\uparrow}(x_a,\mathbf{k}_{a\perp},\vec{S}_\perp)\\ &\quad\times f_{b/B}(x_b,k_{b\perp})\,\frac{1}{16\pi^2\hat{s}}\left|\overline{\mathcal{M}}_{ab\to\ell}\right|^2\delta(\hat{s}+\hat{t}+\hat{u})\,,\end{aligned} \tag{5.22}$$

where $\hat{s}$, $\hat{t}$, and $\hat{u}$ are the Mandelstam variables and the leading order partonic scattering amplitude square, $\left|\overline{\mathcal{M}}_{ab\to\ell}\right|^2$, is given by

$$\left|\overline{\mathcal{M}}_{ab\to\ell}\right|^2 = \frac{8(\mathrm{G}_F M_W^2)^2}{3}\frac{\hat{u}^2}{(\hat{s}-M_W^2)^2+M_W^2\,\Gamma_W^2} \tag{5.23}$$

for partonic channels $ab = d\bar{u}, s\bar{u}, \bar{d}u, \bar{s}u$;

$$\left|\overline{\mathcal{M}}_{ab\to\ell}\right|^2 = \frac{8(\mathrm{G}_F M_W^2)^2}{3}\frac{\hat{t}^2}{(\hat{s}-M_W^2)^2+M_W^2\,\Gamma_W^2} \tag{5.24}$$

for the rest light flavor channels $ab = \bar{u}d, \bar{u}s, u\bar{d}, u\bar{s}$. Γ_W in Eqs. (5.23) and (5.24) is the W leptonic decay width.

Substituting Eq. (5.7) into Eq. (5.22), we derive both the spin-averaged and spin-dependent

cross sections as

$$\frac{d\sigma_{A^\uparrow B\to\ell(p)}(\vec{S}_\perp)}{dy\,d^2\mathbf{p}_\perp} = \sum_{a,b}|V_{ab}|^2\int dx_a\,d^2\mathbf{k}_{a\perp}\int dx_b\,d^2\mathbf{k}_{b\perp}f_{a/A}(x_a,k_{a\perp}) \times f_{b/B}(x_b,k_{b\perp})\,\frac{1}{16\pi^2\hat{s}}\left|\overline{\mathcal{M}}_{ab\to\ell}\right|^2\delta(\hat{s}+\hat{t}+\hat{u}), \tag{5.25}$$

$$\frac{d\Delta\sigma_{A^\uparrow B\to\ell(p)}(\vec{S}_\perp)}{dy\,d^2\mathbf{p}_\perp} = \sum_{a,b}|V_{ab}|^2\int dx_a\,d^2\mathbf{k}_{a\perp}\int dx_b\,d^2\mathbf{k}_{b\perp}\vec{S}_\perp\cdot(\hat{p}_A\times\hat{\mathbf{k}}_{a\perp})\Delta^N f^{\rm DY}_{a/A^\uparrow}(x_a,k_{a\perp}) \times f_{b/B}(x_b,k_{b\perp})\,\frac{1}{16\pi^2\hat{s}}\left|\overline{\mathcal{M}}_{ab\to\ell}\right|^2\delta(\hat{s}+\hat{t}+\hat{u}), \tag{5.26}$$

from which we evaluate the SSAs of inclusive lepton production from W decay numerically.

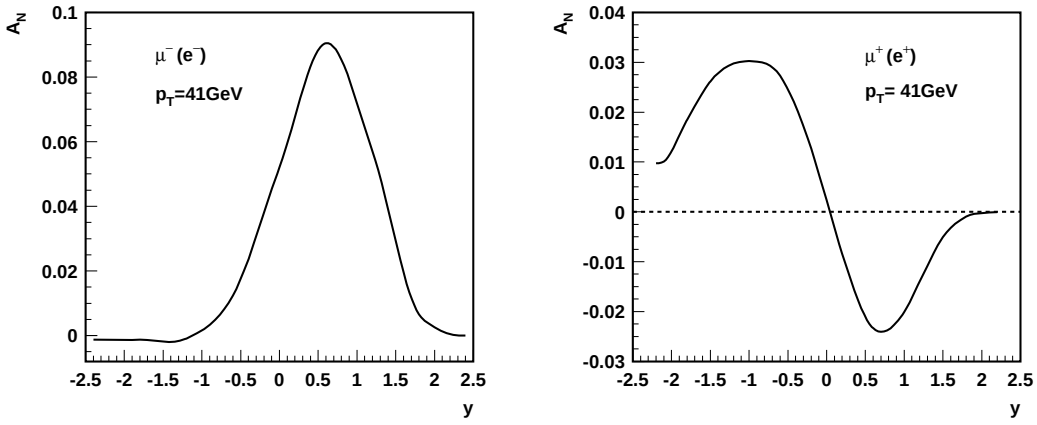

Figure 5.3 A_N as a function of lepton rapidity at $p_T = 41$ GeV for negative lepton (left) and positive lepton (right).

In Figs. 5.3 and 5.4, we present our predictions for the inclusive lepton asymmetry from the decay of W bosons at RHIC energy. Although the decay diluted the size of the asymmetry, the lepton inherited all key features of the W asymmetry in Figs. 5.1 and 5.2. As shown in Fig. 5.4, the lepton asymmetry is sharply peaked at $p_T \sim 41$ GeV, which should help control the potential background. The difference in rapidity dependence of the W^+ and W^- in Fig. 5.3 provides the excellent flavor separation of the Sivers function, as well as rich information on the functional form. For a good range of rapidity, the lepton asymmetry is measurable at RHIC and should be a good channel to test the time-reversal modified universality of the Sivers functions.

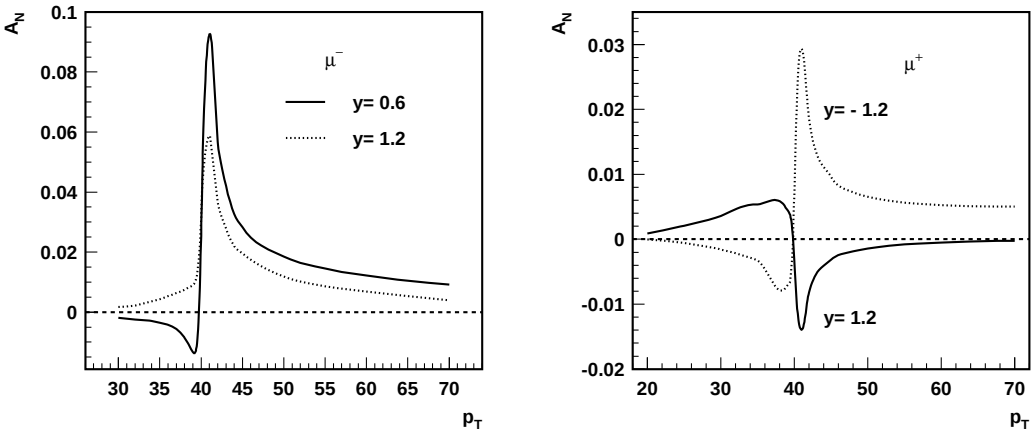

Figure 5.4 A_N as a function of lepton transverse momentum at different rapidity for negative lepton (left) and positive lepton (right).

CHAPTER 6. Nuclear dependence: Overview

We investigated the three parton correlation functions inside a polarized hadron in last four chapters by taking advantage of the spin-dependnece of the collisions. In this and next chapter we will use the nuclear dependence in high energy nuclear collisions to probe the four parton correlation functions.

Since 1970s it has been observed [68] that inclusive cross sections for single high transverse momentum particle produced in hadron-nucleus scattering show an anomalous nuclear dependence, in which the cross section at fixed transverse momentum might rise faster than linearly with atomic number A. Since typical energy exchange in a high transverse-momentum scattering process is over GeV, the hard scattering should take place at a distance scale less than 1/5 fm, which is certainly localized within a single nucleon. Because of the weak nuclear dependence of the nuclear density, a linear A dependence was expected for single scattering process. The anomalous nuclear dependence is often attributed to multiple scattering of partons inside nuclear matter [69, 70, 71, 72, 98]. For a recent review, see Ref. [73].

In terms of factorization at higher twist [18, 19], Luo, Qiu and Sterman (LQS) have developed a consistent treatment of multiple scattering at partonic level [98]. According to this generalized factorization theorem, the double scattering contribution (the first nontrivial term in multiple scattering) can be expressed in terms of universal four-parton correlation functions in nuclei and the corresponding short-distant hard parts can be calculated in perturbation theory systematically.

Since then, this formalism has been widely used to study the multiple scattering effect in hadron nucleus and heavy-ion collisions. Originally LQS applied this formalism to single particle inclusive and single-jet production in deep inelastic scattering and photo-production

[98]. Guo [89] used the formalism to study the so-called transverse momentum broadening, $\Delta\langle q_T^2\rangle \equiv \langle q_T^2\rangle|_{AB} - \langle q_T^2\rangle|_{hh}$, which is defined as a difference between the averaged transverse momentum square in hadron-nucleus collision and that in hadron-hadron collision. The averaged transverse momentum square that will be defined in the next Chapter could be perturbatively more stable than the transverse momentum distribution itself. Qiu and Vitev [74] studied the role of the partonic multiple scattering in understanding the nuclear shadowing of the structure functions in lepton deep inelastic scattering off a large nucleus. More recently, Guo, Wang and Zhang [75] extended this multiple scattering formalism to the heavy ion collision and studied the jet quenching phenomena [76, 77]: an energetic parton loses its energy when passing through the hot and dense medium formed in high energy nucleus-nucleus collisions. These studies have been successful in explaining the data observed in hadron-nucleus and nucleus-nucleus collisions. For a review, see Ref. [96].

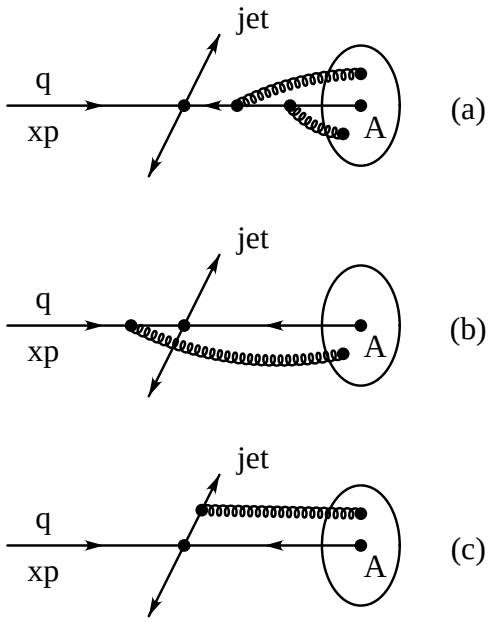

Figure 6.1 Clascification of parton multiple scattering in nuclear medium: (a) interactions internal to the nucleus, (b) initial-state interactions, and (c) final-state interactions.

To discuss the multiple scattering effect in a bit more detail, let us classify the multiple scattering into the following three categories: (a) initial-state interactions internal to the

nucleus, (b) initial-state parton-nucleus interactions (ISI), and (c) final-state parton-nuclues interactions (FSI), as sketched in Fig. 6.1. Here, we only consider the multiple scattering between the hard probes and the soft partons in the medium and do not consider the soft parton interactions between two heavy ions and those that are responsible for the formation of the hot and dense medium. The formation of the hot and dense medium observed at RHIC is very interesting and is beyond the scope of this thesis.

Initial-state interactions internal to the nucleus as shown in Fig. 6.1(a) will change the parton distributions of the nucleus. Consequently the effective parton distribution functions in a large nucleus (nPDFs) are different from a simple sum of individual nucleons parton distribution functions. The perturbatively calculable short-distance single scattering is infrared safe and is therefore the same for hadron scattering on a proton or a large nucleus. The nPDFs and the normal PDFs in a proton share the same operator definition except the proton state is replaced by the nuclear state. Since they share the same operator, the nPDFs and the normal PDFs obey the same DGLAP evolution equations [48] at the leading power of the large momentum exchange. Consequently, only nuclear dependence of the leading power nPDFs is from the boundary conditions, the input nPDFs, which are needed to solve the DGLAP evolution equations. Several groups have been trying to find consistent sets of nPDFs by the global fitting with all the existing experimental data in lepton-nuclues and hadron-nucleus collisions. Currently there are at least five parameterizations of nPDFs available for the community to use: EKS98 [78], dFS2003 [79], HKM [80], EPS08 [81], and EPS09 [82]. Although all of them are consistent with the experimental data, the nuclear dependence of the x behavior of nPDFs are quite different from each other, especially for nuclear gluon distribution. Recently, we have shown that the low-mass lepton pair production at large transverse momentum could be a very sensitive probe to the nuclear gluon distribution and should help to better pin down the nuclear gluon distribution [83].

The initial-state interactions internal to the nucleus not only change the absolute value of the nPDFs, they could also change the evolution of these parton distributions. Recently using DIS as an example, we are able to calculate the leading nuclear size enhanced power

corrections to the DGLAP evolution equations [84]. By doing so, we were able to include the process independent nuclear dependence to nPDFs not only from the input distributions but also from the dynamics of evolution. We find that these power corrections significantly slow down the growth of gluon density at small-x, which could drive the parton distribution at small-x into the saturation regime [85].

On the other hand, the process dependent initial-state and final-state parton-nucleus interactions, as shown in Fig. 6.1(b) and (c), directly change the physical cross sections and corresponding momentum distributions. Since the multiple scattering involves at least two physically polarized partons from the nucleus, the effect of these multiple scattering are power suppressed for the inclusive cross section or momentum distributions. However, as we will show in detail in next chapter, these effects are enhanced by the nuclear size and significant. The partonic multiple scattering might be the most important mechanics for generating the anomalous nuclear dependence. In next chapter, we will use this generalized factorization formalism to study the transverse momentum broadening of vector boson production in both hadron-nucleus and nucleus-nucleus collisions.

CHAPTER 7. Transverse momentum broadening of vector boson production in high energy nuclear collisions

In this chapter, we apply the generalized factorization theorems developed by LQS [98] to study the transverse momentum broadening of heavy vector boson production in high energy nuclear collisions.

7.1 Why transverse momentum broadening

The transverse momentum distribution of a heavy vector boson, such as a virtual photon with a large invariant mass, a heavy quarkonium, and a Z (or W) boson, is calculable in perturbative QCD when the transverse momentum q_T is also large [12, 86]. When $q_T \ll Q$ (invariant mass of vector boson), the q_T distribution calculated in the conventional fixed-order perturbation theory receives a large logarithm, $\ln\left(Q^2/q_T^2\right)$, at every power of α_s, which is a direct consequence of emission of soft and collinear gluons by the incoming partons (sometimes referred as "parton shower"). In order to have a reliable prediction, one need to resum these large logarithms. This so-called Sudakov resummation formalisms [52, 53] are classical ones and have been applied extensively in phenomenological studies [87].

In high energy nuclear collisions, partonic multiple scattering in a nuclear medium could modify the distribution of the vector boson's transverse momentum q_T. Each rescattering is likely to change the momentum spectrum by an order of the typical transverse momentum of the partons inside the nuclear matter, which is significantly softer than the momentum exchange in the hard collision. Therefore, the change to the transverse momentum spectrum, $d\sigma/dq_T^2$, should be most significant when q_T is relatively small. But, the rescattering effect on the low q_T spectrum is unlikely to be calculable in perturbative QCD [47, 88, 96, 98]. Furthermore,

the potential interference between the rescattering and the parton shower could complicate the resummation of the logarithms and lead to even less control on the low q_T spectrum. On the other hand, an averaged transverse momentum square of the produced heavy vector boson,

$$\langle q_T^2 \rangle \equiv \int dq_T^2 \, q_T^2 \, \frac{d\sigma_{hh\to V^*}}{dq_T^2} \Big/ \int dq_T^2 \, \frac{d\sigma_{hh\to V^*}}{dq_T^2} \ , \tag{7.1}$$

is much more inclusive. If we integrate over all kinematically allowed q_T, the $\langle q_T^2 \rangle$ depends on only one single hard scale, Q, the mass of the vector boson and is perturbatively calculable [47, 58, 88, 96]. The large logarithmic contribution to the q_T^2-distribution from the power of $\ln(Q^2/q_T^2)$ is suppressed by the q_T^2 weight.

The accumulative change from the rescattering to the averaged transverse momentum square - transverse momentum broadening, $\Delta\langle q_T^2 \rangle \equiv \langle q_T^2 \rangle|_{AB} - \langle q_T^2 \rangle|_{hh}$, defined as a difference between the calculable transverse momentum square in nuclear collision and that in hadron-hadron collision, should be calculable too [47, 96]. Some time ago, by taking into account the initial-state multiple scattering between the partons of the incoming beam and nuclear matter, Guo [89] has studied the Drell-Yan transverse momentum broadening. The broadening was shown to be proportional to the target size or to have the $A^{1/3}$-type nuclear dependence. The calculated nuclear dependence was found to be consistent with both Fermilab and CERN data.

On the other hand, as shown in Ref. [90], there have been difficulties in understanding the same broadening in the production of heavy quarkonia (J/ψ and Υ). At the leading order of perturbative calculation, the Drell-Yan dilepton production is dominated by a quark-antiquark annihilation subprocess, while the heavy quarkonium production in hadronic collision is dominated by a gluon-gluon fusion subprocess. One thus expects that the ratio of broadening of heavy quarkonium over Drell-Yan is close to the ratio of the multiple scattering effect of a gluon over that of a quark (or an antiquark) inside a nuclear medium [91]. At the lowest order, the ratio is approximately equal to the ratio of color factors of the lowest order gluon and (anti)quark rescattering, $C_A/C_F = 9/4$, with $C_A = N_c = 3$ and $C_F = (N_c^2 - 1)/(2N_c) = 4/3$. Although the data on heavy quarkonium broadening in hadron-nucleus collisions shows the expected $A^{1/3}$-type nuclear dependence, the ratio to the Drell-Yan broadening could be as

large as 5, twice of the naive expectation [90].

In this chapter, we will start with a study on the transverse momentum broadening of the heavy quarkonium in hadron nucleus collisions. We will show that the net broadening is a combined effect of the initial-state interaction and final-state rescattering between the produced heavy quark pair and the nuclear matter. Since the final-state interaction is sensitive to the non-perturbative formation mechanism of the bound state, we calculate the broadening of heavy quarkonium production in both non-relativistic QCD (NRQCD) model [92] and Color Evaporation model [93]. In the NRQCD model, the non-perturbative dynamics for a heavy quark pair to form a bound quarkonium is organized through matrix elements of operators that are characterized by an expansion in the relative velocity of the pair and the pair's rotational and color quantum numbers. On the other hand, in the Color Evaporation model, all heavy quark pairs with invariant mass less than the mass threshold of producing a pair of open flavor heavy mesons have the same probability to become a bound quarkonium regardless the pair's rotational and color quantum numbers. Rescattering of the heavy quark pair in nuclear medium could change the pair's rotational and color quantum numbers. Therefore, these two models could lead to different predictions for the nuclear dependence of heavy quarkonium production in nuclear collisions. If the difference is significant, an accurate measurement of the nuclear dependence could provide important information on the hadronization. We find that the heavy quarkonium broadening calculated in these two models have different analytical expressions. But, numerically, these two models predict a very similar result for the broadening of J/ψ and Υ in hadron-nucleus collision. The calculated broadening is close to $2C_A/C_F$, which is consistent with Fermilab data [90, 94].

We further extend our calculations of heavy quarkonium's transverse momentum broadening in hadron-nucleus collisions to the broadening in nucleus-nucleus collisions. The net broadening in nucleus-nucleus collisions will depend on whether there is hot medium produced in nucleus-nucleus collisions. As shown in Ref. [95], the Relativistic Heavy Ion Collider (RHIC) at Brookhaven National Laboratory has produced good evidence that a new state of hot and dense matter of quarks and gluons, the quark-gluon plasma (QGP), was formed in

ultra-relativistic heavy-ion collisions. We discuss the broadening in this kind of situation and investigate the role of transverse momentum broadening in probing the properties of the dense and hot QCD matter. We also propose to use the broadening of Z (as well as W) bosons to independently study the initial-state interaction and extract the medium density. We make the predictions for the broadening of Z (or W) bosons in relativistic heavy ion collisions at the future Large Hadron Collider (LHC) to test our formalism.

To set up the notation and terminology, we first review the perturbative QCD calculation for the transverse momentum broadening for Drell-Yan production in a covariant gauge, in which the calculation of broadening is the easiest. We then derive the transverse momentum broadening of heavy quarkonium production in hadron-nucleus collision in Sec. 7.3. We calculate both initial-state and final-state multiple scattering. We evaluate the transverse momentum broadening in both NRQCD model and Color Evaporation model. We then extend the calculation to the broadening of heavy quarkonium production in nucleus-nucleus collisions. In Sec. 7.4, we calculate the broadening of Z (as well as W) boson production in both hadron-nucleus and nucleus-nucleus collisions at the LHC. We argue that the transverse momentum broadening of Z (or W) bosons that are reconstructed from their leptonic decay channels is an excellent probe for initial-state rescattering and the medium density at an early stage of relativistic heavy ion collisions. We present our numerical study of the transverse momentum broadening of vector boson production in Sec. 7.5. We discuss the extrapolation of the non-perturbative matrix elements from the fixed target energies to collider energies. We compare our calculations with data from both fixed-target experiments at Fermilab, and collider experiments at RHIC. We also predict the broadening at the LHC energy.

7.2 Transverse momentum broadening in Drell-Yan production

Consider the Drell-Yan process in hadron-nucleus collisions,

$$h(p') + A(p) \to \gamma^*(q)[\to \ell^+\ell^-] + X, \tag{7.2}$$

where q, p', p are the four momentum of the virtual photon, the incoming hadron, and the nucleus (per nucleon) with atomic weight A, respectively. In nuclear collisions, it is very likely that the energetic incoming parton can have several scatterings with soft partons inside the nuclear matter before the hard collision to produce the vector boson (γ^*). Such initial-state multiple scattering could induce more soft radiation from the incoming parton and broaden the parton's transverse momentum. The additional parton transverse momentum at the hard collision leads to the broadening of the observed vector bosons.

In terms of contributions with different number of rescattering, the Drell-Yan cross section can be written as

$$\sigma_{hA} = \sigma_{hA}^{S} + \sigma_{hA}^{D} + \dots \tag{7.3}$$

with superscript S for single scattering, D for double scattering, and etc. As explained earlier, single hard scattering is localized in space and time, and is unlikely to provide the target length (or the $A^{1/3}$-type nuclear size) enhancement to the cross section, although it can get a weaker nuclear dependence to the cross section from nuclear parton distributions [96]. The leading contribution to the broadening of the dilepton's transverse momentum square comes from the double scattering [89],

$$\Delta\langle q_T^2\rangle_{\rm DY} \approx \int dq_T^2\, q_T^2\, \frac{d\sigma_{hA}^{D}}{dQ^2 dq_T^2} \Big/ \frac{d\sigma_{hA}}{dQ^2}\ , \tag{7.4}$$

with the inclusive Drell-Yan cross section given by

$$\frac{d\sigma_{hA}}{dQ^2} \approx \frac{d\sigma_{hA}^{S}}{dQ^2} \approx A \sum_q \int dx'\, f_{\bar{q}/h}(x') \int dx\, f_{q/A}(x)\, \frac{d\hat{\sigma}_{q\bar{q}}}{dQ^2}\,, \tag{7.5}$$

where A is the atomic weight of the nucleus, $\sum_q$ runs over all quark and antiquark flavors, $f_{\bar{q}/h}$ and $f_{q/A}$ represent the hadron and nuclear partonic distribution functions, respectively, and $d\hat{\sigma}_{q\bar{q}}/dQ^2$ is the lowest partonic $q\bar{q}$ annihilation cross section to a lepton pair of invariant mass Q.

In Fig. 7.1, we sketch the leading order Feynman diagram that contributes to the double scattering cross section, $d\sigma_{hA}^{D}$: an antiquark of momentum $x'p'$ from the incoming hadron scatters off a gluon from the nucleus (indicated by the bottom blob) before it annihilates with a quark from the nucleus to form a vector boson of large invariant mass, Q, which then decays into a lepton pair. The interference diagrams, that have both gluons in the same side of the final-state cut (the dashed line), do not contribute to the broadening in a covariant gauge calculation [89], while they are very important in the light-cone gauge calculation [97]. It is clear from the diagram that the momentum of the observed vector boson is only sensitive to the total momentum from the nucleus, which is equal to a sum of the gluon and quark momentum. Therefore, the gluon (or quark) momentum in the scattering amplitude (the left of the dashed line) is not necessary to be equal to the gluon (or quark) momentum on the right of the final-state cut. This is a consequence of the fact that there could be an arbitrary momentum flow from the nucleus through the quark line, the internal antiquark line, and back to the nucleus from the gluon line without changing both initial- and final-state. To drive the double scattering contribution to the cross section, we need to integrate over this loop momentum for both the amplitude and complex conjugate of the amplitude, or equivalently, the momentum flows through those two gluons in Fig. 7.1. The internal antiquark propagator following the gluon rescattering can be very large if the gluon momentum is very soft, and it can actually diverge if the gluon momentum vanishes. But, it is easy to verify that the singularity of the internal antiquark propagator when gluon momentum vanishes is not pinched. The integration of the gluon momentum can be deformed far away from the on-shell singularity into a perturbative off-shell region at the order of the hard scale Q; and the net result from the integration is given by the residue of the pole of the antiquark propagator [96, 98].

Following the derivation in a covariant gauge as in Ref. [89], the contribution from the double scattering diagram in Fig. 7.1 to the q_T^2-moment of Drell-Yan cross section can be

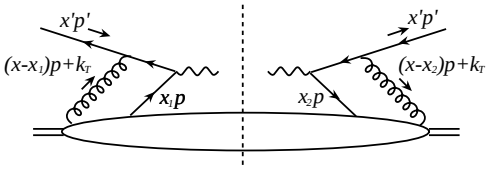

Figure 7.1 Lowest order double scattering Feynman diagram that contributes to the broadening of Drell-Yan transverse momentum distribution, which shows an antiquark of momentum $x'p'$ of incoming hadron scatters off a gluon of a nucleus (the bottom blob) before it annihilates a quark to produce a vector boson.

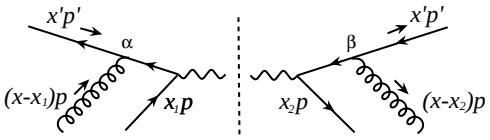

Figure 7.2 Lowest-order double scattering diagram that leads to the factorized partonic part, H, in Eq. (7.10).

expressed as

$$\int dq_T^2\, q_T^2\, \frac{d\sigma_{hA}^D}{dQ^2 dq_T^2} = \sum_q \int dq_T^2\, q_T^2 \int dx' f_{\bar{q}/h}(x') \int dx\, dx_1\, dx_2\, d^2k_T\, \overline{T}_{Aq}(x, x_1, x_2, k_T, p) \times \overline{H}(x, x_1, x_2, k_T, p, q, x'p')\, \delta(q_T^2 - k_T^2)\,, \tag{7.6}$$

where the matrix element $\overline{T}_{Aq}$ is given by the bottom blob in Fig. 7.1, which includes the propagators of all quarks and gluons connecting to the blob,

$$\overline{T}_{Aq}(x, x_1, x_2, k_T, p) = \int \frac{dy^-}{2\pi} \frac{dy_1^-}{2\pi} \frac{dy_2^-}{2\pi} \int \frac{d^2y_T}{(2\pi)^2}\, e^{ix_1 p^+ y_1^-}\, e^{i(x-x_1)p^+ y^-}\, e^{-i(x-x_2)p^+ y_2^-}\, e^{-ik_T\cdot y_T} \times \frac{1}{2}\langle p_A | A^+(y_2^-, 0_T)\bar{\psi}(0)\gamma^+\psi(y_1^-)A^+(y^-, y_T)|p_A\rangle\,, \tag{7.7}$$

where the subscript "Aq" indicates that the matrix element is made of the gluon and quark field operators. The partonic part $\overline{H}$ in Eq. (7.6) is given by the top partonic part of the diagram in Fig. 7.1 with two antiquark lines traced with $(\gamma\cdot p')/2$, two quark lines from the nucleus traced with $(\gamma\cdot p)/2$, and the Lorentz indices of two gluon lines from the nucleus contracted by $p^\alpha p^\beta$ [89].

The separation of the partonic part $\overline{H}$ from the hadronic matrix element $\overline{T}_{Aq}$ in Eq. (7.6) is not yet a gauge invariant factorization. The matrix element $\overline{T}_{Aq}$ in Eq. (7.7) has an explicit dependence on the gluon field operator A^+, which is not gauge covariant. That is, the matrix element $\overline{T}_{Aq}$ cannot be made gauge invariant by the insertion of ordered gauge links between the field operators [96]. To achieve a gauge invariant factorization, it is necessary to convert the gluon field operator A^+ in the matrix element into corresponding gluon field strength, $F^{+\alpha}$, with a transversely polarized Lorentz index α. We can achieve this conversion in a covariant gauge as follows. We first expand the k_T in the partonic part, $\overline{H}$, around $k_T^2 = 0$, because $k_T^2 \ll Q^2$, and keep the first nonvanishing term, $H(x, x_1, x_2, p, q, x'p') = \overline{H}(x, x_1, x_2, k_T = 0, p, q, x'p')$, which is given by the diagram in Fig. 7.2. We then write the transverse momentum square, q_T^2 in Eq. (7.6) as k_T^2 by taking advantage of the $\delta(q_T^2 - k_T^2)$, and convert $k_T^2\, A^+(y_2^-, 0_T)A^+(y^-, y_T)$ to $F_\alpha{}^+(y_2^-, 0_T)F^{+\alpha}(y^-, y_T)$ by a partial integration [89]. Finally, up to the power corrections in $\langle k_T^2\rangle/Q^2$, we can rewrite the q_T^2-moment in Eq. (7.6) as

$$\int dq_T^2\, q_T^2\, \frac{d\sigma_{hA}^D}{dQ^2 dq_T^2} = \sum_q \int dx'\, f_{\bar{q}/h}(x') \int dx\, dx_1\, dx_2\, T_{Fq}^{(I)}(x, x_1, x_2, p)\, H(x, x_1, x_2, p, q, x'p') \quad (7.8)$$

where T_{Fq} is a twist-4 parton correlation function defined as

$$\begin{aligned} T_{Fq}^{(I)}(x, x_1, x_2, p) &= \int \frac{dy^-}{2\pi}\, \frac{dy_1^-}{2\pi}\, \frac{dy_2^-}{2\pi}\, e^{ix_1 p^+ y_1^-}\, e^{i(x-x_1)p^+ y^-}\, e^{-i(x-x_2)p^+ y_2^-} \\ &\quad \times \frac{1}{2}\langle p_A | F_\alpha{}^+(y_2^-)\bar{\psi}(0)\gamma^+\psi(y_1^-)F^{+\alpha}(y^-)|p_A\rangle\,, \end{aligned} \quad (7.9)$$

with the superscript "(I)" indicates the matrix element corresponding to the initial-state rescattering [89]. The leading order contribution to the partonic hard part from the diagram in Fig. 7.2 is [89]

$$H(x, x_1, x_2, p, q, x'p') = \frac{8\pi^2\alpha_s}{N_c^2 - 1}\, C_F \left[\frac{1}{2\pi}\frac{1}{x_1 - x - i\epsilon}\frac{1}{x_2 - x + i\epsilon}\right] \frac{d\hat{\sigma}_{q\bar{q}}}{dQ^2}\,, \quad (7.10)$$

where two unpinched poles are from the two antiquark propagators in Fig. 7.2. Substituting

Eq. (7.10) to Eq. (7.8), and integrating over x_1, x_2, by taking the residues of the unpinched poles (the leading pole approximation [96]), we obtain

$$\int dq_T^2\, q_T^2\, \frac{d\sigma_{hA}^D}{dQ^2 dq_T^2} = \sum_q \int dx'\, f_{\bar{q}/h}(x') \int dx\, T_{q/A}^{(I)}(x)\, \frac{d\hat{\sigma}_{q\bar{q}}}{dQ^2} \left(\frac{8\pi^2 \alpha_s}{N_c^2 - 1} C_F \right) , \tag{7.11}$$

with the measurable twist-4 quark-gluon correlation function [89, 96],

$$\begin{aligned} T_{q/A}^{(I)}(x) = & \int \frac{dy^-}{2\pi}\, e^{ixp^+y^-} \int \frac{dy_1^- dy_2^-}{2\pi}\, \theta(y^- - y_1^-)\, \theta(-y_2^-) \\ & \times \frac{1}{2} \langle p_A | F_\alpha{}^+(y_2^-) \bar{\psi}_q(0) \gamma^+ \psi_q(y^-) F^{+\alpha}(y_1^-) | p_A \rangle , \end{aligned} \tag{7.12}$$

where the superscript "(I)" again indicates the initial-state rescattering. From Eq. (7.4), we obtain the leading double scattering contribution to the Drell-Yan broadening [89],

$$\Delta \langle q_T^2 \rangle_{\rm DY} \approx \frac{\sum_q \int dx'\, f_{\bar{q}/h}(x') \int dx\, T_{q/A}^{(I)}(x)\, \frac{d\hat{\sigma}_{q\bar{q}}}{dQ^2} \left(\frac{8\pi^2 \alpha_s}{N_c^2 - 1} C_F \right)}{A \sum_q \int dx'\, f_{\bar{q}/h}(x') \int dx\, f_{q/A}(x)\, \frac{d\hat{\sigma}_{q\bar{q}}}{dQ^2}} . \tag{7.13}$$

By using the model proposed for the twist-4 parton correlation functions [89, 98]

$$T_{q/A}^{(I)}(x) = \lambda^2\, A^{4/3}\, f_{q/A}(x) , \tag{7.14}$$

we can express the Drell-Yan broadening in a much simpler form [89]

$$\Delta \langle q_T^2 \rangle_{\rm DY} = C_F \left(\frac{8\pi^2 \alpha_s}{N_c^2 - 1}\, \lambda^2\, A^{1/3} \right) , \tag{7.15}$$

with an unknown non-perturbative parameter λ^2 defined in Eq. (7.14). The leading contribution to the Drell-Yan broadening in Eq. (7.15) shows a clear $A^{1/3}$-type dependence and is proportional to the color factor C_F from the rescattering between an antiquark (or a quark) and a gluon.

7.3 Transverse momentum broadening in heavy quarkonium production

In this section we use the same technique reviewed in last section to calculate the transverse momentum broadening of heavy quarkonium production in both hadron-nucleus and nucleus-nucleus collisions.

The heavy quarkonium's transverse momentum broadening in hadron-nucleus collision was often attributed to the initial-state multiple scattering between the active parton of the projectile and soft partons of the nuclear target before the hard collision to produce the heavy quark pair [91]. Calculation of such initial-state rescattering should be very similar to that for the Drell-Yan broadening, except that the quark-antiquark annihilation is accompanied by a much larger gluon-gluon fusion subprocess. If one considers only the gluon-gluon fusion subprocess, one should expect to have Eq. (7.15) for the heavy quarkonium broadening with the overall color factor C_F replaced by $C_A = N_c = 3$ due to the difference in color factors between gluon rescattering and quark rescattering. The initial-state rescattering alone leads to the naive expectation for the ratio of broadening between heavy quarkonium and Drell-Yan as $C_A/C_F = 2.25$, which is much smaller than the data [90].

However, since a heavy quarkonium is unlikely to be formed at the same time when the heavy quark pair was produced [99], the final-state interaction between the heavy quark pair and the nuclear medium could generate additional broadening. Since the final-state rescattering is sensitive to the detailed dynamics that transmutes a heavy quark pair into a bound quarkonium, we calculate the final-state contribution to heavy quarkonium broadening in both NRQCD and Color Evaporation models.

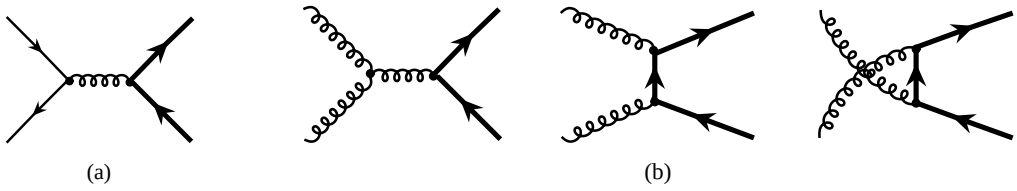

Figure 7.3 Lowest order Feynman diagram for light quark-antiquark annihilation (a) and for gluon-gluon fusion to a pair of heavy quark.

7.3.1 Color Evaporation Model

In the Color Evaporation model (CEM), heavy quarkonium production is factorized into two steps: the production of a pair of heavy quarks with an invariant mass Q followed by a non-perturbative hadronization process with an universal transition probability for the pair to become a bound quarkonium [93]. It was assumed that the transition probability is the same for all heavy quark pairs whose invariant mass is less than the mass threshold of producing two open flavor heavy mesons, and the cross section for producing a heavy quarkonium, H, can be written as [93]

$$\sigma^{\rm CEM}_{hA\to H} = F_{Q\bar{Q}\to H} \int_{4m_Q^2}^{4M_Q^2} dQ^2 \, \frac{d\sigma_{hA\to Q\bar{Q}}}{dQ^2} \,, \tag{7.16}$$

where $F_{Q\bar{Q}\to H}$ is a non-perturbative transition probability and is independent of the color and angular momentum of the heavy quark pair, m_Q and M_Q are the mass of the heavy quark and open flavor heavy meson, respectively. There is one transition probability for each heavy quarkonium state, H. In Eq. (7.16), the inclusive cross section for producing a pair of heavy quarks of invariant mass Q can be factorized as [100]

$$\frac{d\sigma_{hA\to Q\bar{Q}}}{dQ^2} = A \sum_{a,b} \int dx' \, f_{a/h}(x') \int dx \, f_{b/A}(x) \, \frac{d\hat{\sigma}_{ab\to Q\bar{Q}}}{dQ^2} \,, \tag{7.17}$$

where $\sum_{a,b}$ sum over all parton flavors, and $d\hat{\sigma}_{ab\to Q\bar{Q}}/dQ^2$ is a short-distance hard part for two partons of flavor a and b to produce a pair of heavy quarks of invariant mass Q. At the lowest order, they are given by the light quark-antiquark annihilation and gluon-gluon fusion subprocess, as sketched in Fig. 7.3. The transition probability in Eq. (7.16) is assumed to be universal and independent of how the heavy quark pair was produced. It fixes the overall normalization for the cross section of heavy quarkonium production in different collision processes and provides the predictive power of the model. The model has been reasonably successful when comparing with data of inclusive heavy quarkonium production [101, 102].

Similar to Fig. 7.2, the leading order double scattering diagrams for producing a heavy quark pair are sketched in Fig. 7.4 for quark-antiquark annihilation subprocess, and in Fig. 7.5

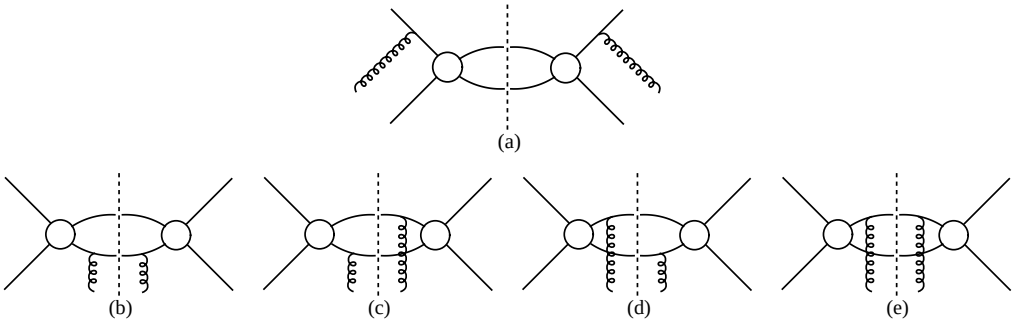

Figure 7.4 Leading order double scattering diagrams for $q\bar{q} \to Q\bar{Q}$: initial-state double scattering (a), and final-state double scattering (b), (c), (d), and (e).

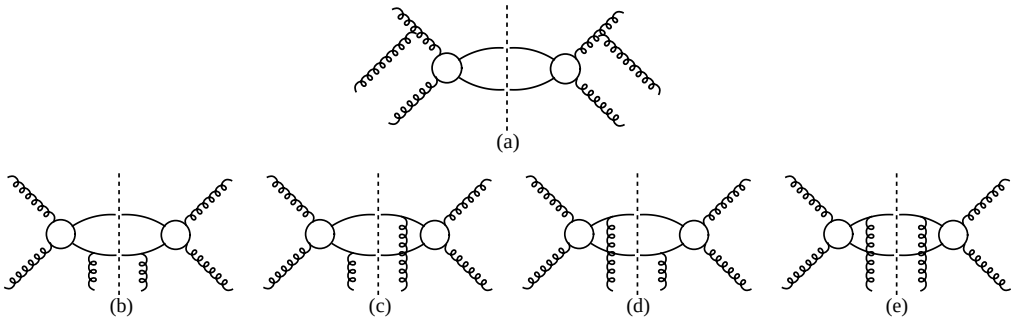

Figure 7.5 Leading order double scattering diagrams for $gg \to Q\bar{Q}$: initial-state double scattering (a), and final-state double scattering (b), (c), (d), and (e).

for gluon-gluon fusion subprocess, respectively. The blob in the quark-antiquark annihilation subprocess in Fig. 7.4 is given by the diagram in Fig. 7.3(a), and the blob in the gluon-gluon fusion subprocess in Fig. 7.5 is given by a sum of the three diagrams in Fig. 7.3(b).

In CEM, the transverse momentum broadening of a heavy quarkonium is equal to the transverse momentum broadening of the parent heavy quark pair, since the transition probability from a heavy quark pair to a bound quarkonium is given by a constant, $F_{Q\bar{Q}\to H}$. We use the same method reviewed in last section to calculate the transverse momentum broadening of the

heavy quark pairs. Similar to Eq. (7.8) in the Drell-Yan case, we have

$$\begin{aligned}\int dq_T^2\, q_T^2\, \frac{d\sigma^D_{hA\to Q\bar{Q}}}{dQ^2 dq_T^2} &= \sum_q \int dx' f_{\bar{q}/h}(x') \int dx\, dx_1\, dx_2 \\ &\times \big[T^{(I)}_{Fq}(x,x_1,x_2,p) H^{(I)}_{q\bar{q}\to Q\bar{Q}}(x,x_1,x_2,p,q,x'p') \\ &+ T^{(F)}_{Fq}(x,x_1,x_2,p) H^{(F)}_{q\bar{q}\to Q\bar{Q}}(x,x_1,x_2,p,q,x'p')\big] \\ &+ \int dx' f_{g/h}(x') \int dx\, dx_1\, dx_2 \\ &\times \big[T^{(I)}_{FF}(x,x_1,x_2,p) H^{(I)}_{gg\to Q\bar{Q}}(x,x_1,x_2,p,q,x'p') \\ &+ T^{(F)}_{FF}(x,x_1,x_2,p) H^{(F)}_{gg\to Q\bar{Q}}(x,x_1,x_2,p,q,x'p')\big]\,, \end{aligned} \tag{7.18}$$

where the superscripts, "(I)" and "(F)", indicate the initial-state and final-state rescattering, respectively, and the matrix element $T^{(I)}_{Fq}$ is given in Eq. (7.9). $T^{(I)}_{FF}$ is given by

$$\begin{aligned} T^{(I)}_{FF}(x,x_1,x_2,p) = \int \frac{dy^-}{2\pi}\frac{dy_1^-}{2\pi}\frac{dy_2^-}{2\pi} e^{ix_1 p^+ y_1^-} e^{i(x-x_1)p^+ y^-} e^{-i(x-x_2)p^+ y_2^-} \\ \times \langle p_A | {F_\alpha}^+(y_2^-) F^{\sigma+}(0) F^+_\sigma(y_1^-) F^{+\alpha}(y^-) | p_A\rangle\,. \end{aligned} \tag{7.19}$$

The matrix elements with final-state rescattering, $T^{(F)}_{Fq}$ and $T^{(F)}_{FF}$, have the same expressions as corresponding matrix elements with initial-state rescattering, since the field operators in the definition of the multiparton matrix elements in the collinear factorization approach commute on the light-cone [96].

The diagram with initial-state rescattering in Fig. 7.4(a) contributes to $H^{(I)}_{q\bar{q}\to Q\bar{Q}}$ as

$$H^{(I)}_{q\bar{q}\to Q\bar{Q}} = H^{(7.4a)}_{q\bar{q}\to Q\bar{Q}} = \frac{8\pi^2\alpha_s}{N_c^2-1} C_F \left[\frac{1}{2\pi}\frac{1}{x_1 - x - i\epsilon}\frac{1}{x_2 - x + i\epsilon}\right] \frac{d\hat{\sigma}_{q\bar{q}\to Q\bar{Q}}}{dQ^2}\,. \tag{7.20}$$

All four diagrams with the final-state rescattering, in Figs. 7.4(b), (c), (d), and (e), contribute to $H^{(F)}_{q\bar{q}\to Q\bar{Q}}$ as

$$H^{(F)}_{q\bar{q}\to Q\bar{Q}} = H^{(7.4b+7.4c+7.4d+7.4e)}_{q\bar{q}\to Q\bar{Q}} = \frac{8\pi^2\alpha_s}{N_c^2-1} C_A \left[\frac{1}{2\pi}\frac{1}{x_1 - x + i\epsilon}\frac{1}{x_2 - x - i\epsilon}\right] \frac{d\hat{\sigma}_{q\bar{q}\to Q\bar{Q}}}{dQ^2}\,. \tag{7.21}$$

Here $d\hat{\sigma}_{q\bar{q}\to Q\bar{Q}}/dQ^2$ represents the lowest order partonic cross section from $q\bar{q}$ annihilation to

a heavy quark pair of invariant mass Q, and it is given by [103],

$$\frac{d\hat{\sigma}_{q\bar{q}\to Q\bar{Q}}}{dQ^2} = \frac{2}{9}\frac{4\pi\alpha_s}{3Q^2}\left(1+\frac{1}{2}\gamma\right)\sqrt{1-\gamma}, \tag{7.22}$$

with $\gamma = 4m_Q^2/Q^2$. The final-state contribution in Eq. (7.21) is very similar to the initial-state contribution in Eq. (7.20) except the overall color factor and the location of the unpinched poles. The difference in the location of the unpinched poles, indicated by the sign difference of the $i\epsilon$, is a consequence of the order of the rescattering taken place either before or after the hard collision. The overall color factor for the final-state interaction, C_A in Eq. (7.21), indicates that as far as the color is concerned, the rescattering of a heavy quark pair is effectively the same as that of a color-octet gluon when the effect is calculated in the Color Evaporation model.

Similarly, we evaluate the double scattering diagrams from gluon-gluon fusion subprocess in Fig. 7.5 and obtain their contribution to the partonic hard part,

$$H^{(I)}_{gg\to Q\bar{Q}} = H^{(7.5a)}_{gg\to Q\bar{Q}} = \frac{8\pi^2\alpha_s}{N_c^2-1}\,C_A\left[\frac{1}{2\pi}\frac{1}{x_1-x-i\epsilon}\frac{1}{x_2-x+i\epsilon}\right]\frac{d\hat{\sigma}_{gg\to Q\bar{Q}}}{dQ^2}\,, \tag{7.23}$$

for the initial-state double scattering, and

$$H^{(F)}_{gg\to Q\bar{Q}} = H^{7.5b+7.5c+7.5d+7.5e}_{gg\to Q\bar{Q}} = \frac{8\pi^2\alpha_s}{N_c^2-1}\,C_A\left[\frac{1}{2\pi}\frac{1}{x_1-x+i\epsilon}\frac{1}{x_2-x-i\epsilon}\right]\frac{d\hat{\sigma}_{gg\to Q\bar{Q}}}{dQ^2}\,, \tag{7.24}$$

for the final-state double scattering. The lowest order partonic cross section from gg fusion to a heavy quark pair of invariant mass Q, $d\hat{\sigma}_{gg\to Q\bar{Q}}/dQ^2$, is given by [103],

$$\frac{d\hat{\sigma}_{gg\to Q\bar{Q}}}{dQ^2} = \frac{\pi\alpha_s}{3Q^2}\left[(1+\gamma+\frac{1}{16}\gamma^2)\ln\left(\frac{1+\sqrt{1-\gamma}}{1-\sqrt{1-\gamma}}\right)-\left(\frac{7}{4}+\frac{31}{16}\gamma\sqrt{1-\gamma}\right)\right]. \tag{7.25}$$

Compare Eqs. (7.23) and (7.24), we find that the contribution to the gluon-gluon fusion subprocess from the final-state double scattering is the same as that from the initial-state interaction. That is because the rescattering effect of a heavy quark pair is the same as that of a color-octet gluon when the effect is calculated in the Color Evaporation model.

Substituting the partonic hard parts in Eqs. (7.20), (7.21), (7.23), and (7.24) into Eq. (7.18), integrating over the momentum fractions, x_1 and x_2 of the rescattering gluons under the leading pole approximation, we obtain the leading double scattering contribution to the q_T^2-moment of producing a heavy quark pair in hadron-nucleus collisions,

$$\begin{aligned}
&\int dq_T^2\, q_T^2\, \frac{d\sigma^D_{hA\to Q\bar{Q}}}{dQ^2 dq_T^2} \\
&= \left[\frac{8\pi^2\alpha_s}{N_c^2-1}\right]\left(\sum_q \int dx' f_{\bar{q}/h}(x') \int dx \left[C_F\, T^{(I)}_{q/A}(x) + C_A\, T^{(F)}_{q/A}(x)\right] \frac{d\hat{\sigma}_{q\bar{q}\to Q\bar{Q}}}{dQ^2}\right. \\
&\qquad\left. + \int dx' f_{g/h}(x') \int dx \left[C_A\, T^{(I)}_{g/A}(x) + C_A\, T^{(F)}_{g/A}(x)\right] \frac{d\hat{\sigma}_{gg\to Q\bar{Q}}}{dQ^2}\right), \quad (7.26)
\end{aligned}$$

where the quark-gluon correlation function, $T^{(I)}_{q/A}$, is given in Eq. (7.12), the $T^{(I)}_{g/A}$ is given by

$$\begin{aligned}
T^{(I)}_{g/A}(x) &= \int \frac{dy^-}{2\pi}\, e^{ixp^+y^-} \int \frac{dy_1^- dy_2^-}{2\pi}\, \theta(y^- - y_1^-)\, \theta(-y_2^-) \\
&\quad \times \frac{1}{xp^+} \langle p_A | F_\alpha{}^+(y_2^-) F^{\sigma+}(0) F^+_\sigma(y^-) F^{+\alpha}(y_1^-) | p_A \rangle\,, \quad (7.27)
\end{aligned}$$

and $T^{(F)}_{q/A}$ and $T^{(F)}_{g/A}$ are given by the same expressions in Eq. (7.12) and Eq. (7.27), respectively, except the θ-functions are replaced as [96]

$$\theta(y^- - y_1^-)\, \theta(-y_2^-) \to \theta(y_1^- - y^-)\, \theta(y_2^-)\,, \quad (7.28)$$

due to the different order of rescattering (or the sign of the $i\epsilon$ for the unpinched poles).

By integrating over the invariant mass of the heavy quark pair we can derive the heavy quarkonium transverse momentum broadening in CEM as

$$\Delta\langle q_T^2\rangle^{\rm CEM}_{\rm HQ} \approx \int dq_T^2\, q_T^2 \int_{4m_Q^2}^{4M_Q^2} dQ^2\, \frac{d\sigma^D_{hA\to Q\bar{Q}}}{dQ^2 dq_T^2} \Bigg/ \int_{4m_Q^2}^{4M_Q^2} dQ^2\, \frac{d\sigma_{hA\to Q\bar{Q}}}{dQ^2}\ . \quad (7.29)$$

As pointed out in Ref. [96], the field operators on the light-cone in the definition of the multiparton matrix elements, as those in Eqs. (7.12) and (7.27) commute. The matrix element with initial-state rescattering is equal to corresponding matrix element with final-state rescattering,

if the phase space interaction of these two matrix elements, such as the $\int dy^- \, dy_1^- \, dy_2^- \theta(y^- - y_1^-)\theta(-y_2^-)$ in Eq. (7.12) for initial-state rescattering and $\int dy^- \, dy_1^- \, dy_2^- \theta(y_1^- - y^-)\theta(y_2^-)$ for the corresponding final-state rescattering, are the same [89]. However, the phase space integration for the final-state interaction in heavy quarkonium production may not cover the full size of the nuclear medium if the heavy quark pair becomes a physical quarkonium or transmutes into a color singlet pre-hadron quarkonium state before the pair exits the nuclear medium. Rescattering between a quarkonium and nuclear medium and that between a colored heavy quark pair and the same medium could be different, and lead to a different heavy quarkonium broadening.

It was argued in Ref. [99] that a physical quarkonium state is likely to form outside nuclear matter in hadron-nucleus collision. Therefore, the matrix elements with final- and initial-state rescattering could have the same phase space interaction. If we assume that the matrix elements with the final- and initial-state rescattering are the same, $T_{q/A}^{(F)}(x) = T_{q/A}^{(I)}(x)$ and $T_{g/A}^{(F)}(x) = T_{g/A}^{(I)}(x)$, and assume the same model for both twist-4 quark-gluon and gluon-gluon correlation functions,

$$T_{g/A}^{(I)}(x) = \lambda^2 \, A^{4/3} \, f_{g/A}(x) \,, \tag{7.30}$$

we can express the heavy quarkonium broadening in hadron-nucleus collisions as,

$$\Delta\langle q_T^2 \rangle_{\rm HQ}^{\rm CEM} = \left(\frac{8\pi^2 \alpha_s}{N_c^2 - 1} \, \lambda^2 \, A^{1/3} \right) \frac{(C_F + C_A) \, \sigma_{q\bar{q}} + 2 \, C_A \, \sigma_{gg}}{\sigma_{q\bar{q}} + \sigma_{gg}} \,, \tag{7.31}$$

where $\sigma_{q\bar{q}}$ and σ_{gg} are the lowest order inclusive cross sections from the $q\bar{q} \to Q\bar{Q} \to H$ and $gg \to Q\bar{Q} \to H$ subprocess, respectively. They are given by [103, 116]

$$\sigma_{q\bar{q}} = F_{Q\bar{Q}\to H} \int_{4m_Q^2}^{4M_Q^2} dQ^2 \sum_q \int dx' f_{\bar{q}/h}(x') \int dx \, f_{q/A}(x) \, \frac{d\hat{\sigma}_{q\bar{q}\to Q\bar{Q}}}{dQ^2} \tag{7.32}$$

$$\sigma_{gg} = F_{Q\bar{Q}\to H} \int_{4m_Q^2}^{4M_Q^2} dQ^2 \int dx' f_{g/h}(x') \int dx \, f_{g/A}(x) \, \frac{d\hat{\sigma}_{gg\to Q\bar{Q}}}{dQ^2} \,, \tag{7.33}$$

where the lowest order partonic cross sections to produce a pair of $Q\bar{Q}$ are given in Eqs. (7.22)

and (7.25). If the gluon-gluon subprocess dominates the heavy quarkonium production rate, $\sigma_{gg} \gg \sigma_{q\bar{q}}$, we have

$$\Delta\langle q_T^2\rangle_{\rm HQ}^{\rm CEM} \approx 2\,C_A \left(\frac{8\pi^2\alpha_s}{N_c^2-1}\,\lambda^2\,A^{1/3}\right) . \tag{7.34}$$

By comparing the Drell-Yan broadening in Eq. (7.15) and the leading heavy quarkonium broadening in Eq. (7.34), we conclude that the leading contribution to heavy quarkonium transverse momentum broadening in hadron-nucleus collision, calculated in CEM, is about $2\,C_A/C_F = 4.5$ times Drell-Yan broadening.

7.3.2 Non-Relativistic QCD Model

The application of NRQCD to the production of a heavy quarkonium H in hadronic collisions relies on the proposed factorization formalism [92],

$$\sigma_{hA\to H}^{\rm NRQCD} = A\sum_{a,b}\int dx'\,f_{a/h}(x')\int dx\,f_{b/A}(x)\left[\sum_n H_{ab\to Q\bar{Q}[n]}\langle\mathcal{O}^H(n)\rangle\right] \tag{7.35}$$

where a and b run over all parton flavors, and $H_{ab\to Q\bar{Q}[n]}$ are perturbatively calculable coefficient functions for producing the heavy $Q\bar{Q}[n]$ states. The state of the heavy quark pair, $[n]$, is characterized by the pair's rotational, $^{2s+1}L_J$, and color quantum numbers. The coefficient function for producing each $Q\bar{Q}[n]$ state is perturbatively calculable in a power series of the strong coupling constant, α_s. The matrix elements of $\langle\mathcal{O}^H(n)\rangle$ in Eq. (7.35) describe the non-perturbative hadronization dynamics and give the probability for the pair to become a physical heavy quarkonium H [92, 104]. The matrix elements should be universal. That is necessary for the predictive power of the NRQCD formalism. The expansion in Eq. (7.35) is organized according to the effective power of the heavy quark pair's relative velocity. Although it still lacks a fully compelling proof for the NRQCD factorization formula in Eq. (7.35) [104], the formalism for heavy quarkonium production has had many successes, in particular, its success in interpreting the CDF data on J/ψ and ψ' production as a function of transverse momentum [113, 105].

In NRQCD model of heavy quarkonium production, the transition probability from a heavy quark pair to a bound quarkonium is sensitive to the pair's rotational and color quantum numbers. Partonic multiple scattering has a potential to change not only the heavy quark pair's momentum, but also the pair's color and other quantum numbers. Therefore, the transverse momentum broadening calculated in NRQCD model is not necessary the same as that calculated in CEM in last subsection. If the difference is significant, a precise measurement of transverse momentum broadening could shed some lights on heavy quarkonium's production mechanism.

We assume that the q_T^2-moment of heavy quarkonium production, $\int dq_T^2 (q_T^2)^n d\sigma_{hA\to H}^{\rm NRQCD}/dq_T^2$ with $n \geq 0$, can be factorized in the same way as the $0^{\rm th}$-moment given in Eq. (7.35). We calculate the leading double scattering contribution to the broadening of the first moment. Like the calculation done in CEM in last subsection, the partonic double scattering diagrams are given in Figs. 7.4 and 7.5. Similar to Eq. (7.18), we obtain

$$\begin{aligned}
\int dq_T^2\, q_T^2\, \frac{d\sigma_{hA\to H}^{D}}{dq_T^2} \;=\; & \sum_q \int dx' f_{\bar{q}/h}(x') \int dx\, dx_1\, dx_2 \\
& \times \big[T_{Fq}^{(I)}(x,x_1,x_2,p) H_{q\bar{q}\to H}^{(I)}(x,x_1,x_2,p,q,x'p') \\
& + T_{Fq}^{(F)}(x,x_1,x_2,p) H_{q\bar{q}\to H}^{(F)}(x,x_1,x_2,p,q,x'p') \big] \\
& + \int dx' f_{g/h}(x') \int dx\, dx_1\, dx_2 \\
& \times \big[T_{FF}^{(I)}(x,x_1,x_2,p) H_{gg\to H}^{(I)}(x,x_1,x_2,p,q,x'p') \\
& + T_{FF}^{(F)}(x,x_1,x_2,p) H_{gg\to H}^{(F)}(x,x_1,x_2,p,q,x'p') \big] \,, \qquad (7.36)
\end{aligned}$$

with the partonic cross sections defined as

$$\begin{aligned}
H_{q\bar{q}\to H}^{(I,F)}(x,x_1,x_2,p,q,x'p') &= \sum_n H_{q\bar{q}}^{(I,F)}(n) \left\langle \mathcal{O}^H(n) \right\rangle , \\
H_{gg\to H}^{(I,F)}(x,x_1,x_2,p,q,x'p') &= \sum_n H_{gg}^{(I,F)}(n) \left\langle \mathcal{O}^H(n) \right\rangle , \qquad (7.37)
\end{aligned}$$

where $\sum_n$ sums over all possible $Q\bar{Q}$ states, n, with appropriate spin and color quantum numbers [106], and $H_{q\bar{q}}^{(I,F)}(n)$ and $H_{gg}^{(I,F)}(n)$, whose dependence on parton momentum fractions

and kinematic variables are suppressed, represent partonic hard parts for producing a heavy quark pair at a quantum state n from quark-antiquark annihilation subprocess and gluon-gluon fusion subprocess, respectively.

The partonic parts for the quark-antiquark annihilation subprocess, $H_{q\bar{q}}^{(I,F)}(n)$ in Eq. (7.37), are derived from diagrams in Fig. 7.4. The single diagram in Fig. 7.4(a) contributes to $H_{q\bar{q}}^{(I)}(n)$. Under the leading pole approximation, the initial-state rescattering does not change the nature of the s-channel $q\bar{q} \to Q\bar{Q}$ subprocess, which produces a heavy $Q\bar{Q}$ pair in a color octet and spin-1 state: $n = {}^3S_1^{(8)}$. The corresponding hard part is given by

$$H_{q\bar{q}}^{(I)}({}^3S_1^{(8)}) = \frac{8\pi^2\alpha_s}{N_c^2-1} C_F \left[\frac{1}{2\pi} \frac{1}{x_1 - x - i\epsilon} \frac{1}{x_2 - x + i\epsilon}\right] H_{q\bar{q}}^{(0)}({}^3S_1^{(8)}) \,, \tag{7.38}$$

where $H_{q\bar{q}}^{(0)}({}^3S_1^{(8)})$ is the lowest order short-distance coefficient for $q\bar{q} \to Q\bar{Q}({}^3S_1^{(8)})$ subprocess and is given by

$$H_{q\bar{q}}^{(0)}({}^3S_1^{(8)}) = \frac{\pi^3\alpha_s^2}{M^3} \frac{16}{27} \delta(\hat{s} - M^2) \,, \tag{7.39}$$

with the mass of a quarkonium: $M = 2m_Q$. The final-state rescattering effect to the $q\bar{q}$ annihilation subprocess comes from the four diagrams in Figs. 7.4(b), (c), (d), and (e). The additional gluon rescattering in the final-state allows more quantum states for the produced $Q\bar{Q}$ pair. At this order, we have the following nonvanishing states: $n = {}^3S_1^{(8)}, {}^3P_{J=1,2}^{(1,8)}$, and corresponding hard parts,

$$\begin{aligned} H_{q\bar{q}}^{(F)}({}^3S_1^{(8)}) &= \frac{8\pi^2\alpha_s}{N_c^2-1} C_A \left[\frac{1}{2\pi} \frac{1}{x_1 - x + i\epsilon} \frac{1}{x_2 - x - i\epsilon}\right] H_{q\bar{q}}^{(0)}({}^3S_1^{(8)}) \,, \\ H_{q\bar{q}}^{(F)}({}^3P_{J=1,2}^{(1,8)}) &= \frac{8\pi^2\alpha_s}{N_c^2-1} \left[\frac{1}{2\pi} \frac{1}{x_1 - x + i\epsilon} \frac{1}{x_2 - x - i\epsilon}\right] H_{q\bar{q}}^{(1)}({}^3P_{J=1,2}^{(1,8)}) \,, \end{aligned} \tag{7.40}$$

where $H^{(0)}_{q\bar{q}}({}^3S_1^{(8)})$ is given in Eq. (7.39) and the leading order P-wave contribution is given by

$$\begin{aligned} H^{(1)}_{q\bar{q}}({}^3P_1^{(8)}) &= \frac{5}{3}H^{(1)}_{q\bar{q}}({}^3P_2^{(8)}) = \frac{\pi^3\alpha_s^2}{M^3}\frac{40}{27}\frac{1}{3m_Q^2}\delta(\hat{s}-M^2)\,, \\ H^{(1)}_{q\bar{q}}({}^3P_1^{(1)}) &= \frac{5}{3}H^{(1)}_{q\bar{q}}({}^3P_2^{(1)}) = \frac{\pi^3\alpha_s^2}{M^3}\frac{64}{81}\frac{1}{3m_Q^2}\delta(\hat{s}-M^2)\,. \end{aligned} \tag{7.41}$$

The nonvanishing contribution to the ${}^3P_{J=1,2}^{(1,8)}$ states is a consequence of the gluon rescattering, which effectively provides a $gg \to Q\bar{Q}$ subprocess.

Similarly, partonic parts for the gluon-gluon fusion subprocess, $H_{gg}^{(I,F)}(n)$ in Eq. (7.37), are derived from diagrams in Fig. 7.5. Unlike the quark-antiquark annihilation subprocess, the heavy quark pair produced in gluon-gluon subprocess can have more than one quantum state. For the initial-state rescattering diagram in Fig. 7.5(a), the heavy quark pair with $n = {}^1S_0^{(1,8)}, {}^3P_{J=0,2}^{(1,8)}$ can all give nonvanishing contribution to $H_{gg}^{(I)}(n)$. The four final-state rescattering diagrams in Figs. 7.5(b), (c), (d), and (e) can produce heavy quark pairs with $n = {}^1S_0^{(8)}$ and ${}^3P_{J=0,2}^{(8)}$. We obtain the hard parts from gluon-gluon fusion diagrams in Fig. 7.5 as

$$\begin{aligned} H_{gg}^{(I)}({}^1S_0^{(1,8)}, {}^3P_{J=0,2}^{(1,8)}) &= \frac{8\pi^2\alpha_s}{N_c^2-1}\,C_A\left[\frac{1}{2\pi}\frac{1}{x_1-x-i\epsilon}\frac{1}{x_2-x+i\epsilon}\right] \\ &\quad \times H_{gg}^{(0)}({}^1S_0^{(1,8)}, {}^3P_{J=0,2}^{(1,8)})\,, \end{aligned} \tag{7.42}$$

$$\begin{aligned} H_{gg}^{(F)}({}^1S_0^{(8)}, {}^3P_{J=0,2}^{(1,8)}) &= \frac{8\pi^2\alpha_s}{N_c^2-1}\,C_A\left[\frac{1}{2\pi}\frac{1}{x_1-x+i\epsilon}\frac{1}{x_2-x-i\epsilon}\right] \\ &\quad \times H_{gg}^{(0)}({}^1S_0^{(8)}, {}^3P_{J=0,2}^{(8)})\,, \end{aligned} \tag{7.43}$$

where $H_{gg}^{(0)}({}^1S_0^{(1,8)}, {}^3P_{J=0,2}^{(1,8)})$ are the lowest order cross sections without the rescattering,

$$\begin{aligned} H_{gg}^{(0)}({}^1S_0^{(1,8)}) &= \frac{\pi^3\alpha_s^2}{M^3}B_n\delta(\hat{s}-M^2)\,, \\ H_{gg}^{(0)}({}^3P_0^{(1,8)}) &= \frac{\pi^3\alpha_s^2}{M^3}B_n\frac{3}{m_Q^2}\delta(\hat{s}-M^2)\,, \\ H_{gg}^{(0)}({}^3P_2^{(1,8)}) &= \frac{\pi^3\alpha_s^2}{M^3}B_n\frac{4}{5m_Q^2}\delta(\hat{s}-M^2)\,, \end{aligned} \tag{7.44}$$

with a color factor $B_n = 2/9$ for a color-singlet state and $5/12$ for a color-octet state, respec-

tively.

Having obtained the short-distance hard parts, we can derive the leading double scattering contribution to the q_T^2-moment of heavy quarkonium production in Eq. (7.36). We limit ourselves to the *direct* production of spin-1, S-wave heavy quarkonia, such as J/ψ, Υ and etc. After neglecting the color singlet $Q\bar{Q}$ states not equal to $^3S_1$, we are left with the following $Q\bar{Q}$ states, which contribute to the direct production of a $H(^3S_1)$ heavy quarkonium,

$$\begin{aligned} q\bar{q} &\to Q\bar{Q}(^3S_1^{(8)}, {}^3P_{J=1,2}^{(8)}) \to H(^3S_1)\,, \\ gg &\to Q\bar{Q}(^1S_0^{(8)}, {}^3P_{J=0,2}^{(8)}) \to H(^3S_1)\,. \end{aligned} \tag{7.45}$$

From Eq. (7.37), we obtain by summing over all $Q\bar{Q}$ states in Eq. (7.45),

$$\begin{aligned} H^{(I)}_{q\bar{q}\to H} &= \frac{8\pi^2\alpha_s}{N_c^2-1}\left[\frac{1}{2\pi}\frac{1}{x_1-x-i\epsilon}\frac{1}{x_2-x+i\epsilon}\right] C_F\, H^{(0)}_{q\bar{q}}(^3S_1^{(8)})\langle\mathcal{O}^H(^3S_1^{(8)})\rangle \\ &= \frac{8\pi^2\alpha_s}{N_c^2-1}\left[\frac{1}{2\pi}\frac{1}{x_1-x-i\epsilon}\frac{1}{x_2-x+i\epsilon}\right] C_F\,\hat{\sigma}^{(0)}_{q\bar{q}}\,, \end{aligned} \tag{7.46}$$

where the lowest order quark-antiquark annihilation cross section is defined as

$$\hat{\sigma}^{(0)}_{q\bar{q}} \equiv H^{(0)}_{q\bar{q}}(^3S_1^{(8)})\,\langle\mathcal{O}^H(^3S_1^{(8)})\rangle = \frac{\pi^3\alpha_s^2}{M^3}\frac{16}{27}\delta(\hat{s}-M^2)\,\langle\mathcal{O}^H(^3S_1^{(8)})\rangle \tag{7.47}$$

with the nonperturbative NRQCD matrix element, $\langle\mathcal{O}^H(^3S_1^{(8)})\rangle$, for a $Q\bar{Q}[^3S_1^{(8)}]$ pair to become a heavy quarkonium H. Similarly, we have the final-state rescattering contribution,

$$\begin{aligned} H^{(F)}_{q\bar{q}\to H} &= \frac{8\pi^2\alpha_s}{N_c^2-1}\left[\frac{1}{2\pi}\frac{1}{x_1-x+i\epsilon}\frac{1}{x_2-x-i\epsilon}\right]\Big(C_A\, H^{(0)}_{q\bar{q}}(^3S_1^{(8)})\langle\mathcal{O}^H(^3S_1^{(8)})\rangle \\ &\quad + H^{(1)}_{q\bar{q}}(^3P_1^{(8)})\langle\mathcal{O}^H(^3P_1^{(8)})\rangle + H^{(1)}_{q\bar{q}}(^3P_2^{(8)})\langle\mathcal{O}^H(^3P_2^{(8)})\rangle\Big) \\ &= \frac{8\pi^2\alpha_s}{N_c^2-1}\left[\frac{1}{2\pi}\frac{1}{x_1-x+i\epsilon}\frac{1}{x_2-x-i\epsilon}\right]\Big(C_A\,\hat{\sigma}^{(0)}_{q\bar{q}} + \hat{\sigma}^{(1)}_{q\bar{q}}\Big)\,, \end{aligned} \tag{7.48}$$

where we defined the P-wave contribution as

$$\begin{aligned}\hat{\sigma}_{q\bar{q}}^{(1)} &\equiv H_{q\bar{q}}^{(1)}({}^3P_1^{(8)})\langle\mathcal{O}^H({}^3P_1^{(8)})\rangle + H_{q\bar{q}}^{(1)}({}^3P_2^{(8)})\langle\mathcal{O}^H({}^3P_2^{(8)})\rangle \\ &= \frac{\pi^3\alpha_s^2}{M^3}\frac{80}{27}\,\delta(\hat{s}-M^2)\,\langle\mathcal{O}^H({}^3P_0^{(8)})\rangle\,. \end{aligned} \tag{7.49}$$

In deriving the last equation, we used the heavy quark spin symmetry [106],

$$\langle\mathcal{O}^H({}^3P_J^{(8)})\rangle = (2J+1)\langle\mathcal{O}^H({}^3P_0^{(8)})\rangle\,. \tag{7.50}$$

From Eqs. (7.42) and (7.43), after we neglect the color singlet channels that have wrong spin and angular momentum quantum numbers, the gluonic contribution from the initial-state and final-state rescattering to the direct production of $H({}^3S_1)$ are effectively the same except the sign of the $i\epsilon$ for the unpinched poles,

$$\begin{aligned} H_{gg\to H}^{(I)} &= \frac{8\pi^2\alpha_s}{N_c^2-1}\left[\frac{1}{2\pi}\frac{1}{x_1-x-i\epsilon}\frac{1}{x_2-x+i\epsilon}\right]C_A\,\hat{\sigma}_{gg}^{(0)}\,, \\ H_{gg\to H}^{(F)} &= \frac{8\pi^2\alpha_s}{N_c^2-1}\left[\frac{1}{2\pi}\frac{1}{x_1-x+i\epsilon}\frac{1}{x_2-x-i\epsilon}\right]C_A\,\hat{\sigma}_{gg}^{(0)}\,, \end{aligned} \tag{7.51}$$

where the gluon-gluon fusion cross section is defined as

$$\hat{\sigma}_{gg}^{(0)} \equiv \frac{\pi^3\alpha_s^2}{M^3}\frac{5}{12}\,\delta(\hat{s}-M^2)\left[\langle\mathcal{O}^H({}^1S_0^{(8)})\rangle + \frac{7}{m_Q^2}\langle\mathcal{O}^H({}^3P_0^{(8)})\rangle\right]. \tag{7.52}$$

In deriving Eq. (7.51), the heavy quark spin symmetry in Eq. (7.50) was used again.

Substituting the partonic cross sections in Eqs. (7.46), (7.48), and (7.51) into Eq. (7.36), and integrating over gluon momentum fractions, x_1 and x_2, we obtain the double scattering

contribution to the q_T^2-moment of heavy quarkonium production in NRQCD model as,

$$\begin{aligned}
&\int dq_T^2\, q_T^2\, \frac{d\sigma^D_{hA\to H}}{dq_T^2} \\
&= \left[\frac{8\pi^2\alpha_s}{N_c^2-1}\right]\left(\sum_q \int dx' f_{\bar{q}/h}(x') \int dx\, \left[T^{(I)}_{q/A}(x)\, C_F\, \hat{\sigma}^{(0)}_{q\bar{q}} + T^{(F)}_{q/A}(x)\, \left(C_A\, \hat{\sigma}^{(0)}_{q\bar{q}} + \hat{\sigma}^{(1)}_{q\bar{q}}\right)\right]\right. \\
&\left. + \int dx' f_{g/h}(x') \int dx \left[T^{(I)}_{g/A}(x)\, C_A\, \hat{\sigma}^{(0)}_{gg} + T^{(F)}_{g/A}(x)\, C_A\, \hat{\sigma}^{(0)}_{gg}\right]\right), \qquad (7.53)
\end{aligned}$$

which has a very similar expression as that in Eq. (7.26) derived in CEM in last subsection.

If we use the same model for the quark-gluon and gluon-gluon correlation functions as that used in CEM calculation in last subsection, we obtain the heavy quarkonium broadening in NRQCD model as

$$\Delta\langle q_T^2\rangle^{\rm NRQCD}_{\rm HQ} = \left(\frac{8\pi^2\alpha_s}{N_c^2-1}\,\lambda^2\, A^{1/3}\right)\frac{(C_F+C_A)\,\sigma^{(0)}_{q\bar{q}} + 2C_A\,\sigma^{(0)}_{gg} + \sigma^{(1)}_{q\bar{q}}}{\sigma^{(0)}_{q\bar{q}} + \sigma^{(0)}_{gg}}\,, \qquad (7.54)$$

where the leading order cross sections calculated in NRQCD model are given by

$$\begin{aligned}
\sigma^{(0,1)}_{q\bar{q}} &= \sum_q \int dx'\, f_{\bar{q}/h}(x') \int dx\, f_{q/A}(x)\, \hat{\sigma}^{(0,1)}_{q\bar{q}}\,, \\
\sigma^{(0)}_{gg} &= \int dx'\, f_{g/h}(x') \int dx\, f_{g/A}(x)\, \hat{\sigma}^{(0)}_{gg}\,, \qquad (7.55)
\end{aligned}$$

with the partonic cross sections given in Eqs. (7.47), (7.49), and (7.52), respectively.

From the transverse momentum broadening in Eq. (7.31) calculated in CEM in last subsection and that in Eq. (7.54) calculated in NRQCD model, it is clear that the leading double scattering contribution to the broadening calculated in these two models have the same expression if one neglects the P-wave contribution in NRQCD approach. Since the P-wave contribution is smaller than the S-wave contribution, and the gluon-gluon fusion subprocess dominates the heavy quarkonium cross section, we expect that $\Delta\langle q_T^2\rangle^{\rm NRQCD}_{\rm HQ} \approx \Delta\langle q_T^2\rangle^{\rm CEM}_{\rm HQ} \approx (2\,C_A/C_F)\Delta\langle q_T^2\rangle_{\rm DY}$.

In both CEM and NRQCD approach to the production of quarkonia, $H(^3S_1)$, we can also calculate the broadening effect on those quarkonia that were produced from the decay of either

excited or high spin states of produced quarkonia, known as the feeddown mechanism of the quarkonium production. Since the q_T^2-moment is normalized by the cross section (the 0^{th}-moment), and the rescattering takes place at the parton-level, we expect that the feed-down mechanism is not very sensitive to the quarkonium broadening while it is much more sensitive to the quarkonium production rate. We will come back to the role of the feeddown mechanism in quarkonium broadening in Sec. 7.5 when we present our numerical results.

7.3.3 Transverse momentum broadening in nucleus-nucleus collisions

In this subsection, we extend our calculations of heavy quarkonium's transverse momentum broadening in hadron-nucleus collisions to the broadening in nucleus-nucleus collisions. We discuss the similarities and differences between the hadron-nucleus and nucleus-nucleus collisions, and the role of transverse momentum broadening in probing the properties of the dense and hot QCD matter created in high energy nucleus-nucleus collisions.

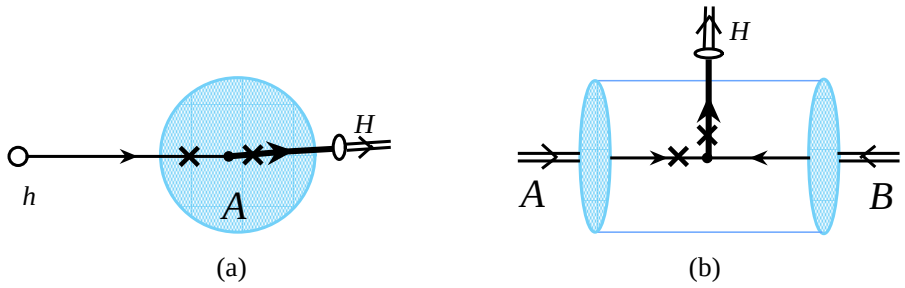

Figure 7.6 Sketch of heavy quarkonium production in hadron-nucleus collisions as viewed in the target rest frame (a), and that in nucleus-nucleus collisions as viewed in the center-of-mass frame (b). The thin and thick lines indicate the incoming parton and the outgoing heavy quark pair, respectively. The cross indicates potential rescattering point with soft partons of the nuclear medium.

The broadening of heavy quarkonium's transverse momentum is a consequence of both initial-state and final-state rescattering in nuclear medium. In high energy hadron-nucleus collisions, both initial-state and final-state rescattering probe the same properties of a normal nuclear matter. If the scattering process is viewed in the rest frame of the nucleus, as sketched

in Fig. 7.6(a), the incoming active parton and the produced heavy quark pair move very fast along the direction of the incoming hadron and interact with only partons of the nucleus near the same impact parameter. This picture supports our approximation that the correlation functions for final-state interaction are about the same as that for initial-state interaction. If the same process is viewed in the center of mass frame, we get the same conclusion that only nuclear partons near the same impact parameter can participate in the rescattering because the nuclear matter is moving very fast in this frame.

However, in high energy nucleus-nucleus collisions, the situation can be very different. If, other than the hard parton-parton scattering to produce the heavy quark pair and corresponding rescattering discussed above, other partons from two colliding nuclei did not interact in the collision, the transverse momentum broadening of heavy quarkonium production would be a simple superposition of the broadening in hadron-nucleus collision. In this picture, the leading contribution to the broadening in a collision between a nucleus A and a nucleus B would be given by the same expression in Eq. (7.34) with the $A^{1/3}$ replaced by $A^{1/3} + B^{1/3}$ or more precisely by L_{AB}/r_0, where $r_0 \approx 0.8$ fm and L_{AB} is an effective medium length in nucleus-nucleus collision calculated in the Glauber model [107]. The value of r_0 is obtained by letting $L_{pA} \approx r_0 A^{1/3} \approx (3/4)R_A$ with the nuclear radius R_A.

But, as indicated by the RHIC data [95], soft partons from two nuclei do interact to form a dense and hot QCD quark-gluon medium in high energy nucleus-nucleus collisions. The final-state rescattering between the produced heavy quark pair of transverse momentum q_T and the almost stationary or slowly expanding hot QCD medium in the center of mass frame of nucleus-nucleus collision, as sketched in Fig. 7.6(b), is very unlikely to broaden the pair's transverse momentum. Instead, the final-state interaction could suppress the production rate of the leading (or large momentum) colored and coherent heavy quark pair due to the energy loss [108], which is responsible for the observed jet quenching (or the suppression of leading hadrons or heavy quarks) at RHIC [95], and decrease the averaged transverse momentum $\langle q_T^2 \rangle$. On the other hand, the initial-state interaction in nucleus-nucleus collisions is likely to broaden the transverse momentum of the active parton in the same way as that in hadron-nucleus

collisions. Therefore, the measured $\langle q_T^2 \rangle$ in nucleus-nucleus collision is a consequence of two competing effects: the initial-state interaction tries to broaden the transverse momentum while the final-state rescattering in a slowly expanding medium tends to reduce the pair's transverse momentum. The detailed analysis and calculation of the competing final-state effects on the quarkonium broadening in nucleus-nucleus collisions requires a careful modeling of the hot and dense medium, and we will not discuss in this work.

Precise measurements of transverse momentum broadening of heavy quarkonium production in relativistic heavy ion collisions should provide very valuable information on the formation of the dense and hot quark-gluon medium and its properties. In nucleus-nucleus collisions, a deviation of the transverse momentum broadening from the simple superposition of that measured in hadron-nucleus collisions clearly indicates a change of nuclear matter properties from the interaction between soft partons of colliding nuclei. It should indicate the formation of a dense quark-gluon medium when the measured transverse momentum broadening is equal or less than the expected broadening from the initial-state interaction alone.

If the long-range interaction of soft partons from two colliding nuclei is quick and strong, and the dense quark-gluon medium is formed very early in relativistic heavy ion collisions, the initial-state interaction in nucleus-nucleus collisions could be different from a superposition of the initial-state effect in hadron-nucleus collisions due to the modification of nuclear matter. In order to independently test the initial-state effect from the final-state rescattering, we calculate the transverse momentum broadening of Z (as well as W) bosons in relativistic heavy ion collisions at the LHC in next section.

7.4 Transverse momentum broadening of Z (and W) production at the LHC

The lack of the final-state interaction of a Z (or a W) boson when it is reconstructed from its leptonic decay channels makes its transverse momentum broadening in high energy nuclear collisions an ideal probe for the initial-state interaction, in particular, the density of nuclear medium in the early stage of relativistic heavy ion collisions [109]. If the long-range

soft gluon interactions between two incoming heavy ions were so strong and a dense nuclear medium was formed before the short-distance creation of a Z (or a W) boson, the transverse momentum broadening would be a clean probe of the density of the dense medium. Otherwise, the transverse momentum broadening of Z (or W) bosons in nucleus-nucleus collisions would be a simple superposition of that in hadron-nucleus collision. Therefore, by measuring the broadening of Z (or W) bosons in both hadron-nucleus and nucleus-nucleus collisions, we could learn valuable information on whether the dense quark-gluon medium could be formed at a very early stage in relativistic heavy ion collisions [110].

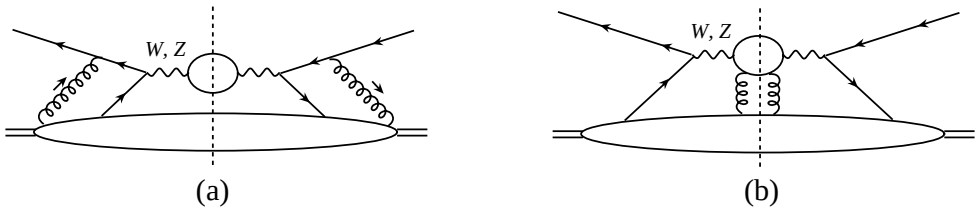

Figure 7.7 Leading order double scattering diagrams for production of a Z (or a W) boson in hadron-nucleus collisions via the initial-state interaction (a) and the possible final-state rescattering if the vector boson is reconstructed from its hadronic decay.

In Fig. 7.7, we sketch the leading double scattering diagrams for the Z (or W) production in hadron-nucleus collisions. The diagram in Fig. 7.7(a), which is almost identical to that for the Drell-Yan transverse momentum broadening, represents the initial-state interaction, while that in Fig. 7.7(b) represents the possible final-state rescattering if the vector boson could be reconstructed from its hadronic decay channels. For the Z and W bosons reconstructed from their leptonic decay channels, their transverse momentum broadening is mainly caused by the initial-state interaction, just like the broadening of the virtual photon in the Drell-Yan production. From the leading double scattering diagram in Fig. 7.7(a) and following the same derivation for the Drell-Yan broadening in Sec. 7.2, we obtain the leading transverse

momentum broadening of Z (or W) bosons in hadron-nucleus collisions as,

$$\begin{aligned}\Delta\langle q_T^2\rangle_{hA}^{Z} &= C_F\,\frac{8\pi^2\alpha_s(M_Z)}{N_c^2-1}\,\lambda_Z^2\,A^{1/3}\,,\\ \Delta\langle q_T^2\rangle_{hA}^{W} &= C_F\,\frac{8\pi^2\alpha_s(M_W)}{N_c^2-1}\,\lambda_W^2\,A^{1/3}\,,\end{aligned}\tag{7.56}$$

where λ_Z^2 (λ_W^2) is the nonperturbative scale for the double scattering production of Z (or W) bosons. It is defined in the same was as that in Eq.(7.14) and represents a ratio of nuclear four parton correlation function over a corresponding normal parton distribution. It is proportional to an averaged gluon field strength square in nuclear matter, $\langle F^{+\alpha}F^{+}_{\alpha}\rangle$ [74]. The λ_Z should be proportional to the typical transverse momentum or effective virtuality of soft gluons participating in the double scattering. As we will discuss in next section, the value of the λ_Z^2 (or λ_W^2) could depend on the momentum exchange of the hard collision, $Q\sim M_Z$ (or M_W), as well as the collision energy.

If we assume that the dense quark-gluon medium in relativistic heavy ion collisions is not formed before the creation of the heavy vector boson Z (or W), we could apply our formula in Eq. (7.56) to the broadening in nucleus-nucleus collisions as a simple superposition of the hadron-nucleus collision, and obtain the transverse momentum broadening in nucleus-nucleus collision as

$$\Delta\langle q_T^2\rangle_{AB}^{V} \approx C_F\,\frac{8\pi^2\alpha_s(M_V)}{N_c^2-1}\,\lambda_V^2\,\frac{L_{AB}}{r_0}\,,\tag{7.57}$$

where $V=Z,W$ for the Z and W production, respectively. If the long-range soft gluon interactions between two colliding heavy ions are so strong that the dense quark-gluon medium was formed before the short-distance creation of a Z (or a W) boson, we expect the same formula in Eq. (7.57) to be valid for the leading contribution to the transverse momentum broadening, but, with a new λ_V^2 different from that of a normal nuclear matter. The value of the effective λ_V^2 and its dependence on the collision geometry and collision energy should provide valuable informations on the formation of the QCD medium and its properties.

7.5 Numerical results

In this section, we provide a numerical comparison between our calculated heavy quarkonium broadening in nuclear collisions with existing data from Fermilab and RHIC experiments, and make predictions for the transverse momentum broadening at the LHC.

We have calculated the transverse momentum broadening of vector boson production in nuclear collisions in terms of the QCD factorization approach. We factorized the rescattering contribution to the broadening into two parts: (1) the non-perturbative, but, well-defined universal parton-parton correlation functions, which represent the probability to find the scattering centers in the nuclear medium, and (2) corresponding parton-level rescattering subprocess, which are infrared safe and perturbatively calculable. As a result of the factorization, the normalization for the transverse momentum broadening from partonic double scattering is uniquely fixed by the size of the non-perturbative quark-gluon and gluon-gluon correlation functions. If we use the model in Eqs. (7.14) and (7.30) to parameterize the correlation functions, the numerical results of our calculated transverse momentum broadening should be directly proportional to the value of the λ^2.

The value of the λ^2, or more precisely, the value of the parton-parton correlation functions should not depend on which vector boson was produced. This is because of the universality and the long-distance nature of the correlation functions. However, the value of the correlation functions or the λ^2 should depend on the momentum scale at which the hard part of the partonic scattering was evaluated.

As explicitly demonstrated in last three sections, all phase space integrations for the partonic rescattering can be deformed into perturbative region, and both initial- and final-state parton-level rescattering are evaluated at a hard scale $Q \sim 2m_Q$ or M_Z (or M_W) for heavy quarkonium or Z (or W) production, respectively. From the model in Eq. (7.14) (or (7.30)), the non-perturbative parameter, λ^2, represents a ratio of nuclear four parton correlation function over a normal parton distribution. As demonstrated in Ref. [74] by approximately decomposing a nuclear state into a product of nucleon states, the ratio (so as the λ^2) can be expressed in terms of an averaged gluon field strength square, $\langle F^{+\alpha}F^{+}_{\alpha}\rangle$. In this picture, the λ represents

the virtuality or the typical transverse momentum of the partons participating in the partonic rescattering, and certainly depends on the momentum exchange of the hard collision, Q, as well as the collision energy, $\sqrt{s}$, which determines the available phase space for the collision. For hadron-nucleus collisions with a large momentum transfer, Q, we expect the λ^2 to be proportional to $\ln(Q^2)$ from the parton shower leading to the hard collision. If the collision energy $\sqrt{s}$ is very large and the momentum fraction of the active parton, x, is very small, we would expect the λ^2 to be proportional to the saturation scale $Q_s^2 \propto 1/x^\delta$ with $\delta \approx 0.3$ [111, 112]. For the vector boson production, the typical momentum fraction of an active parton, $x \sim Q/\sqrt{s}$. Therefore, we expect $\lambda^2(Q) \propto \ln(Q^2)\,(\sqrt{s}/Q)^\delta$.

We use data on the Drell-Yan broadening in hadron-nucleus collisions, which were measured by Fermilab experiments at the fixed target energy, $\sqrt{s} = 38.8$ GeV [90], to extract the $\lambda^2_{\rm DY}$. From the value of $\lambda^2_{\rm DY}$, we estimate the value of λ^2 for producing a vector boson of invariant mass Q at a collision energy $\sqrt{s}$ as follows,

$$\lambda^2(Q) \approx \lambda^2_{\rm DY}\,\frac{\ln(Q^2)}{\ln(\langle Q^2_{\rm DY}\rangle)}\,\left(\frac{\sqrt{s}/Q}{38.8/\langle Q_{\rm DY}\rangle}\right)^\delta\,, \tag{7.58}$$

with the $\sqrt{s}$ in unit of GeV, $\langle Q_{\rm DY}\rangle \sim 6$ GeV, and $\delta \sim 0.3$.

Fermilab experiments: E772, E789, and E866 have measured the transverse momentum broadening of the Drell-Yan, as well as J/ψ, ψ', and Υ production in hadron-nucleus collisions [90, 94]. In Fig. 7.8, we plot the data on both the Drell-Yan and heavy quarkonium broadening as a function of atomic weight of nuclear targets. The broadening for the data was defined as a difference between the q_T^2-moment in proton-nucleus and proton-deuteron collisions: $\Delta\langle q_T^2\rangle = \langle q_T^2\rangle_{pA} - \langle q_T^2\rangle_{pD}$. By fitting the data on the Drell-Yan broadening as a function of $A^{1/3} - 2^{1/3}$, we obtain $\lambda^2_{\rm DY} \approx 0.01$ GeV^2, which gives the bottom solid line for the Drell-Yan broadening in Fig. 7.8, and is consistent with the value extracted in Ref. [89].

In Fig. 7.8(a), we plot our theoretical calculations of transverse momentum broadening of *direct* heavy quarkonium production in hadron-nucleus collisions at the Fermilab fixed target energy, $\sqrt{s} = 38.8$ GeV. To obtain the numerical results of theoretical calculations, we use CTEQ6L for nucleon parton distribution functions [13] and EKS98 parametrization for nuclear

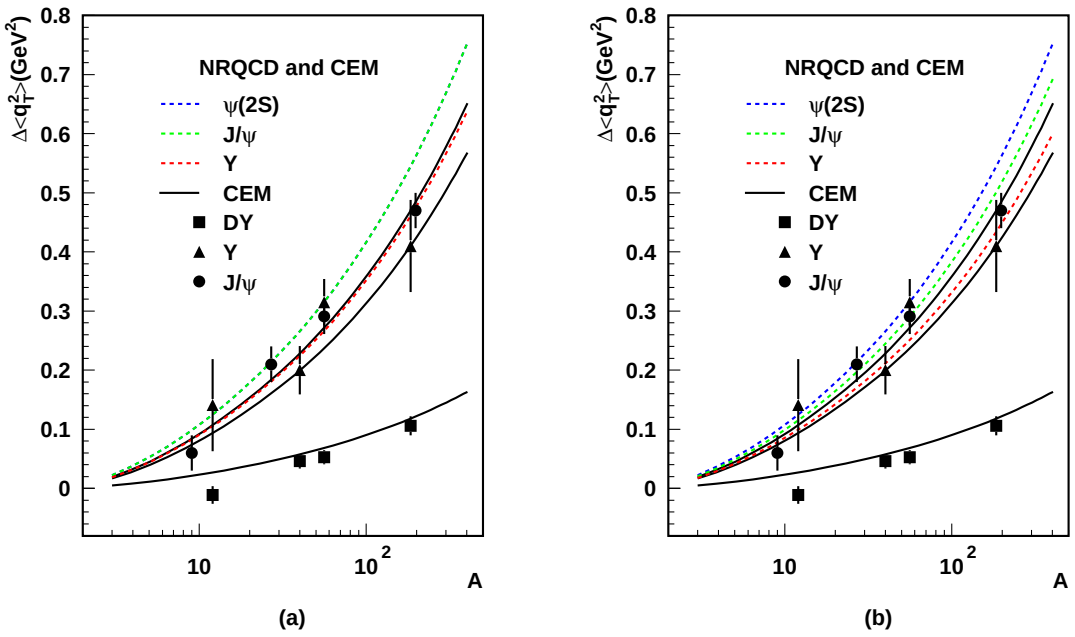

Figure 7.8 Data on transverse momentum broadening of heavy quarkonium as well as Drell-Yan production in hadron-nucleus collisions. Also plotted are theoretical calculations using Eq. (7.31) (solid lines) and Eq. (7.54) (dashed lines), derived by using CEM and NRQCD model, respectively. Three solid lines (from the top to bottom) correspond to J/ψ, Υ, and Drell-Yan, while three dashed lines represent ψ', J/ψ, and Υ production from NRQCD model. The quarkonium broadening calculated in NRQCD model is evaluated with (a) and without (b) quarkonia from the feeddown mechanism.

parton distributions (nPDF) [78] to evaluate the leading order production cross sections in Eqs. (7.31) and (7.54). The non-perturbative parameter, λ^2, in Eqs. (7.31) and (7.54) could be slightly different for J/ψ and Υ production due to the difference in the scale of hard collision, $Q \sim 2m_Q$. Using $\lambda^2_{\rm DY} \approx 0.01$ GeV^2, $M_{\rm J/\psi} = 3.1$ GeV, $M_\Upsilon = 9.5$ GeV, we estimate from Eq. (7.58) that $\lambda^2_{\rm J/\psi} \approx 0.008$ GeV^2 and $\lambda^2_\Upsilon \approx 0.011$ GeV^2 at $\sqrt{s} = 38.8$ GeV. We use Eq. (7.54) to evaluate the broadening for ψ', J/ψ, and Υ (the dashed lines) in NRQCD model. The NRQCD matrix elements are taken from Refs. [113, 114]. The small difference between the broadening of J/ψ and Υ is caused by the relative size between the quark and gluon contribution due to different sizes of matrix elements and the range of parton momentum fractions. For the direct production, J/ψ and ψ' have almost the identical broadening as shown in Fig. 7.8(a).

Similarly, we use Eq. (7.31) to evaluate the broadening for J/ψ (top solid line) and Υ (middle solid line) in CEM with $m_Q = 1.5$ GeV and $M_Q = 1.85$ GeV for J/ψ and $m_Q = 4.5$ GeV and $M_Q = 5.3$ GeV for Υ production, respectively. The transition probability, $F_{Q\bar{Q}\to H}$, cancels between the numerator and the denominator in Eq. (7.31). The small difference between these two solid lines are again caused by the relative size of the quark and gluon contribution due to the slightly different ranges of parton momentum fractions for J/ψ and Υ production.

We also test the effect of transverse momentum broadening on heavy quarkonia produced by the feeddown mechanism. Using the partonic hard parts derived in Sec. 7.3.2, we calculate in NRQCD model the transverse momentum broadening of quarkonia in high spin or excited states, which then decay into the observed spin-1 and S-wave quarkonia, $H(^3S_1)$. We plot the calculated broadening with this feeddown mechanism in Fig. 7.8(b). Although the feeddown mechanism could provide as much as 40% of J/ψ production rate, its net effect on the transverse momentum broadening is very small because of the fact that the broadening defined is normalized by the inclusive cross section.

For a large nucleus with the atomic weight $A \geq 10^2$, some of the produced heavy quark pairs could transmute to a color singlet pre-quarkonium state (or even a physical quarkonium) before exiting the nuclear matter. Comparing to a colored heavy quark pair, these color singlet states should have a weaker interaction with the nuclear matter and get less broadening in transverse momentum. Therefore, we expect the theoretical curves in Fig. 7.8 to be slightly less steep than what were shown when $A \geq 10^2$.

From Fig. 7.8, we conclude that perturbative QCD calculations of the quarkonium broadening based on both CEM and NRQCD model give a good description of existing experimental data in hadron-nucleus collisions. The major difference between the heavy quarkonium and the Drell-Yan broadening is naturally explained by the role of final-state interactions. Although the production mechanism in CEM and NRQCD model is different, these two models of heavy quarkonium production predict almost the same functional form for the transverse momentum broadening, as shown in Eq. (7.31) and Eq. (7.54), respectively. Since the P-wave contribution is relatively small, as shown in Fig. 7.8, these two models predict almost the same transverse

momentum broadening. In addition, both models predict that J/ψ and Υ have effectively the same broadening in hadron-nucleus collisions other than a small difference caused by the available phase space (i.e., the available range of parton momentum fractions).

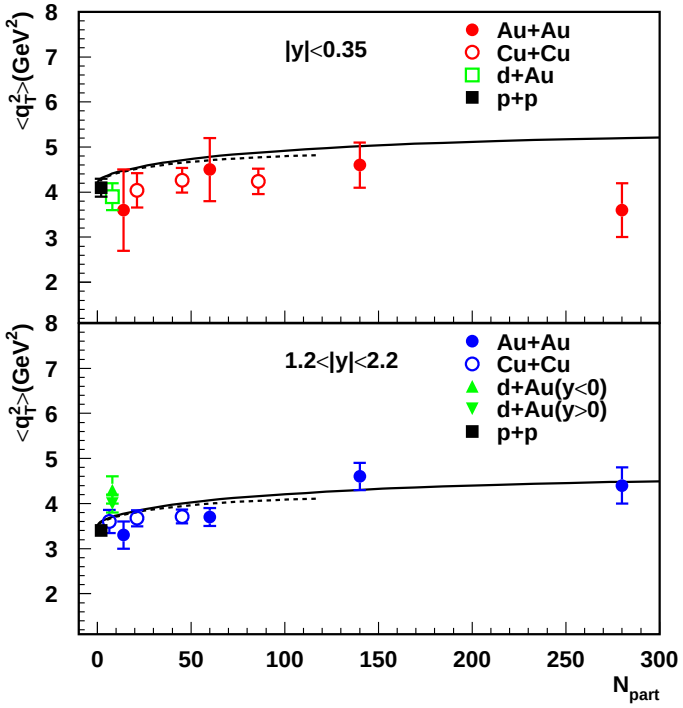

Figure 7.9 RHIC data on averaged transverse momentum square of J/ψ production as a function of the number of participants [115]. The top panel is for the J/ψ's produced in the central rapidity region while the bottom panel is for those produced in more forward or backward region. Also plotted are theoretical calculations using Eq. (7.59). Solid lines for Au-Au collisions and dashed lines for Cu-Cu collisions, respectively.

In Fig. 7.9, we plot PHENIX data on averaged transverse momentum square of J/ψ production at RHIC energies as a function of the number of participants, $N_{\rm part}$ [115]. The top panel is for the J/ψ produced in the central rapidity region with $|y| < 0.35$, and the bottom is for those produced in the forward and backward region with $1.2 < |y| < 2.2$. We also plot our theoretical calculations of the transverse momentum square by using

$$\langle q_T^2 \rangle_{AB} \approx \langle q_T^2 \rangle|_{pp-exp} + \Delta\langle q_T^2 \rangle_{AB} \,, \tag{7.59}$$

where $\langle q_T^2\rangle|_{pp-exp}$ is fixed by the data point from proton-proton collision in Fig. 7.9 and $\Delta\langle q_T^2\rangle_{AB}$ is given by our calculation. We evaluate $\Delta\langle q_T^2\rangle_{AB}$ in nucleus-nucleus collisions with an effective medium length L_{AB} as

$$\Delta\langle q_T^2\rangle_{AB\to \mathrm{J}/\psi}^{\mathrm{CEM}} = \left(\frac{8\pi^2\alpha_s}{N_c^2-1}\,\lambda_{\mathrm{J}/\psi}(\mathrm{RHIC})^2\,\frac{L_{AB}}{r_0}\right)\frac{(C_F+C_A)\,\sigma_{q\bar{q}}+2\,C_A\,\sigma_{gg}}{\sigma_{q\bar{q}}+\sigma_{gg}} \tag{7.60}$$

in CEM. Eq. (7.60) is obtained from Eq. (7.31) by replacing the $A^{1/3}$ by L_{AB}/r_0. We can calculate the broadening in NRQCD model by applying the same replacement to Eq. (7.54). At the RHIC energy, we obtain $\lambda_{\mathrm{J}/\psi}(\mathrm{RHIC})^2 \approx 0.013$ GeV^2 from Eq. (7.58). We calculate the L_{AB} in Glauber model and convert it to $\mathrm{N_{part}}$ [107].

In nucleus-nucleus collisions, soft gluons from the colliding ions can interact even if the collision is not a head-on or a central collision. Such interaction in a non-central collision may not be strong enough to stop all soft partons to form an almost stationary or slowly expanding hot medium of quarks and gluons. It certainly can slow down some of the colliding soft partons to change the characteristics of the nuclear matter, which could alter the final-state interactions. As a result, the final-state interaction between the produced heavy quark pairs and the modified nuclear matter in nucleus-nucleus collisions, as sketched in Fig. 7.6(b), generates less transverse momentum broadening if it does not reduce the transverse momentum due to energy loss. In Fig. 7.9, we plot our calculations of J/ψ transverse momentum broadening by using Eqs. (7.59) and (7.60), and keeping only the contribution from initial-state rescattering. The solid lines are for the Au-Au collision, while the dashed lines are for the Cu-Cu collision. Our calculations are consistent with the data in both rapidity regions.

In the central Au-Au collision, a hot and dense medium is produced. As discussed above, the averaged transverse momentum could be reduced, instead of the broadening, due to the energy loss of the produced heavy quark pairs when they interact with the hot and slowly expanding medium. A more detailed study of the momentum shift of the heavy quark pairs in such a hot medium could provide a more accurate description of the data in central region, and help the extraction of medium properties.

Transverse momentum broadening of Z (or W) bosons in high energy nuclear collisions

could provide a clean measurement of initial-state interactions, and help isolating final-state rescattering effect in heavy quarkonium production. However, because of the heavy mass of Z (or W) boson, only the LHC has a chance to measure the broadening reliably [110].

We use Eq. (7.58) to estimate the λ^2 for the heavy vector boson production at $\sqrt{s} = 5.5$ TeV, the averaged nucleon-nucleon collision energy in relativistic heavy ion collisions at the LHC. We obtain $\lambda^2(\mathrm{LHC}) \approx 0.035, 0.05$ and 0.05 GeV^2 for the production of J/ψ, Υ, and the heavy vector boson Z (or W), respectively. Although the Υ mass is much smaller than that of a Z boson, the Υ and Z have the same $\lambda^2(\mathrm{LHC})$ for the transverse momentum broadening due to the larger available phase space for Υ production [117]. In Fig. 7.10, we present our predictions for the transverse momentum broadening of vector boson production at the LHC. Using the estimated $\lambda^2_{Z/W}(\mathrm{LHC}) \approx 0.05$ GeV^2 and Eq. (7.56), we evaluate the transverse momentum broadening of Z (and W) bosons reconstructed from their leptonic decays, and plot the predictions for hadron-nucleus collisions as a function of atomic weight of the nucleus, A, in Fig. 7.10(a). We also plot the expected transverse momentum broadening of J/ψ and Υ production in hadron-nucleus collisions in Fig. 7.10(a). The curves for heavy quarkonium broadening are evaluated by using $\lambda^2_{\mathrm{J}/\psi}(\mathrm{LHC}) \approx 0.035$ GeV^2 and $\lambda^2_{\Upsilon}(\mathrm{LHC}) \approx 0.05$ GeV^2, and Eq. (7.31) from CEM without contributions from the feeddown mechanism. Eq. (7.54) derived from NRQCD model gives the similar results. The heavy quarkonium broadening in Fig. 7.10(a) is much larger than that of Z (or W) bosons because of the additional final-state effect, and the difference in color factor and the strength of the strong coupling constant, $\alpha_s(Q)$.

In Fig. 7.10(b), we plot the expected transverse momentum broadening of vector boson production in Pb-Pb collision at $\sqrt{s} = 5.5$ TeV at the LHC as a function of the number of participants, $\mathrm{N_{part}}$ [107]. We calculate the L_{AB} in Glauber model with inelastic nucleon-nucleon cross section $\sigma^{in}_{NN} = 70$mb at the LHC energy and convert it to $\mathrm{N_{part}}$ in Pb-Pb collisions [107]. For the Z (and W) broadening, we use $\lambda_{Z/W}(\mathrm{LHC})^2 \approx 0.05$ GeV^2, the same value used for the broadening in hadron-nucleus collisions in Fig. 7.10(a). Since the transverse momentum broadening is directly proportional to the λ^2, which is proportional to the gluon strength in

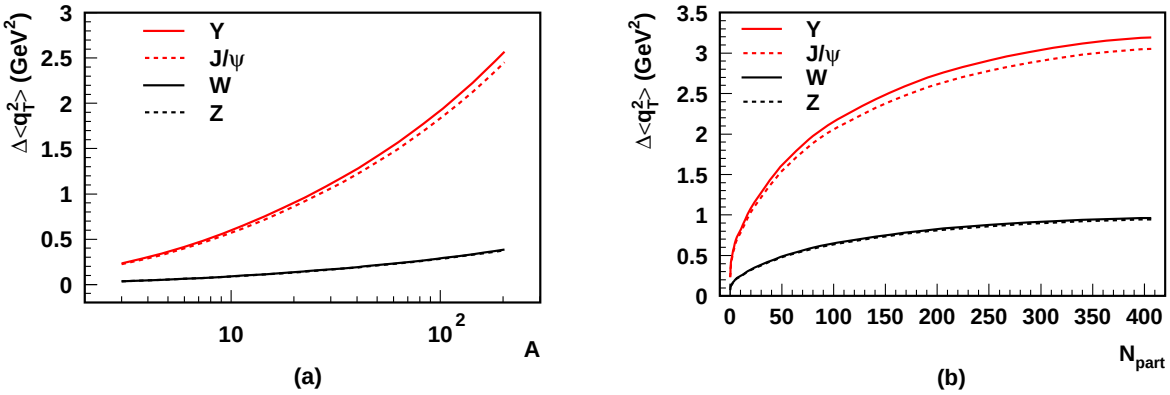

Figure 7.10 Transverse momentum broadening of Z and W (lower set of curves) in hadron-nucleus collisions (a) and nucleus-nucleus collisions (b) at $\sqrt{s} = 5.5$ TeV as a function of atomic weight of nuclear beam and the number of participants, N_{part}, respectively. Also plotted are predictions (upper set of curves) for the transverse momentum broadening of heavy quarkonium production in hadron-nucleus collision at the LHC energy (a); and the initial-state only broadening in nucleus-nucleus collision at the same energy (b).

the medium, a deviation from the predicted curves in Fig. 7.10(b) signals the formation of the hot quark-gluon medium before the creation of the heavy Z (or W) bosons.

For J/ψ and Υ production in Fig. 7.10(b), we use $\lambda^2_{J/\psi}(\mathrm{LHC}) \approx 0.035$ GeV^2 and $\lambda^2_{\Upsilon}(\mathrm{LHC}) \approx 0.05$ GeV^2, and Eq. (7.31) from CEM to evaluate the quarkonium broadening. Eq. (7.54) from NRQCD model gives similar predictions. The plotted curves for J/ψ and Υ production in Fig. 7.10(b) include only initial-state interaction. As discussed in Sec. 7.3.3, the final-state rescattering in nucleus-nucleus collisions is more likely to reduce the transverse momentum broadening due to the energy loss, if a slowly expanding medium was produced. Therefore, we expect the curves in Fig. 7.10(b) to represent the maximum broadening of J/ψ and Υ that will be seen in relativistic heavy ion collisions at the LHC [110].

If we could reconstruct Z and W bosons from their hadronic decay (e.g., into two jets), which might be impossible to do in the LHC environment, the hadronic jets from Z and W decay will have to interact with the nuclear medium. The final-state multiple scattering could generate momentum imbalance between these two jets and effectively introduce an apparent

mass shift for the Z and W boson [47]. Such mass shift would provide additional information on the properties of the hot quark-gluon medium.

CHAPTER 8. SUMMARY AND OUTLOOK

Perturbative QCD has made up the most amazing story of Quantum Chromodynamics because of the asymptotic freedom and factorization theorems. With factorization theorems, the physical observables in high energy scattering processes can be factorized into short-distance hard parts convoluted with universal long-distance parton distribution functions (PDFs) at *leading power*. The factorization assures that both the short distance hard parts and the PDFs could be interpreted as probabilities evaluated at two very different momentum scales. All quantum correlations between physics at these two different scales are proved to be suppressed by the power of the ratio of these two momentum scales. The short-distance hard parts are often referred as the partonic cross sections with all collinear divergences removed. With the asymptotic freedom, we are able to calculate the short-distance hard parts in terms of a power series expansion in the QCD coupling α_s. The universal PDFs are interpreted as probability densities to find a parton of various flavors inside a hadron with a given momentum fraction. Once the process independent PDFs are extracted from some experiments, they can be used to make predictions for observables in other experiments. This so-called *leading power (twist)* QCD factorization formalism has been very successful in interpreting and predicting high energy scattering processes.

In this thesis, we investigated QCD dynamics and hadron structure beyond what have been learned from this probability picture. Using the generalized factorization theorems, by taking advantage of spin and nuclear dependence, we were able to explore the three-parton and four-parton quantum correlations inside a hadron.

We have shown that the single transverse spin asymmetries (SSAs) are sensitive to three-parton correlation functions inside a polarized hadron. We constructed two sets of twist-

3 three-parton correlation functions relevant to the SSAs. The quark-gluon and tri-gluon correlation functions represent the role that quark and gluon have played in generating the SSAs, respectively. Since gluon is an essential component of QCD dynamics and has played a dominant role in many high energy hadronic scattering processes, we investigated the potential role of gluons in generating the SSAs in both lepton-hadron and hadron-hadron collisions. We derived for the first time the leading order (LO) formalism for the SSAs of open charm meson production in both SIDIS and hadronic collisions. We found that the SSAs are likely dominated by the contribution of the tri-gluon correlation functions, thus the observation of any significant single-spin asymmetry in these processes would be a clear indication of the presence of tri-gluon correlations inside a polarized hadron. We also found that the two tri-gluon correlation functions could play very different role in generating the SSAs for production of D and $\bar{D}$ mesons. These features make the SSAs in open charm production excellent probes of tri-gluon correlation functions.

We could easily generalize the current formalism to study the contribution of tri-gluon correlation functions in other processes, such as single jet production $p^{\uparrow}p \to jet + X$, single inclusive pion production $p^{\uparrow}p \to \pi + X$, prompt photon production $p^{\uparrow}p \to \gamma + X$, J/ψ production $p^{\uparrow}p \to J/\psi + X$, and Drell-Yan production $p^{\uparrow}p \to [\gamma^* \to \ell^+\ell^-] + X$. Once we derive the formalisms for all these processes, we could try to extract the first information on the tri-gluon correlation functions through a global QCD fitting procedure. These studies are under way and will be available in the near future.

Although the twist-3 collinear factorization approach to the SSAs at the leading power in α_s has had some successes phenomenologically, there are still many challenges. One of the challenges is the strong dependence on the choice of the renormalization scale μ as well as the factorization scale μ_F, while the physically observed SSAs are independent of any of these scales. The strong dependence on the choice of renormalization and factorization scale is an artifact of the lowest order perturbative calculation. A significant cancellation of the scale dependence between the leading and the next-to-leading order (NLO) contribution is expected from the QCD factorization theorem and has been proved to be true for many processes at

the leading power (or leading twist). In order to really test QCD dynamics for SSAs, it is necessary to calculate the evolution (or the scale dependence) of the universal long-distance distributions and to evaluate the perturbative short-distance contribution beyond the lowest order in α_s.

We introduced the Feynman diagram representation for the twist-3 quark-gluon and tri-gluon correlation functions relevant to SSAs in QCD collinear factorization approach. We derived the cut vertices to connect the hadronic matrix elements of these correlation functions to the forward scattering Feynman diagrams. In terms of the Feynman diagram representation, we derived for the first time a closed set of evolution equations for these quark-gluon and tri-gluon correlation functions. We calculated evolution kernels relevant to the gluonic pole contribution to the SSAs at the order of α_s. We found that all evolution kernels are infrared safe and have a lot in common to the DGLAP evolution kernels of unpolarized parton distributions (not the polarized helicity distributions). Having derived evolution equations for these correlation functions, we will be able to systematically compute NLO corrections to the SSAs, which represents a necessary step moving toward the goal of global analysis of QCD dynamics beyond what have been explored by the very successful leading power QCD collinear factorization formalism.

We further extended our current study on the SSAs to the two-scale observables. Using the TMD approach, we studied the SSAs of W production in terms of the Sivers functions and found that the measurable lepton asymmetry from W decay at RHIC is an excellent observable for testing the time-reversal modified universality of the Sivers functions.

We also explored the opportunities to study the four-parton correlation functions by taking the advantage of nuclear dependence in high energy nuclear collisions. We found that the nuclear-size dependent effect are sensitive to the four-parton correlation functions in nuclei. We investigated the transverse momentum broadening of vector boson production in hadron-nucleus and nucleus-nucleus collisions in terms of parton-level multiple scattering. We factorized the contribution to transverse momentum broadening into the calculable short-distance partonic rescattering multiplied by universal parton-parton correlation functions, which could

be interpreted as the probabilities to find coherent rescattering centers in a nuclear medium. We derived the short-distance hard parts by evaluating the partonic rescattering diagrams at a perturbative hard scale Q which is of the order of vector boson mass. We verified the universality of the non-perturbative parton-parton correlation functions by fitting the data on both the Drell-Yan broadening and the broadening of J/ψ and Υ production, and demonstrated clearly the predictive power of the QCD factorization approach.

For the Drell-Yan virtual photon and Z (or W) boson production, we evaluated transverse momentum broadening from purely initial-state multiple scattering. We discussed the scale dependence of the non-perturbative parameter, λ^2, and extrapolated it from its value at the fixed-target energy to the collider energies. We calculated the broadening of Z (and W) bosons in both hadron-nucleus and nucleus-nucleus collisions at the LHC. We evaluated the Z (and W) boson broadening in nucleus-nucleus collisions as a superpostion of its broadening in hadron-nucleus collisions, and argued that a deviation from our calculation is a clear signal indicating that strong interactions between soft partons of colliding heavy ions took place before the short-distance creation of the heavy vector bosons. That is, the transverse momentum broadening of Z (or W) bosons could be a clean and excellent probe of the early stage dynamics of relativistic heavy ion collisions.

For J/ψ and Υ production, we demonstated that the final-state interaction between the produced heavy quark pair and the nuclear medium is very important in understanding the existing data. We calculated the broadening in both CEM and NRQCD model, and clearly showed that the two models generate a small difference in the broadening and the broadening has a weak dependence on the feeddown mechanism. That is, the transverse momentum broadening is insensitive to the details of the hadronization mechanism and perturbatively reliable. We found that the leading contribution to heavy quarkonium broadening in hadron-nucleus collisions is about $2C_A/C_F = 4.5$ times the corresponding Drell-Yan broadening, which gives a good description of the existing Fermilab data.

We argued that the role of the final-state interaction to the transverse momentum broadening in nucleus-nucleus collisions could be very different from that in hadron-nucleus collisions.

In hadron-nucleus collisions, both initial-state and final-state interactions involve only soft partons of the nucleus near the same impact parameter, and therefore, provide similar contributions to the transverse momentum broadening as long as the heavy quark pair stays in a colored state. On the other hand, soft partons from two colliding nuclei could strongly interact to produce a slowly expanding quark-gluon medium. This new medium could interact with the produced heavy quark pair as shown in Fig. 7.6. The interaction could be very weak if the pair is in a singlet state. On the other hand, the interaction could be very strong if the pair is in a color octet state, but, is unlikely to increase the pair's transverse momentum if it does not reduce the momentum due to the pair's medium induced energy loss.

This generalized factorization approach could also be applied to study the nuclear dependence of quarkonium cross sections in high energy nuclear collisions, as well as the nuclear dependence of the quarkonium's rapidity and transverse momentum distributions if the transverse momentum q_T is large enough. Quantum suppression was proposed as one of the most reliable signals for the formation of quark-gluon plasma in relativistic heavy ion collisions. Since the temperature of the hot medium in heavy ion collisions is comparable with the binding energy of a physical heavy quarkonium meson, understanding the formation of a heavy quarkonium in the medium can not only provide valuable information on the medium properties but also shed some lights on how a bound and color singlet (or confined) physical meson was formed from a pair of colored heavy quarks produced at the very short distance. This is another direction that my future research will be focused on.

QCD has been proven to be very successful in interpreting many complex phenomena observed in high energy experiments, and serves the basis of predictions and tests for new physics beyond the Standard Model. However, QCD is a very rich theory and is much more complex than the theory of Quantum Electrodynamics, which is the fundamental quantum theory behind all excitements of condensed matter phenomena. After more than 35 years since it was first proposed, we have only learned a very small part of QCD dynamics. We do not know how quarks and gluons, and their color degree of freedom were confined to form the bound hadrons, and we have not found the robust way to derive the basic properties of

the hadrons, such as its mass and spin, from the first principle calculation of QCD dynamics. Our work presented in this thesis does represent an important effort to better understand the QCD dynamics by exploring the quantum interference and quantum correlations between its fundamental fields/particles: quarks and gluons. We derived from QCD new predictions and proposed experimental measurements to test our predictions. With data arriving from the current and future experiments around the world, we will be able to learn features of QCD dynamics and its role in understanding the physics of the strong interaction.

BIBLIOGRAPHY

[1] M. Gell-Mann, Phys. Lett. **8**, 214 (1964).

[2] G. Zweig, CERN preprint TH401, 412 (unpublished), 1964.

[3] E. D. Bloom *et al.*, Phys. Rev. Lett. **23**, 930 (1969).

[4] J. I. Friedman and H. W. Kendall, Ann. Rev. Nucl. Part. Sci. **22**, 203 (1972).

[5] J. D. Bjorken and E. A. Paschos, Phys. Rev. **185**, 1975 (1969).

[6] C. G. . Callan and D. J. Gross, Phys. Rev. Lett. **22**, 156 (1969).

[7] R. P. Feynman, Phys. Rev. Lett. **23**, 1415 (1969).

[8] C. N. Yang and R. L. Mills, Phys. Rev. **96**, 191 (1954).

[9] H. Fritzsch, M. Gell-Mann and H. Leutwyler, Phys. Lett. B **47**, 365 (1973).

[10] D. J. Gross and F. Wilczek, Phys. Rev. Lett. **30**, 1343 (1973).

[11] H. D. Politzer, Phys. Rev. Lett. **30**, 1346 (1973).

[12] for reviews, see: J. C. Collins, D. E. Soper and G. Sterman, Adv. Ser. Direct. High Energy Phys. **5**, 1 (1988), [arXiv:hep-ph/0409313].

[13] J. Pumplin, D. R. Stump, J. Huston, H. L. Lai, P. Nadolsky and W. K. Tung, JHEP **0207**, 012 (2002) [arXiv:hep-ph/0201195]; P. M. Nadolsky *et al.*, Phys. Rev. D **78**, 013004 (2008) [arXiv:0802.0007 [hep-ph]], and references therein.

[14] A. D. Martin, R. G. Roberts, W. J. Stirling and R. S. Thorne, Eur. Phys. J. C **23**, 73 (2002) [arXiv:hep-ph/0110215]; A. D. Martin, W. J. Stirling, R. S. Thorne and G. Watt, Phys. Lett. B **652**, 292 (2007) [arXiv:0706.0459 [hep-ph]], and references therein.

[15] C. Amsler *et al.* [Particle Data Group], Phys. Lett. B **667**, 1 (2008).

[16] J. W. Qiu and G. Sterman, Phys. Rev. Lett. **67**, 2264 (1991); Phys. Rev. D **59**, 014004 (1998).

[17] J. W. Qiu and G. Sterman, Nucl. Phys. B **378**, 52 (1992).

[18] J. W. Qiu and G. Sterman, AIP Conf. Proc. **223**, 249 (1991);

[19] J. w. Qiu and G. Sterman, Nucl. Phys. B **353**, 105 (1991); Nucl. Phys. B **353**, 137 (1991).

[20] G. Bunce *et al.*, Phys. Rev. Lett. **36**, 1113 (1976).

[21] D. L. Adams *et al.* [E581 and E704 Collaborations], Phys. Lett. B **261**, 201 (1991); D. L. Adams *et al.* [FNAp-E704 Collaboration], Phys. Lett. B **264**, 462 (1991); K. Krueger *et al.*, Phys. Lett. B **459**, 412 (1999).

[22] A. Bravar [Spin Muon Collaboration], Nucl. Phys. A **666**, 314 (2000); A. Airapetian *et al.* [HERMES Collaboration], Phys. Rev. Lett. **84**, 4047 (2000); Phys. Rev. D **64**, 097101 (2001); Phys. Rev. Lett. **94**, 012002 (2005) [arXiv:hep-ex/0408013]; V. Y. Alexakhin *et al.* [COMPASS Collaboration], Phys. Rev. Lett. **94**, 202002 (2005) [arXiv:hep-ex/0503002]; E. S. Ageev *et al.* [COMPASS Collaboration], Nucl. Phys. B **765**, 31 (2007) [arXiv:hep-ex/0610068]; M. Alekseev *et al.* [COMPASS Collaboration], Phys. Lett. B **673**, 127 (2009) [arXiv:0802.2160 [hep-ex]]; S. Levorato [COMPASS Collaboration], talk presented at "Second International Workshop on Transverse Polarisation Phenomena in Hard Processes (Transversity 2008)", May 2008, Ferrara, Italy; H. Avakian, P. E. Bosted, V. Burkert and L. Elouadrhiri [CLAS Collaboration], AIP Conf. Proc. **792**, 945 (2005) [arXiv:nucp-ex/0509032].

[23] J. Adams *et al.* [STAR Collaboration], Phys. Rev. Lett. **92**, 171801 (2004) [arXiv:hep-ex/0310058]; B. I. Abelev *et al.* [STAR Collaboration], Phys. Rev. Lett. **99**, 142003 (2007) [arXiv:0705.4629 [hep-ex]]; Phys. Rev. Lett. **101**, 222001 (2008) [arXiv:0801.2990 [hep-ex]]; S. S. Adler *et al.* [PHENIX Collaboration], Phys. Rev. Lett. **95**, 202001 (2005) [arXiv:hep-ex/0507073]; M Chiu [PHENIX Collaboration], talk presented at "The 18th International Symposium on Spin Physics (Spin 2008)", Charlottesville, Virginia, Oct. 2008; I. Arsene *et al.* [BRAHMS Collaboration], Phys. Rev. Lett. **101**, 042001 (2008) [arXiv:0801.1078 [nucp-ex]].

[24] for reviews, see: U. D'Alesio and F. Murgia, Prog. Part. Nucl. Phys. **61**, 394 (2008).

[25] G. L. Kane, J. Pumplin and W. Repko, Phys. Rev. Lett. **41**, 1689 (1978).

[26] A. V. Efremov and O. V. Teryaev, Sov. J. Nucl. Phys. **36**, 140 (1982) [Yad. Fiz. **36**, 242 (1982)]; A. V. Efremov and O. V. Teryaev, Phys. Lett. B **150**, 383 (1985).

[27] C. Kouvaris, J. W. Qiu, W. Vogelsang and F. Yuan, Phys. Rev. D **74**, 114013 (2006) [arXiv:hep-ph/0609238].

[28] H. Eguchi, Y. Koike and K. Tanaka, Nucl. Phys. B **752**, 1 (2006) [arXiv:hep-ph/0604003]; Nucl. Phys. B **763**, 198 (2007) [arXiv:hep-ph/0610314].

[29] Y. Koike and K. Tanaka, Phys. Lett. B **646**, 232 (2007) [Erratum-ibid. B **668**, 458 (2008)] [arXiv:hep-ph/0612117]; Phys. Rev. D **76**, 011502 (2007) [arXiv:hep-ph/0703169].

[30] R. b. Meng, F. I. Olness and D. E. Soper, Nucl. Phys. B **371**, 79 (1992); Y. Koike and J. Nagashima, Nucl. Phys. B **660**, 269 (2003).

[31] A. Mendez, Nucl. Phys. B **145**, 199 (1978).

[32] X. Ji, J. W. Qiu, W. Vogelsang and F. Yuan, Phys. Rev. Lett. **97**, 082002 (2006) [arXiv:hep-ph/0602239], Phys. Rev. D **73**, 094017 (2006) [arXiv:hep-ph/0604023], Phys. Lett. B **638**, 178 (2006) [arXiv:hep-ph/0604128]; Y. Koike, W. Vogelsang and F. Yuan, Phys. Lett. B **659**, 878 (2008) [arXiv:0711.0636 [hep-ph]].

[33] F. Yuan and J. Zhou, Phys. Lett. B **668**, 216 (2008) [arXiv:0806.1932 [hep-ph]].

[34] C. J. Bomhof and P. J. Mulders, JHEP **0702**, 029 (2007) [arXiv:hep-ph/0609206]; Nucl. Phys. B **795**, 409 (2008) [arXiv:0709.1390 [hep-ph]].

[35] X. D. Ji, Phys. Lett. B **289**, 137 (1992).

[36] T. Kneesch, B. A. Kniehl, G. Kramer and I. Schienbein, Nucl. Phys. B **799**, 34 (2008) [arXiv:0712.0481 [hep-ph]].

[37] A. Deshpande, R. Milner, R. Venugopalan and W. Vogelsang, Ann. Rev. Nucl. Part. Sci. **55**, 165 (2005) [arXiv:hep-ph/0506148].

[38] M. Cacciari, S. Frixione, M. L. Mangano, P. Nason and G. Ridolfi, JHEP **0407**, 033 (2004) [arXiv:hep-ph/0312132].

[39] H. Liu [PHENIX Collaboration], talk presented at "The 18th International Symposium on Spin Physics (Spin 2008)", Charlottesville, Virginia, Oct. 2008.

[40] R. Nouicer and f. t. P. Collaboration, PoS **VERTEX2007**, 042 (2007) [arXiv:0801.2947 [nucl-ex]].

[41] W. Vogelsang and F. Yuan, arXiv:0904.0410 [hep-ph].

[42] A. H. Mueller, Phys. Rept. **73**, 237 (1981).

[43] J. C. Collins and J. W. Qiu, Phys. Rev. D **39**, 1398 (1989).

[44] R. K. Ellis, W. Furmanski and R. Petronzio, Nucl. Phys. B **212**, 29 (1983).

[45] J. W. Qiu, Phys. Rev. D **42**, 30 (1990).

[46] R. L. Jaffe, Nucl. Phys. B **229**, 205 (1983).

[47] M. Luo, J. W. Qiu and G. Sterman, Phys. Rev. D **49**, 4493 (1994).

[48] Yu. Dokshitzer, Sov. Phys. JETP **46**, 1649 (1977); V. N. Gribov and L. N. Lipatov, Sov. Nucl. Phys. **15**, 438 (1972); **15**, 675 (1972); G. Alteralli and G. Parisi, Nucl. Phys. B **126**, 298 (1977).

[49] V. Barone, A. Drago and P. G. Ratcliffe, Phys. Rept. **359**, 1 (2002) [arXiv:hep-ph/0104283]; X. Artru and M. Mekhfi, Z. Phys. C **45**, 669 (1990); J. C. Collins, Nucl. Phys. B **396**, 161 (1993) [arXiv:hep-ph/9208213].

[50] Z. B. Kang and J. W. Qiu, Phys. Rev. D **78**, 034005 (2008) [arXiv:0806.1970 [hep-ph]]; Z. B. Kang, J. W. Qiu, W. Vogelsang and F. Yuan, Phys. Rev. D **78**, 114013 (2008) [arXiv:0810.3333 [hep-ph]].

[51] D. Boer, P. J. Mulders and F. Pijlman, Nucl. Phys. B **667**, 201 (2003) [arXiv:hep-ph/0303034].

[52] J. C. Collins and D. E. Soper, Nucl. Phys. B **193**, 381 (1981) [Erratum-ibid. B **213**, 545 (1983)]; Nucl. Phys. B **197**, 446 (1982).

[53] J. C. Collins, D. E. Soper and G. Sterman, Nucl. Phys. B **250**, 199 (1985).

[54] J. C. Collins, Phys. Lett. B **536**, 43 (2002).

[55] D. Boer, P. J. Mulders and F. Pijlman, Nucl. Phys. B **667**, 201 (2003).

[56] X. d. Ji, J. P. Ma and F. Yuan, Phys. Lett. B **597**, 299 (2004), Phys. Rev. D **71**, 034005 (2005).

[57] J. C. Collins and A. Metz, Phys. Rev. Lett. **93**, 252001 (2004).

[58] J. Collins and J. W. Qiu, Phys. Rev. D **75**, 114014 (2007).

[59] D. W. Sivers, Phys. Rev. D **41**, 83 (1990), **43**, 261 (1991).

[60] J. C. Collins, Nucl. Phys. B **396**, 161 (1993).

[61] M. Anselmino *et al.*, Eur. Phys. J. A **39**, 89 (2009)

[62] J. C. Collins *et al.*, Phys. Rev. D **73**, 094023 (2006).

[63] G. Bunce, *et al.*, "Plans for the RHIC Spin Physics Program 2008".

[64] X. d. Ji and F. Yuan, Phys. Lett. B **543**, 66 (2002); A. V. Belitsky, X. Ji and F. Yuan, Nucl. Phys. B **656**, 165 (2003).

[65] for example, see: Z. B. Kang and J. W. Qiu, Phys. Rev. D **79**, 016003 (2009), and references therein.

[66] S. J. Brodsky, D. S. Hwang and I. Schmidt, Phys. Lett. B **553**, 223 (2003); I. Schmidt and J. Soffer, Phys. Lett. B **563**, 179 (2003).

[67] M. Gluck, E. Reya and A. Vogt, Eur. Phys. J. C **5**, 461 (1998).

[68] J. W. Cronin, H. J. Frisch, M. J. Shochet, J. P. Boymond, R. Mermod, P. A. Piroue and R. L. Sumner, Phys. Rev. D **11**, 3105 (1975); L. Kluberg, P. A. Piroue, R. L. Sumner, D. Antreasyan, J. W. Cronin, H. J. Frisch and M. J. Shochet, Phys. Rev. Lett. **38**, 670 (1977); R. L. McCarthy *et al.*, Phys. Rev. Lett. **40**, 213 (1978); D. Antreasyan, J. W. Cronin, H. J. Frisch, M. J. Shochet, L. Kluberg, P. A. Piroue and R. L. Sumner, Phys. Rev. D **19**, 764 (1979); H. Jostlein *et al.*, Phys. Rev. D **20**, 53 (1979); P. B. Straub *et al.*, Phys. Rev. Lett. **68**, 452 (1992).

[69] P. M. Fishbane and J. S. Trefil, Phys. Rev. D **12**, 2113 (1975); J. H. Kuhn, Phys. Rev. D **13**, 2948 (1976); M. J. Longo, Nucl. Phys. B **134**, 70 (1978); A. Krzywicki, J. Engels, B. Petersson and U. Sukhatme, Phys. Lett. B **85**, 407 (1979); V. V. Zmushko, Sov. J. Nucl. Phys. **32**, 127 (1980) [Yad. Fiz. **32**, 246 (1980)].

[70] M. Lev and B. Petersson, Z. Phys. C **21**, 155 (1983); K. Kastella, G. Sterman and J. Milana, Phys. Rev. D **39**, 2586 (1989).

[71] E. M. Levin and M. G. Ryskin, Sov. J. Nucl. Phys. **47**, 889 (1988) [Yad. Fiz. **47**, 1397 (1988)]; G. T. Bodwin, S. J. Brodsky and G. P. Lepage, Phys. Rev. D **39**, 3287 (1989).

[72] X. N. Wang, Phys. Rev. C **61**, 064910 (2000) [arXiv:nucl-th/9812021].

[73] A. Accardi, arXiv:hep-ph/0212148.

[74] J. W. Qiu and I. Vitev, Phys. Rev. Lett. **93**, 262301 (2004) [arXiv:hep-ph/0309094].

[75] X. f. Guo and X. N. Wang, Phys. Rev. Lett. **85**, 3591 (2000) [arXiv:hep-ph/0005044]; Nucl. Phys. A **696**, 788 (2001) [arXiv:hep-ph/0102230]; B. W. Zhang, E. Wang and X. N. Wang, Phys. Rev. Lett. **93**, 072301 (2004) [arXiv:nucl-th/0309040]; Nucl. Phys. A **757**, 493 (2005) [arXiv:hep-ph/0412060].

[76] M. Gyulassy and M. Plümer, Phys. Lett. **B243**, 432 (1990); M. Gyulassy,M. Plümer, M. H. Thoma and X.-N. Wang, Nucl. Phys. A **538** (1992).

[77] X.-N. Wang and M. Gyulassy, Phys. Rev. Lett. **68**, 1480 (1992).

[78] K. J. Eskola, V. J. Kolhinen and C. A. Salgado, Eur. Phys. J. C **9**, 61 (1999) [arXiv:hep-ph/9807297]; K. J. Eskola, V. J. Kolhinen and P. V. Ruuskanen, Nucl. Phys. B **535**, 351 (1998) [arXiv:hep-ph/9802350].

[79] D. de Florian and R. Sassot, Phys. Rev. D **69**, 074028 (2004) [arXiv:hep-ph/0311227].

[80] M. Hirai, S. Kumano and T. H. Nagai, Phys. Rev. C **70**, 044905 (2004) [arXiv:hep-ph/0404093]; Phys. Rev. C **76**, 065207 (2007) [arXiv:0709.3038 [hep-ph]].

[81] K. J. Eskola, H. Paukkunen and C. A. Salgado, JHEP **0807**, 102 (2008) [arXiv:0802.0139 [hep-ph]].

[82] K. J. Eskola, H. Paukkunen and C. A. Salgado, JHEP **0904**, 065 (2009) [arXiv:0902.4154 [hep-ph]]; arXiv:0903.1956 [hep-ph].

[83] Z. B. Kang, J. W. Qiu and W. Vogelsang, Phys. Rev. D **79**, 054007 (2009) [arXiv:0811.3662 [hep-ph]].

[84] Z. B. Kang and J. W. Qiu, J. Phys. G **34**, S607 (2007) [arXiv:hep-ph/0702040].

[85] For a review, see A. H. Mueller, arXiv:hep-ph/0111244.

[86] E. L. Berger, J. W. Qiu and X. f. Zhang, Phys. Rev. D **65**, 034006 (2002) [arXiv:hep-ph/0107309].

[87] See, for example, G. A. Ladinsky and C. P. Yuan, Phys. Rev. D **50**, 4239 (1994) [arXiv:hep-ph/9311341]; J. W. Qiu and X. F. Zhang, Phys. Rev. D **63**, 114011 (2001) [arXiv:hep-ph/0012348]; F. Landry, R. Brock, P. M. Nadolsky and C. P. Yuan, Phys. Rev. D **67**, 073016 (2003) [arXiv:hep-ph/0212159], and references therein.

[88] X. f. Guo, J. W. Qiu and X. f. Zhang, Phys. Rev. Lett. **84**, 5049 (2000) [arXiv:hep-ph/9911476]; Phys. Rev. D **62**, 054008 (2000) [arXiv:hep-ph/9912361].

[89] X. f. Guo, Phys. Rev. D **58**, 114033 (1998).

[90] P. L. McGaughey, J. M. Moss and J. C. Peng, Annu. Rev. Nucl. Part. Sci. **49**, 217 (1999); J. C. Peng, arXiv:hep-ph/9912371.

[91] M. J. Leitch, Eur. Phys. J. C **43**, (157-160) 2005.

[92] G. T. Bodwin, E. Braaten and G. P. Lepage, Phys. Rev. D **51**, 1125 (1995) [Erratum-ibid. D **55**, 5853 (1997)] [arXiv:hep-ph/9407339].

[93] M.B. Einhorn and S.D. Ellis, Phys. Rev. D**12**, 2007 (1975); H. Fritzsch, Phys. Lett. B**67**. 217 (1977); M. Glück, J.F. Owens and E. Reya, Phys. Rev. D17, 2324 (1978); J. Babcock, D. Sivers and S. Wolfram, Phys. Rev. D18, 162 (1978).

[94] E772 Collaboration, D.M. Alde et al., Phys. Rev. Lett. **66**, 2285 (1991); E772 Collaboration, D.M. Alde et al., Phys. Rev. Lett. **64**, 2479 (1990); E789 Collaboration, M.J. Leitch et al., Phys. Rev. D **52**, 4251 (1995); M.A. Vasiliev et al., Phys. Rev. Lett. **83**, 2304 (1999).

[95] I. Arsene *et al.* [BRAHMS Collaboration], Nucl. Phys. A **757**, 1 (2005) [arXiv:nucl-ex/0410020]; B. B. Back *et al.*, Nucl. Phys. A **757**, 28 (2005) [arXiv:nucl-ex/0410022]; J. Adams *et al.* [STAR Collaboration], Nucl. Phys. A **757**, 102 (2005) [arXiv:nucl-

ex/0501009]; K. Adcox *et al.* [PHENIX Collaboration], Nucl. Phys. A **757**, 184 (2005) [arXiv:nucl-ex/0410003].

[96] For a review, see J. W. Qiu and G. Sterman, Int. J. Mod. Phys. E **12**, 149 (2003); J. W. Qiu, Eur. Phys. J. C **43**, 239 (2005) [arXiv:hep-ph/0507268].

[97] R. J. Fries, Phys. Rev. D **68**, 074013 (2003) [arXiv:hep-ph/0209275].

[98] M. Luo, J. W. Qiu and G. Sterman, Phys. Lett. B **279** (1992) 377; Phys. Rev. D **50**, 1951 (1994).

[99] S. J. Brodsky and A. H. Mueller, Phys. Lett. B **206**, 685 (1988).

[100] J. C. Collins, D. E. Soper and G. Sterman, Nucl. Phys. B **263**, 37 (1986).

[101] R. Gavai, D. Kharzeev, H. Satz, G. A. Schuler, K. Sridhar and R. Vogt, Int. J. Mod. Phys. A **10**, 3043 (1995) [arXiv:hep-ph/9502270].

[102] J. F. Amundson, O. J. P. Eboli, E. M. Gregores and F. Halzen, Phys. Lett. B **390**, 323 (1997) [arXiv:hep-ph/9605295].

[103] C. J. Benesh, J. W. Qiu and J. P. Vary, Phys. Rev. C **50**, 1015 (1994) [arXiv:hep-ph/9403265], and references therein.

[104] G. C. Nayak, J. W. Qiu and G. Sterman, Phys. Lett. B **613**, 45 (2005) [arXiv:hep-ph/0501235]; Phys. Rev. D **72**, 114012 (2005) [arXiv:hep-ph/0509021]; Phys. Rev. D **74**, 074007 (2006) [arXiv:hep-ph/0608066].

[105] E. Braaten, S. Fleming and T. C. Yuan, Ann. Rev. Nucl. Part. Sci. **46**, 197 (1996) [arXiv:hep-ph/9602374];
M. Kramer, Prog. Part. Nucl. Phys. **47**, 141 (2001) [arXiv:hep-ph/0106120];
J. P. Lansberg, Int. J. Mod. Phys. A **21**, 3857 (2006) [arXiv:hep-ph/0602091].

[106] P. Cho and A. K. Leibovich, Phys. Rev. D **53**, 150 (1996); P. Cho and A. K. Leibovich, Phys. Rev. D **53**, 6203 (1996); M. Beneke and I. Z. Rothstein, Phys. Rev. D **54**, 2005 (1996); P. Ko, J. Lee and H. S. Song, Phys. Rev. D **54**, 4312 (1996).

[107] M. L. Miller, K. Reygers, S. J. Sanders and P. Steinberg, Ann. Rev. Nucl. Part. Sci. **57**, 205 (2007) [arXiv:nucl-ex/0701025].

[108] Y. L. Dokshitzer and D. E. Kharzeev, Phys. Lett. B **519**, 199 (2001) [arXiv:hep-ph/0106202]; M. Djordjevic and M. Gyulassy, Nucl. Phys. A **733**, 265 (2004) [arXiv:nucl-th/0310076].

[109] A. Accardi *et al.*, arXiv:hep-ph/0308248, and references therein.

[110] Z. B. Kang and J. W. Qiu, arXiv:0707.0276 [hep-ph].

[111] K. Golec-Biernat and M. Wusthoff, Phys. Rev. D **59**, 014017 (1999).

[112] For a review, see E. Iancu and R. Venugopalan, arXiv:hep-ph/0303204, and references therein.

[113] For a review, see N. Brambilla *et al.* [Quarkonium Working Group], arXiv:hep-ph/0412158, and references therein.

[114] E. Braaten, S. Fleming and A. K. Leibovich, Phys. Rev. D **63**, 094006 (2001) [arXiv:hep-ph/0008091].

[115] A. Adare *et al.* [PHENIX Collaboration], Phys. Rev. Lett. **98**, 232002 (2007) [arXiv:hep-ex/0611020]; Phys. Rev. C **77**, 024912 (2008) [arXiv:0711.3917 [nucl-ex]]; Phys. Rev. Lett. **98**, 232301 (2007) [arXiv:nucl-ex/0611020]; Phys. Rev. Lett. **101**, 122301 (2008) [arXiv:0801.0220 [nucl-ex]].

[116] J. W. Qiu, J. P. Vary and X. F. Zhang, Phys. Rev. Lett. **88**, 232301 (2002) [arXiv:hep-ph/9809442]; Nucl. Phys. A **698**, 571 (2002) [arXiv:nucl-th/0106040].

[117] E. L. Berger, J. W. Qiu and Y. l. Wang, Phys. Rev. D **71**, 034007 (2005) [arXiv:hep-ph/0404158].